Study of the fast domain wall dynamics in thin magnetic wires

Kornel Richter

Laboratory of Solid State Physics
University Paris-Sud 11
and
Faculty of Science
Pavol Jozef Šafárik University in Košice

Thesis

Presented to obtain

THE DEGREE OF DOCTOR OF PHILOSOPHY
at the
UNIVERSITY PARIS XI IN ORSAY
and at the
PAVOL JOZEF ŠAFÁRIK UNIVERSITY IN KOŠICE

by

Kornel RICHTER

Subject:

Study of the fast domain wall dynamics in thin magnetic wires

Discipline: Solid state physics

Defended on August, 28 2013 in front of the commission:

Larissa Panina . . . . . Referee
Ivan Skorvanek . . . . . Referee
Vincent Cros. . . . . Examiner
Anne-Lise Adenot . . . . . Examiner
Peter Samuely . . . . . Examiner
Alexander Feher . . . . . Examiner
André Thiaville. . . . . Director
Rastislav Varga. . . . . Director

Laboratoire de Physique des Solides
University Paris XI
and
Faculty of Science
Pavol Jozef Šafárik University in Košice

Thesis

Presented to obtain

THE DEGREE OF DOCTOR OF PHILOSOPHY
at the
UNIVERSITY PARIS XI IN ORSAY
and at the
PAVOL JOZEF ŠAFÁRIK UNIVERSITY IN KOŠICE

by

Kornel RICHTER

Subject:

Study of the fast domain wall dynamics in thin magnetic wires

Discipline: Solid state physics

Defended on August, 28 2013 in front of the commission:

Larissa Panina	Referee
Ivan Skorvanek	Referee
Vincent Cros.	Examiner
Anne-Lise Adenot	Examiner
Peter Samuely	Examiner
Alexander Feher	Examiner
André Thiaville.	Director

Acknowledgement

This work was done within the frame of cotutelle agreement between Pavol Jozef Šafárik University in Košice and Laboratoire de Physique des Solides (LPS) which takes part at Université Paris-Sud 11 in Orsay. Due to the different time-length of the PhD. study in Slovakia and in France I spent the first year of my postgradual studies solely in Slovakia. After that, a possibility to finish my PhD. study in France appeared, so I switched to the "cotutelle" program and the next three years I continued my study in a series of one-half-year stays that have been held alternatively in Košice and Orsay.

First of all, I would like to owe my deepest gratitude to my Slovak supervisor Rastislav Varga, who introduced me to the main problems related to my work during the initial stage of my research and who provided the guidance and specific help in my work during the whole time of my PhD. study. Thanks to the friendly working atmosphere that he usually held in the lab I was always feeling very comfortable which helped me to be fully concentrated on my work.

I also wish to express thank my French supervisor André Thiaville, for providing me the opportunity to spend three marvelous stays at LPS. Under his supervision I was introduced to the new experimental techniques enabling direct observation of the surface domain structure by use of MOKE. His continuous effort to mould me into magneto-optics gave me many practical skills that are useful not only for recent work, but I will use it in my future research.

In the same way I would like to thank all members of IDMAG group for permanent support in different aspects of my research project as well as for many group-meetings which extended my understanding in the field of their research in magnetism.

I thank much stuff of LPS which helped me with practical realization of my experiments. Especially, I want to express thank Stanislas Rohart for his help with glass-removing by acid during my first stay as well as all technician stuff which helped me with preparation of my hand-made sample holders and setups.

I am happy to thank all members of the current and extended research group in Košice; namely Janka Gamcová and my recent colleagues Yuriy Kostyk, Peter Klein and Tomáš Ryba for permanent help and the cooperation in the field of our study.

I owe thank my family for strong support during the whole PhD. study, especially my parents, who made me feel that I have still the place where I can come back. It was giving me more power to go ahead. I would be remiss if I did not acknowledge my two sisters Mária and Daniela. I certainly thank Susan who was there for me through thick and thin.

Most of my activities during my PhD. study would not be possible to do without financial funding. I would like to thank French government which provided financial covering of my stays in France by *Bourse du gouvernement français (BGF)*. I would like to thank French embassy in Bratislava which mediated this fellowship.

Finally, I thank funding agencies for supporting my work within the frame of following projects:

NanoCEXmat Nr. ITMS 26220120019, Slovak MVTS 6RP/Manuet/UPJS/08 grant, Slovak VEGA grant No.1/0060/12, Slovak VEGA grant No.1/0076/09, Slovak VEGA grant No. 1/3035/06, Slovak grant APVV-0027-11, Slovak grant APVV-0266-10, Slovak grant APVT-20-007804, University grant VVGS UPJS No.30/09-10, University grant VVGS PF 36/2010/F, University grant VVGS PF No. 34/2011/F, University grant VVGS UPJS 2/12-13, SPP Hlavička Fellowship, EU ERANET program under project 'SoMaMicSens' (MANUNET-2010), MICINN Project No. MAT2007-65420-C02-01 MICINN Project No. MAT2010-18914, Saiotek 10 MIMAGURA project (SPE11UN087)

Table of contents

Introduction

The magnetization process of domain wall movement has become the topic of investigation since the introduction of domain theory which was done by French physicist Pierre-Ernest Weiss in 1907 (1). He proposed that ferromagnetic material is not magnetically homogeneous, but it is spontaneously divided into separate magnetic domains characterized by parallel orientation of magnetic moments within them. The boundary between two domains was later identified as a *domain wall*. The direction of magnetic moments was proposed to be arbitrary in magnetic domains, so that the net magnetization of specimen is nearly zero. However, if magnetic field is applied to such specimen, the magnetic domains with magnetization pointed toward external field start to increase volume and the ferromagnetic material becomes magnetically polarized. Although Weiss has never used the term “domain wall” in his work; practically, he was the first one who introduced the idea of domain wall existence being partially responsible for magnetization reversal.

A first experimental confirmation of Weiss theory was done by Barkhaussen (2). He found out that magnetic reversal of iron bulk is not continuous process, but it occurs as a series of small jumps giving rise to characteristic noise that can be heard by use of amplifier. In fact, this noise could be attributed to domain switching performed by domain wall propagation.

Further investigation of domain wall dynamics tried to find specimens in which the individual domain wall propagation takes place instead of multiple processes as it was in Barkhausen experiment.

The first observation on single domain wall propagation was done by Sixtus and Tonks (3) – (6) in 1931. In this pioneering work the magnetic field dependence of domain wall velocity in series of Ni-Fe amorphous wires held under mechanical stress was measured. For those compositions with positive magnetostriction and small crystalline anisotropy the applied tension stress provided magnetic bistability of studied wire. The measured domain wall velocity reached high values (1 km/s) and it was experimentally found to be direct proportional to a driving field in wide range of chemical compositions. In order to explain such measured data, Sixtus and Tonks suggested the domain wall velocity must be limited by eddy-currents that accomplish change of magnetic flux during domain wall movement. Later Dijkstra and Snoek (7) extended

their experiment. With their results they were able to confirm the shape of domain wall which was found to be conical.

Such results inspired Bloch (8) to analyze theoretically the transition boundary between two domains. He found out that the walls must have a width of several hundred lattice constants due to exchange interaction that opposes an abrupt magnetization change between two domains. His assumption was later experimentally confirmed by Bitter (9).

In a parallel development, the effect of anisotropy, magnetostriction and other factors involved on individual domain wall velocity in different samples were studied by others authors.

Williams and Shockely (10) in the late forties of 20th century used single crystal of silicon iron cut in the form of a hollow rectangular loop with {100} surface planes and with legs parallel to {100} crystal axes (picture frame) in their experiments. In this case, the domain structure was governed solely by magnetocrystalline anisotropy as opposed to magnetoelastic one in Sixtus-Tonks experiment. Later Williams, Shockley, and Kittel (11) observed the velocity of domain wall as a function of applied field in this specimen. Their experimental results showed that the movement is solely limited by eddy current as it was in Sixtus experiments.

Essentially similar experiments were carried out by Bean and Rodbell (12) using magnetically annealed Ni-Fe tapes. However, they pointed out firstly, that the domain wall braking cannot be explained with eddy currents since the thickness of the samples became smaller than 10 μm. A similar behavior of domain wall velocity in ferrites reported by Galt was explained by Kittel (13) in the frame of an additional magnetic relaxation domain wall damping.

Further investigation on individual domain wall dynamic was carried out in the late fifties by DeBlois (14). He observed the single domain wall propagation at high velocity of 50km/s in 10 μm thick iron-whisker specimens. Two regimes of domain wall propagation were explained in term of the domain wall structure change that occurs at high velocities.

The domain wall movement became in the centre of study due to investigation of losses in conducting ferromagnetic materials in the works of Becker (15) in the sixties of 20th century. In parallel, the ferromagnetic behavior of glassic metallic alloys was discovered that time (16). Such material was studied extensively in the next decade when the first specimens (wires and ribbons) became available in a form suitable for domain wall dynamics measurements (17) (18). The soft magnetic properties of such

specimens were compared favorably with Permalloy and were improved by thermal treatment (19) or stress (20). Another promising material for magneto-optic observation of domain wall movement was found in iron-garnets films (21) in the late seventies of 20^{th} century.

The ultra-fast magnetization process in the orthoferrites was intensively studied in the eighties of 20^{th} century (22). The strong orthorhombic anisotropy of the orthoferrites prevents substantial change of the structure of the moving domain wall. Moreover, the magnetic reorientation field was found to be very strong, about 80 kOe. This increased the range of fields in which the magnetization was due to domain wall displacement, and permitted the domain-wall dynamics in orthoferrites investigation in fields substantially stronger than in other ferromagnets. As a result of high domain wall velocity, the interaction of domain wall with phonons (23) (30) or spin waves (24) was observed in this kind of specimens.

Nowadays, more than 80 years after the first observation of domain wall dynamics made by Sixtus and Tonks, the phenomenon of domain wall movement is employed in many practical applications including a wide range of sensor and nano-sized data storage devices. However, most of the recent challenges in domain wall dynamics are related to its potential application in spintronics.

Spintronic, or spin – oriented electronic is a new emerging technology that makes use of magnetic moment of electron to transport and store information. One of spintronics concepts is based on magnetic transport properties of uniaxial ferromagnetic wires. Two states of bistable magnetic wires are used for coding two Boolean basis states of a logic system. Practically, the logic value is coded by direction of magnetization, whereas the change of logic value is performed by domain wall propagation.

D. A. Allwood (25) and D. Atkinson (26) proposed magnetic domain wall logic built on the basis of thin Permalloy planar nanowires. Due to the absence of magnetocrystalline and magnetoelastic anisotropies, the used wires are magnetically soft. The strongest magnetic anisotropy in this case arises from the elongated shape of nanowires (shape anisotropy). Fig. 1 shows prototypes of domain wall-based logical gates “AND” and “NOT”. Logical operations are performed by moving domains walls driven by an in-plane rotating magnetic field. Small dimensions of used wires are responsible for low

energy cost that is needed to change logic value. The energy needed to reverse the magnetic wire by domain wall propagation is $E = 2M_S H_c \mu_0 V_{nd}$, where the volume of the wire is V_{nd}. For nanowires this energy is of the order of $10^{-5}\ pJ$.

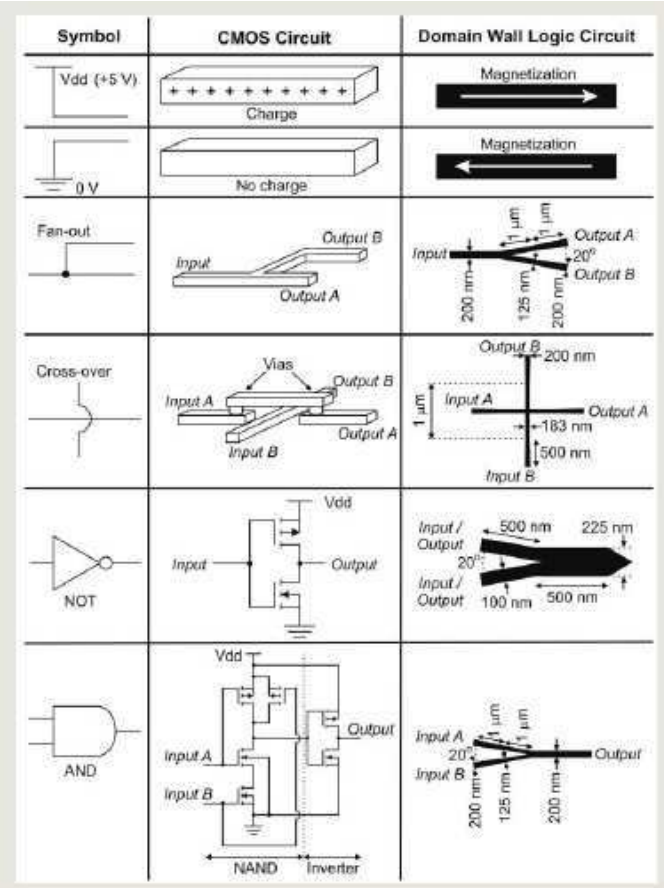

Fig. 1 Schematic drawing of the four basic junctions employed in domain wall logic devices. The logical values are coded by magnetization direction. "Fan-out" and "Cross-over" junctions serve for building complex 3D structures. Logical gates "not" and "and" are working under the condition of in-plane rotating magnetic field, in which one full rotation represents one computing cycle. The dimensions illustrated in the figure are critical for valid operation. Negation by logical gate "not" is provided by changing the domain wall structure from head to head into tail to tail. Figure adopted from (26).

Another spintronic device based on domain wall propagation is the domain wall diode (Fig. 2) proposed by Allwood et al. (27). The domain wall diode has a form of triangle, with one nanowire emanating from its apex and one from its base. A domain wall arriving at the triangle apex, under an applied magnetic field, is able to overcome pinning through the diode and continue through the opposite nanowire. However, a domain wall arriving at the triangle base is unable to overcome the significant pinning energy presented by the sudden change in track width.

Fig. 2 Domain wall movement-based diode. Image adopted from (27).

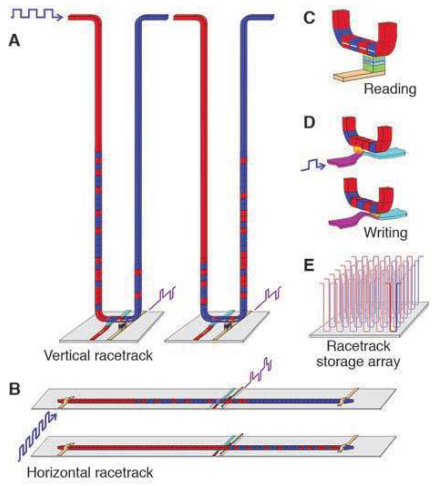

Fig. 3 Schematic drawing of domain wall-based spintronic memory Race-track. As in the previous devices, the logic value is coded by magnetization direction in the wire, in which one cell is carrying the information of one bit. Reading and writing of information is provided by synchronous domain wall movement. Figure adopted from (28).

A non-volatile domain wall-based spintronic memory was proposed by Parkin (28). Race-track memory consists of an array of thin ferromagnetic wires arranged horizontally or vertically on a silicon chip (Fig. 3). Individual reading and writing spintronic nanodevices are used to modify or read information stored in magnetic domains by synchronous movement of 10 to 100 domain walls.

As it is seen, in all these devices, the change of logic value is provided by domain wall movement. For this reason, recent interest in development of spintronics devices based on uniaxial magnetic wires is focused at two main challenges:

1, Understanding and controlling the behavior of domain walls as they propagate through complex geometry planar magnetic nanowires. This knowledge is critical for the successful development of magnetic logic circuits containing complex structures like loops or corners. Better understanding of micromagnetic processes involved pinning of domain wall is essential for enhancing of functional stability of such devices.

2, Understanding the magnetic field dependence of domain wall velocity. Since the logical value is changed by domain wall propagation, the operational speed of such devices is determined by domain wall velocity. Knowledge of the domain wall velocity and its dependence on magnetic field when combined with magnetic logic path-length information allows estimates of device operating times and equivalent clock speeds.

This work is related to the problem number 2. In the previous works (29) the domain wall velocity in microwires was found to reach very high values that exceed 15 km/s. Such high velocities are not possible to explain within the present models. The

understanding and knowledge of the control of fast domain wall velocities in microwires becomes in the centre of fundamental interest due to potential employment of microwires in practical applications based on domain wall movement.
The main goal of this thesis is to understand better the main factors that allow the fast magnetic reversal in microwires as well as the knowledge of controlling such high domain wall velocities with a special interest paid to potential application.

The manuscript is organized in following manner:

Chapter1: First, the similarity between the domain wall propagation and the motion of mass point in viscous media is discussed. Based on such analogy, a mechanical model of domain wall propagation is introduced. Within the mentioned model, two parameters: (a) a domain wall mobility and (b) a critical field are found to be responsible for the high domain wall velocities. The domain wall damping is shown to be the most important parameter determining the domain wall mobility. Three main contributions to the domain wall damping are presented. Basic physical principles of critical field are discussed.

Chapter 2: Here, the main properties of domain wall propagation in wires beyond the limit of viscous regime are briefly presented. It is shown that the domain wall dynamics beyond viscous regime is strongly determined by the geometry of material: in cylindrical wires, the transverse domain wall chirality is not restricted to any direction, whereas in wires with rectangular cross-section the Walker regime occurs. The change of the domain wall structure beyond Walker limit and its influence on a domain wall velocity is presented. Finally, the recent methods used to enhance the domain wall velocities in magnetic wires are briefly discussed.

Chapter 3: This chapter contains the description of main experimental techniques used in the thesis. Firstly, it is the improved Sixtus-Tonks setup and data software acquisition that were built within this work. It is followed by the description of Kerr-effect setup used in magneto-metric measurements. The standard technique of magneto-optic observation by use of polarizing microscope and the furnace for thermal annealing under the mechanical stress are described at the end.

Chapter 4: Initially, this chapter deals with magnetic and mechanical properties of amorphous glass-coated microwires. The fabrication of amorphous glass-coating microwire is shown to be responsible for the domain structure. Next, previous measurements on domain wall dynamic in microwires are presented with special interest paid to the domain wall velocity. The negative critical field and the two regimes of domain wall dynamics in microwires are shown to be responsible for high velocities exceeding the speed of sound in such material. At the end, three possible factors that might be responsible for such high domain wall velocities in microwires are discussed.

The main scientific results obtained in this thesis are presented in three chapters.

Chapter 5: In this chapter, the influence of magnetic anisotropy on fast domain wall propagation is analyzed. Since the magnetoelastic anisotropy was found to be the dominant one in case of amorphous glass-coated microwires, the magnetic anisotropy is tuned in three ways. In the first measurements, the domain wall dynamic under the externally applied axial tension is observed. It is shown that the domain wall damping arising from structure relaxation results in three different regimes of domain wall propagation. The influence of conventional annealing and annealing under the tensile stress on domain wall dynamics in microwires are compared. Finally, the effect of current annealing on domain wall velocity is studied.

Chapter 6: This chapter deals with the influence of the surface domain structure on high domain wall velocities. The surface magnetic structure is observed by combination of three experimental techniques. Firstly, the determination of the surface magnetization direction is performed by measuring the angular dependence of hysteresis loops with laser MOKE. Such results are compared with the surface domain pattern obtained by Bitter colloid and by magneto-optic observation with polarizing microscope. The comparison of surface domain structure in the samples with high and low domain wall velocity allows us to discuss on its possible influence on domain wall velocity. In the final magneto-optic experiment the domain wall trapped in a potential well and the shape of the domain wall are discussed.

Chapter 7: The domain wall velocity is measured in microwires with reduced diameter from 2.7 μm down to 1 μm in this chapter. The different ratio of glass-coating thickness

and metallic core diameter was previously found to be an important parameter for geometry of residual mechanical stresses introduced to the wire during its preparation process. The samples are treated by conventional thermal annealing and by thermal annealing in a perpendicular field. It is shown that the thermal treatment in perpendicular field results in rapid increase of domain wall mobility. The presence of strong perpendicular anisotropy in microwires is confirmed by the measurements of temperature dependence of remanent magnetization by MPMS.

Chapter 1
Mechanical model of domain wall propagation

Already the first measurements of domain wall dynamics revealed that the braking force opposed the domain wall motion can be expressed as a linear function of domain wall velocity (3) (10) (13). Moreover, Döring (31) showed that the domain wall exhibits inertia. Due to such analogies of domain wall propagation with the movement of a body in viscous medium, the domain wall dynamics is studied in mechanical model, in parallel to the other (micromagnetic) approaches.

Let's assume a magnetic domain wall to be a mass point of a total effective mass m_{DW} which is located at a potential well described by a harmonic potential:

$$\varphi = \frac{1}{2}\alpha_p x^2 \tag{1}$$

were α_p is a restoring force constant and x is the displacement of the domain wall from equilibrium position. If an external magnetic field *H* parallel to the magnetization direction in the domain is applied, the domain wall movement becomes described by the equation of linear harmonic oscillator:

$$m_{DW}\frac{d^2x}{dt^2} + \beta\frac{dx}{dt} + \alpha_p x = 2\mu_0 M_S H \tag{2}$$

where β is the domain wall damping coefficient, $\alpha_p x$ is the first derivative of pinning potential φ , μ_0 the permeability of vacuum, M_S saturation magnetization and the right side of equation correspond to the driving force per unit of wall surface arising from external magnetic field H. Assuming the domain wall propagates at constant velocity, the acceleration term in eq. 2 becomes zero. Moreover, the effect of local inhomogenities, impurities and other factors tending to impede the motion of the wall can be described by an average retarding field (called critical field) H_0, whose magnitude is like the ordinary coercive force. Assume the pining force of defects can be replaced by internal field H_0 oriented in opposite direction relative to the driving field. According to the eq. 2 the value of critical field is related to the shape of pining potential φ:

$$F = 2\mu_0 M_S H_0 \tag{3}$$

Then, the domain wall velocity can be expressed as a linear function of driving tic field:

$$v = S(H - H_0) \tag{4}$$

where the coefficient

$$S = 2\mu_0 M_S / \beta \tag{5}$$

is so-called domain wall mobility. Measurements of domain wall dynamics on magnetic wires confirm this relation. As it is seen from eq.(4), the high domain wall velocities can be achieved either by high domain wall mobility or by low (if it is possible even by a negative) critical field.

1.1 The domain wall mobility

Within the mechanical model, the domain wall mobility is directly proportional to the saturation magnetization M_S and indirectly proportional to the domain wall damping β (eq. 5). It is well-known from experiments, that the domain wall mobility S in microwires (32) (33) (34) as well as in the other magnetic materials (36) (37) usually exhibits positive temperature dependence as opposed to a negative temperature dependence of saturation magnetization M_S. Hence, the value of domain wall mobility must be predominantly determined by the domain wall damping in these specimens.

Recently, three contributions to the domain wall damping are recognized:

1, Eddy-current contribution – arises in any conducting magnetic material as a result of flux density change that occurs during the domain wall propagation. The exact calculation of the eddy-current contribution to the total domain wall damping must be performed with respect to the geometry of the wire and to the structure of the moving domain wall.

In the case of the amorphous glass-coated microwires, the domain wall propagates in cylindrical axial domain, which is surrounded by outer shell of radial domains. For such case, the eddy-current damping for planar domain wall was evaluated (35) in the form:

$$\beta_e = \frac{\mu_0^2 M_S^2 r_b}{\rho}\left(\ln\frac{r_0}{r_b} + 0.93\right) \tag{6}$$

where r_0 is the radius of the metallic nucleus, r_b is the axial domain radius and ρ is the electric resistance of material. This formula has been extended to satisfy the situation in bistable amorphous magnetic wires with very small residual stresses (35).

The eddy-current contribution to the total domain wall damping was firstly recognized in magnetic materials, where the domain wall velocity was limited by eddy-currents. (14) (3) – (6). The eddy-currents domination in such materials usually influenced the shape of the domain wall. At low magnetic fields (and velocities), the planar domain wall appeared as a result of small magnetic field induced by eddy currents. Transition velocities were characterized by conical domain wall which were followed by cylindrical domain wall collapsing inward the wire at the highest magnetic fields (14).

Although the eddy-current contribution was able to explain experimental data in many magnetic materials (12) (15), it failed in case of the strong domain wall damping observed in magnetic insulators (ferrites). For this reason, another contribution has had to be taken into account.

2, Magnetic relaxation domain wall damping: arises from the fact that domain wall cannot move faster than the magnetic moments which domain wall consists of. Firstly assume the case of single individual magnetic moment. If a dipolar moment is placed into external magnetic field, the directional change of magnetic moment does not occur immediately, but it takes a specific relaxation time τ to point toward the field. The switching process of a magnetic moment in effective magnetic field $\vec{H}_{eff}$ is described by famous Landau-Lifshitz equation (38):

$$\frac{d\vec{M}}{dt} = -\gamma_0(\vec{M}\times\vec{H}_{eff}) - \frac{\alpha\gamma}{|M_S|}\vec{M}\times(\vec{M}\times\vec{H}_{eff}) \tag{7}$$

where γ_0 is gyromagnetic ratio and α dimensionless Gilbert damping. The first term on the right side of equation is called the gyromagnetic term, whose analytical solution with the left side corresponds to the precessional motion:

$$\begin{aligned} M_x &= M_S \sin\upsilon_0 e^{i\omega_0 t} \\ M_y &= M_S \sin\upsilon_0 e^{i\omega_0 t + i\pi/2} \\ M_z &= M_S \cos\upsilon_0 \end{aligned} \tag{8}$$

where the values of angular velocity $\omega_0 = \gamma_0 H_{eff}$ and azimuthal angle υ_0 are constant.

$$\frac{d\vec{M}}{dt} = -|\gamma|\vec{M}\times\vec{H} \qquad \frac{d\vec{M}}{dt} = -|\gamma|\vec{M}\times\vec{H}^{eff} + \alpha\frac{d\vec{M}/dt\times\vec{M}}{|M|}$$

Fig. 4 Trajectory of magnetic moment subjected to magnetic field. Left, the intrinsic damping is zero, right; non-zero damping results in spiral motion toward magnetic field.

The gyromagnetic term in Landau-Lifshitz equation is conservative. Being the only one at right side of the equation, the magnetization performs precessional motion around the magnetic field and it would be never pointed to the field (fig. 4). However, it is well – known from experiments that magnetic materials are able to be magnetized. It is a result of dissipative processes that lead the magnetic moment to fall by spiral trajectory toward the direction of magnetic field. The general solution with dissipative term can be expressed in the similar form as it was in precessional motion of undamped case (39):

$$\begin{aligned} M_x &= M_S \sin\upsilon\, e^{i\omega t} \\ M_y &= M_S \sin\upsilon\, e^{i\omega t + i\pi/2} \\ M_z &= M_S \cos\upsilon \end{aligned} \tag{9}$$

but neither azimuthal angle υ nor angular velocity ω are not the same as before:

$$\tanh\frac{\upsilon}{2} = \tanh\frac{\upsilon_0}{2}e^{-t/\tau} \tag{10}$$

$$\omega = \frac{\omega_0}{1+\alpha^2} = \frac{\omega_0}{1+(1/(\omega_0\tau_0))^2} \tag{11}$$

Now, assume that the Bloch domain wall consists of magnetic moments, whose motion is described by above discussed Landau-Lifshitz equation (7). Moreover, assume the domain wall motion is damped solely due to relaxation of magnetic moments. The domain wall velocity is studied by the switching of magnetic moment situated in the centre of the domain wall (Fig. 5). For this magnetic moment:

$$M_x = M_S \tag{12}$$

$$M_y = M_z = O \tag{13}$$

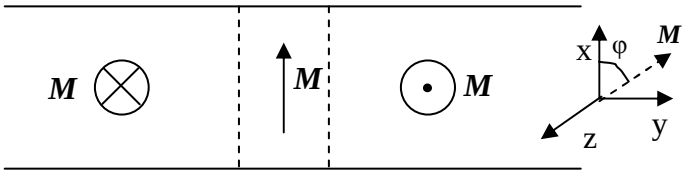

Fig. 5 Schematic drawing of Bloch domain wall between two adjacent domains. The central magnetic moment is oriented parallel to x axis and perpendicular to y axis.

Applying the external magnetic field H_Z in direction parallel to the magnetization in adjacent domains, the central magnetic moment starts to precess around *z* axis as it was described by eq. 8. However, after very short time *dt*, $\cos\varphi \cong 1$ and $dM_x/dt = 0$ can be assumed**.** According to the eq. 7 and eq. 13**,** the time derivatives of all others magnetization component can be evaluated:

$$\frac{dM_x}{dt} = 0 \quad \frac{dM_y}{dt} = \gamma_0 M_S H_Z \quad \frac{dM_z}{dt} = \alpha\gamma_0 M_S H_Z \tag{14}$$

Taking into account the small value of Gilbert damping $(\alpha << 1)$, the magnetic moment inclines from *y* and *x* axis significantly, but inclination of magnetic moment from *z* axis can be neglected (39). Then, denoting φ the inclination angle between the magnetic moment and *x*-axis, the components of magnetic moment within the centre of domain wall can be expressed:

$$M_x = M_S \cos\varphi, M_y = M_S \sin\varphi, M_z = 0 \tag{15}$$

Above mentioned rotation of magnetic moment gives rise to the creation of demagnetizing field. If the domain wall is approximated by thin, infinite long desk in *xy*-plane, the demagnetizing field is defined by corresponding demagnetizing factors:

$$N_x = N_z = 0, N_y = 1 \tag{16}$$

The total effective magnetic field applied to the magnetic moment is then given by the sum of externally applied magnetic field H_Z and demagnetizing field with components:

$$H_x = 0, H_y = M_S \cos\varphi, H_z = H_z \tag{17}$$

However, this magnetic field must fulfill LLG equation again. By introduction of all the components to the eq. 7 one may obtain:

$$\begin{aligned} \frac{dM_x}{dt} &= -\gamma_0 M_S H_z \sin\varphi + \alpha\gamma_0 M_S^2 \cos\varphi \sin^2\varphi, \\ \frac{dM_y}{dt} &= \gamma_0 M_S H_z \cos\varphi - \alpha\gamma_0 M_S^2 \cos^2\varphi \sin\varphi \\ \frac{dM_z}{dt} &= \gamma_0 M_S^2 \cos\varphi \sin\varphi + \alpha\gamma_0 M_S H_z \end{aligned} \tag{18}$$

If the domain wall propagation is restricted to the direction of y- axis, the first derivatives of magnetization components in *y* and *x* direction are zero for stationary motion:

$$\frac{dM_x}{dt} = \frac{dM_y}{dt} = 0 \tag{19}$$

Introducing this relation to the set of eq. 18, one may obtain:

$$H_z = \alpha M_S \cos\varphi \sin\varphi \tag{20}$$

Taking into account the magnetization profile of the domain wall being in the form (39):

$$M_z = M_S \tanh(y/\Delta) \tag{21}$$

where Δ denotes the domain wall width and assuming $\tanh(e) = e$ for $e << 1$, the time derivative of magnetization (eq. 18) yields:

$$\frac{dM_z}{dt} = \frac{M_S}{\Delta}\frac{dy}{dt} = \frac{M_S}{\delta}v_y \tag{22}$$

Comparing this equation with eq. 21

$$\frac{M_S}{\Delta}v_y = \gamma_0 M_S^2 \cos\varphi\sin\varphi + \alpha\gamma_0 M_S H_z \tag{23}$$

the relation containing the domain wall velocity can be obtained:

$$v_y = \gamma_0\Delta(M_S\cos\varphi\sin\varphi + \alpha H_z) \tag{24}$$

Assuming the above mentioned relation:

$$\cos\varphi\sin\varphi = \frac{H_z}{\alpha M_S} \tag{25}$$

the formula for domain wall propagation can be written:

$$v_y = \gamma_0\Delta(\frac{H_z}{\alpha} + \alpha H_z) = \frac{\gamma_0\Delta}{\alpha}(H_z + \alpha^2 H_z) = \frac{\gamma_0\Delta H_z}{\alpha}(1+\alpha^2) \tag{26}$$

If $\alpha << 1$, the field dependence of the domain wall velocity can be expressed in the form (39):

$$v_y = \frac{\gamma_0\Delta}{\alpha}H_z \tag{27}$$

As it is seen, even if the domain wall is not braked by macroscopic eddy-currents, the domain wall velocity is restricted by intrinsic damping of magnetic moments of the domain wall. The relation between the damping coefficient α (which express the intrinsic damping of magnetic moments) and the part of the total domain wall damping β (which express the damping of the whole domain wall) was first time introduced by Kittel and Galt (13) for high-resistance ferrites, where eddy-current failed to describe observed domain wall mobility. The domain wall damping was found to be proportional

to the magnetic anisotropy. The corresponding formula of domain wall damping arising from magnetic relaxation of magnetic moments can be expressed:

$$\beta_r = \frac{F}{v} = \frac{2M_S H_z \mu_0}{H_z \gamma_0 \Delta/\alpha} = 2\alpha M_S \mu_0 \gamma_0^{-1} (K/A)^{1/2} \tag{28}$$

as it was considered by many authors before (13), (14), (44). The magnetic relaxation domain wall damping β_r is then proportional to the Gilbert damping α and inversely proportional to the domain wall width δ. Physically this dependence comes about because for a given domain wall velocity the spins in a thin wall must rotate more rapidly than in a thick one (14).

In this sense, the minimization of magnetic relaxation domain wall damping can be performed by minimizing the switching time of magnetic moments. However, the switching time of individual magnetic moments was not found to be the monotonous function of effective field. For very low value of Gilbert damping $\alpha << 1$, spins perform too many rotations (eq. 7) in order to point toward magnetic field. Then, the total switching time is high (in the limit case of zero Gilbert damping, the switching time is infinite). On the other side, a high value of Gilbert damping makes the magnetic moments less mobile and even if they perform less rotations, the total switching time is higher due to the higher damping. Hence, there must be a critical value of Gilbert domain damping, at which the switching time of magnetic moments is minimal and the domain wall propagation is fast. Such idea was used to enhance the domain wall velocities in the ferrites (40), where the magnetic relaxation takes the most important contribution to the total domain wall damping. The minimum switching time was found:

$$\tau_{\min} = \frac{2}{\omega_0} = \frac{2}{\gamma_0 H} \tag{29}$$

Taking into account $g = 2$ and $H = 20000\,Oe$:

$$\tau_{\min} = 5.7 \times 10^{-9}\,s \tag{30}$$

The switching time was found to be one order higher in ferromagnetic resonance experiments. However, this value can be decreased by eddy currents. If the magnetization reversal occurs in cylindrical wire, the total magnetic field induced by eddy-currents can be expressed:

$$H_{dam} = \int_0^{r_0} i(r)dr = -\frac{r_0^2}{4\rho}\frac{dM}{dt} \tag{31}$$

On the other side, the damping field can be evaluated from eq. 7:

$$H_{dam} = \frac{\alpha}{\gamma_0 M_s}\frac{dM}{dt} \tag{32}$$

Comparing the last two equations and taking into account the values of constants $\gamma_0 = 2{,}21\times10^5 mA^{-1}s^{-1}$, $\mu_0 = 4\pi\times10^{-7}$, $M_S = 1{,}6\times10^6 Am^{-1}$, $\rho = 10^{-7}\Omega m$ the condition of minimal time is met in the wire with the total diameter (40):

$$r_0 = 1{,}35\mu m \tag{33}$$

Thin magnetic wires are typical by fast domain wall velocities. One of the reasons for that may arise from Gilbert damping being optimized by eddy-currents.

The eddy-current and magnetic relaxation domain wall damping were used to describe the observed domain wall mobility in wide range of magnetic materials including high-resistance ferrites and wires with high residual mechanical stress. However, they failed to explain the high observed values of domain wall damping which appears at low temperatures in amorphous materials (41). For this reason, the so-called structural contribution to the domain wall damping has had to be introduced.

3, Domain wall damping by structural relaxation – arises from the interaction of atomic mobile defects with a domain wall. Such structural relaxation domain wall damping was introduced at the basis of thermodynamics of the two-level systems (42) (43). In the simplest case the mobile defect can take place at two metastable positions (fig. 6) characterized by interaction energies e_{ff}^1 and e_{ff}^2. In the neighbourhood of a free volumes the atoms and atomic clusters (mobile defects) posses an increased mobility, thus assisting rearrangements of the atoms. The total interaction energy of mobile defect

with amorphous matrix in each of both positions can be assumed to be the sum of dipole-dipole, exchange and magnetoelastic anisotropy (42) (43):

$$e_{eff} = e_{eff}^{dipole-dipole} + e_{eff}^{exchange} + e_{eff}^{magnetoelastic} \tag{34}$$

The energy difference between the two orientations of the atom pair is given by splitting energy:

$$2\Delta = e_{ff}^{1} - e_{ff}^{2} \tag{35}$$

At high temperature $kT >> 2\Delta$ the mobile defect can overcome the energy barrier by thermal activation very easy and the occupation probability is the same for both positions. However, at low temperatures $kT \approx \Delta$ the occupation of both levels becomes described by a distribution function. Assume the mobile defect takes place at a position with a certain magnetization direction. However, such a direction of local magnetization is changed during the domain wall propagation.

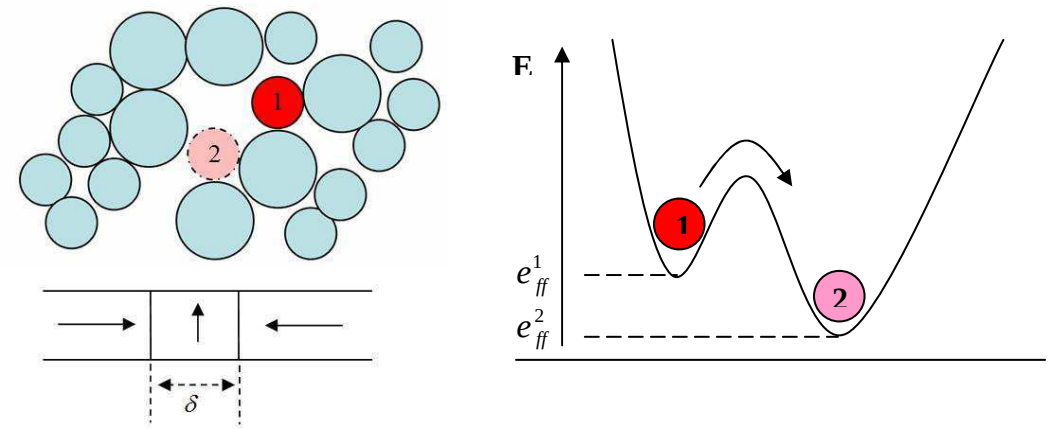

Fig. 6 In the simplest case, the mobile defect represented in the picture by red and pink circles can occupy only two metastable positions, each characterized by different interaction energy with local magnetization.. Assume the domain wall of total width δ propagates at constant velocity v through the mobile defect. It takes the total time $t = \delta / v$ to cross the mobile defect. Depending on the balance between the relaxation time τ of mobile defect and the crossing time t a structural relaxation can appear in different regimes.

The total interaction energy of mobile defects with domain wall can be defined as the energy acquired by mobile defects reoccupation to the states of lowest energy. Since the transition of the mobile defects between the metastable positions is determined by stochastic processes, the probability of domain wall's interaction with mobile defect increases with time. The total energy transferred between the domain wall and the mobile defects can be expressed as (42):

$$E = \frac{\delta}{15}\frac{c_0}{kT}\left\langle \varepsilon^2 \right\rangle \left(1 - \exp(-t/\tau)\right) \tag{36}$$

where δ denotes the domain wall width, c_0 the volume concentration of mobile defects, $\left\langle \varepsilon^2 \right\rangle$ is the mean value of squares of interaction energies of mobile defect. Note, that total energy acquired by the interaction of the domain wall with mobile defects increases with time from $E_{t=0} = 0$ at t = 0 to the maximum value $E_{t=\infty} = \frac{\delta}{15}\frac{c_0}{kT}\left\langle \varepsilon^2 \right\rangle$. If the domain wall has a thickness δ and it propagates with velocity v, the time it is needed to cross the mobile defects is $t = \delta / v$. Then, the eq. 36 can be transformed:

$$E = \frac{vt}{15}\frac{c_0}{kT}\left\langle \varepsilon^2 \right\rangle \left(1 - \exp(-t/\tau)\right) \tag{37}$$

The domain wall damping by structural relaxation plays an important role unless the crossing time is comparable to the relaxation time of mobile defects:

$$t \approx \tau \tag{38}$$

Taking into account eq. 5 and eq. 37, the total energy can be written:

$$E = \frac{v\tau}{15}\frac{c_0}{kT}\left\langle \varepsilon^2 \right\rangle \left(1 - \exp(-t/\tau)\right) \tag{39}$$

If the energy for reoccupation of mobile defect is consumed from the domain wall propagation, the corresponding damping term was evaluated (15) as:

$$\beta_S = \frac{\tau}{15}\frac{c_0}{kT}\left\langle \varepsilon^2 \right\rangle \left(1 - \exp(-t/\tau)\right) \tag{40}$$

The structural relaxation domain wall damping was introduced in this form in order to explain the high domain wall damping in microwires measured at low temperatures (45).

Being t_1 the time, which the domain wall needs to cross the position of atomic mobile defects ($t_1 = \delta / v$, where δ is the domain wall width and v the domain wall velocity), the two other parameters for the structural relaxation are important:

τ - The relaxation time of atomic mobile defects obeying Arrhenius law $\tau = \tau_0 e^{E_Q / kT}$

t_2 - The time between two domain wall propagations (i.e. the period of the measurement in our experiment that corresponds to a measuring frequency *f*: $t_2 \sim 2/f$)

Depending on the relation between t_1, τ and t_2 respectively, five regimes of structural relaxation were recognized (46), (47), (48), (49) :

1, Metastable range: $\tau > t_2 > t_1$ - here, the mobile defects have no time to relax (they are frozen in the amorphous matrix) and the amplitude of the structural relaxation is given by the history of the material (e.g. if the material was stabilized, by annealing below Curie temperature, the structural relaxation damping is high. On the other side, if the system was destabilized, by heating above Curie temperature, the structural relaxation is low.)

2, Structural relaxation range: $\tau \approx t_2 > t_1$ - the defects are able to stabilize the domain structure between two domain wall propagations. This makes the structural relaxation damping to increase that results in a hindering of the domain wall propagation. By properly selected frequency of measurements, the range can be moderated and the structural relaxation damping can be modified.

3, Adiabatic range: $t_2 > \tau > t_1$. The system of defects is in equilibrium state and the structural relaxation damping reaches its maximum at given temperature, but the defect cannot follow the propagating domain wall (fig. 7).

4, Diffusion- damped range: $t_2 > t_1 \approx \tau$. In this range, the time at which the domain wall crosses a single defect is comparable to its relaxation time. The defect relaxes during the domain wall propagation that results in a decrease of the domain wall velocity.

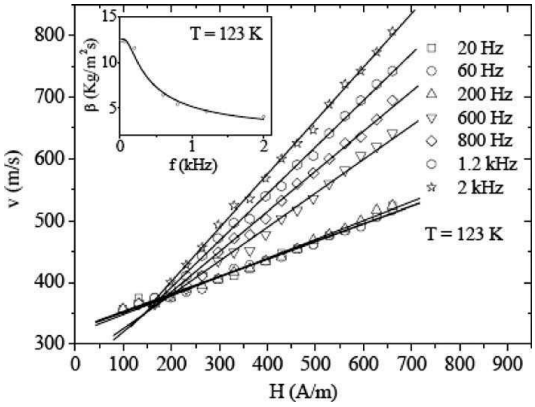

Fig. 7 Field dependence of domain wall velocity is a function of measuring frequency. This can be explained with the term of structural relaxation. If the time interval between two domain wall propagations is too high, the mobile defects have time to relax, which results in lower domain wall velocity. The inset shows frequency dependence of domain wall damping. Image adopted from (48).

Increasing the applied field amplitude, the domain wall velocity increases until $t_1 < \tau$, when the domain wall is able to detach from defect and goes into adiabatic regime (fig. 8).

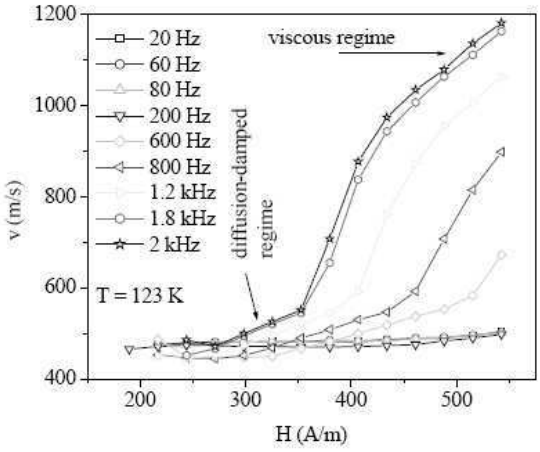

Fig. 8 If the domain wall crosses the mobile defect during the time, which is higher than the relaxation time of mobile defects, the domain wall is no more retarded by structure relaxation (viscous regime). The image was adopted from (49).

5, Isothermal regime: $t_2 > t_1 > \tau$. Although, the whole system relaxes between two domain wall propagations, the relaxation time of defects is short and they are able to follow rapidly the domain wall during its propagation. Structural relaxation damping term is small and the domain wall velocity increases. Such regime usually appears at high temperatures only.

1.2 Critical propagation field of the domain wall

The second considered parameter governing the domain wall velocity is the critical propagation field. If the bistable wire is fully magnetized in one direction by

axial magnetic field, and the field is then removed, the wire remains magnetized fully in that direction. In order to start the magnetization reversal, some magnetic field greater than material's intrinsic coercitive force must be applied in opposite direction. The calculation of critical field (eq. 3) considers usually two mechanisms involved in this process: mechanism of domain wall nucleation and mechanism of domain wall deppining. In case of amorphous glass-coated microwires, the domain wall nucleates itself during the reversal process; hence, the value of critical field is determined solely by deppining mechanism.

Recently, at least two contributions to the critical field in amorphous glass-coated microwires are recognized:

1, Contribution from magnetoelastic anisotropy – since amorphous glass-coated microwires has a large enough positive magnetostriction, it is reasonable to assume that the switching field is mostly driven by magnetoelastic interaction between internal stresses and the domain walls at the ends of wire (54). Assume that that the process of domain wall deppining is accompanied by increase of its effective length.

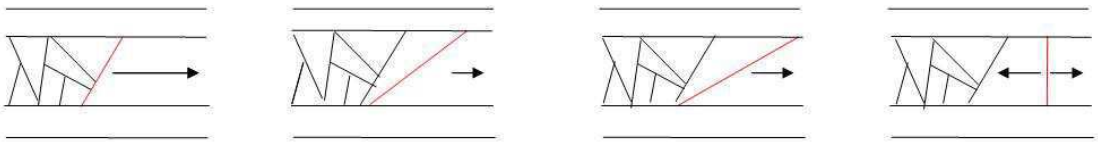

Increasing the total domain wall length, more magnetic moments are rotated out of easy axis and the domain wall energy becomes higher. The value of critical field arising from magnetoelastic anisotropy could be derived from eq. 3:

$$\frac{1}{2} M_S H_0^{\sigma} \mu_0 = K \tag{50}$$

As it will be shown later, the most important magnetic anisotropy in the case of amorphous glass-coated microwires arise from the magnetoelastic contribution:

$$K = \frac{3}{2} \lambda_S \sigma \tag{51}$$

where λ_S is the saturation magnetostriction coefficient of metallic nucleus and σ the total mechanical stress applied to the sample either by external load or by rapid

quenching and drawing during the fabrication process. Combining such relation with eq. 50, the critical field can be found to be proportional to the mechanical stress:

$$H_0^{\sigma} \approx 2K/M_S\,\mu_0 = 3K\lambda_S\sigma/\mu_0 M_S \qquad (52)$$

A similar dependence has been measured in previous experiments (54).

2, Contribution from structure relaxation – Decrease in the critical field at low frequency in microwires (54) was explained satisfactory within the frame of magnetic-after effect (42). As a result of microwire preparation by rapid cooling, the structure of amorphous wires is associated with the metastable state of the amorphous structure, and for this reason a quite large relaxation effect can be expected (54). Within the domain wall, the mobile defects are relaxed in the direction of local magnetization in the wall, whereas the mobile defects in adjacent magnetic domains are relaxed to the axial magnetization. The domain wall starts to move as soon as the total force from external magnetic field exceeds the force needed for rearrangement of relaxed mobile defects from their metastable positions.

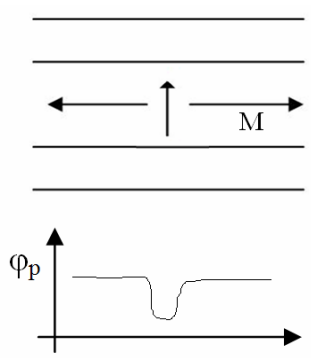

Fig. 10 Schematic drawing of the domain wall together with the potential which arises from structural relaxation. The mobile defects are relaxed to the local magnetization direction in whole volume of domain wall. In the same way, the mobile defects in adjacent domains are relaxed to the direction of magnetization.

The critical field arising from structure relaxation has explained the frequency dependence of the critical field in microwires. As the measuring frequency decreased, the measuring time increased and the stabilization of the domain structure by structure relaxation took place.

The contribution of structural relaxation to the critical field was introduced in the form (55):

$$H_0^{s} \approx \varepsilon_{eff}^2\, c_0 \left(1-\exp(-t/\tau)\right)/M_S kT \qquad (53)$$

where ε_{eff} is the effective interaction energy of the mobile defect with amorphous matrix, c_0 is volume concentration of mobile defects, t is the interaction time of domain wall with mobile defect, τ is relaxation time of mobile defect, M_S is the saturation magnetization, k is Boltzman constant and T is the thermodynamic temperature.

Such effect has been found to be explaining the observed temperature dependence of critical field in microwires (51), (52), (53).

Chapter 2

Beyond the viscous regime

In the previous chapter the mechanical model of the domain wall propagation was introduced. It was shown that the braking force opposing the domain wall motion can be expressed as a linear function of domain wall velocity. Then, the domain wall velocity can be evaluated as a linear function of magnetic field. Such model was confirmed by field dependence of domain wall velocity measurements in various magnetic materials, where a linear relation between the domain wall velocities and the driving field was found. However, such phenomenological approach has its own limitation, which consists in the non-linear dynamics process that starts to take place in very fast domain wall. In this way a question about the domain wall dynamics beyond the limitation of viscous regime appears, which is briefly discussed in this chapter.

In the previous chapter, the movement of Bloch wall considered as a simple chain (1D) has been studied. It has been shown that application of magnetic field in the direction of domain wall propagation leads to the rotation of central magnetic moment within the domain wall out of the x-axis by eq. 26. Such rotation of magnetic moment generates the demagnetizing field which was found elsewhere to be responsible for effective domain wall mass. As it is seen from eq. 26, the rotation angle φ is increasing with the applied driving field:

$$H_z = 1/2\,\alpha M_S \sin 2\varphi \tag{54}$$

and the maximum of angle φ ($\sin(2\varphi) = 1$) is achieved at the value of magnetic field (from eq. 54):

$$H_w = 1/2\,\alpha M_S \tag{55}$$

which corresponds to the domain wall velocity (according to the eq. 27):

$$v_w = \frac{\gamma_0 \delta}{\alpha} H_w = 1/2\,\gamma_0 \delta M_S \tag{56}$$

This velocity is so-called Walker velocity (or limit) and it is the maximum velocity, at which the domain wall can propagate in its initial (Bloch) configuration.

An exact solution of 1D movement of 180° domain wall was firstly done by Schryrer and Walker (56) in 1974. A polar coordinate system with the polar axis along the hard axis (Fig. 11) was used in his numerical calculations. The driven magnetic field was applied along the easy axis $\theta = 90°$. The wall motion was described by the change in the value of angle θ from $\theta = -90°$ to $\theta = 90°$. The type of the domain wall structure is given by the angle Φ of magnetic moment in the centre of the wall. The angle Φ indicates the character of the wall, being $\Phi = 90°$ for stray-field free Bloch wall and $\Phi = 0°$ the Néel wall.

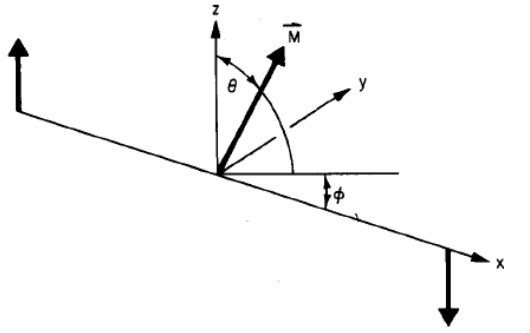

Fig. 11 Cartesian and polar coordinate system. The easy magnetization direction is parallel to z axis. Image adopted from (56).

Walker considered the total domain wall energy per unit area (in CGS) in the form:

$$E = \int_{-\infty}^{+\infty} (-\mathrm{H}_0 \mathrm{M}_z + 2\pi \mathrm{M}_x^2 - \frac{\mathrm{K}}{\mathrm{M}_0^2} \mathrm{M}_z^2 + \frac{\mathrm{A}}{\mathrm{M}_0^2} \left| \frac{\partial \vec{\mathrm{M}}}{\partial \mathrm{x}} \right|^2) dx \qquad (57)$$

where the first term in parentheses represents the Zeeman energy density, the second term corresponds to the magnetostatic energy density, the third term refers to energy density of uniaxial anisotropy and the last one to the exchange energy density.

By use of Landau-Lifshitz-Gilbert equation in arbitrary coordinate system and assuming the wall moving at a constant velocity v along the x axis, the following equations were derived (56) (17) for steady motion:

$$\begin{aligned} -vc\theta' &= 2\gamma_0 / J_S \left[-A(c^2\Phi') + \mathrm{K}_d c^2 \sin\Phi\cos\Phi \right] - \alpha v c^2 \Phi' \\ -vc\Phi' &= 2\gamma_0 / J_S \left[A\theta'' + \mathrm{cs}(\mathrm{K}_u + \mathrm{K}_d \sin^2\Phi + A\Phi'^2) \right] + H\gamma_0 c + \alpha v \theta' \end{aligned} \qquad (58)$$

Where $c = \cos\theta$ and $S = \sin\phi$.

One of the solutions of these equations corresponds to the constant angle Φ through the wall, for which the last two terms (eq. 58) representing the driving force and the dissipation force cancel each other (17). Such a solution represents the motion of the wall with a constant configuration of magnetization. The domain wall velocity is found to be directly proportional to the driving field. The maximum velocity for this kind of propagation was found to be directly proportional to quality factor:

$$v_p = \gamma_0 \sqrt{\frac{2AQ}{u_0}} f(Q), Q = \frac{K_u}{K_d},\ f(\mathrm{Q}) = \sqrt{1+1/\mathrm{Q}} - 1 \qquad (59)$$

where Q is the factor quality.

It means, beyond this value, no steady state of the domain wall is possible. In order to investigate the domain wall movement beyond Walker limit, a system of rotating coordinates was used in his calculations. The main results are shown in fig. 12 and fig. 13.

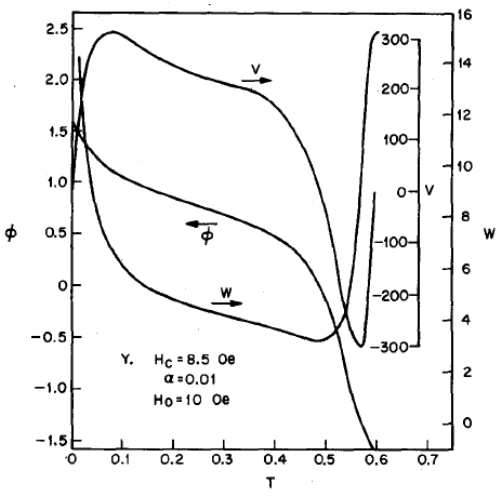

Fig. 12 The relation between the domain wall velocity and the main coordinates which characterize the domain wall structure transformations from Bloch to Néel one beyond Walker limit. Image adopted from (56). *T* denotes time, ϕ is polar angle of magnetic moment within the domain wall centre (see text below) and *v* denotes the domain wall velocity.

Fig. 12 shows the relation between the polar angle Φ ($\Phi = \pi/2$ for Bloch wall and $\Phi = 0$ for Néel domain wall) and the domain wall velocity. Within the initial acceleration of the domain wall, the decrease of polar angle from the value of $\Phi = \pi/2$ can be observed. If the central magnetization vector becomes tilted of around $\Phi = 1.25$, the domain wall velocity starts to decrease. Close to the angle $\Phi = 1$ the velocity is zero. However, further transformation of the Bloch wall into the Néel one is accompanied by the backward domain wall motion (negative velocity). The domain wall velocity remains negative until the Néel wall is transformed to the opposite Bloch wall and the whole process is repeating in the same way (Fig. 12).

Walker was the first one, who showed that beyond the critical field (Walker field) no stable solution of the domain wall propagation exists. In this regime, the domain wall transforms its structure periodically from the Bloch to Néel configuration, while the wall itself oscillates back and forth. Such non-stationary domain wall propagation results in the rapid decrease of average domain wall velocity, which can be recognized as a breakdown in the field dependence of domain wall velocity. The domain wall has the negative domain wall mobility in this regime, where average velocity decreases with increasing applied field.

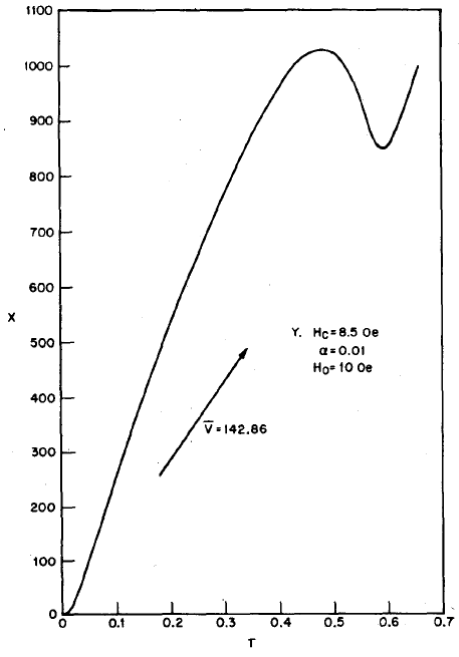

Fig. 13 The field dependence of the average domain wall velocity as it was calculated by Walker. The steady regime of domain wall propagation can be recognized in the initial linear part. The domain wall mobility becomes negative beyond the Walker limit. In this regime, the stationary solutions must be replaced by inhomogeneous chaotic modes. Image adopted from (56).

Walker considered the infinite magnetic medium in his model. The demagnetizing field arises from the domain wall magnetization precession that accompanies domain wall movement. Even if the situation is more complex in real material, the Walker solution has been found to be qualitatively valid in wide range of magnetic materials.

2.1 The domain wall dynamics in thin planar magnetic nanowires

The domain wall dynamics was extensively studied on thin planar nanowires (57) (58) (59). They have been constructed on the basis of thin ferromagnetic stripes with length *L*, width *w* and total thickness *t* (L >> w > t). The structure of the domain wall in such material depends on balance between exchange and anisotropy energies. The exchange energy is minimized by parallel orientation of magnetic moments, whereas

the anisotropy energy encourages the orientation along a particular direction. In soft magnetic materials (like Permalloy) the shape anisotropy is the most important and the spontaneous magnetization lies along the wire axis. The domain wall separating two adjacent domains come in two configurations: transverse and vortex wall. The transverse structure is characterized by continuous rotation of magnetization vector across the wall. This reduces the exchange energy at the expense of the free magnetic poles at the edges. The resulting magnetostatic energy increases with *w* and *t*. As either of these dimensions increases, the system eventually favors closure structure like vortex domain wall. Here, the magnetization vector circulates in a plane about a small core with perpendicular magnetization within. The closure configuration of vortex domain wall minimizes the free poles but increases the exchange energy.

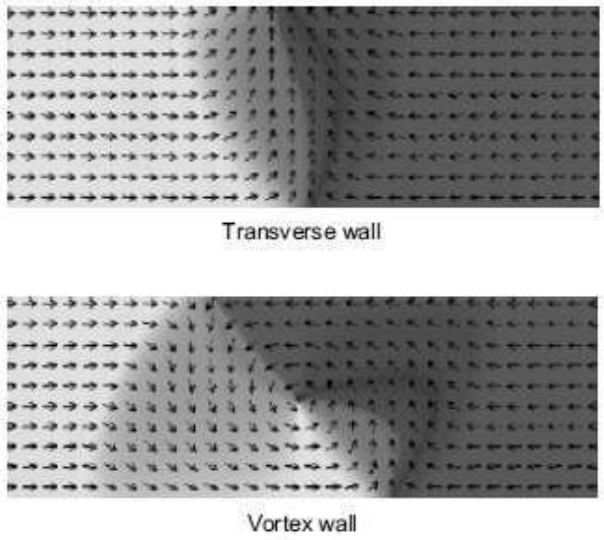

Fig. 14 The structure of Transverse and Vortex domain wall in thin ferromagnetic strip. Image adopted from (60).

By magnetostatic energy comparison of the transverse domain wall with additional exchange energy attributed to the vortex domain wall a phase diagram was determined (60) (61) (62):

$$wt = 60L_{ex}^2 \tag{60}$$

where L_{ex} denotes exchange length (which is for permalloy around 5 nm). As it is seen in Fig. 5, the transverse domain walls are preferable for thin and narrow nanowires, whereas the vortex domain structure is table if dimensions are increased.

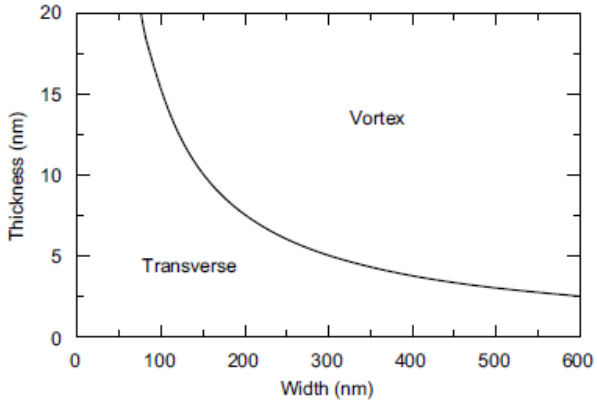

Fig. 15 The phase boundary for transverse and vortex domain wall in thin ferromagnetic nanowires. Image adopted from (60).

Consider a thin ferromagnetic strip oriented in x axis with transverse domain wall. Such a nanowire is characterized by three regions: two adjacent domains, each uniformly magnetized and a domain wall with core magnetization direction being oriented in y axis (Fig. 14). If the driving field is applied along x – direction, the magnetization within the domains does not respond because of domains being parallel oriented to the field. However, damping toward the applied field leads to the rotation of the domain wall magnetization toward the x- axis. Precession of the magnetic moments around the driving field results in domain wall magnetization tilting out of the plane at angle θ. If the magnetization is tilted out from xy – plane, it is no longer antiparallel to the demagnetization field. The component of demagnetization field perpendicular to the magnetization is proportional to the tilting angle θ (63):

$$H_d = M_S (N_z - N_y) \cos\theta \sin\theta \qquad (61)$$

where N_z, N_y are demagnetizing factors in the region of the domain wall. It means, for non-zero tilting angle θ, the component of demagnetization field is non-zero too and the domain wall magnetization precesses around it, contributing to the rotation toward x – axis (i.e. to the domain wall propagation along x axis).

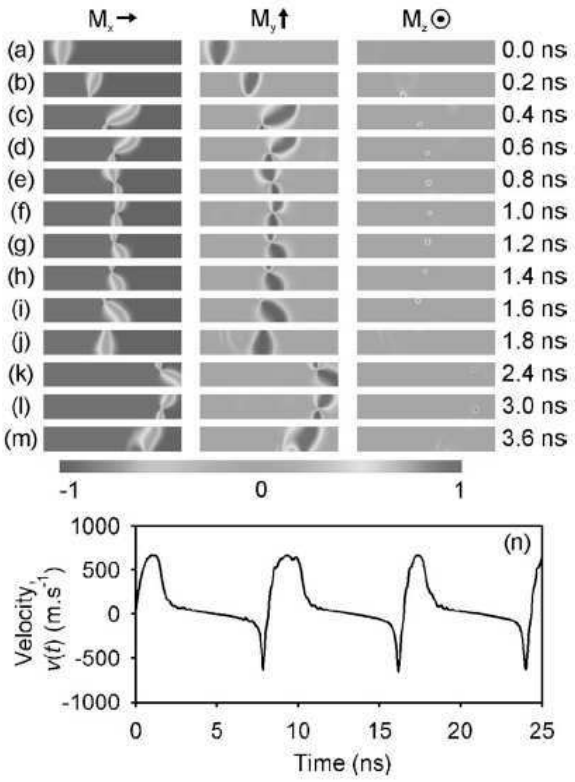

Fig. 16 The micromagnetic simulation of the transverse domain wall propagation in thin ferromagnetic planar nanowire beyond the Walker limit. If the tilting angle reach its maximum value (which is given by the dimensions of the wire), a small vortex core is nucleated at the apex of the transverse wall. As the vortex core starts to move within the transverse wall, the propagation velocity becomes negative (retrograde domain wall motion). If the vortex reaches the second edge, the transverse wall is recovered, but it sense (chirality) is reversed. Image adopted from (60).

The domain wall velocity is then proportional to the component of demagnetization field perpendicular to the magnetization:

$$(1+\alpha^2)v = (\gamma\pi^{-1})(H_d + H\alpha)\alpha \qquad (62)$$

This formula shows that when the driving field H is removed, the precession around demagnetizing field sustains the momentum of the wall (63). This behaviour was attributed to the effective domain wall mass. However, damping of the magnetic moments drags the energy from the movement in this case, which results in decrease of tilting angle θ and, consequently, in decrease of demagnetizing field H_d which bring the domain wall to a stop.

As it is clearly seen from eq. 61, the higher value of tilting angle, the higher domain wall velocity is achieved. For each strip geometry there is a tilt angle θ maximizing the domain wall velocity that occurs at $max\ H_d$.

From the domain wall dynamics point of view, two regimes of domain wall propagation can be recognized with respect to the driving field (63):

1, $H < \alpha M_s (N_x - N_y)/2$ - if the value of applied magnetic field is small, the tendency to increase the tilt angle is balanced by the tendency of damping to push the tilt angle back to zero (63). The tilt angle is constant at a given value of driving field and the domain wall velocity is proportional to the field.

2, $H > \alpha M_s (N_x - N_y)/2$ - if the driving field is increased, the tilt angle continues to grow. When the value of tilt angle exceeds $\pi/2$, the precession and damping accelerate the magnetization back to the plane. Though precession continues clockwise around the demagnetizing field, the transverse direction of magnetization is reversed, so that precession moves the wall in the reverse direction. The domain wall velocity becomes negative in this case (63). When the magnetization passes through the plane of the strip and the direction of core magnetization is reversed, it causes the precession direction to reverse, yielding another reversal of wall direction and whole the process is repeating.

Fig. 16 shows the result of micromagnetic simulation of the transverse domain wall propagation above the Walker limit in a thin planar nanowire. The magnetization direction within the core of the transverse domain wall is oriented in y – axis at the beginning. If the domain wall reaches critical velocity (Walker limit) a small vortex is nucleated at the apex of transverse wall. Further movement of the vortex across the transverse wall is accompanied by forward motion of the wall and then it begins to move backward as the vortex crosses the wire midpoint (retrograde motion). If the vortex reaches other side of the wall, the transverse structure is recovered, but its sense (chirality) is reversed. The whole process containing the domain wall acceleration followed by Walker limit and vortex nucleation periodically appears in the same way. The retrograde motion of the domain wall (which occurs during the vortex movement) is responsible for the breakdown of the average velocity as compared to the case below Walker limit (Fig. 17).

Walker breakdown appears in thin planar nanowire at much lower magnetic field as compared to the above discussed Walker solution. It is because a small magnetic vortex is nucleated at much lower tilting angle than $\varphi = \pi/4$.

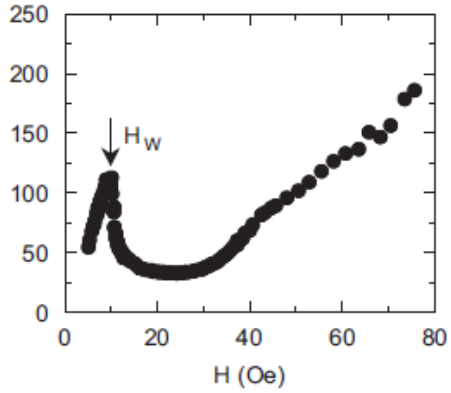

Fig. 17 The field dependence of the domain wall velocity measured in thin 490 x 20 nm planar ferromagnetic nanowire. Image adopted from (60).

It has been shown (60) that the field dependence of transverse domain wall velocity below the Walker limit can be evaluated similarly to the Walker solution as a linear function of applied magnetic field:

$$v = \frac{\gamma_0 \delta}{\alpha} H \tag{63}$$

where δ denoting the domain wall width is obtained by fitting of experimental data. In the region far beyond the Walker limit, the field dependence can be evaluated:

$$\bar{v} = \frac{\alpha \gamma_0 \bar{\delta}}{1+\alpha^2} H \tag{64}$$

where $\bar{\delta}$ denotes the average domain wall width. Since the Gilbert damping in most material $\alpha << 1$, the domain wall mobility beyond the Walker limit is found to be much higher than below breakdown.

As it is seen, the main results of the Walker model (existence of the critical velocity and two regimes of domain wall propagation) well describe the real observed domain wall dynamics in thin magnetic wires. At low field, the domain wall is moving in linear regime (which was discussed in the preliminary chapter) where the structure of the moving domain wall is constant during its propagation. As soon as the domain wall reaches the critical value of the velocity, the movement becomes characterized by complex periodical changes that occur within the wall.

2.2 Tailoring the domain wall velocity in nanowires

In order to increase the domain wall velocity in nanowires several methods have been proposed in previous works. As it was shown in the previous chapters the Walker breakdown appears as a result of periodical dynamical changes that occur within the moving domain wall. Such processes are related to the rotation around polar angle φ in the case Bloch domain wall (according to denotation used in fig. 5) and to the vortex back and forth movement within the transverse domain wall in case of thin planar nanowires. It was show in the previous works that the presence of additional perpendicular (71) (54) (64) field is able to stabilize the processes that occurs within the transverse domain wall and, consequently, to suppress the Walker limit.

Consider the simplest case of Bloch wall between two adjacent domains with spontaneous magnetization oriented along x-axis. Under the application of magnetic field H_x in x- axis, the magnetic moments are rotated out of the easy magnetization axis by angle ψ. Then, the components of magnetic field can be evaluated (39):

$$\begin{aligned} H_x &= 0 \\ H_y &= M_S \sin\psi - M_S Q \sin\psi + H_y \\ H_z &= M_S \cos\psi \end{aligned} \tag{65}$$

where $Q = \dfrac{2K}{\mu_0 M_S^2}$ is so-called factor of quality which express the strength of uniaxial anisotropy with respect to the demagnetization energy. The condition for stable configuration is given by zero torque acting on the moments:

$$\mathbf{M} \times \mathbf{H} = 0 \tag{66}$$

The x- component (39):

$$(\mathbf{M} \times \mathbf{H})_x = M_S^2 Q \cos\psi \sin\psi - H_\perp M_S \cos\psi \tag{67}$$

fullfils the condition given by eq. 66 if

$$\sin\psi = H_{\perp}/M_S Q \tag{68}$$

Then, the y-component of effective field can be evaluated (39):

$$H_y = H_{\perp}/Q + H_{\perp} \tag{69}$$

The movement of Bloch wall (characterized by small angle ψ) is examined by use LLG equation similarly as it was done in chapter 1. Moreover a small domain wall velocity is considered, which results in low value of polar angle φ.The effective magnetic field in the core of the domain wall is given by set of equations::

$$\begin{aligned} H_x &= M_S \cos\varphi \\ H_y &= H_{\perp}/Q + H_{\perp} \\ H_z &= H_z \end{aligned} \tag{70}$$

Then, the eq. 67 can be written in the form:

$$\begin{aligned} \frac{dM_x}{dt} &= -\gamma_0 M_S H_z \sin\varphi + \alpha\gamma_0 M_S (M_S \cos\varphi \sin^2\varphi - \frac{H_{\perp}(Q+1)}{Q}\cos\varphi\sin\varphi) \\ \frac{dM_y}{dt} &= \gamma_0 M_S H_z \sin\varphi - \alpha\gamma_0 M_S (M_S \cos^2\varphi \sin\varphi - \frac{H_{\perp}(Q+1)}{Q}\cos^2\varphi) \end{aligned} \tag{80}$$

If the domain wall movement along y direction is considered, the polar angle φ within the core of the wall is constant:

$$\frac{dM_x}{dt} = \frac{dM_y}{dt} = 0 \tag{81}$$

Assuming this relation, the z- component of the effective field can be evaluated:

$$H_z = \alpha M_S (\cos\varphi\sin\varphi - \frac{H_{\perp}(Q+1)}{M_S Q}\cos\varphi) \tag{82}$$

and the eq. 80 becomes transformed to:

$$\frac{dM}{dt} = \frac{dM_z}{dt} = \frac{M_S v_y \cos\psi}{\delta_s} \tag{83}$$

By using the eq. 82 :

$$\frac{dM_z}{dt} = \frac{M_S v_y \cos\psi}{\delta_s}\sqrt{\left[1-(H_\perp / M_S Q^2)\right]} = (\frac{H_\perp M_S (Q+1)}{Q}\cos\varphi - M_S^2 \cos\varphi\sin\varphi) - \alpha M_S H_z \tag{84}$$

If this equation is compared to eq. 83 a field dependence of the domain wall velocity under the influence of perpendicular field can be obtained in the form:

$$v_y = \frac{\gamma_0 \delta(1+\alpha^2)}{\alpha\sqrt{1-(H_\perp / M_S Q)^2}} H \tag{85}$$

For zero perpendicular fields $H_\perp = 0$ such equation is transformed to:

$$v_y = \frac{\gamma_0 \delta}{\alpha}(1+\alpha^2)H \tag{86}$$

which is in a good agreement with previously derived formula without perpendicular field. Application of the perpendicular field leads to the increase of the walker limit:

$$v_w = \frac{2v_w(\cos\varphi_m \sin\varphi_m + \frac{H_\perp (Q+1)}{M_S Q}\cos\varphi_m)}{\sqrt{1-(H_\perp / M_S Q)^2}} \tag{87}$$

Here, angle φ_m denotes the maximal angle at which a Walker breakdown occurs (39):

$$\varphi_m = \arcsin\frac{-d+\sqrt{(d^2+8)}}{4} \tag{88}$$

where *d* denotes the complex parameter described elsewhere (39). Comparing the eq. 85 and eq. 87, one may conclude that the application of perpendicular field leads to the suppression of the Walker regime and to the effective increase of domain wall velocity below Walker regime.

However, the application of perpendicular field is not the only one method for suppression of Walker regime. Nakatani et al. showed (69) that surface roughness inhibits creating of vortexes inside the transversal domain wall, which prevents Walker breakdown so that constant velocity above Walker limit could be obtained. A similar way of Walker breakdown suppression was proposed by Kunz (71), who used the strong out of plane oriented perpendicular field to keep the vortex close to the edge of the transversal domain wall (fig. 18).

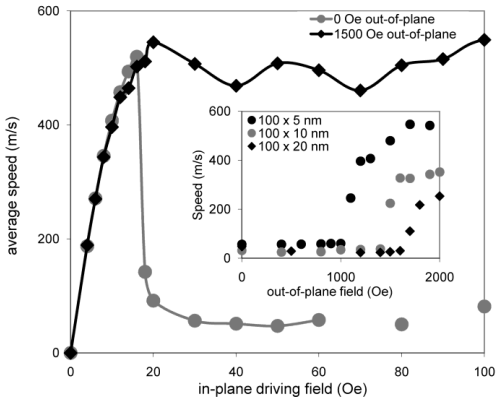

Fig. 18 The field dependance of domain wall velocity in 5 x 100 nm long permalloy strip. Perpendiculary oriented out-of plane magnetic field keeps the vortex at the edge of strip, which prevents the periodical changes within the transverse wall beyond Walker limit. As a result, velocity breakdown does not occur beyond critical velocity, but the velocity saturation can be observed. Image adopted from (71).

The importance of perpendicular anisotropy on fast domain wall propagation was demonstrated by Cowburn (70). He showed that the Walker breakdown can be totally suppressed by the series of cross-shaped perpendicular domains that acts to prevent transformations of the domain wall structure and increase the domain wall velocity by a factor of four compared to the maximum velocity on a plain strip (fig. 19).

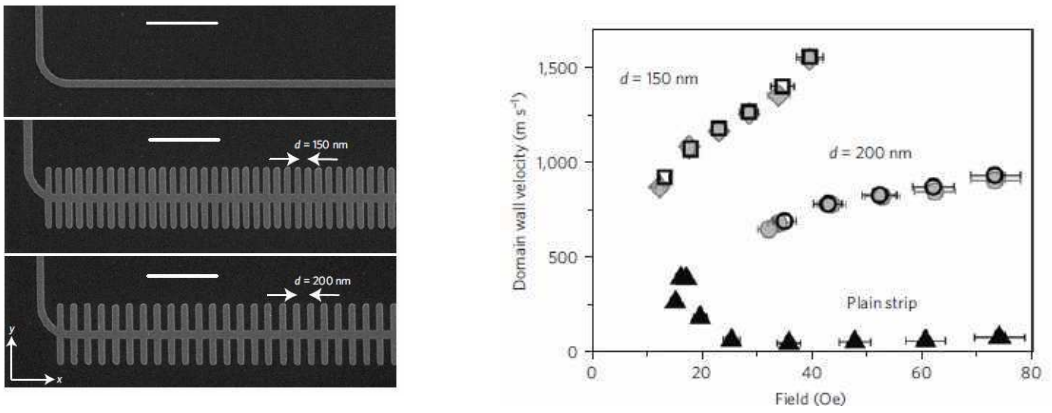

Fig. 19 Comparison of the field dependance of domain wall velocity measured at nanostrips with different surface comb structure. As it is seen, a significant velocity breakdown occurs beyond walker regime in plane strip. The presence of surface comb structure at the surface of the wire prevents the creation of vortex inside the transverse wall. This results in a positive domain wall mobility at the value of field, where walker breakdown was observed previously. Image adopted from (70).

Chapter 3

Amorphous glass-coated microwires

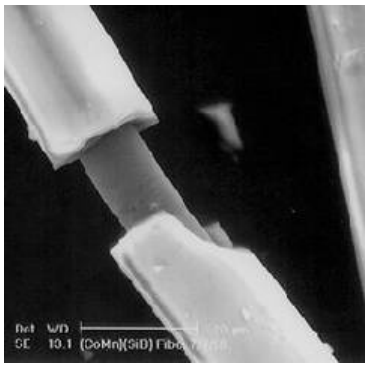

Fig. 20 The image of amorphous glass-coated microwire made by scanning electron microscopy (88).

Amorphous glass-coated microwires are a composite material consisting of a metallic nucleus that is covered by an insulating glass coat (Fig.20). Most of the magnetic properties of amorphous-glass coated microwires are mainly given by their fabrication process. The classical preparation method was first proposed by Taylor in 1924 (73). The technique consisted essentially of filling a glass tube with the metal from which the wire was drawn, placing this in a heated cylinder or flame and drawing it out at the proper rate by use of muffle made from copper rod. The selected glass tube had to be softened at a temperature between the melting and boiling point of metal used and had not to react chemically with the metal at high temperature. This was usually achieved at the melting temperature of glass-coating about 1400°C that was around 200°C higher than that of the metal depending on the composition. The glass-coating served as insulation and could be removed by acid etching. The as-prepared filaments were characterized by higher tensile strength than wires of ordinary size. This technique was proved to be quite useful for obtaining a broad spectrum of chemical compositions for metallic nucleus, including copper, aluminum and iron microwires with diameters down to 1 μm and with length of 0.5 cm – 1.5 cm. However, the main disadvantage of such hand-made producing method was bad reproducibility of prepared samples that was strongly determined by many factors, especially by proper selected temperature of melted master-alloy and by the speed of microwires drawing. In early fifties Ulitovski (74) (75) improved Taylor's production by automation of procedures involved in drawing of the wire. Further development in fabrication of more homogeneous microwires was carried out in sixties and seventies (76) (77) (78) by modification of Taylor method and by combining with Ulitovski improvements. These modifications finally resulted in Taylor-Ulitovski method that allows producing microwires with metallic core diameter of 1 μm - 30 μm (in special cases even down to 100nm (87)) and with glass thickness 2- 20 μm (79). Fig.21 shows the schematic drawing of microwire fabrication process. A few grams of

master alloy is put into Pyrex-like glass tube and placed in the middle of induction heating coil. As soon as the temperature of master alloy was sufficient to soften the glass tube, a small drop is formed at the bottom of the tube. The portion of the glass tube adjacent to the melted alloy envelopes the metal droplet. A glass capillary is then drawn from the softened glass portion and wound on a rotating coil. At suitable drawing conditions, the molten metal fills the glass capillary and a microwire is thus formed where the metal core is completely coated by a glass shell. The amount of glass used in the process is balanced by the continuous feeding of the glass tube through inductor zone, whereas the formulation of the metallic core is restricted by the initial quantity of the master alloy droplet (79). Note that the entire solidification process of microwires does not occur homogeneously in all volume, but starts from the periphery of the wire and is following through the all diameter. A final piece of microwire is stock on the rotating cylinder that provides both functions: pulling out the sample and wounding the as-prepared microwires. In the solidification process by flowing water stream, the cooling rate of 10^5 K/s – 10^7 K/s is obtained. Such rate is sufficient to achieve the amorphous state of prepared microwires.

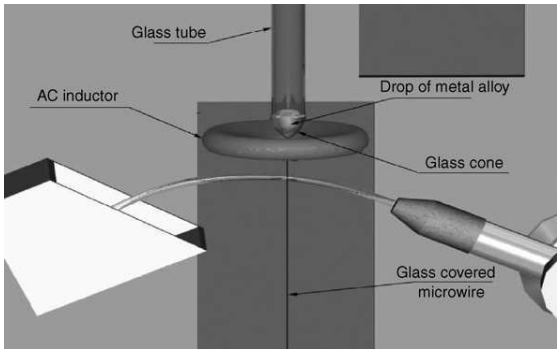

Fig. 21 schematic picture of microwire preparation by Taylor-Ulitovski process (79).

The main advantages of the microwire fabrication by Taylor-Ulitovski method are (a,) good reproducibility of samples, (b,) control of geometrical dimensions of as-prepared wires (the ratio between the metallic core and glass-coating) and (c,) continuous preparation of long pieces (tens of kilometers from a couple grams of master-alloy).

As a result of rapid quenching and drawing process during such preparation technique strong internal stresses are introduced to as-prepared microwires. The standard calculation of internal stress distributions in microwires (80) (81) (82) involves two stages of preparation process. The first stage is the glass transition of the metal that is assumed (80) to take place simultaneously with the hardening of the glass at the temperature T_{glass}. During this stage the internal stresses are introduced due to the

solidification of metal as the solidification front proceeds radial inward to the centre of the wire. Such process creates the radial and circular stresses. The second stage is the cooling of the metal-glass from T_{glass} to room temperature. During this stage, axial and radial internal stresses are introduced due to the contraction of both materials (glass and metal) characterized by different thermal coefficients:

$$\sigma(T) = E_M(\alpha_g - \alpha_m)\Delta T \tag{89}$$

where E_M denotes the Young modulus of metallic core, α_g and α_m the thermal expansion coefficient of glass-coating and metallic nucleus and ΔT the difference between melted alloy temperature and as-prepared microwire temperature.

Moreover, the stretching of composite during fabrication process induces additional axial stresses. The resulting stress distribution is then evaluated by superposition of all stresses originated by the progressive solidification of microwire and it has a tensor character. The corresponding components of internal stress tensor can be roughly evaluated (83):

$$\begin{aligned} \sigma_{axial}(r) &= 2\nu A - KT(r) \\ \sigma_{radial}(T) &= -K(1/r^2)I(R) + A - B/r^2 \\ \sigma_{azimutal}(r) &= K(1/r^2)I(r) + A - B/r^2 - KT(r) \end{aligned} \tag{90}$$

with $K = \alpha_m E_m/(1/\nu)$ where ν is Poisson's coefficient, A and B are integrating parameters determined by boundary conditions. As it is roughly seen, axial stresses are linear function of the distance from wire centre. The evolution of radial and circumferential stresses strongly depends on integrating parameters A,B determined by many factors, namely the radius of metallic core and the ratio between the metallic core and glass thickness.

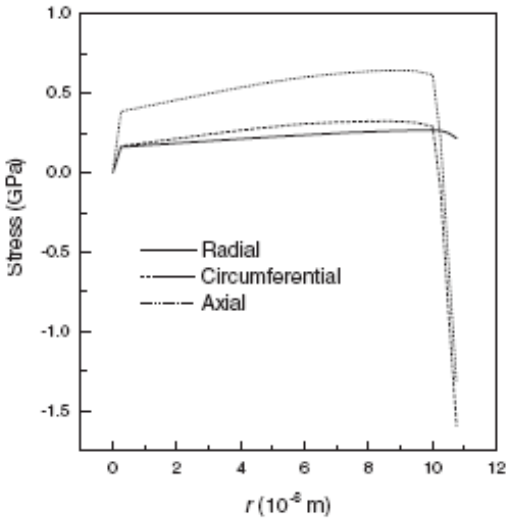

Fig. 22 Distribution of internal stresses in FeSiB glass-coated microwires according to (84).

Fig. 22 shows the calculated strength of internal residual stresses in microwire of radius $R = 11.2\ \mu m$. As it is seen, the stresses are not homogeneous through the radius, but

one can see complex distribution. The axial stresses are dominant from r = 0 μm to approximately r = 10 μm. Within the interval from 10 μm to 10.5 μm the axial stress is still dominant, but circular stresses prevails radial ones. In the thin layer just below the surface of the wire (10.5 μm -11 μm) the radial and circumferential stresses are the strongest. As it is seen at fig. 22, not only the value, but the sign of stress is not constant across the microwire radius, too. The radial stresses are tensile everywhere in range (0, R), while the axial and azimuthal stresses are tensile from r = 0 to approximately 93% of R, changing sign close to the surface where it becomes compressive. Generally, the stresses are tensile in central part of the wire, whereas compressive stresses are present at the surface of the wire. The schematic picture depicting the directions dominating stresses is shown in Fig. 23.

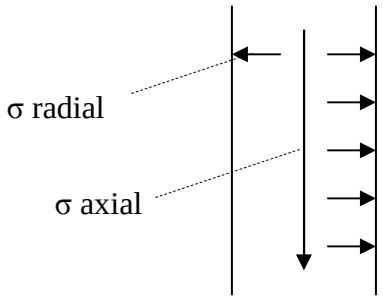

Fig. 23 Schematic drawing of dominating internal stresses introduced to microwires during Taylor-Ulitovski production method.

3.1 The domain structure of microwires

It is well known from experiment that the domain structure of microwires (with length of 0.5cm and more) is given by the sign of magnetostriction coefficient (Fig. 24). While microwires with negative magnetostriction are characterized by hysteresis loops containing rotation of magnetic moments in wide interval of field, the microwires with positive magnetostriction are characterized by magnetic bistability. It proves that the most important magnetic anisotropy of microwires arises from the magnetoelastic coupling between the spontaneous magnetization and residual stresses. The energy associated with the magnetoelastic coupling can be expressed:

$$F_\sigma = -\frac{3}{2}\lambda_S \sigma \cos^2 \varphi \qquad (91)$$

where λ_S is a coefficient of saturation magnetostriction, σ residual stresses and φ is the angle between the direction of magnetization and the direction of residual stress. According to the distribution of internal stresses and possible values of magnetostriction coefficient, three groups of microwires are generally recognized with respect to their domain structure:

1, microwires with negative magnetostriction, usually Co-based with $\lambda_S \approx -2\times10^{-6}$: the minimum of magnetoelastic energy is achieved if direction of spontaneous magnetization is perpendicular to the direction of internal stress. Taking into account above mentioned stress distribution in microwires, one may see that the magnetoelastic energy gives rise to the easy axis in direction perpendicular to microwire axis. The magnetoelastic energy exceeds the magnetostatic energy and the magnetization aligns perpendicular to the radial and axial stresses (circumferential direction). The domain structure of such wires consists of circular domains (85). This proves that the magnetoelastic anisotropy is stronger than magnetostatic one. With the application of axial magnetic field, the magnetization rotates from circular to axial orientation exhibiting minimal hysteresis (Fig. 24)

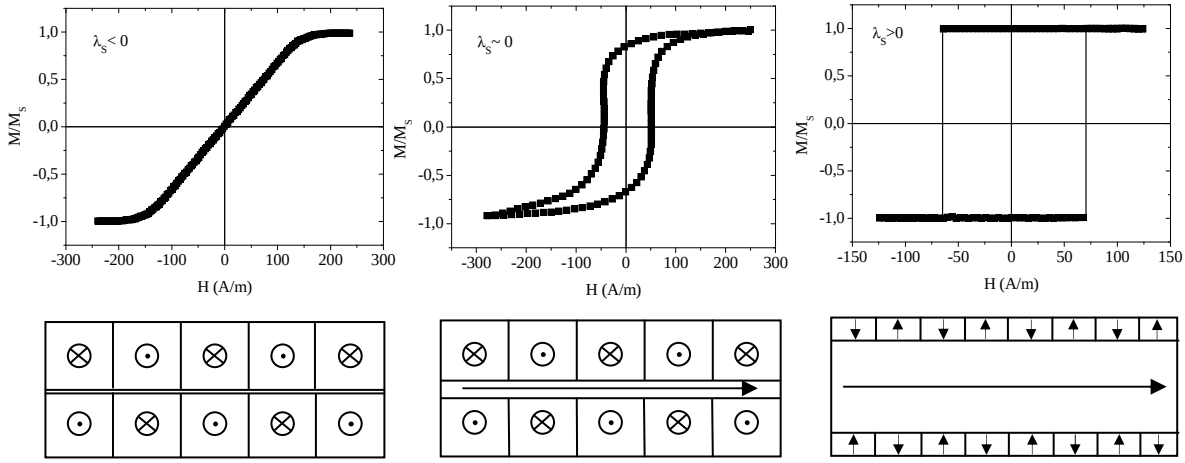

Fig. 24 Comparison of axial hysteresis loops of amorphous glass-coated microwires made from negative (a,) nearly zero (b,) and positive (c,) magnetostriction coefficient of metallic nucleus. The schematic drawing of domain structure is showed down. As it is seen, the domain structure is not given by shape anisotropy, but magnetostriction coefficient is the most important parameter determining the domain structure of microwires. Note, the size of radial and axial structures in schematic drawing does not correspond to the real case.

2, microwires with nearly zero magnetostriction – usually Co-based with small amount of Fe or Mn $\lambda_S \approx 1\times10^{-7}$ - in this case the magnetoelastic energy becomes fully balanced (or exceeded) by magnetostatic energy. A condition of magnetostatic minimum energy is fulfilled by axial orientation of magnetization in whole volume of microwires. In turn, magnetoelastic anisotropy gives rise to circular domain structure (as it was in above mentioned wires with negative magnetostriction). The competition between both anisotropies usually results in compromise: the domain structure of such wires consist of axial domains surrounded by thick shell of circumferential domains (86). However, the direction of magnetization in this kind of wires is strongly dependant on chemical compositions of metallic nucleus. Generally, the reversal magnetization process takes place firstly by domain wall propagation in small volume followed by rotation of magnetic moments. (Fig. 24)

3, microwires with (high) positive magnetostriction - usually Fe-rich samples with $\lambda_S \approx 3\times10^{-5}$ - axial hysteresis loop is characterized by large Barkhausen jump followed by magnetization rotation in surface region of the wire fig. 24. Due to the high magnetoelastic coupling, the metallic part of wire forms easy (hard) axis of magnetization parallel to internal tensile (compress) stresses. The condition of magnetoelastic minimum tends the magnetization to follow the direction of internal stresses introduced to the sample during Taylor-Ulitovski production. According to the specific stress distribution discussed in previous chapter, the domain structure of such wires consists of large axial domain surrounded by many radial domains (Fig. 24). Moreover, two closure domains appear at the end of microwire in order to decrease magnetostatic energy. If such microwire is submitted to axial magnetic field, the domain wall between closure and axial domain starts to reverse the whole volume of axial domain (Fig. 25).

For this reason, the amorphous glass-coated microwires with positive magnetostriction are ideal material to study the propagation of single, well-defined domain wall.

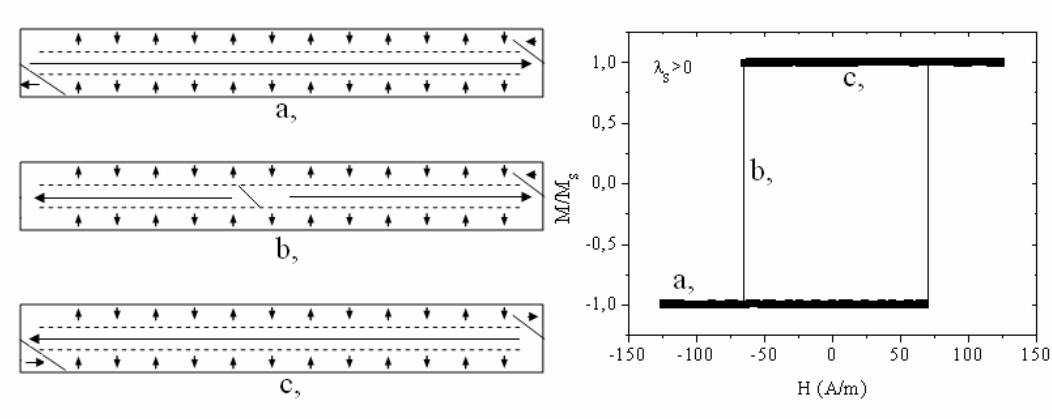

Fig. 25 Schematic drawing of Large Barkhaussen jump that gives rise to the square-shpaed axial hysteresis loop.

3.2 The domain wall dynamics in amorphous glass-coated microwires

The main properties of fast domain wall dynamics in microwires are demonstrated at the samples with composition of $Fe_{77.5-x}Ni_xSi_{7.5}B_{15}$ with $x \in (0; 38.8)$. These alloys are characterized by soft magnetic properties and by the variable value of magnetostriction and magnetization constants, which allows comparing the influence of such parameters on domain wall dynamics in microwires.

As it was mentioned in chapter 1, the domain wall velocity in viscous model is directly proportional to the driving field (eq. 4). As it is seen in Fig. 26 (a,) (b,) such model is in a good agreement with the domain wall dynamics observed in microwires of composition $Fe_{77.5}Si_{7.5}B_{15}$ and $Fe_{62}Ni_{15..5}Si_{7.5}B_{15}$. The domain wall velocity in these samples is directly proportional to the driving field (eq. 4) and thanks to the low anisotropy the velocity reaches a very high value of about 2.2 km/s. By the linear extrapolation of measured data, one can obtain negative critical field H_0. The negative critical field has already been found in amorphous microwires and it is taken to be one of the most important mechanisms to increase the domain wall velocity even in case of low domain wall mobility.

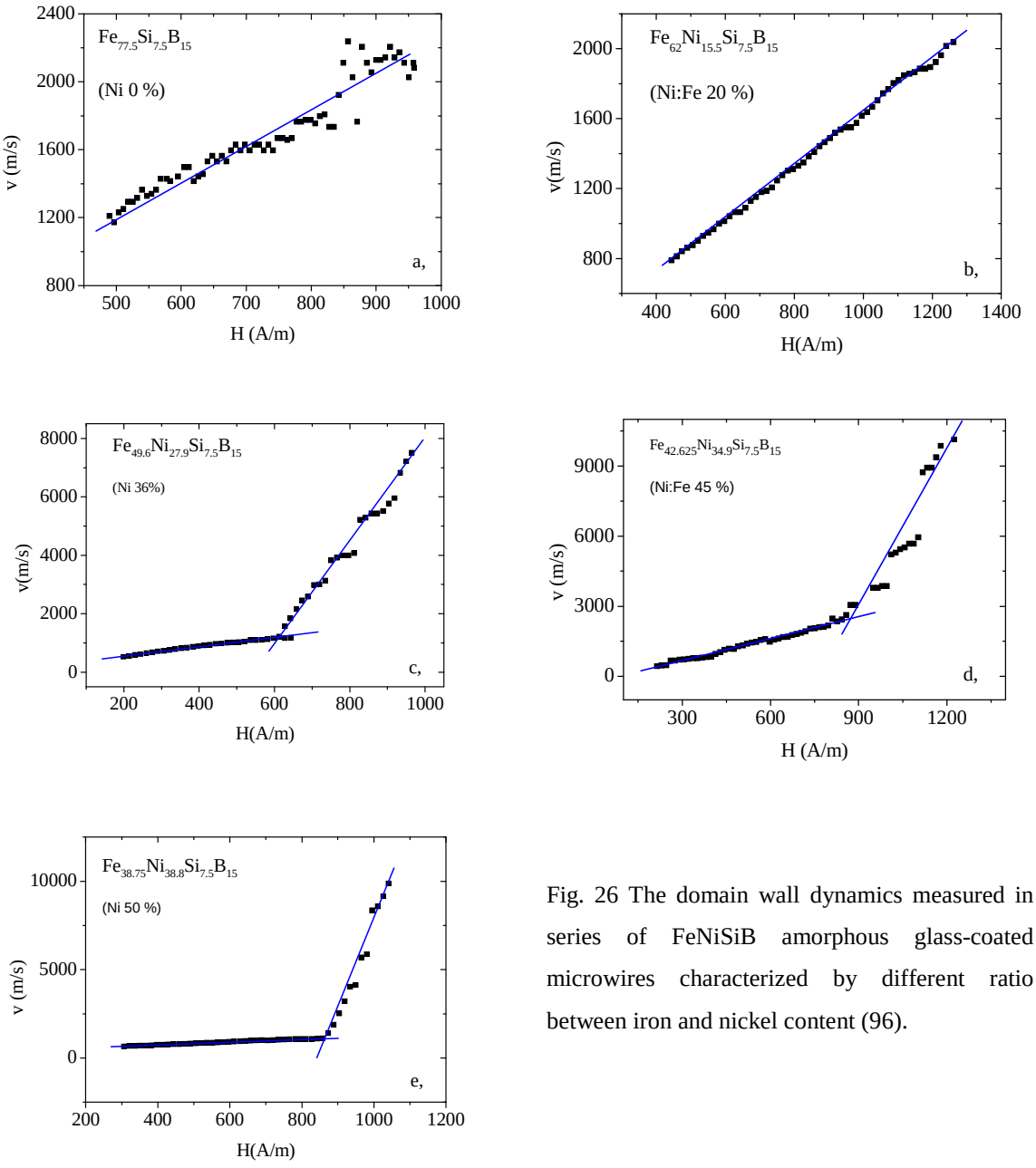

Fig. 26 The domain wall dynamics measured in series of FeNiSiB amorphous glass-coated microwires characterized by different ratio between iron and nickel content (96).

The domain wall dynamics in microwires becomes more complex in case of the samples with higher nickel content. At low fields, the velocity follows linear dependence on the driving field, but only up to the certain value of velocity (1.5 km/s – 2 km/s), when domain wall mobility steeply increases (fig. 26 c, d, e). Then the domain wall jumps to the secondary linear regime with maximum velocity around 10 km/s. As it is seen in tab. 1 the secondary regime in all samples is characterized by domain wall mobility of order of tens m^2/A.s as opposed to the primary one with mobility of units m^2/A.s (tab.1).

Sample $Fe_{100-x}Ni_x$	Domain wall regime	v_0 (m/s)	H_0 (A/m)	S (m^2/ A s)	β (kg m^{-2} s^{-1})
$Fe_{77.5}Si_{7,5}B_{15}$	Primary	201	-98	2.0	1.14
$Fe_{62}Ni_{15.5}Si_{7.5}B_{15}$	Primary	99	-64	1.5	1.31
$Fe_{49.6}Ni_{27.9}Si_{7.5}B_{15}$	Primary	268	-178	1.4	1.15
	Secondary		534	16.4	0.10
$Fe_{42.6}Ni_{34.9}Si_{7.5}B_{15}$	Primary	92	-76	3.1	0.92
	Secondary		764	22.3	0.12
$Fe_{38.75}Ni_{38.8}Si_{7.5}B_{15}$	Primary	402	-478	0.8	3.1
	Secondary		857	54.3	0.02

Tab. 1 The main parameters of domain wall dynamics fitted by mechanic model described in chapter 1.

3.2.1 Two regimes of domain wall propagation

One of possible explanation of such transformation could be attributed to the change of domain wall structure. It was shown by means of micromagnetic calculation (89) as well as by the simulation (90) that in case of cylindrically symmetric wires at least two structures of domain walls could appear. These two structures have become known as the transverse (in case of cylindrical wires as a corkscrew mode (91)) and vortex wall (or localized curling mode) fig. 27. The first of them refers to the thin ferromagnetic wires. Transverse domain wall has lower energy and lower domain wall mobility. It produces a strong stray field that interacts with shell of surface domains and the domain wall velocity is lower. On the other side, the vortex domain wall is characterized by closed magnetic flux, which prevents the interaction with the surface and the domain wall velocity is higher. Moreover, vortex domain wall needs higher energy to be created and appears in thicker wires.

Taking into account the above mentioned properties of domain walls with microwires, one may expect the transverse domain wall to be present at low field due to the presence of perpendicular anisotropies (axial and radial). Axial anisotropy is dominant in the center of the wire, whereas the radial becomes stronger just below the surface of the wire.

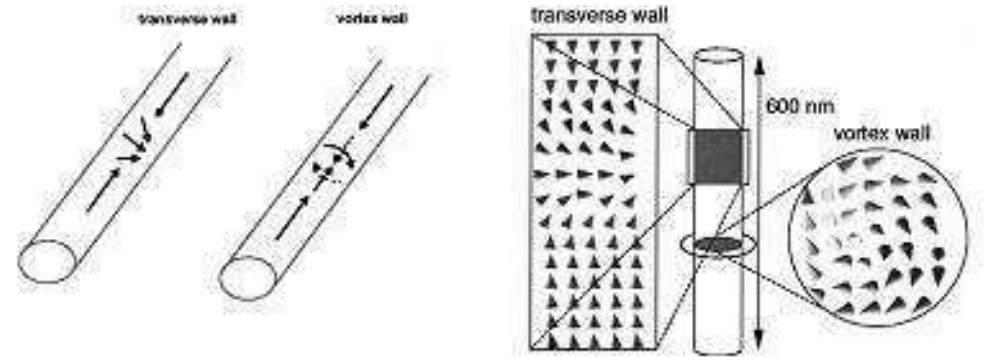

Fig. 27 The vortex and transverse domain wall structure in cylindrically symmetric wires. Image adopted from (92).

At lower magnetic field there is not enough energy to create the complex structure of vortex domain wall and therefore the transversal domain wall with low domain wall mobility and lower domain wall velocity is preferred. However, at higher fields, the energy stored to the domain wall can be assumed to be higher. Then the system has more energy to create the structure of the vortex wall which is not favorable at low fields. One of possible reasons that the vortex domain wall is nucleated at high field may consist in mechanism of domain wall deppining. In the Sixtus-Tonks experiment, the magnetic field is produced by function generator plugged to the primary coil. Due to the relaxation time of primary coil, it takes same time to raise the magnetic field at constant value.

It is worth mentioning that increase in the driving axial magnetic field leads to the increase in the axial domain's diameter which could favors the vortex structure (97) too. Once the domain wall with defined structure becomes created, it does not change its structure during the domain wall propagation (98). Especially, a very similar behavior is observed at the transition between primary and secondary regime (around 600 A/m in $Fe_{49.6}Ni_{27.9}Si_{7.5}B_{15}$, see fig. 26, d). Such region is characterized by non-stability of the nucleated structure of the domain wall hence the both wall structure can appear (fig. 26 c, d, e.).

However, the experimental proof confirming that the transformation of domain wall structure is responsible for secondary regime is missing. Anyway, some indirect experimental fact point to this statement. First of all, it is a measurement of domain wall velocity fluctuation. As a result of interaction of domain wall with local structure of microwire, the domain wall does not cross the wire in the exactly same time during each reversal process, but one can observe smooth fluctuations of velocities. The comparison

of domain wall's fluctuation for primary and secondary regime is shown in fig. 28. The velocity of primary regime (transverse domain wall) is well defined with deviations less than 1%. Then the domain wall moves in stable velocity, somewhere called steady-state regime. If the velocity of domain wall approaches the transition between primary and secondary regime (around 1.5 km/s in fig. 28), the value of fluctuations steeply increase up to 35 %. However, this increase is perhaps related to the metastability of both regimes, rather than the change in way of individual domain wall's fluctuations. In contrary, the secondary regime (vortex) is characterized by one order higher fluctuations than the primary one. One of possible explanation consists in term of different domain wall structure. The vortex domain wall has higher volume (width) that interacts with local structure and consequently the lower stability of the velocity occurs.

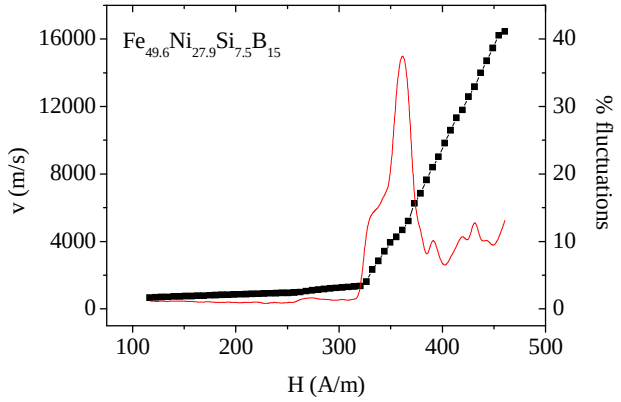

Fig. 28 Comparison of domain wall velocity fluctuations for primary and secondary regime in amorphous FeNiSiB glass-coated microwire.

Another important experimental fact is related to the sign of critical field H_0. The critical field of primary regime (see tab.1) is negative because the domain wall already exists at zero magnetic fields. On the other side, the critical field of secondary regime is positive because the vortex domain wall must be nucleated at high field when enough energy is supplied by the external field. The evolution of critical field for primary and secondary regime is shown in Fig. 29. As it is seen, the negative critical field of primary (transverse wall) regime decreases with nickel content as opposed to the secondary one. This is quite surprising result because one can expect lower magnetoelastic anisotropy with higher nickel content.

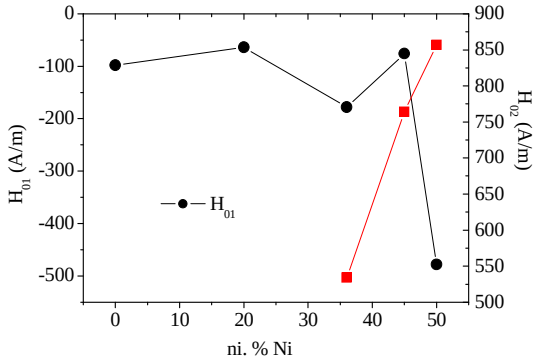

Fig. 29 Compositional dependence of domain wall mobility and critical field for primary regime S_1, H_{01} and secondary regime S_2 H_{02} in amorphous FeNiSiB glass-coated microwires (96).

Moreover, the transversal domain wall produces strong surface stray field (fig.10) that interacts with shell of radial domains in microwires and slows the domain wall velocity. In this regard the vortex domain wall is advantaged by closure magnetic flux that prevents such interaction with surface shell domains and consequently it allows reaching high domain wall velocities. As a result, the domain wall mobility is increased by one order and the maximum domain wall velocity increases almost 5 times up to 8 km/s (fig. 26).

The two regimes of domain wall propagation have be seen observed in other samples with nominal composition of $Fe_{42.62}Ni_{34.9}Si_{7.5}B_{15}$ and $Fe_{38.75}Ni_{38.8}Si_{7.5}B_{15}$. It is important to note, that the transition between the primary and secondary regime appears around the same domain wall velocity (1 km/s – 2 km/s) in all samples and it doesn't seem to be the effect of driving field. As in the previous samples, the highest domain wall velocities are achieved by secondary regime and reach up 9 km/s and 10 km/s respectively. Such increase of maximum velocity can be associated with the magnetic anisotropy decrease with nickel content.

Regardless to the origin of secondary regime, it is worth mentioning that the secondary regime of domain wall propagation was observed in microwires of many different compositions, where it was attributed to the Walker field or multiple domain wall propagation by many authors (99) (100) (101).

3.2.2 The high domain wall velocities in microwires

Regardless to the origin of secondary regime, one may conclude the domain wall velocities in microwires reach high enough values. Similarly high velocities have been previously measured only in small group of magnetic materials including orthoferrites (up to 60 km/s) (24) or iron whiskers (up to 30 km/s) (95). In case of amorphous glass-coated microwires the highest velocities are usually obtained by secondary regime: in primary regime the maximum velocities do not exceed 1 – 2 km/s. In turn, thanks to the positive critical field and higher domain wall mobility, the maximum domain wall velocities in secondary regime is one order higher as compared to the primary one. The relation between the domain wall mobility and saturation magnetization for primary and secondary regime is compared in fig. 30. As it is seen, the domain wall mobility decreases with nickel content in the same way as the saturation magnetization for primary regime. On the other side, domain wall mobility of secondary regime increase with saturation magnetization decrease (fig. 30). It was shown in chapter 1 that the domain wall mobility in viscous model is directly proportional to the magnetization and indirectly proportional to the domain wall damping. The domain wall mobility in secondary regime must be determined mainly by the domain wall damping, since the domain wall mobility decreases with nickel content and the saturation magnetization increases.

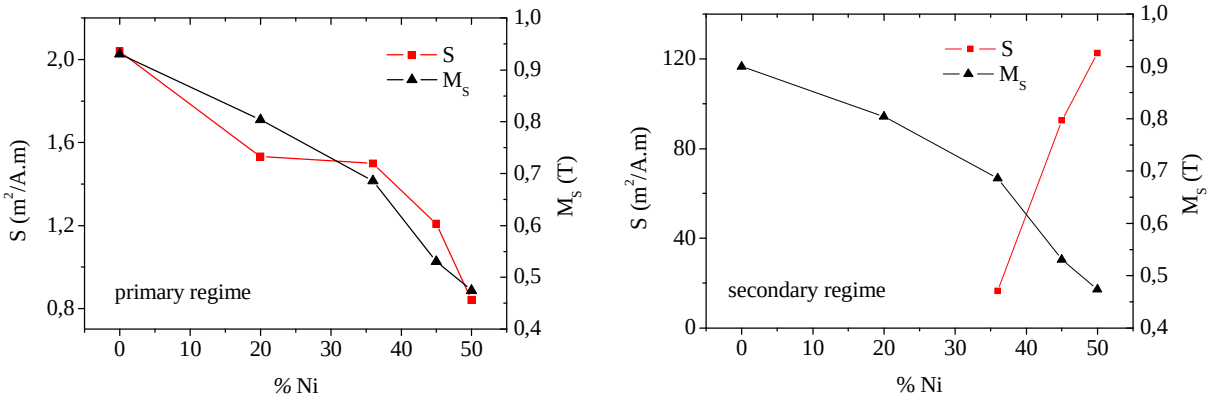

Fig. 30 Compositional dependence of domain wall mobility S and saturation magnetization M_S for primary and secondary regime in amorphous FeNiSiB glass-coated microwires (96).

It was shown in the previous works (93) that the main contribution to the domain wall damping in amorphous glass-coated microwires arises from magnetoelastic interaction of magnetic moments with local mechanical stresses. Hence, the fast domain wall

velocities of secondary regime should be related to the low anisotropy of microwires resulting from magneto-elastic coupling. The domain wall dynamics under the influence of tailored magnetoelastic anisotropy is discussed in chapter 5.1. Another factor that can help to achieve fast domain walls in microwire could be related to the presence of two perpendicular anisotropies. Both anisotropies compensate each other that results in the effective axial anisotropy decrease. Finally, the radial surface domain structure shields the domain wall from pinning on the surface defects, which helps to increase the domain wall velocity (discussed in chapter 6). The aim of this work is to investigate the influence of above mentioned factors on fast domain wall propagation in microwires.

The most typical aspects of the fast domain wall dynamics were introduced in this chapter: (1,) two regimes of domain wall propagation, (2,) the negative value of critical fields and (3,) the high domain wall velocities. The domain wall velocity in both regimes is well-described by viscous model of domain wall propagation, in which the domain wall velocity is directly proportional to the driving field. The measurements of domain wall dynamics provided by Sixtus-Tonks method show that the domain wall in microwires can achieve very high velocities that reach up 15 km/s. Three possible factors allowing such high velocities in microwires were introduced.

Chapter 4

Experimental part

This chapter contains the description of the main experimental techniques used in this work. Although it involves standard methods (thermal annealing, Sixtus-Tonks experiment), many of setups have had to be modified with respect to particular properties of amorphous glass-coated microwires discussed in this chapter.

4.1 Improved Sixtus-Tonks experiment for domain wall velocity measurements

4.1.1 Description of method

The classical experiment proposed by Sixtus and Tonks determined the domain wall velocity by the time *T*, which domain wall needs to cross the known distance *L*. Such method was adapted in later works to various experimental setups using different ways of domain wall detection including optical (103) (113), sensor (111) (112) (123) or inductive methods (102) (104) (114).

The position of domain wall is sensed by series of pick-up coils in the induction method. Assume a 180° domain wall which crosses the pick-up coil. According to Faraday law of induction, the total induced voltage is proportional to change of flux in the coil:

$$U = -\frac{d\Phi}{dt} \tag{92}$$

If the pick-up coil with cross-section S_C is wired from *n* turns, the total induced voltage is proportional to time derivative of magnetic flux density *B*:

$$U = -S_c n \frac{dB}{dt} \tag{93}$$

The magnetic flux density *B* is given by material relation: $B = \mu_0 H + \mu_0 M$. Then the eq. 93 may be written in the form:

$$U = -n\mu_0((S_c - S_n)\frac{dH}{dt} + \mathrm{S_n}\left[\frac{dM}{dt} + \frac{\mathrm{dH}}{\mathrm{dt}}\right]) \tag{94}$$

where S_n denotes the cross-section of the metallic core. As it is seen, the voltage induced in pick-up coil results from two effects. The first term is associated with the voltage inducted by the time change of magnetic field *H* (given by the solenoid inductance and by the function generator used in experiment), whereas the second term is related to change of magnetization direction that occurs as a result of domain structure change. The main reversal process at low field is related to the domain wall propagation in axial domain in the case of positive magnetostriction microwire. Hence, the induction method can provide the detection of moving domain wall that crosses the pick-up coil.

The magnetic bistability of the studied wire was achieved by an externally applied tension stress in the experiment proposed by Sixtus and Tonks. However, this is not necessary to do in the case of positive magnetostriction microwires due to the strong residual stresses introduced to wires during fabrication process. The schematic drawing of experimental apparatus for domain wall dynamics measurements in microwires is shown in fig. 31. It consists of a solenoid powered by a function generator with square waveform providing constant magnetic field in solenoid during each half-period. As it is seen, the microwire is placed to the solenoid asymmetrically with one end being out of the coil in order to avoid the multiple domain wall propagation from both sides. The length of the sample must be selected properly with respect to the size of solenoid. If the studied piece of microwire is too short, the domain wall propagation occurs from both sides. Otherwise, the microwire is not fully reversed (the domain wall stops at low field outside the coil) if too long microwire is used for measurements. The optimal length in our experiments (with respect to the length of solenoid and to the field distribution in solenoid discussed later) was found to be around 10 cm with 1 cm - 1.5 cm part being outside the solenoid.

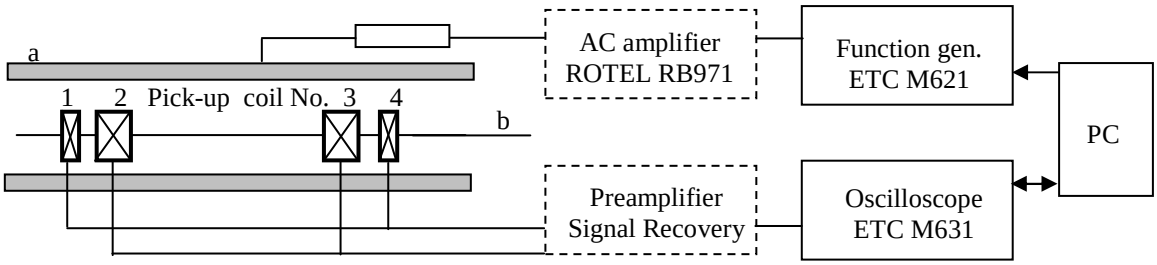

Fig. 31 Schematic picture of Sixtus-Tonks setup used for domain wall dynamics measurements in amorphous glass-coated microwires (a,) solenoid (b,) sample under investigation

The position of domain wall in microwire was sensed by series of four pick-up coils plugged to the oscilloscope providing time resolution of induced voltage in pick-up coils. In order to be sure that the series of induced peaks at oscilloscope screen does not correspond to multiple domain wall propagation, the number of pick-up coils was increased to four (in comparison with previous experiments). Both pairs of pick-up coils (outer and inner one, see fig. 31) were wired in series and opposite in order to avoid the voltage induced by change of magnetic field intensity *H* (first term in eq. 94) and for enhancing the effective signal arising from domain wall propagation (second term in eq. 94). The pair of outer pick-up coils serves for the direction of domain wall propagation determination. They contain less turns than inner pick-up coils in order to distinguish peaks at the oscilloscope screen. Fig. 32 shows the typical oscilloscope traces of the voltage induced by flux reversal at 4 pick-up coils when the domain walls (a,) propagate from microwire centre (b,) propagates from one end to the another one (regular case) (c,) propagates from both sides of microwire.

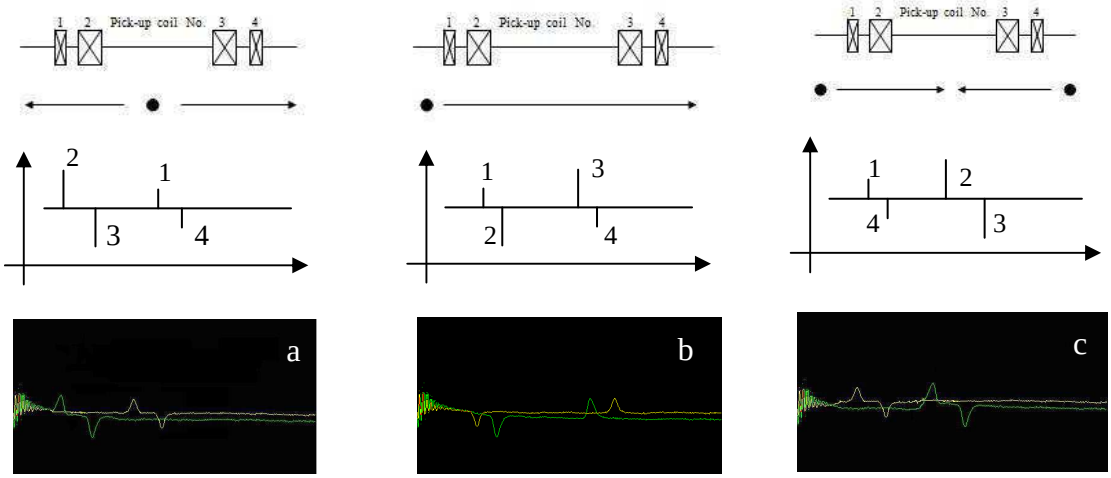

Fig. 32 Sequences of peaks induced at the oscilloscope screen when the domain wall propagates (a,) from the centre of wire, (b,) from one end to another one (regular case) (c,) from both sides of wire. The driving field in (b,) was opposite to the direction of field used in (a,).

The inner pair of pick-up coils serves for the domain wall velocity measurements. They are spaced 6 cm apart in order to get the domain wall propagation in uniform magnetic field (see magnetic field profile of solenoid in Fig. 33). By measuring the time interval T between two peaks formed by internal pair of pick-up coils distanced apart L, the domain wall velocity can be easy calculated:

$$v = \frac{L}{T} \tag{95}$$

Changing the value of magnetic field H at which the domain wall propagation occurs and measuring the domain wall velocity; one may obtain the dependence of domain wall velocity on applied magnetic field (v-H dependence).

Such dependence is very useful for domain wall dynamics study because it reveals important parameters related to domain wall propagation. The slope of curve in v-H dependence is inversely proportional to the domain wall damping; therefore it reflects various mechanisms contributing to the domain wall braking during its propagation. Another important parameter is related to the area under the v-H curve. The total power used to move the domain wall at constant velocity v by force F (in our case arising from external magnetic field, (eq. 2) is equal to $P = F.v$. Hence:

$$P = 2M_S \mu_0 Hv \tag{96}$$

which is proportional to the area under the curve in v-H dependence.

4.1.2 Design of apparatus

The entire hand-made sample holder used in Sixtus-Tonks setup consists of 3 main parts:

1, solenoid (primary coil)

2, sample holder made from thin glass capillary

3, pick-up coils wound around thin glass capillary and inserted into the solenoid

The driving field was furnished by 10 cm solenoid containing 1224 turns made of copper wire with diameter of 0.5 mm being wound on glass-tube in six layers. Fig. 33 compares the magnetic field profiles measured at the axis of solenoid. The uniform part of the field was calculated as:

$$H = 12240.i \tag{97}$$

where i denotes the current passing the coil in amperes. The constant of coil was determined by fitting the magnetic field intensity measured along the axis of solenoid

for different values of electric voltage applied to solenoid. The decrease of magnetic field from the middle of coil is less than 2 %.

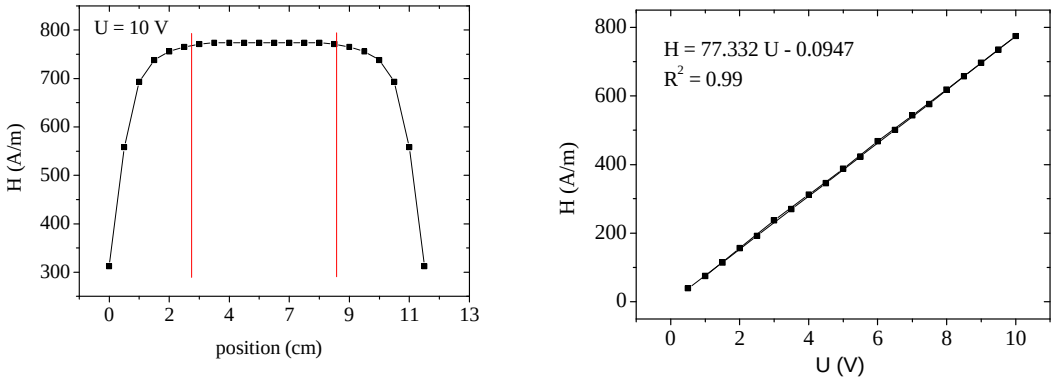

Fig. 33 left: the axial magnetic field intensity measured at the axis of solenoid used in experiments for applied voltage of U = 10V. Red lines denote the interval where the domain wall velocity is measured. right: fit of coil constant

The microwire under the investigation was held in the axis of the solenoid by use of sample holder made from thin glass capillary with diameter of 100 μm inserted into the solenoid. A series of four pick-up coils were wound around the capillary. The outer pick-up coils were wounded from 350 turns of thin copper wire with diameter of 30 μm. The inner pair of pick – up coils consists of two coils with 650 turns in order to achieve higher sensitivity. Adjacent pick-up coils were separated by glass tube that holds the sample holder in solenoid axis.

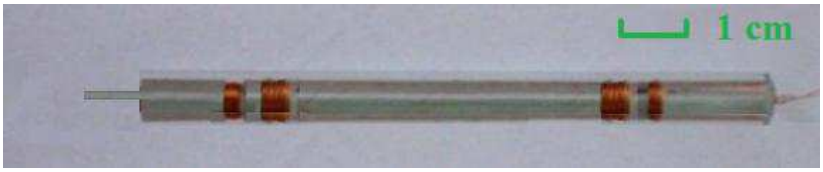

Fig. 34 shows the detail of as-prepared sample holder containing thin capillary and series of four pick-up coils wound around it.

The solenoid was powered by a ETC M621 function generator via 46 ohm resistor in order to match the solenoid resistance to the output impedance of Function Generator (50 ohms). The signal from pick-up coils was gathered by ETC M631 oscilloscope. Both equipments were controlled by data acquisition software written in Visual Basic. The software automatically measures the time interval between peaks induced in the

internal pair of pick-up coils, while increasing the magnetic field by use of function generator. The program's main user-interface is shown in fig. 35.

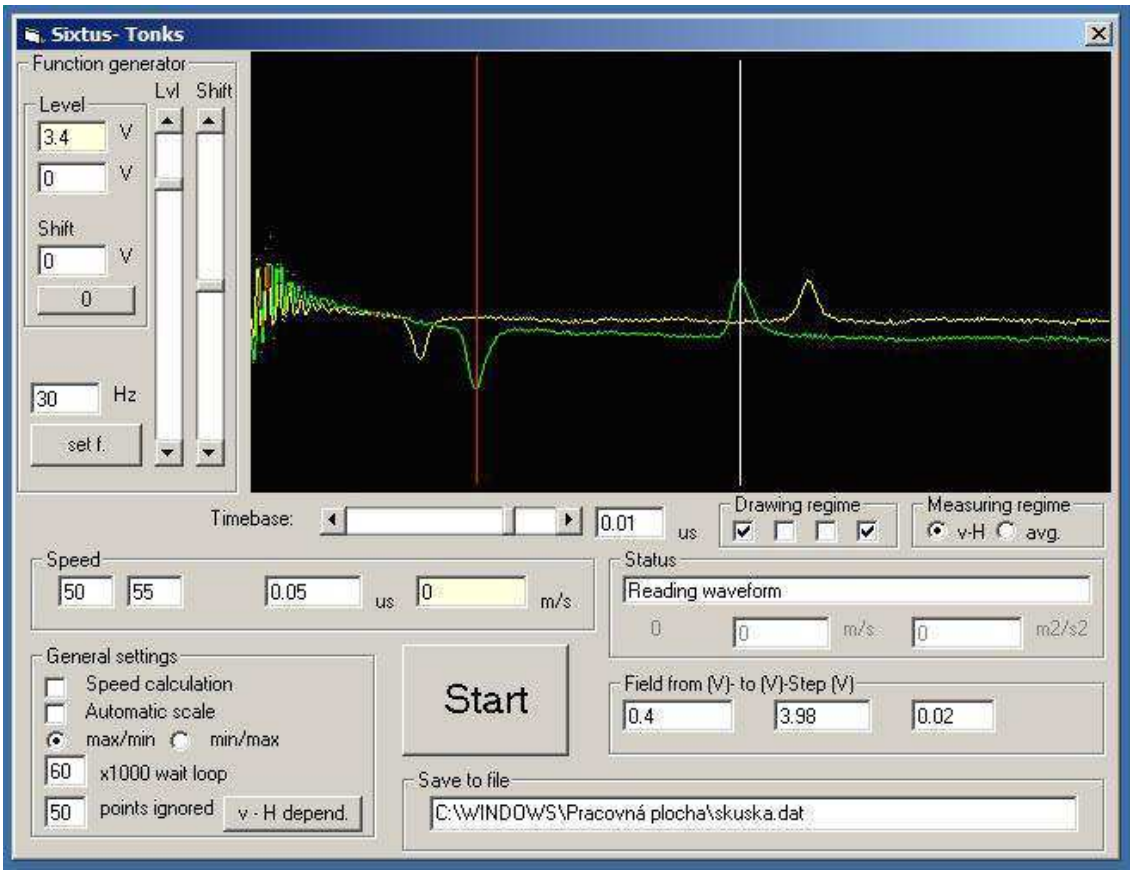

Fig. 35 The main screen of Sixtus-Tonks software used for automatic measurements of domain wall velocity.

The whole user-interface table is divided in following sub-panels:

1, Screen panel – provides actual oscilloscope screen in real-time. The program can distinguish whether the sequence of induced peaks corresponds to the proper domain wall propagation from one end of microwire to another (case b in fig. 32). The signal from the first channel of function generator is figured by yellow curve (outer pair of pick-up coils), whereas signal from channel B by green curve (inner pair of pick-up coils). The position of minimal and maximal peaks used in domain wall velocity calculation is searched by short software procedure and the result is depicted by red and white vertical cursors.

2, Function generator- this panel enables to control base settings of function generator (level, shift and frequency) that are used during domain wall velocity measurements in Sixtus-Tonks experiments. Moreover, it allows checking the proper sequence of induced peaks in the whole interval of magnetic field before measurement.

3, Measuring regime- contains two options: in "v-H" option, the program provides quick measurement of v-H curve by one measurement of domain wall velocity per one value of magnetic field. The second option "avg" means that the software calculates average domain wall velocity from 100 values measured at the same field intensity value.

4, Drawing regime- allows to switch on/off vertical cursors drawing and the signal from both channels at the screen panel. Such option is useful for the computer speed increase (and thus the data rate increase).

5, Timebase- provides setting of oscilloscope timebase.

6, General settings- *"speed calculation"* allows to switch off the speed calculation. Especially, this is useful to avoid the error messages during replacement of microwire samples when the sample holder is empty. *"Automatic scale"*- option used for switch on/off the automatic change of timebase during measurement. This setting is usually necessary during the sample replacement. Options *"max/min" and "min/max"* defines which sequence for domain wall velocity calculation is used to. *"wait loop"* allows to slow-down the time interval between measurements of domain wall velocity. *"points ignored"*- this label defines how many preliminary points are ignored in software procedure for the domain wall velocity calculation. Button "v-H" serves for drawing v-H dependence in real-time.

7, Status- informs user, which part of software loop is being executed. The white label shows average velocity and dispersion of measured velocities in *"avg"* mode.

8, Field from-to-step- defines the interval of magnetic field (in volts) in which the domain wall velocities are going to be measured.

9, Save to file- path where the file containing output data is saved.

The data output of program is a text (ASCII) file containing measurements settings (date, time, sample composition) followed by data in seven columns: magnetic field H (in A/m), position of minimum in channel A (outer pair of pick-up coils) PA_1 (in pixels), position of maximum in channel A PA_2 (in pixels), position of minimum in channel B PB_1 (in pixels), position of maximum in channel B PB_2 (in pixels), timebase T (in us/pixel), time interval between peaks induced by interval pick-up coils $(PB_2 - PB_1)*T$ (in us) and corresponding domain wall velocity (in m/s).

4.2 Magneto-metrical and magneto-optical measurements

4.2.1 Origin of Kerr-effect

Incident electromagnetic wave is said to be linearly polarized if the vector of electric field intensity oscillates in a plane. This oscillating vector is oriented perpendicularly to the propagation direction of wave which is defined by the wave vector *k* (fig. 36). If the vector of electric field is oriented perpendicularly to the plane of incidence, the electromagnetic wave is called “s – polarized” (abbreviation from German word *senkrecht* = perpendicular). Parallel orientation of electric vector (of linearly polarized light) to the plane of incidence is usually called “ p - polarization” (p - parallel).
If electromagnetic wave is reflected from surface medium, the reflected beam lies in the plane of incidence given by incident vector *k* and normal *n*. Generally, the reflected ray remains linearly polarized if the incident ray is fully “p” or fully “s” polarized.

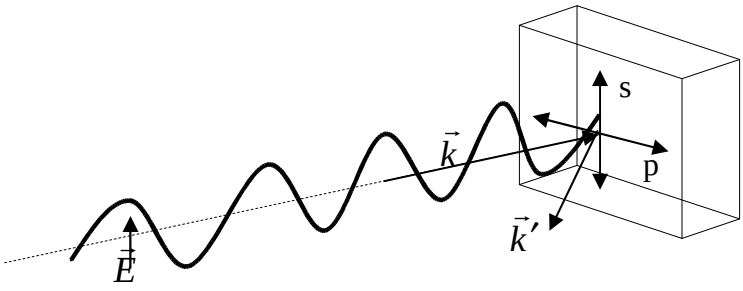

Fig. 36 Schematic drawing of linearly s-polarized incident electromagnetic wave. The plane of incidence is given by wave vectors $\vec{k}$ and $\vec{k}'$.

In order to explain the Kerr-effect it is useful to visualize the linearly polarized light as a linear combination of left-circularly and right-circularly polarized lights (109). These two modes must be in phase relative to each other in order to obtain fully polarized light. In general the propagation velocity of each mode depends on the direction of propagation. In that case, the medium is called anisotropic and the corresponding dielectric constant becomes 3 x 3 tensor. Dielectric tensor ε can be symmetric, antisymetric or it can be combination of both of them. The symmetric part of dielectric tensor contains three values that determine the dielectric constant in any direction. If these values are identical, the medium is called isotropic.

For the case of magnetic sample characterized by spontaneous magnetization *M*, the corresponding dielectric tensor is evaluated (118):

$$\vec{\vec{\varepsilon}} = \varepsilon \begin{pmatrix} 1 & iQ_Z & -iQ_Y \\ -iQ_Z & 1 & iQ_X \\ iQ_Y & -iQ_X & 1 \end{pmatrix} \tag{98}$$

where $N = \sqrt{\varepsilon}$ is the refractive index of not magnetized medium and *Q* is Voigt magneto-optic parameter proportional to the magnetization *M* of medium. When a linearly polarized light wave penetrates the medium it decomposes into left-circularly polarized and right-circularly polarized modes which experiences different refractive indexes (115) *n*: $n = N(1 \pm \vec{Q}.\vec{k})$. Since these two modes have different refractive indexes, they propagate with different velocities:

$$c = \frac{1}{\sqrt{\mu_r \varepsilon_r}} c_0 = \frac{c_0}{n} \tag{99}$$

When light is reflected from medium surface, the left-circularly polarized mode and the right-circularly polarized light modes (now, characterized by different propagation velocity and phase shift) recombine into polarized state with rotated plane of polarization and ellipticity. The differential attenuation results in ellipticity and phase difference accounts for rotation of plane. The off-diagonal components of dielectric tensor ε are responsible for Kerr-effect, while diagonal constant accounts for reflection of light wave from not magnetized medium. If it is assumed to be isotropic, the diagonal constants are equal.

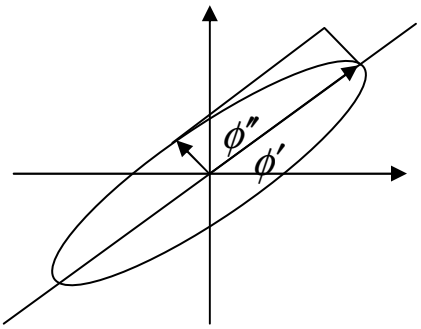

Fig. 37 Schematic drawing of Kerr rotation and Kerr elipticity angle in reflected light wave

4.2.2 Measurement of Kerr – rotation

In measurements employing magneto-optical Kerr effect, there are three major configurations of optical setup, differing in geometry : longitudinal, transversal and polar.

a, Polar Kerr – effect : here, magnetization lies perpendicularly to the surface and parallel to the plane of incidence. This geometry is sensitive to the change of perpendicular magnetization component to the surface and yields Kerr rotation in plane parallel to the surface (fig. 38). This arrangement produces the greatest rotation of the plane polarization as much as 20 minutes (108). The effect is proportional to the cosine of incident angle; hence the biggest signal is obtained in direction parallel to the surface normal. Whether s- or p- linearly polarized light is used in the measurements, the signal is the same for both of them (119) (120).

b, Longitudinal Kerr – effect : the magnetization lies in the plane of incidence and also in the plane of reflecting surface. This geometry is sensitive to the in – plane magnetization change. The rotation produced by longitudinal Kerr-effect is considerably less, by factor of about 5 than that of the polar Kerr-effect. For small angles it is proportional to sine of incident angle. The rotation is found to be zero at normal incidence, increasing to a maximum for angles of incidence of about 60° (105). Rotation angle of s-linearly and p-linearly polarized light is the same for longitudinal orientation in absolute scale. They differ by opposite sign (120).

c, Transverse Kerr-effect : the magnetization lies again in the plane of reflecting surface, but also in a plane perpendicular to the plane of incidence. In this case, there is no Kerr – rotation of the plane of polarization and the transverse effect appears due to the changes in the reflection coefficient of the surface for light polarized in the plane of incident (p-polarization). For this reason, the analyzer can be removed during the experiment. The whole essential signal is arising from alternating intensity of reflected light. The plane of polarization of s-polarized incident light wave is not rotated by reflection in transverse Kerr-effect.

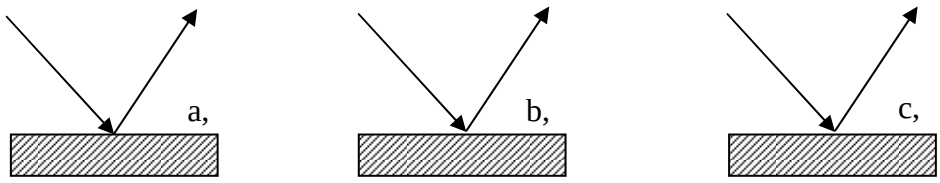

Fig. 38 The disposition of magnetization with respect to the plane of incidence for polar (a), longitudinal (b) and transverse (c) Kerr effect of electromagnetic wave reflected at magnetic surface.

Most obviously, the Kerr-signal in the real experiment is measured as a combination of longitudinal and polar effect due to the geometrical restriction (zero incidence angle is not possible to achieve). A several ways of separating longitudinal and polar Kerr-signals was proposed in previous works (121).

4.2.3 MOKE-based loop tracer

A schematic drawing of laser MOKE loop tracer is shown in fig. 39. It consists of 5 mW THORLABS HRP050 – 1 He-Ne laser providing linearly polarized beam with wavelength of 632.8nm. The size of laser spot is 1.2 mm. The beam reflected from the microwire surface is incident on THORLABS PDA 100A – EL CCD detector. The main advantage of this detector is the high sensitivity which is achieved by the built-in amplifier with adjustable output gain from 0 – 70dB. The signal from CCD detectors is then amplified and DC part of the signal (time constant background) is removed by use of SIGNAL RECOVERY 5113 preamplifier working in AC mode with adjustable bandpass filter. The signal is finally treated by two channels TEKTRONIX TDS 2024B oscilloscope. The plane of incidence is given by the mutual orientation of laser source and CCD camera. The plane of incidence was horizontal during all experiments in this work (fig. 39).

The magnetic field was applied by Helmholtz coils providing the magnetic field up to 1000 A/m. The whole construction of coils was done with respect to the geometrical restriction in Kerr-effect: the sample being under investigation is placed in the centre of the coil and big diameter of the coil (20 cm) allows directing the laser beam in a

requested incident angle. The triangular ac signal of HAMEG function generator amplified by ROTEL RB971 ac-amplifier was used for feeding the Helmholtz coils. Hysteresis loops were measured by oscilloscope working in 100-times averaging mode. The obtained data were saved to flash memory by USB interface.

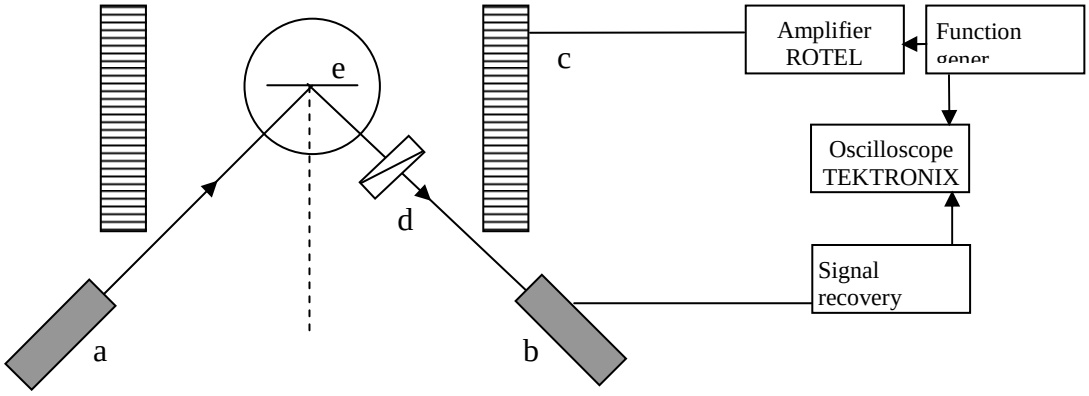

Fig. 39 The basic MOKE setup components (a) laser source, (b) ccd sensor, (c) Helmholtz coils, (d) polarisator (analyser) and (e) microwire sample mounted on a rotating holder. The plane of incidence was oriented in horizontal direction. The analyzer was removed during the measurements of transverse Kerr – effect.

The most important feature of magneto-optical observation of microwires is related to their cylindrical shape. The laser beam reflected from cylindrical surface forms a diverging cone. Hence, the signal intensity is indirectly proportional to square of distance between the wire and CCD detector. For this reason, the position of CCD camera was permanently attached at the same place in close proximity to the sample.

The second important feature of magneto-optical observation of microwires is associated with the glass-coat of the microwire. The Kerr - signal is arising from the light reflected at metallic surface which takes only certain part of total light reflected from microwire. In order to understand better the light reflection from composite material, the calculation of reflection and transmission coefficients was performed for bilayer planar interface consisting from metal and glass of the same thickness as in microwires (fig. 40). The reflection coefficient for p- and s- linearly polarized light was calculated by use of Fresnel equations as follows: In first step, the portion of light transmitted by glass surface to the metallic core was calculated at each incidence angle. In second step, the total reflected light from microwire was obtained as a sum of light reflected from the metallic core and the glass-coating. Note, the interference effects were not taken into account due to big thickness of the glass-coat with respect to the

wavelength of light used in the experiments. The refractive index of metal was chosen that of $Fe_{50}Ni_{50}$ alloy (106) which has the similar composition as microwires used in this work (discussed in chapter 4.4).

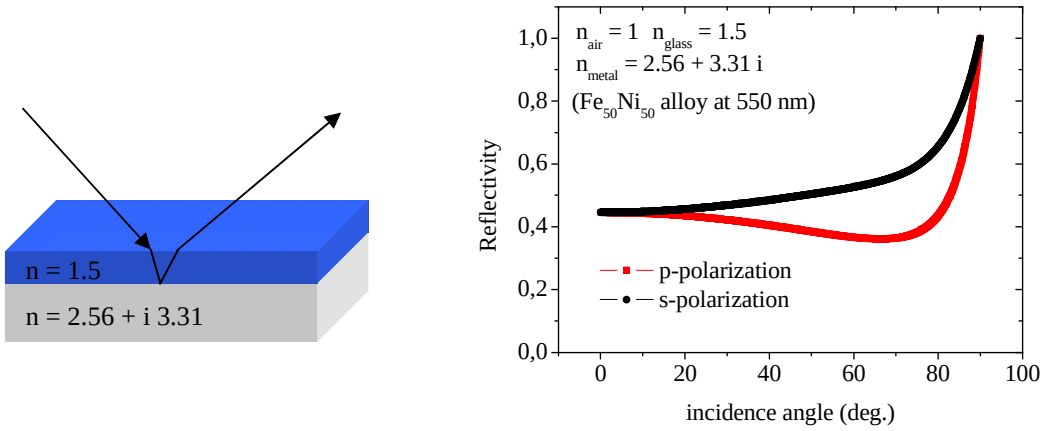

Fig. 40 The incidence angle dependence of light reflectivity calculated for bilayer planar interface consisting of metal covered by glass. The bilayer structure is assumed to be plane (left). The calculation of reflectivity for p- and s- polarized light is shown right.

Fig. 40 compares the angular dependence of reflection coefficients for p- and s-polarized light reflected from planar composite surface. As it is seen, the reflectivity of p-polarization light doesn't drop to zero at Brewster angle as a consequence of the metallic surface presence. However, the difference in reflectivity of s- and p- polarized light is not so high in the whole interval of incident angle. The smallest difference is observed at zero incident angle (corresponding to the polar Kerr-effect). Then it starts to increase and a maximum difference of about 15% is reached at the incident angle of about 66.3°. As it is seen, the reflection intensity of s-polarized light is higher in the whole interval of incident angles. Hence the s-polarization of light seems to be optimal for magneto-optic observations in longitudinal configuration. However, as it was noted above, the light reflected from metallic surface (and thus contributing to the Kerr-effect) takes only one part of total light reflected from microwire. Fig. 41 shows how many percent of light reflected from microwire surface is formed by that light reflected from the metallic core. As it is seen, the highest Kerr-signal is obtained in case of p-polarized light. Almost 92% of scattered light is reflected from the metallic surface at normal incidence for both p- and s- polarizations. The effective Kerr-signal for p - polarization increases with incidence angle and vice versa for s-polarization. The highest portion of

the light reflected from metallic core corresponds to the Brewster angle characterized by the total light transmission at glass-air interface. Note, that the effective Kerr-signal is higher for p-polarized lights in the whole interval of incident angles. However, the difference between them is not so high (less than 20%).

Taking into account above mentioned results, the optimal light polarization for longitudinal MOKE is given by the measurement conditions: if the light intensity is the most important parameter (due to little sensitivity of CCD, for example), the s-polarized incident light is better to use. On the other hand, if the signal is noised (for example, by reflection from glass surface), the p-polarized light is better to use due to more effective reflection from metallic core.

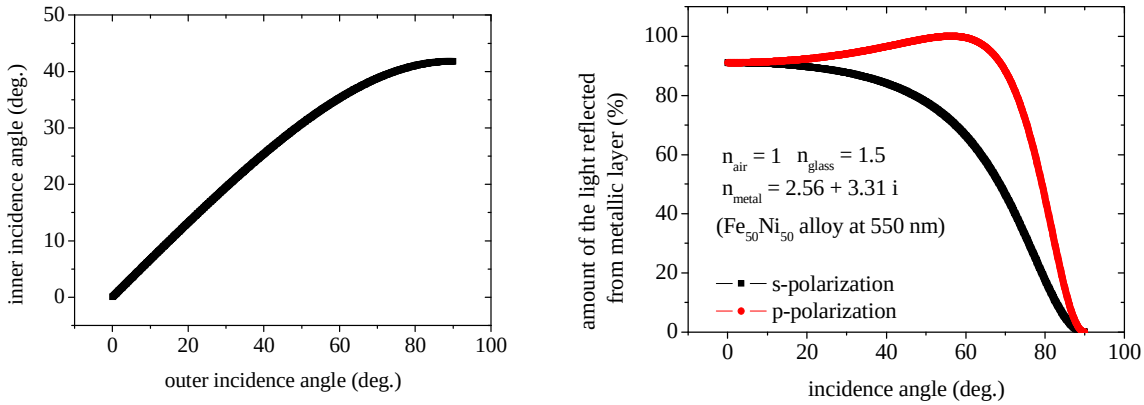

Fig. 41 The relation between the incidence angle at air – glass (outer incidence angle) and glass – metal (inner incidence angle) interface (left). The calculation of the total light reflected from the metallic core (right).

Another important feature of metallic-glass composite observation consists in terms of the different incident angles for glass-air and metal-glass interfaces (fig. 41 leftt). Due to the light refraction at glass surface, the incident angle at metallic core surface (inner incidence angle) becomes smaller than the incidence angle at microwire surface (outer incidence angle which is given by mutual position of laser source and CCD camera in fig. 39). Fig. 41 shows the dependence of inner incidence angle on outer incidence angle. As it is seen, even if the laser beam is directed to the microwire in a high angle, the light cannot be reflected from metallic surface at higher angle than of about 40 degrees. (in the limiting case of outer incident angle of 90 deg., the total internal reflection occurs).

As it was mentioned in previous chapter, the signal intensity from longitudinal Kerr-effect is proportional to sine of incident angle. In this sense, it would be convenient to maximize this angle in order to achieve strong signal. As it is clear from fig. 41 the inner incidence angle cannot exceed the value of 40°. Practically the inner incidence angle that was used in measurements was even smaller due to the interference effect that occur at large outer angles. In the measurements, the optimal outer incidence angle of about 50° was found empirically.

4.2.4 Kerr microscopy

Magneto-optical observations of microwire surface have been performed by use of commercial EVICO-ZEISS Imager.D2m polarizing microscope (Fig. 42). This microscope uses Kohler illumination that allows distinguishing the back-focal plane from the sample plane. The advantage of such system consists in homogeneous sample illumination in a wide interval of objective magnification. The microscope was equipped by 80W short-arc lamp providing continuous band of emitted light.

The magnetic field was applied by series of four magnetizing coils organized in a circle, which makes it possible to apply in-plane magnetic field in each direction. Magnetizing coils were powered by Kepco power supply controlled by commercial software appended to the microscope. More details on the microscope apparatus can be found in firm documentation.

Fig. 42 Evico Zeiss microscope used for magneto-optical observations discussed in this work (left). Detailed picture of sample holder used for measurements (above).

The maximal internal incidence angle was increased by use of ZEISS 518C immersion oil that was applied between the objective and microwire sample. The immersion oil refraction index is very close to that of glass ($n_{oil} = 1.518$ at 23°C). Hence, the application of immersion oil can remove many undesirable optical effect of glass coating. For this reason, the microscope observations are powerful technique especially for longitudinal magneto-optical Kerr effect, where the oblique incident light is used.

4.3 Apparatus for thermal treatment

4.3.1 Annealing furnace

A schematic drawing of annealing furnace used in this work is shown in fig. 43. It consists of two 50 cm long coaxial hollow glass tubes of diameters 5 and 1cm respectively. The inner hollow tube is surrounded by heating coil. The heating coil is wound from high resistive stripe with rectangular cross-section in two layers in order to decrease the Oersted magnetic field arising from current flow. The area between the inner and the outer hollow tube is filled by protecting He atmosphere which is flowed in by two pipes attached to the removable gum bungs carrying the inner hollow tube at both ends. Sample holder made from ceramic rod with diameter of 5 mm is used for carrying the sample to be treated. This holder can be easily slid in and slid out of the inner hollow tube in order to put the sample to the furnace. Note, the protecting atmosphere was not necessary to use in this case, because of the glass-coating of microwires that protects the metallic surface from degradation during the treatment.

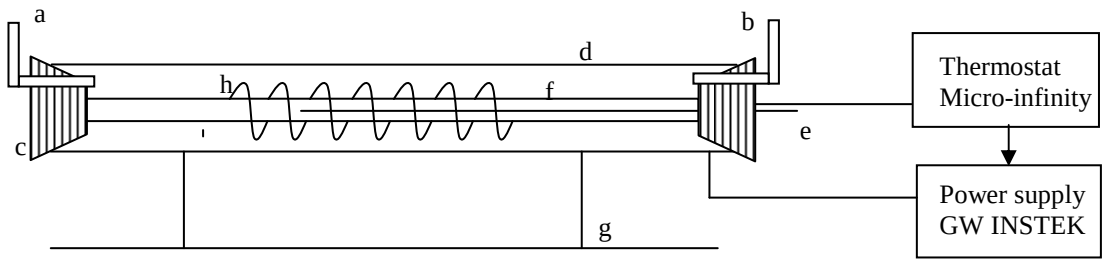

Fig. 43 Schematic drawing of thermal annealing furnace used to treat microwires in this work a, b - input and output glass-pipes for protection atmosphere, c – removable gum bungs, d – outer hollow tube, e – sample holder, f – inner hollow tube, g – furnace support, h – heating spiral coil

A small thermocouple is implanted to the sample holder in close proximity to the heating coil where the temperature is the highest. The heating system of annealing furnace consists of heating spiral coil equipped by 200W Voltcraft VSP 2405HE power supply controlled automatically by MICRO-INFINITY ICN 77 000 thermostat. Such a system is capable to achieve up to 600°C.

Such simple construction of furnace oven allowed its adoption to the (i) annealing in perpendicular field and (ii) for thermo-mechanical annealing.

In order to perform thermal annealing in perpendicular field, the annealing furnace was placed between two flat iron pole pieces of Weiss electromagnet (Fig. 44). It consists of two water-cooled magnetizing coils filled by iron pole-pieces which maximize the magnetic field produced by coils. Magnetic field distribution along the cross-section of pole pieces is show in Fig. 44. As it is seen, the flat shape of pole pieces provided uniform perpendicular magnetic field for microwires during the thermal treatment. Weiss electromagnet was supplied by GW INSTEK PSH 3630A switching power supply that allowed sustained magnetic field up to 1 T. The value of magnetic field was measured by ELIMAG MP – 1 teslameter during the whole treatment.

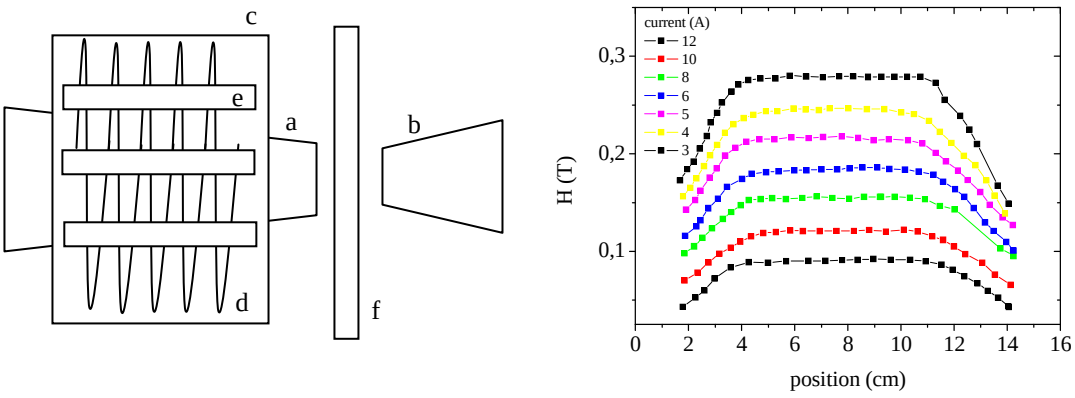

Fig. 44 Schematic drawing of Weiss electromagnet a, b – flat pole-pieces, c – coil body containing d – magnetizing coil and e – water–cooling pipes, f – thermal furnace oven

The above described furnace was used for thermo-mechanical annealing in which microwire was annealed under the mechanical stress. For this purpose, the furnace was positioned vertically. The microwire was placed in the inner hollow tube without use of sample holder. One end of treated microwire was attached to the top gum bung. The bottom end of vertically oriented sample was stock to thin copper wire in order to avoid microwire end damaging by weights. Mechanic tension stress was applied to the microwire by series of laboratory weights hanged to copper wire.

4.3.2 Current annealing

In this kind of thermal annealing, the heat is released by electric current *I* passing into the microwire sample rather than by external heating coil. The total power used to heat the wire is proportional to the electric current *I* squared:

$$P = I^2 R \tag{100}$$

where *R* denotes an electrical resistance of the wire and *P* the total power released by electric current. This kind of thermal treatment takes place under the Oersted field created by flowing current. It allows thermal annealing of microwires in circular (or helical) magnetic field. On the other side, the main disadvantage of such annealing method consists in the proper sample temperature determination during the annealing treatment. The heat produced by current is transferred to neighbor regions by (i) radiation and (ii) thermal flow. The temperature of the microwire is then a complex function of electric current (106). In order to be sure that annealing temperature does not exceed the crystallization point of microwires during current annealing, the whole process of treatment was performed usually in two steps.

1, Firstly, the current dependence of electrical resistance was measured in order to check the value of current at which the crystallization of microwires starts to occur (thermal analysis). A schematic drawing of the setup used for thermal analysis in this work is shown in Fig. 45. The glass-coat was mechanically removed at both ends of small piece of microwire (1 cm in length) in order to make electrical contact. The microwire was attached to high-temperature resistive sample holder by use of two screws that were plugged to Voltcraft VSP 2405HE power supply controlled by data acquisition software running on a personal computer. The program continuously increased the electric current at a defined time intervals and the voltage was measured in order to calculate the electrical resistance of the sample under investigation. Voltage was measured by 4 - points method by use of Hameg precision multimeter.

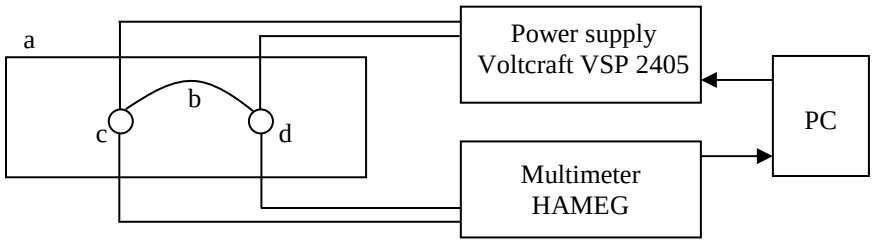

Fig. 45 Schematic drawing of thermal analysis setup a, high-temperature resistive sample holder, b – microwire sample c,d – screw used to make electrical contact to sample of microwire

Fig. 46 shows a typical dependence of electrical resistance on applied electric current. As it is seen, preliminary increase of resistance caused by temperature increase is followed by strong resistance drop that can be associated with the crystallization of sample. Backward trace (decrease of current down to zero) is characterized by lower value of resistance than before crystallization (irreversible structural changes).

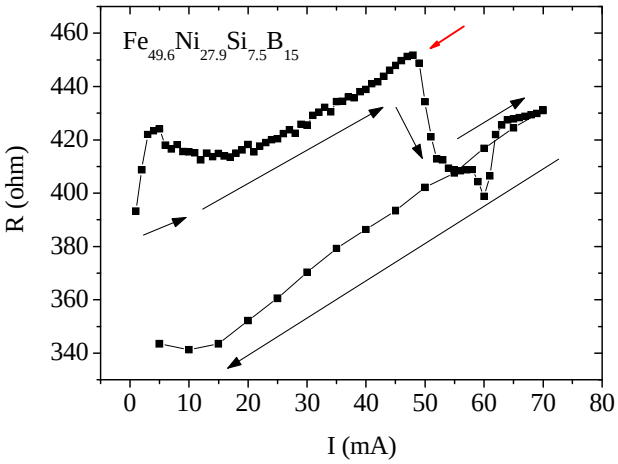

Fig. 46 Thermal analysis of FeNiSiB microwire. The crystallization point is marked by red arrow.

Such a thermal analysis is useful do determine the maximum value of electric current that can be used (without crystallization) in order to maintain the amorphous state of the sample under the investigation during the annealing.

2, Current annealing – the glass-coating of a 10 cm microwire was mechanically removed at the both ends of sample. The value of electric current passing the sample was controlled by programmable HAMEG 2030 power supply controlled by PC. The heating-up rate of 10 mA per 2 seconds was used during annealing. In order to avoid induction of strong mechanical stresses related to the fast cooling process, the sample was cooled down continuously at the rate of 5 mA per 2 seconds.

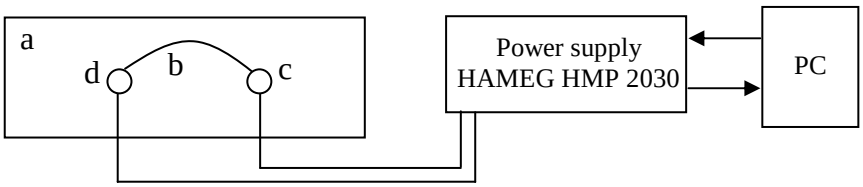

Fig. 47 Schematic drawing of current annealing setup a, high-temperature resistive sample holder, b – microwire sample c,d – screw used to make electrical contact

4.4 Samples used in this work

Two groups of microwire samples have been selected for the investigation, one an iron-nickel based alloy and the other an iron-cobalt alloy. The dimensions and saturation magnetization of these samples are listed in Tab. 2. Iron-rich $Fe_{77.5-x}Ni_xSi_{7.5}B_{15}$ alloy with $x \in (0; 38.8)$ was used in most of experiments. This composition is characterized by positive magnetostriction coefficient, which ensures the magnetic bistability of microwires (Fig. 49). The magnetostriction coefficient of this sample decreases with nickel content (107). For this reason, a special attention was paid to highly-magnetostrictive wires (with high Fe content) in experiments, where the effect of tension stress on domain wall dynamics were studied. Additionally, very high domain wall velocities were reported (96) in this kind of composition. Hence it allows investigation the fast domain wall dynamics which is the subject of this thesis.

A second group of $(Fe_{97}Co_3)_{75}Si_{7.5}B_{15}$ microwires was chosen in order to study the effect of microwire diameter on domain wall velocities (discussed in chapter 7). This composition is characterized by lower saturation magnetization and magnetostriction coefficient (tab. 2)

Composition	D (μm)	d_m (μm)	d_m/D	d_{inner} (μm)	$\mu_0 M_S$ (T)
$Fe_{77.5}Si_{7.5}B_{15}$	31	12	0.38	11.7	1.07
$Fe_{49.6}Ni_{27.9}Si_{7.5}B_{15}$	30	11	0.37	10.3	0.87
$Fe_{42.6}Ni_{34.9}Si_{7.5}B_{15}$	32	12	0.38	10.1	0.64
$(Fe_{97}Co_3)_{75}Si_{7.5}B_{15}$	9	1	0.11	0.8	0.81
	10	1.6	0.16	1.5	0.81
	11	2	0.18	1.9	0.81
	10	2,8	0.28	2.6	0.81

Tab. 2 Table of microwire samples used in this work. D denotes the total diameter, d_m diameter of metallic nucleus, d_{inner} diameter of inner axial domain and M_S saturation magnetization (at 300 K).

The dimensions of microwires (the metallic core diameter and the total diameter) were determined by use of optical microscope in transmission mode (fig. 48). In this case, the

transmitted light penetrates glass-coating, but not the metallic core. Credibility of the optical method was confirmed by use of scanning electron microscopy (SEM).

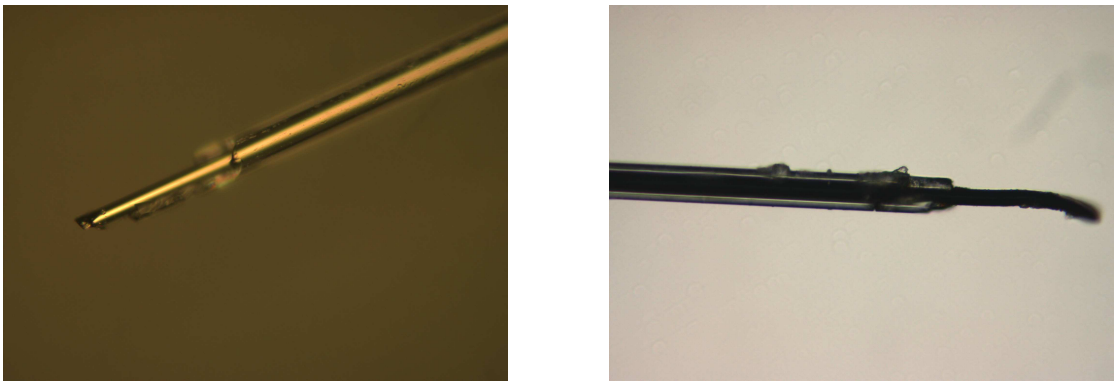

Fig. 48. Optical image of amorphous FeSiB glass-coated microwire obtained by use of polarizing microscope in reflection (left) and transmission (right) mode.

The surface radial domain structure thickness as well as the diameter of inner axial domain was obtained from hysteresis loops by method described elsewhere (122). Since the spontaneous magnetization of surface domain structure does not contribute to the axial magnetization, the thickness of the surface domain structure can be calculated from saturation and remanent magnetization in following way:

$$\frac{M_r}{M_S} \approx \frac{V_a}{V_t} \approx \frac{r_0^2}{r_1^2} \tag{101}$$

where M_S denotes the saturation magnetization, M_R is the remanent magnetization, V_a is the volume of inner axial domain, V_t is total the volume of metallic nucleus, r_0 is the radius of inner axial domain and r_1 is the radius of metallic nucleus.

As it is seen, the difference between the remanent and the saturation magnetization is very small for each composition (Fig. 49). Usually, the surface domain thickness does not exceed 5% of the metallic core radius. This is in a good agreement with previous study performed on this composition (122).

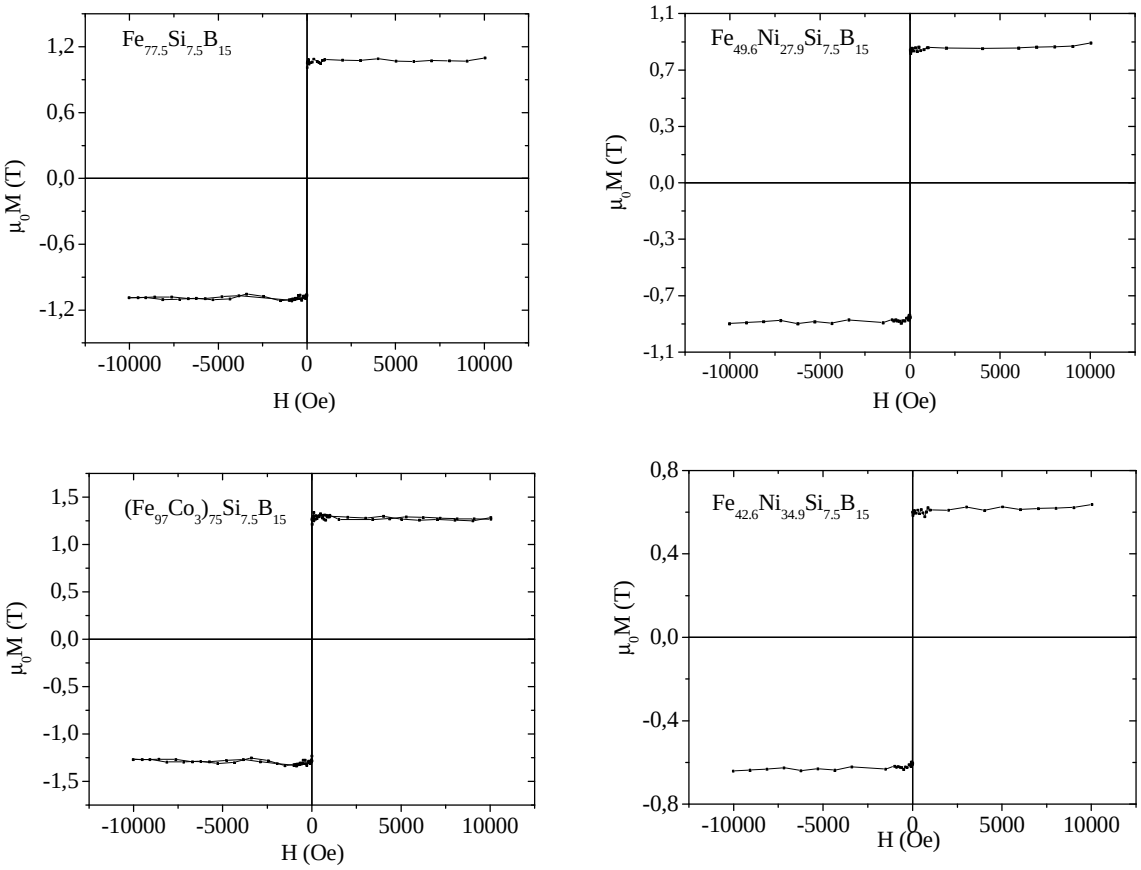

Fig. 49 Hysteresis loops showing Large Barkhausen jump of the samples used in this work. The loops were measured on the pieces of microwires 5 mm in length by use of MPMS at T=300K.

4.4.1 The comparison of microwire magnetization process with Stoner-Wohlfarth model

In order to check how-well the microwires can be described by Stoner-Wohlfarth model (194), the angular dependence of hysteresis loops was measured

The Stoner-Wohlfarth model description

Assume the ferromagnet having a uniaxial magnetic anisotropy described by parameter H_K. The magnetization is pointed toward the easy axis at zero magnetic field. As the field varies, the magnetization rotates in the plane given by applied magnetic field direction and the easy axis. Such configuration can be represented by single angle ϕ_S, the angle between the magnetic field direction and the magnetization. The second parameter is the angle φ_S between the magnetic field direction and the easy axis. The total energy per unit volume of the system can be written:

$$E = K_U \sin^2(\phi_S - \varphi_S) - \mu_0 M_S H \cos\phi_S \tag{102}$$

where M_S is the saturation magnetization, μ_0 is the vacuum permeability and H is the magnetic field intensity. The first term in this equation corresponds to the energy of magnetic anisotropy whereas the second term represents the energy coupling with the applied field (or Zeeman energy). The balance between these two terms for any applied non zero magnetic field intensity H is given by the condition of extreme energy value:

$$0 = \frac{dE}{d\phi_S} = 2K_U \sin(\phi_S - \varphi_S)\cos(\phi_S - \varphi_S) + \mu_0 M_S H \sin\phi_S \tag{103}$$

which yields:

$$K_U \sin 2(\phi_S - \varphi_S) + \mu_0 M_S H \sin\phi_S = 0 \tag{104}$$

$$K_U\left(\sin 2(\phi_S - \varphi_S) + \frac{\mu_0 M_S H}{K_U}\sin\phi_S\right) = 0 \tag{105}$$

$$K_U\left(\sin 2(\phi_S - \varphi_S) + 2\frac{H}{H_K}\sin\phi_S\right) = 0 \tag{106}$$

where $H_K = \frac{2K_U}{\mu_0 M_S}$ is the anisotropy field. For any given values of angle φ_S and magnetic field intensity H, the angle between the magnetization and the applied field can be numerically calculated from eq. 106, and therefore the hysteresis loop can be obtained.

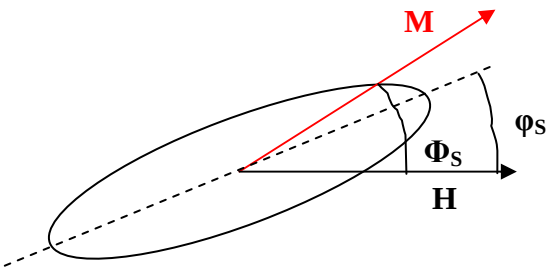

Fig. 50 Schematic drawing of the uniaxial magnetic particle in Stoner-Wohlfarth model.

In order to test how the microwires can be well-described by Stoner-Wohlfarth model (i.e. by uniaxial magnetic anisotropy), the series of following steps was done:

1, firstly, the hysteresis loop of 5 mm microwire sample was measured at a given angle φ_S between the magnetic field and microwire axis. The measurements were performed by use of AGFM in order to determine precisely the angle between the sample and field direction.

2, the software written in C was used to calculate the field dependence of axial magnetization in Stoner-Wohlfarth model. Such calculation requires two input parameters: the saturation magnetization M_S and the angle φ_S between the field and the easy axis direction. The saturation magnetization was obtained by extrapolation of measured data in the first step. The experimental angle φ_S was determined by use of camera equipped by ultra-zoom objective.

3, the uniaxial anisotropy value H_K was determined by least squares method. Here, the software compared the Stoner-Wohlfarth hysteresis loops of different H_K with experimental loop *i*n order to find the value of H_K at which the best agreement of the Stoner-Wohlfarth model with experimental data occurs.

4, Step 1 – 3 was repeated for various angles φ_S .

The angular dependence of the hysteresis loops was measured in two samples (a) as-cast FeSiB microwire and (b) the same FeSiB microwire annealed at 300°C during 1 hour. FeSiB microwires are characterized by the high value of magnetostriction coefficient (due to high iron content) hence a big influence of the thermal annealing on the change in magnetic anisotropy strength was expected.

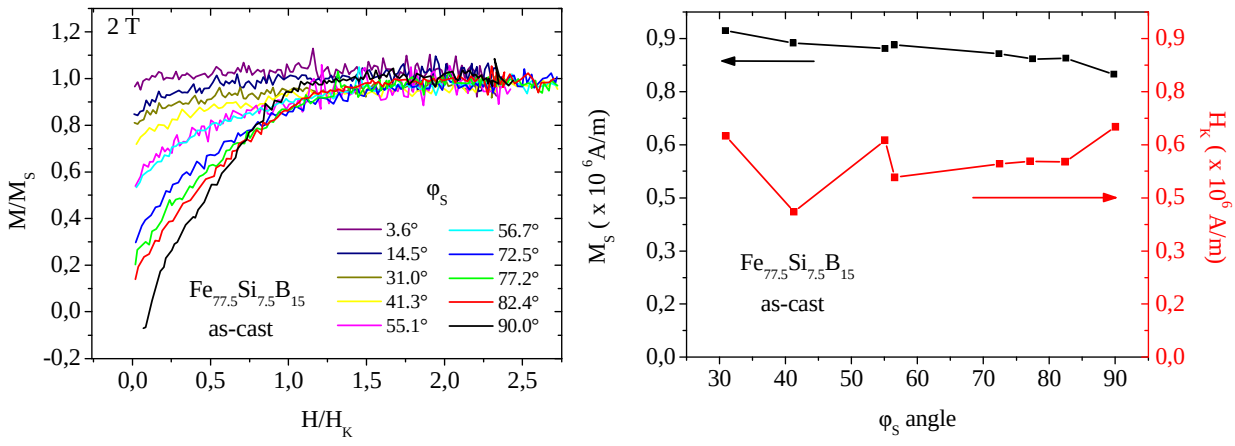

Fig. 51 (Left) The angular dependence of the axial magnetization in as-cast FeSiB amorphous glass-coated microwire. (Right) The parameters obtained by fitting of measured data by Stoner-Wohlfarth model.

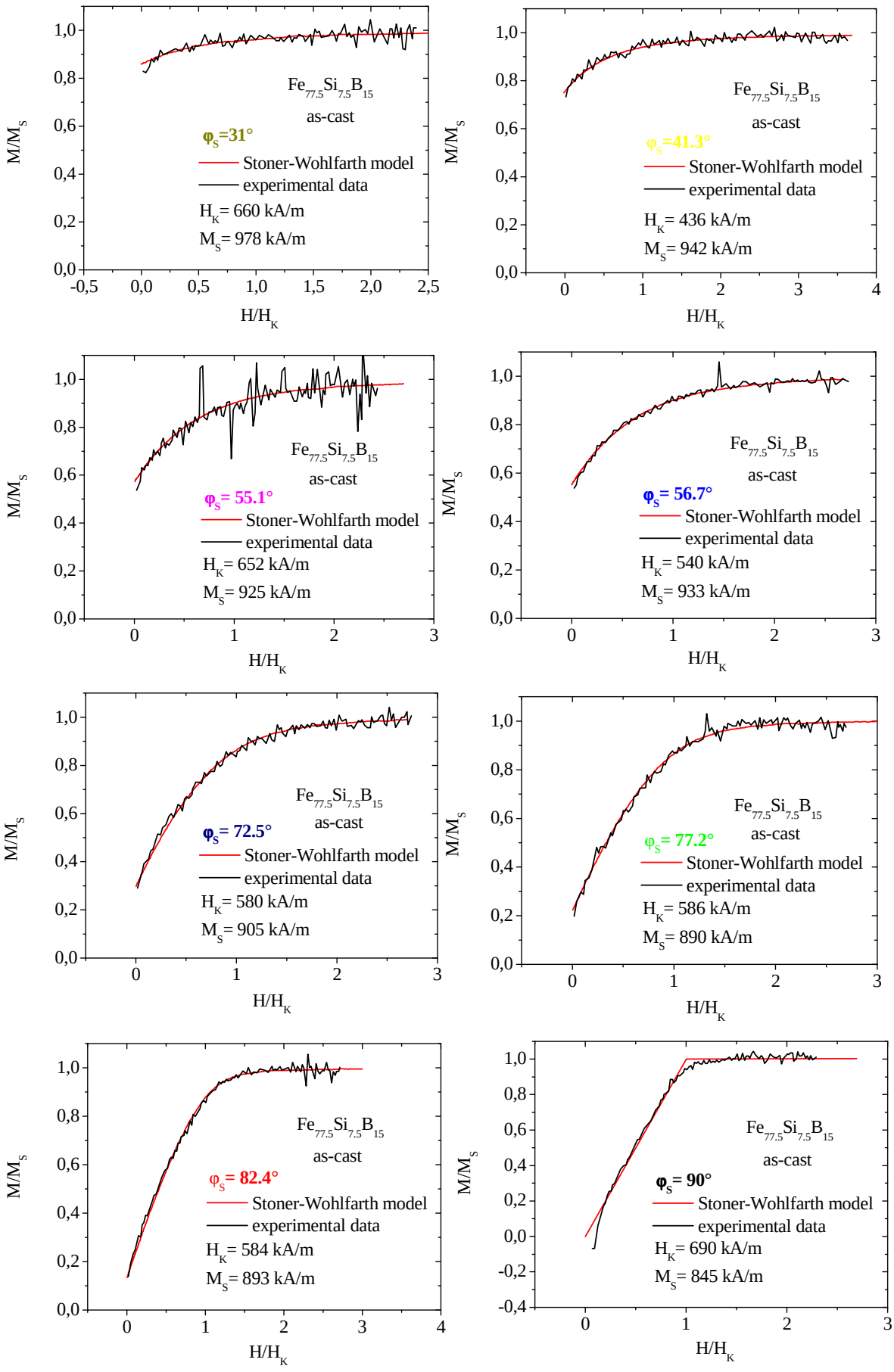

Fig. 52 Fitting of measured data by Stoner-Wohlfarth model in as-cast FeSiB amorphous glass-coated microwire.

As it is seen in Fig. 52, the magnetization process of as-cast FeSiB amorphous glass-coated microwires can be well-described by uniaxial magnetic anisotropy for any angle between the field direction and easy axis. Apparently good agreement of the measured data with Stoner-Wohlfarth model is obtained at each value of φ_S angle. However, the fitted values of anisotropy field H_K and saturation magnetization M_S are not the same. They vary with the angle (Fig. 51), which means that the studied microwire sample is not perhaps perfectly magnetically uniaxial. On the other hand, the average value of anisotropy field (H_K = 591 kA/m) is quite higher than $M_S/2$ (455 kA/m) which means that the shape is not the only one contribution the magnetic anisotropy in his sample. It points indirectly to the presence of additional (magnetoelastic) anisotropy.

The energy density of uniaxial magnetic anisotropy can be evaluated:

$$K = \frac{\mu_0 M_S H_K}{2} \tag{107}$$

with the above obtained average anisotropy field H_K = 591 kA/m and saturation magnetization M_S = 913 kA/m , it yields:

$$K = 3.4 \times 10^5 J/m^3 \tag{108}$$

Such uniaxial magnetic anisotropy includes contributions from two uniaxial magnetic anisotropies in microwires: (i) the magnetoelastic part and (ii) the magnetostatic part which can be related to the shape anisotropy of sample. As far as the demagnetizing field of long, infinite cylinder is $H_{dem} = M_S/2$, the corresponding energy of magnetostatic contribution is $K = \frac{\mu_0 M_S^2}{4}$. For the same values of average anisotropy field and saturation magnetization, it yields:

$$K_{demag} = 2.6 \times 10^5 J/m^3$$

Thus, the uniaxial magnetic anisotropy arising from magnetoelastic coupling is given by K-K_{demag}:

$$K_\sigma = 8 \times 10^4 J/m^3$$

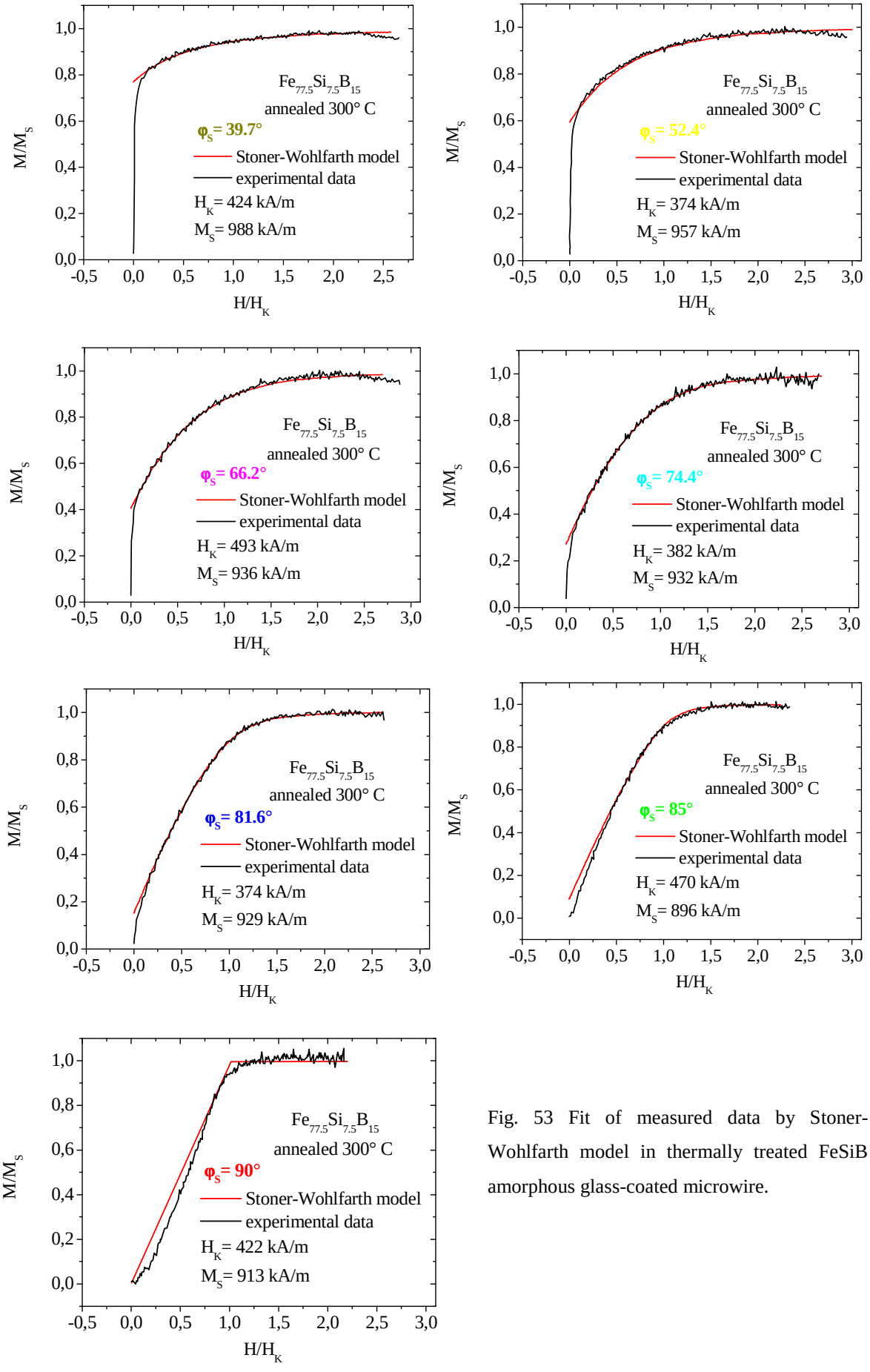

Fig. 53 Fit of measured data by Stoner-Wohlfarth model in thermally treated FeSiB amorphous glass-coated microwire.

The value of magnetoelastic magnetic anisotropy energy density is surprisingly high ($K_\sigma = 8\times10^4 J/m^3$). Table compares this value with the magnetocrystalline energy constant in various materials (108):

Material	K_1	K_2
	J/m^3 at room temperature	
Fe	4.8×10^5	-1.0×10^5
Ni	-4.5×10^4	-2.3×10^4
Co	4.1×10^6	1.5×10^6

Referring to the pure iron value, the magnetoelastic anisotropy energy density is lower, but of comparable magnitude (~1×10^5). As it will be shown later, such high values of magnetic anisotropy in microwires can be responsible for the particular domain wall structure, which can give rise to the apparent high domain wall velocities measured on microwires by the Sixtus-Tonks experiment.

Similar experimental results were obtained on thermally annealed FeSiB microwire. Despite a good agreement of the Stoner-Wohlfarth model with experimental data for each φ_S angle, the remarkable fluctuations of both fitted parameters H_K and M_S can be observed (Fig. 53 and Fig. 54). However, the average value of the fitted anisotropy field is here a bit smaller H_K = 420 kA/m as compared to the as-cast sample (H_K = 591 kA/m). In addition, the value of anisotropy field in annealed microwires (H_K = 420 kA/m) is close to $M_S/2$ (455 kA/m), which means that the magnetoelastic anisotropy was almost completely removed in annealed sample. This can be attributed to the relaxation of the internal stresses during the sample annealing.

It is worth mentioning, that a good agreement of measured data with Stoner-Wohlfarth model was achieved for high angles φ_S only. As the angle φ_S was reduced down to zero, the changes in axial magnetization become comparable to the accuracy of measurements.

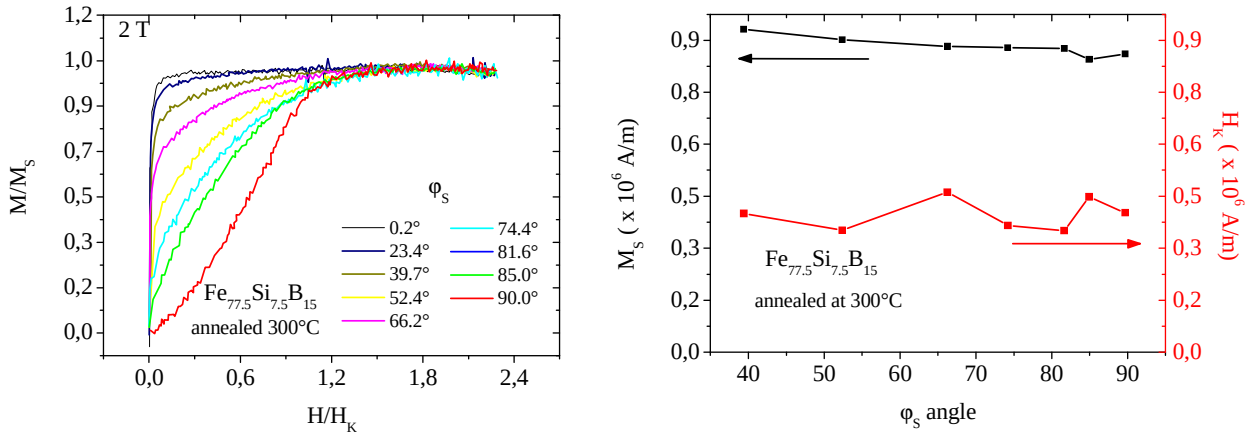

Fig. 54 (Left) The angular dependence of the axial magnetization in thermally treated FeSiB amorphous glass-coated microwire. (Right) The parameters obtained by fitting of measured data by Stoner-Wohlfarth model.

Chapter 5

Tailoring of domain wall dynamics by magnetic anisotropy

The most peculiar property of amorphous glass-coated microwires with positive magnetostriction is related to their spontaneous magnetic bistability characterized by a large Barkhaussen jump that gives rise to square-shaped hysteresis loop. The interpretation of such behavior was found in terms of special geometry of magnetic anisotropies presented in microwires. Comparing the hysteresis loops of amorphous glass-coated microwires with positive and negative magnetostriction coefficient, one may conclude that the most important magnetic anisotropy arises from magnetoelastic effects. In this regard, the domain wall dynamics in microwires was tailored by several methods including the change of internal mechanical stress distribution in this chapter. It was found in chapter 1 that the magnetic anisotropy seems to be a very important parameter determining the domain wall velocity in the mechanical model of domain wall propagation. As it will be shown here, the experimental measurements confirm such statement.

5.1 The influence of tensile mechanical stress on domain wall dynamics in microwires

Most of recent studies on the domain wall propagation in magnetostrictive microwires are inspired by their possible application as a sensor of axial mechanical tension stress. These devices are usually based on the domain wall velocity (124) or critical field (125) measurements. Recent observation of the fast domain wall propagation in microwires makes it possible to enhance the sensitivity as well as the stability of such applications. However, understanding of the influence of externally applied tensile stress on fast domain wall propagation in microwires is essential for further progress in the development of stress - sensitive applications.

Starting from previous chapter, it was demonstrated that the domain wall velocity can reach very high values in as-cast samples, where residual axial stresses σ_0 are present. Here, the additional tension stress σ_e is externally applied to the wire increasing the total

tension $\sigma = \sigma_0 + \sigma_e$. The influence of tensile mechanical stress on domain wall velocity is investigated in detail on the basis of mechanical model discussed in chapter 1.

In order to apply axial tension stress to microwire, the sample was oriented in vertical position. One end of the microwire was attached by glue at the top of primary coil. The mechanical tension in axial direction was applied by series of laboratory weights hanged to the other end of sample. The domain wall velocity was measured by use of Sixtus-Tonks setup supported in vertical position by non magnetic holders.

The applied stress within the metallic nucleus $\sigma_{metallic}$ and glass sheet σ_{glass} has been calculated as (126) (127):

$$\sigma_{metallic} = \frac{\frac{E_G}{E_M} mg}{S_M \frac{E_G}{E_M} + S_G} \tag{109}$$

$$\sigma_{glass} = \frac{mg}{S_M \frac{E_G}{E_M} + S_G} \tag{110}$$

where E_M and E_G is Young modulus of metal and glass coating respectively, S_i is the cross section of metallic core (S_M) and glass shell (S_G) and m is the mass of load. For our samples the following values were considered (128): $E_M = 96GPa$, $E_G = 64GPa$, $S_M = 1.77x10^{-10} m^2$ and $S_G = 6.28x10^{-10} m^2$.

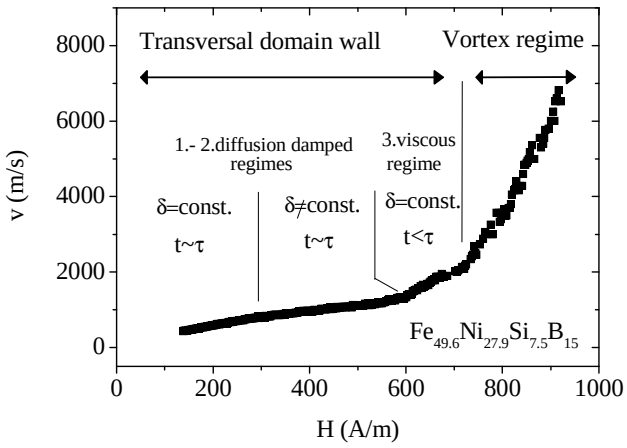

Fig. 55 The domain wall dynamics in $Fe_{49.6}Ni_{27.9}Si_{7.5}B_{15}$ as-cast microwire. Such composition is characterized by four different regimes of domain wall propagation.

The measurements were performed on samples of composition $Fe_{49.6}Ni_{27.9}Si_{7.5}B_{15}$ characterized by multi-regime domain wall dynamics. Fig. 55 shows the dependence of domain wall velocity on applied magnetic field in as-cast sample. As it is seen, four regimes of domain wall propagation can be recognized. Firstly, the domain wall velocity is directly proportional to the magnetic field at low fields (120 A/m – 230 A/m) with negative critical field and low domain wall mobility (2.6 m^2/A.s). In the second range (250 A/m – 600 A/m), the critical field remains negative, but the domain wall mobility slightly decreases. In contrary, the critical field becomes positive in the third regime (600 A/m – 720 A/m) where the domain wall mobility remarkably increases (up to 3.5 m^2/A.s). Fourth regime (720 A/m – 910 A/m) is characterized by the high domain wall mobility (~ 10 m^2/A.s), which was previously attributed to the vortex domain wall.

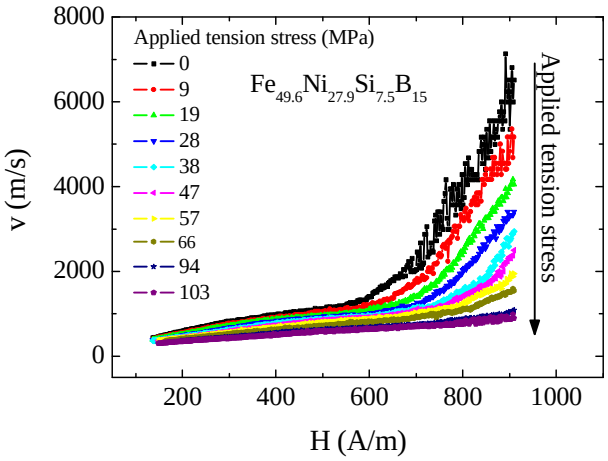

Fig. 56 The domain wall dynamics in $Fe_{49.6}Ni_{27.9}Si_{7.5}B_{15}$ microwire under the influence of axial mechanical stress applied to the microwire.

As expected due to the magnetostrictive character of the sample under study, the domain wall dynamics in microwires exhibits high sensitivity to applied tension stress (fig. 56). In general, the domain wall velocity decreases with applied tension stress. Similar results have been reported in other magnetostrictive microwires (129) (130). However, the multi-regime behavior of domain wall dynamics consisting of the four regions is maintained in whole interval of applied tensions. Comparing the response of each above mentioned regimes to the application of tensile stress, one may conclude that the regimes characterized by lower domain wall velocity seem to be less affected than the regimes with fast domain wall. For this reason, the regimes of domain wall propagation were discussed separately.

1, Diffusion damped regime with a constant thickness of the domain wall
(120 A/m – 250 A/m, 700m/s – 1100 m/s)

The dependence of domain wall velocity on applied tension stress was intensively studied in ferromagnetic magnetostrictive wires in previous works (131). The domain wall mobility in these attempts was found to be a non-monotonous function of applied stress (Fig. 57). At low values of applied tension, the convex stress dependence of domain wall damping was observed. On the other side, the high values of applied tension stress (more than 50 MPa) were characterized by concave shape of measured dependence. The convex part of domain wall damping at low tension was explained within the term of magnetic relaxation domain wall damping which is characterized by square-root dependence on stress (eq. 28). However, the concave part of domain wall damping dependence appearing at high tension stress remained unexplained.

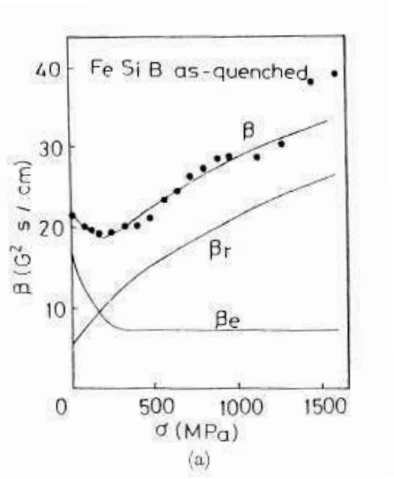

Fig. 57 The stress dependence of domain wall damping parameter in as-cast $Fe_{77.5}Si_{7.5}B_{15}$ amorphous wire. Image adopted from (131).

The tensile stress dependence of domain wall damping in the first regime (120 A/m – 230 A/m) in amorphous FeNiSiB glass-coated microwire is shown in Fig. 58. As it is seen, the increase of tensile stress leads to the more effective domain wall braking which can be recognized in the domain wall damping increase. Similarly to the previous results mentioned above, the domain wall damping exhibits a concave dependence at low values of tension (up to 30 MPa). However, at higher applied tension, the convex shape of curve becomes dominant. Such behavior is not possible to explain within the frame of the eddy-current and the magnetic moments relaxation contributions to the overall domain wall damping ($\beta = \beta_e + \beta_r$) because of their concave stress dependence.

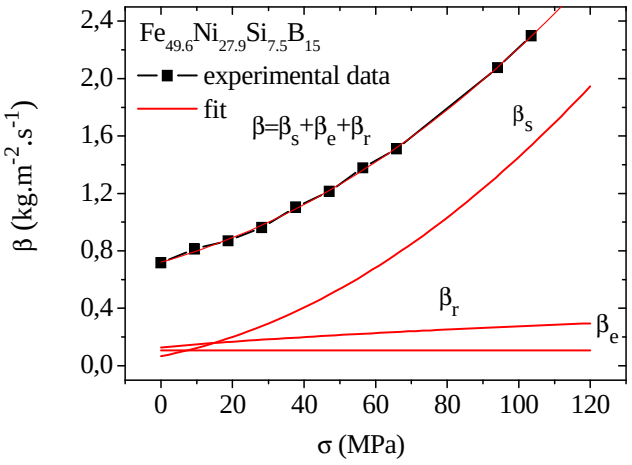

Fig. 58 The tensile stress dependence of domain wall damping in $Fe_{49.6}Ni_{27.9}Si_{7.5}B_{15}$ amorphous glass-coated microwire. Domain wall damping was obtained by fitting the measured domain wall velocities in the first regime.

Hence, additional stress-dependent contribution to the overall domain wall damping must be taken into account in order to get a coincidence of the measured data with the model.

As it was noted in chapter 1, in parallel to the eddy-current domain wall damping and to the magnetic moment relaxation domain wall damping, the motion of the domain wall is damped by structural relaxation, too. The stress dependence of structural relaxation damping arises from the magnetoelastic interaction of mobile defects with amorphous matrix. According to the Kronmuller's model, the interaction energy of a mobile defect with the amorphous matrix can be written as a sum of exchange, dipole-dipole and the magnetoelastic interaction between the magnetic moments of mobile defect and the local mechanic stress (42) (43):

$$e_{eff} = e_{eff}^{dipole-dipole} + e_{eff}^{exchange} + e_{eff}^{magnetoelastic} \tag{111}$$

The magnetoelastic part can be taken in the form:

$$e_{eff}^{magnetoelastic} = \frac{3}{2}\lambda_S \sigma \tag{112}$$

where σ denotes the mechanical stress in close proximity to the mobile defect and the free volume. If the stress dependence of the interaction energy of mobile defect with amorphous matrix is taken into account in this form, the corresponding structural relaxation domain wall damping can be evaluated as a function of tension:

$$\beta_s(\sigma) = P_2(\sigma + \sigma_0)^2 \tag{113}$$

with $P_2 = 9/4\lambda_s^2(c_0/kT)F(T,t)$. Assuming the stress dependence of all the three contributions to the domain wall damping, a good coincidence of measured data with fitting model can be obtained as it can be seen in Fig. 58. At low values of applied tensions (< 30 MPa), the domain wall velocity is limited by magnetic relaxation and eddy-current domain wall damping. However, at higher stresses (> 50 MPa), the structural relaxation domain wall damping becomes dominant as a result of the interaction energy of mobile defects with the local magnetization increase. The domain wall dynamics in this case is governed by structure relaxation, which was studied intensively in previous works (45), (47). Such regime of domain wall propagation was named diffusion damped regime (49). In this regime, the domain wall is damped by diffusion motion of mobile defects that try to follow the magnetization change within the moving domain wall during its propagation. Since the relaxation time of mobile defects is much higher than the inverse switching frequency of magnetic moments within the domain wall, the domain wall is damped by structural relaxation (49).

In order to confirm the dominant role of structure relaxation on domain wall velocity in the first interval of domain wall dynamics, the stress dependence of critical propagation field H_0 was estimated in the next step. Fig. 59 shows the critical propagation field which was obtained by extrapolation of measured curves in Fig. 56 according to eq. 4.

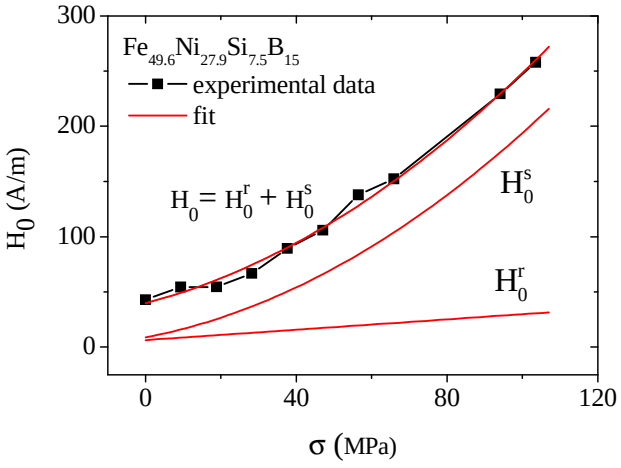

Fig. 59 Stress dependence of the switching field of $Fe_{49.6}Ni_{27.9}Si_{7.5}B_{15}$ amorphous glass-coated microwire in the first regime of domain wall propagation. Values of the switching field were obtained by the extrapolation of linear dependence of domain wall velocity on applied magnetic field.

As it can be clearly seen, the magnetoelastic contribution to the critical propagation field given by eq. 52 alone is not able to describe the measured convex stress dependence of critical propagation field. However, if both contributions to the critical propagation field H_0 (the magnetoelastic one and the structural one) are taken into account a good agreement of measured data with theoretic model is obtained as can be seen on Fig. 59. Here, the contribution from structural relaxation is higher than the magnetoelastic one in the whole interval of applied tensions. This confirms the dominant role of structure relaxation observed in previous measurements. The stress dependence of critical propagation field arises from the stress dependence of the interaction energy of mobile defect with local magnetization (eq. 34 and eq. 36).

2, Diffusion damped regime with reduced domain wall width

(250 A/m – 720 A/m, 1100 m/s – 1700 m/s)

As can be recognized in Fig. 56, the dependence of domain wall velocity on applied magnetic field in the second interval cannot be described by a linear equation, but one may observe a slight saturation of the domain wall velocity at all values of applied tension stress (Fig. 55 and Fig. 56). One of the possible explanations of such behavior could be attributed to the domain wall compression which accompanies the high domain wall velocities. It was shown in the previous works (39) that if the critical domain wall velocity v_c is achieved:

$$v_c = \sqrt{2Q}v_w \tag{114}$$

the domain wall starts to reduce its width significantly according to the relation:

$$\delta' = \delta_0 / \left(1 - \frac{v^2}{2Qv_w^2}\right)^{1/2} \tag{115}$$

where $Q = K / 2M_S^2\mu_0$ denotes the factor of quality, which reflects the strength of uniaxial anisotropy (in our case $Q < 1$), v_w the Walker domain wall velocity and δ_0 the domain wall width at zero domain wall velocity. In this way, the dependence of domain wall

velocity on applied field can be transformed by use of variable domain wall width into the following form:

$$v = S(H - H_0) = S \Big/ \left(1 + \frac{v^2}{2Qv_w^2}\right)^{1/2} (H - H_0) \qquad (116)$$

The comparison of measured domain wall velocity with this model is shown in fig. 60 (the tension stress of 30 MPa was applied in this case). Note, the same good agreement of measured data with this model was obtained in whole interval of applied stresses.

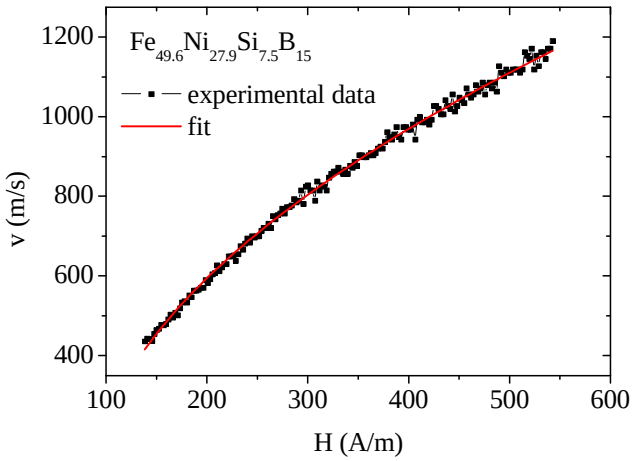

Fig. 60 The domain wall velocity versus applied magnetic field in the second interval of domain wall dynamics in $Fe_{49.6}Ni_{27.9}Si_{7.5}B_{15}$ amorphous glass-coated microwire. The red curve depicts the fit of model containing the domain wall width compression.

3, Viscous regime

(720 A/m – 910 A/m, 1700 m/s – 2100 m/s)

As it was shown above, the first regime of domain wall dynamics is characterized by domination of the structural relaxation domain wall damping (> 50 MPa). Due to the low domain wall velocity, the interaction time of mobile defects with local magnetization within the moving domain wall is higher than the relaxation time of mobile defects. For this reason, the mobile defects are able to follow the magnetization change within the domain wall during propagation and the observable damping by structural relaxation occurs which was indirectly confirmed by fitting of domain wall velocity and switching field by use of stress dependant formulas of structure contributions. However, if the domain wall exceeds the velocity for which the interaction time with mobile defects is lower than relaxation time of mobile defects, the domain wall would be detached from structure relaxation (49). Then the domain wall mobility steeply increases because of lower domain wall damping due to absence of

structural relaxation. This is observed probably in the third interval of domain wall dynamics when the domain wall exceeds the limit of about 1.7 km/s (Fig. 56).

As it can be recognized in fig. 56, the application of tensile stress generally decreases the domain wall velocity and, consequently, the transition field, at which the domain wall becomes detached from mobile defects, is increased.

The plot of total domain wall damping as a function of applied stress for third regime is shown in Fig. 61. In contrary to the previous discussed regimes, the domain wall damping arising from structural relaxation must be neglected in order to obtain a good fit of the measured data.

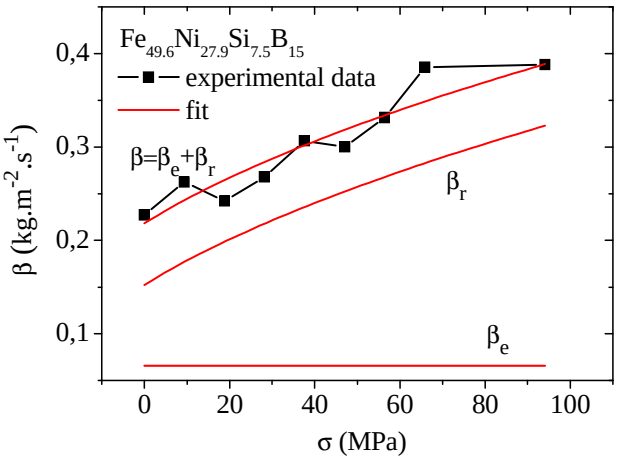

Fig. 61 The domain wall damping as a function of applied tension stress in the third interval of domain wall dynamics in $Fe_{49.6}Ni_{27.9}Si_{7.5}B_{15}$ amorphous glass-coated microwire. The red curve depicts the fit of both contributions to the overall damping.

In order to confirm indirectly that the structural relaxation is not employed to domain wall damping at such high velocities, the tensile stress dependence of critical propagation field was obtained by extrapolation of the measured domain wall velocity in Fig. 56 and it was compared to the fit of the critical propagation field. Here, in order to obtain reasonable physical values of fitted model, the structural relaxation contribution to the switching field (eq. 53) must be neglected. Similarly, the critical propagation field can be successively described within the single term of magnetoelastic contribution given by eq. 52 (Fig. 62).

Here, the switching field is characterized by positive values as opposed to the first and second regime.

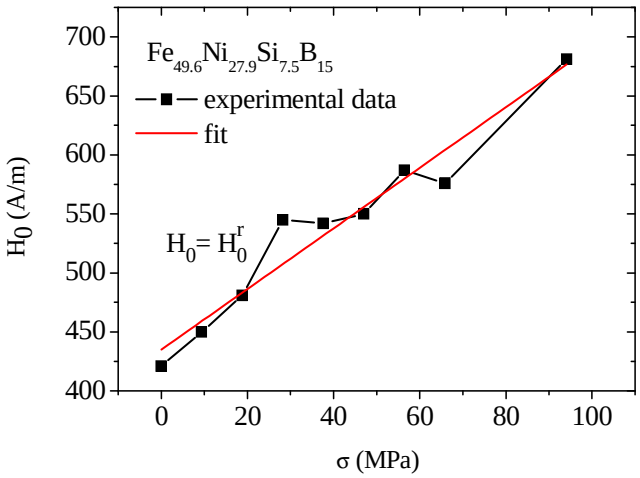

Fig. 62 The critical propagation field as a function of applied tension stress in the third interval of the domain wall dynamics in $Fe_{49.6}Ni_{27.9}Si_{7.5}B_{15}$ amorphous glass-coated microwire. The red curve depicts the fit of the single contribution to the switching field arising from the magnetoelastic effect.

4, Secondary regime

(> 910 A/m, > 2.1 km/s)

The domain wall dynamics in previous regimes was characterized by relatively low domain wall velocity (less than 2 km/s) and low domain wall mobilites (of the order of units). The tension stress dependence of domain wall damping was explained within the terms of the three main contributions to the domain wall damping, which was confirmed indirectly by fitting of experimental data by theoretical models.

However, the situation in fourth regime is more complicated. As the domain wall velocity reaches the value of around 2 km/s in this case (Fig. 55 and Fig. 56), one may observe a rapid domain wall mobility increase up to 12 $A/m^2.s$. Such high domain wall mobility was attributed to the “secondary regime of domain wall propagation” which was discussed in chapters 3 and 4 as a consequence of domain structure transformation (from the transversal one into vortex one, for example). The domain wall damping in fourth regime decreases by almost one order in magnitude as compared to that in viscous regime. This results in significant domain wall mobility increase, which allows achieving very high domain wall velocities up to 8 km/s for the case without applied stress. The low value of domain wall damping which appears in the fourth regime cannot be explained within the above discussed mechanical model, because the fitting gives physically not reasonable values of parameters.

Moreover, as it can be seen in Fig. 63, the response of domain wall damping to the application of tensile stress in fourth regime is a non monotonous function of tensile stress.

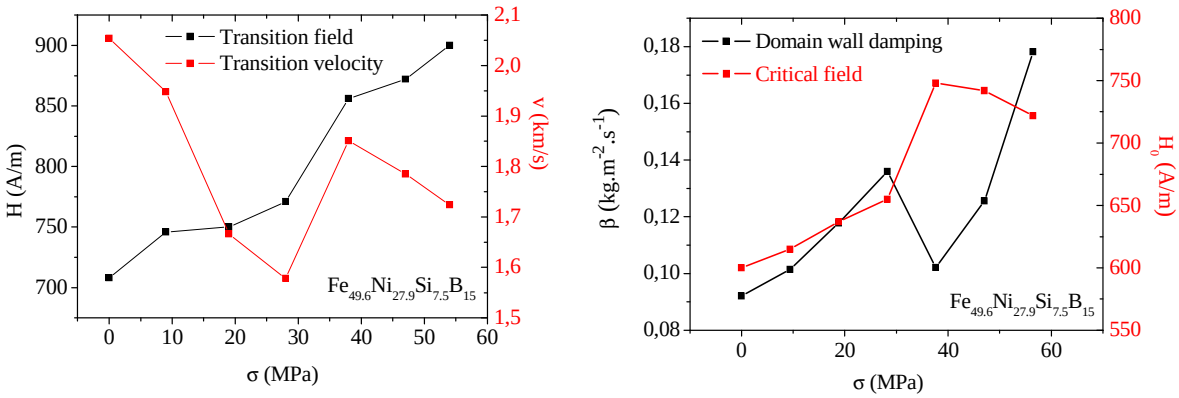

Fig. 63 The transition field and velocity (left) and Critical field and domain wall damping (right) as a function of applied tensile stress in the fourth interval of the domain wall dynamics in $Fe_{49.6}Ni_{27.9}Si_{7.5}B_{15}$ amorphous glass-coated microwire.

The critical propagation field increases almost linearly with applied tensiile stress together with domain wall damping up to 30 MPa. The domain wall dynamics changes steeply above 30 MPa. The critical propagation field continuously increases, however the domain wall damping decreases. One possible explanation may rest on the complex stress distribution and it counter-play on the fast domain wall dynamics that occurs in fourth regime. However, it is not possible to determine the main factor involved, because of the missing model which describes such high domain wall mobility (or low domain wall damping) that occurs in fourth regime.

5.2 The effect of conventional thermal treatment on domain wall dynamics in microwires

As it was shown in previous section, the domain wall dynamics of magnetostrictive Fe-rich microwires can be tailored very effectively by application of tensile stress. Generally, the domain wall velocity was found to be decreasing with applied tension. On the other hand, the highest domain wall velocity was observed at zero applied tension. However, in this case the total tensile stress in as-cast microwires is not zero, but it is equal to the strong residual stresses that can be reduced by a proper thermal treatment (132) (133). In this section, the strong residual stresses are decreased by thermal treatment and the influence of thermal annealing on fast domain wall propagation in microwires is studied. This is especially important for sensor

applications (146), where microwires with well-defined parameters of domain wall propagation (domain wall mobility and critical field) are necessary.

As it was mentioned in chapter 1, the fast domain wall propagation in mechanic model can be attributed to (i) the negative critical field (that can be explained by the interaction of the domain wall with the stray field of microwire (134)) and (ii) to high domain wall mobility. As it was noted in preliminary chapters, a high value of domain wall mobility is mainly given by low value of domain wall damping. Nowadays, three contributions to the domain wall damping are recognized: (a) eddy-current contribution mainly given by the geometry of the domain wall, (b) the magnetic relaxation domain wall damping direct proportional to the value of magnetic anisotropy K and (c) the structural relaxation contribution proportional to the concentration of free volumes c_0.

In $Fe_{77.5}Si_{7.5}B_{15}$ amorphous glass-coated microwires both structural and magnetic relaxation contributions to the domain wall damping are high, due to the amorphous state (high concentration of free volumes c_0) and due to high magnetostriction λ_S of a given chemical composition. This results in a relatively low domain wall velocity that reaches 1.5 km/s in as-cast state (Fig. 64). However, the magnetic relaxation domain wall damping is proportional to the magnetic anisotropy (eq. 28). Since the most important magnetic anisotropy in glass-coated microwires arises from magnetoelastic coupling related to the strong mechanical stresses, the magnetic anisotropy could be decreased by reduction of residual stresses via thermal annealing. However the temperature of thermal treatment must be chosen properly in order to obtain an adequate relaxation of residual stresses.

Fig. 64 and Fig. 65 show that the thermal annealing at 200°C neither changes the domain wall velocity nor the critical field in both samples. This is in a good agreement with previous measurements (135) in which annealing of Fe-rich wires at 200°C resulted only in 10% increase of domain wall velocity as compared to the as-cast state. Thermal treatment at this temperature caused the reversible changes only. A similar result was observed before (143), where annealing of FeSiB samples at 200°C didn't change the magnetic properties of such sample.

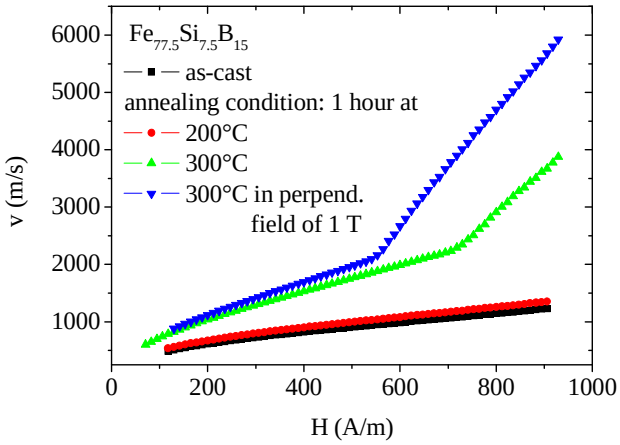

Fig. 64 The influence of thermal treatment on domain wall dynamics in $Fe_{77.5}Si_{7.5}B_{15}$ amorphous glass-coated microwire. Plot shows the average domain wall velocity.

This was confirmed indirectly by the temperature dependence of saturation magnetization measurement (fig. 65). One may determine from the graph that the crystallization temperature of $Fe_{77.5}Si_{7.5}B_{15}$ is equal to T_K = 440°C and Curie temperature to T_C = 390°C. The detail of measured points is shown at inset. As it is seen, the first interval of temperature (10°C - 220°C) is characterized by the high discontinuity of measured data. Such behavior should be attributed to the relaxation of internal stresses. On the other side, the data in second interval (250°C - 550°C) are well-continuous. The magnetization changes smoothly with temperature in this case because the residual stresses are already relaxed during thermal treatment.

Hence, for a more efficient residual stresses decrease, the higher annealing temperature of 300°C was chosen in the next thermal treatment. The domain wall dynamics of as-cast sample is well described by linear equation of motion. The domain wall mobility reaches the order of units $S = 1.2 m^2 / A.s$. Such values have been observed previously in a sample of the same composition (136) and this was attributed to the presence of a transverse domain wall (137).

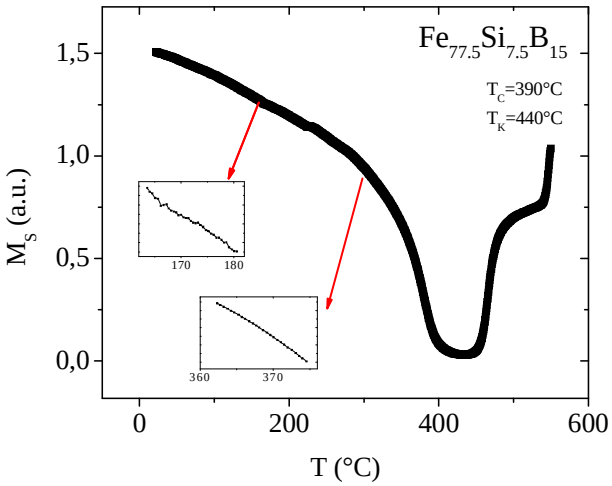

Fig. 65 The temperature dependence of saturation magnetization of $Fe_{77.5}Si_{7.5}B_{15}$ amorphous glass-coated microwire.

The most significant changes of domain wall dynamics were observed in the samples treated at 300°C. Such treatment resulted in two remarkable effects (Fig. 64): (i) abrupt increase of domain wall mobility from $S = 1.2 m^2 / A.s$ to $S = 2.5 m^2 / A.s$ and (ii) introduction of the secondary regime of domain wall propagation characterized by high domain wall mobility ($S = 12 m^2 / A.s$). The increase of domain wall mobility can be explained in term of the magnetic moment relaxation domain wall damping decrease (via magnetic anisotropy decrease) and in terms of structural relaxation domain wall damping decrease (by annealing-out of free volumes). Moreover, the domain wall mobility increase should be attributed to the change of internal stress distribution related to the different thermal expansion coefficient of metallic nucleus and glass-coating. Such internal stresses have a tensor character and the relation between tensor components strongly influences the magnetic properties of microwires (140). It has been shown experimentally (140) and theoretically (141) in previous works, that the axial component of internal stress is much stronger than the radial or circular one. The strength of axial and radial stresses in as-cast microwire depends on the ratio between the volume of glass-coating and the volume of metallic nucleus, which is expressed by factor $x = D^2 / d_m{}^2 - 1$. According to (142), the axial mechanical stress σ_a and radial mechanical stress σ_r can be roughly evaluated:

$$\sigma_a = \sigma_0 \frac{kx}{kx+1} \frac{(k+1)x+1}{(k/3+1)x+4/3} \tag{117}$$

$$\sigma_r = \sigma_0 \frac{kx}{(k/3+1)x+4/3} \tag{118}$$

where $k = E_M / E_G$ denotes the ratio of Young modulus of metal and glass-coating, and $\sigma_0 = E_G(\alpha_G - \alpha_M)(T^* - T)$, T^* is the solidification temperature of microwire during the fabrication process, T the room temperature and α_G, α_M the thermal expansion coefficients of glass coating and metallic nucleus. The proportion between the axial and the radial mechanical stress can be modified by thermal annealing. Such the change of stress distribution can result in change of domain wall dynamics.

As it was noted in previous chapter, the secondary regime with high domain wall mobility (~ 10 m^2/A.s) has been attributed to change of internal domain wall structure

from the transverse into the vortex one. The internal structure of vortex domain wall has much higher amount of magnetic moments rotated out-of easy axis. As a result, the magnetoelastic part of the total domain wall energy takes the more important place in vortex wall as compared to the transverse structure (144). Thermal annealing at 300°C remarkably reduces axial tensile stresses, when the magnetoelastic contribution to the total domain wall energy decreased too and the vortex domain wall could appear even in the wire, where vortex domain wall has not been before (Fig. 64). This observation suggests that the most important parameter allowing the fast vortex domain wall (secondary regime) arises from low value of magnetic anisotropy. However, it seems that the low anisotropy is not the only one condition for fast domain wall propagation. In order to understand better the importance of two perpendicular anisotropies (axial and radial one expressed by eq. 117 and 118) on fast domain wall propagation in FeSiB microwire, annealing in a perpendicular field was performed in the next step. As it is seen (Fig. 64), the thermal treatment in perpendicular field leads to a bit higher domain wall mobility (from $S = 1.2m^2 / A.s$ to $S = 2.7m^2 / A.s$) as compared to the annealing without perpendicular field (from $S = 1.2m^2 / A.s$ to $S = 2.5m^2 / A.s$). The difference between them is probably associated with enhancement of the radial anisotropy during thermal annealing in perpendicular field. Such assumption was confirmed indirectly by temperature dependence of remanent vs. saturation magnetization measurements (Fig. 68). However, the more remarkable effect of thermal treatment consists in the reduction of the transition field at which the change from the primary to the secondary regime of domain wall propagation occurs. This phenomenon can be explained under the assumption of the vortex domain wall being responsible for secondary regime. Induced perpendicular anisotropy is able to favors the multi-axis structure of the vortex domain wall and the magnetoelastic part of the domain wall energy decreases. As a result, the fast secondary regime can appear in the lower magnetic field (Fig. 64).

Regardless to the origin of secondary regime, one may conclude, that the thermal treatment at 300°C resulted in 4 times higher domain wall velocity as compared to the as-cast state (at 800 A/m in Fig. 64). Magnetic anisotropy decreases during the thermal treatment leads to the increase in the domain wall velocity. Especially, this is important for microwires characterized by high values of internal stresses.

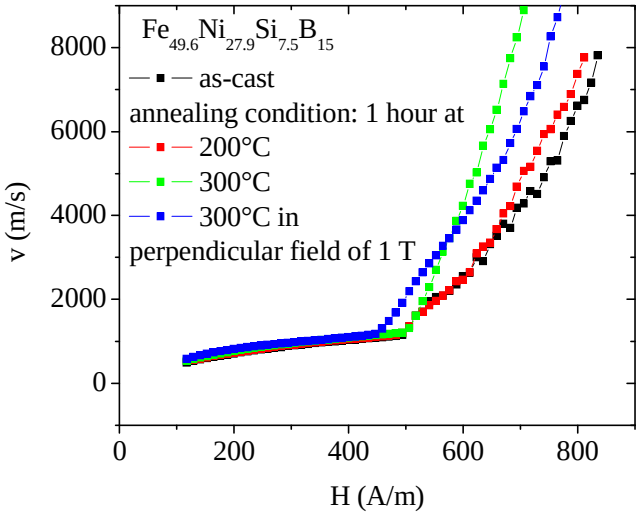

Fig. 66 The influence of thermal treatment on domain wall dynamics in $Fe_{49.6}Ni_{27.9}Si_{7.5}B_{15}$ amorphous glass-coated microwire.

The influence of thermal treatment on fast domain wall dynamics in microwires was studied in next sample with composition of $Fe_{49.6}Ni_{27.9}Si_{7.5}B_{15}$. This sample is characterized by lower value of magnetostriction (145) that results in lower magnetic relaxation contribution to the domain wall damping and, consequently, the higher domain wall velocities can be estimated. The domain wall dynamics of $Fe_{49.6}Ni_{27.9}Si_{7.5}B_{15}$ microwire in as-cast state is shown in Fig. 66. As it is seen, the domain wall dynamics is characterized by two regimes of domain wall propagation as in the previous composition. The primary one with domain wall mobility of $S = 1.6 m^2 / A.s$ and negative critical field is followed by secondary regime with higher domain wall mobility (~ $S = 11.8 m^2 / A.s$). The secondary regime of domain wall propagation appeared as a result of thermal annealing in previously discussed $Fe_{77.5}Si_{7.5}B_{15}$ sample. Here, the secondary regime of domain wall propagation is present in as-cast state. This presence of fast secondary regime of domain wall propagation can be explained within the term of lower magnetic anisotropy resulted from lower value of magnetostriction of $Fe_{49.6}Ni_{27.9}Si_{7.5}B_{15}$ composition. It seems that the fast secondary regime of domain wall propagation appears at low values of mechanical stresses. This was confirmed by measurements of domain wall dynamics under the influence of tensile stress in previous chapter.

As it is seen in fig. 66, the thermal annealing at 200°C neither changes the domain wall mobility nor the critical field, in the same way as it was observed in the previous composition. The thermal annealing at 300°C was sufficient to decrease the transition

field (from 500A/m to 450A/m). However, the thermal annealing at the same temperature in perpendicular did not change the domain wall dynamics significantly.

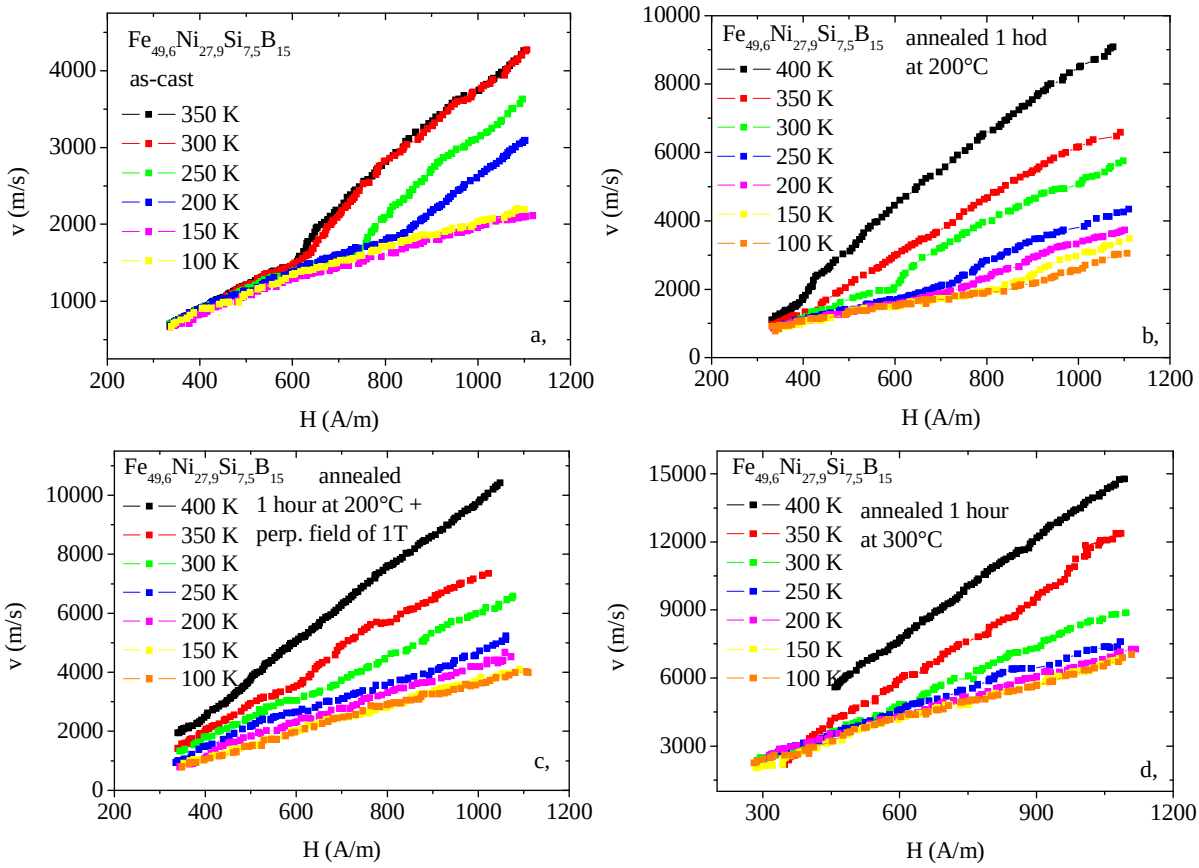

Fig. 67 The temperature dependence of domain wall dynamics in $Fe_{49.6}Ni_{27.9}Si_{7.5}B_{15}$ amorphous glass-coated microwires in as-cast state (a), annealed at 200°C (b), annealed at 200°C in perpendicular field of 1 T (c) and annealed at 300°C (d)

Generally, the effect of thermal treatment of binary alloys below the Curie point can be attributed to the two processes: (1,) induction of magnetic anisotropy related to the pair ordering and (2,) redistribution of the internal stresses during the thermal treatment. Since the two transition metals are present in the alloy with composition of $Fe_{42.6}Ni_{34.9}Si_{7.5}B_{15}$, one would expect the effect of thermal annealing in perpendicular field to be more remarkable (see Fig. 66). However, the effect of pair ordering was probably negligible in comparison to the other effects arising from magnetoelastic coupling.

As it was noted above, the peculiarity of amorphous glass-coated microwires is that they have the additional source of internal stresses related to the different thermal expansion coefficient of glass-coating and metallic nucleus. Generally, the decrease of

temperature leads to the increase of internal stresses in metallic core because of higher thermal expansion of the metallic nucleus as compared to that of glass-coating. From the same reason, the stress induced by temperature decrease can be considered to have tension character. Fig. 67 a shows the temperature dependence of domain wall dynamics in as-cast $Fe_{49.6}Ni_{27.9}Si_{7.5}B_{15}$ microwire. The decrease of temperature is accompanied by two processes: (i) the decrease of domain wall mobility of primary regime and (ii) the shift of the transition field. The decrease of domain wall mobility can be explained in the frame of above discussed mechanic model. Temperature decrease leads to relaxation time of mobile defect decrease and to the internal residual stresses increase. A similar behavior was previously measured on FeSiB microwires (138) (139), where the domain wall damping decreased with temperature. In contrary, the domain wall mobility of secondary regime seems to be not affected by temperature. This confirms our previous statement that domain wall dynamics of secondary regime is not well – described by mechanic model.

Generally, the thermal annealing suppressed the primary regime and the fast secondary regime was observed (Fig. 67 b, c, d) in each sample. Thanks to it, the domain wall velocities achieved very high values, up to 14 km/s. This is 4 times more than the velocity of as-cast samples. However, not only a low anisotropy seems to be responsible for such high values of velocities.

As it was noted above, the change of temperature is accompanied by redistribution of internal stresses, namely the ratio between the axial and radial anisotropy. Fig. 68 shows the temperature dependence of saturation and remanent magnetization of $Fe_{49.6}Ni_{27.9}Si_{7.5}B_{15}$ microwire measured in axial direction. At high temperature, the remanent magnetization follows the curve of saturation magnetization. The difference between them corresponds to the surface domain structure as well as to the volume of closure domains. However, at lower temperature (around 125 K), the perpendicular anisotropy becomes more important than the axial one, which results in a complex change of domain structure. Thermal annealing decreases the ratio between the axial anisotropy and the radial anisotropy which results in more remarkable drop of remanent magnetization at low temperatures (fig. 68 b, d). Such enhanced radial anisotropy then allows reaching higher domain wall velocities in both $Fe_{49.6}Ni_{27.9}Si_{7.5}B_{15}$ (Fig. 66) and $Fe_{77.5}Si_{7.5}B_{15}$ (Fig. 64) samples.

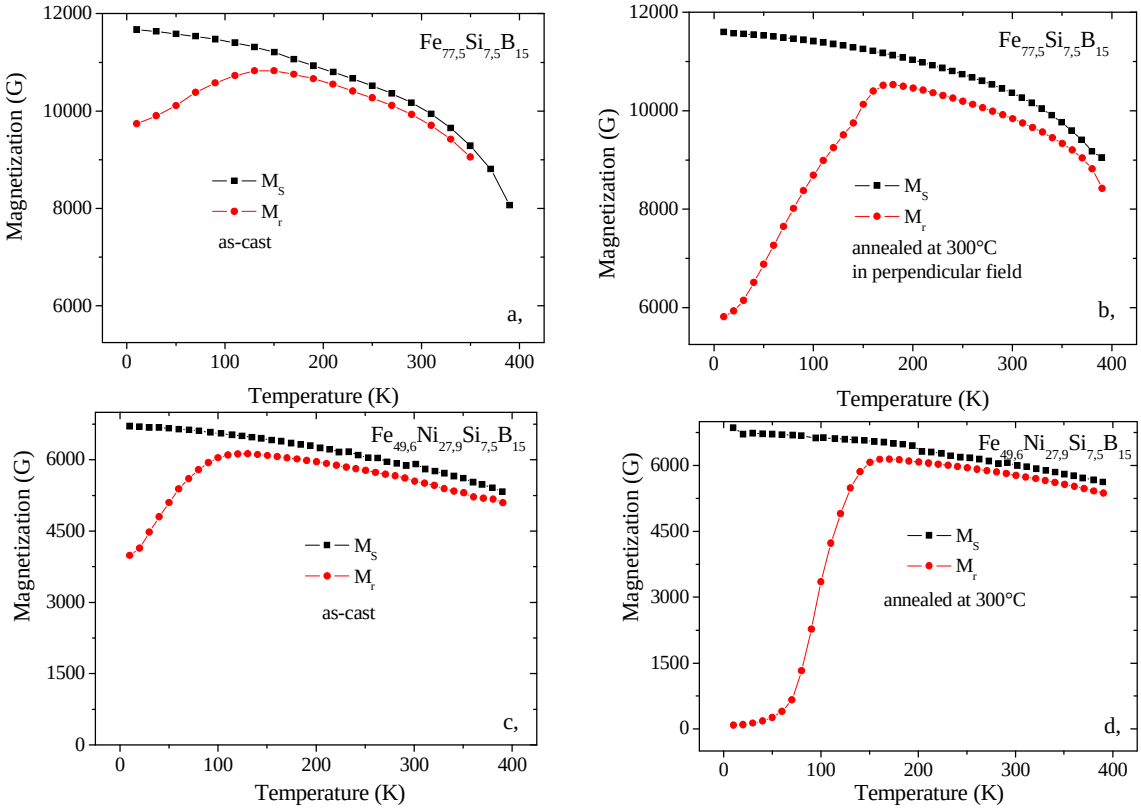

Fig. 68 The comparison of remanent and saturation magnetization of $Fe_{77.5}Si_{7.5}B_{15}$ amorphous glass-coated microwires in as-cast state (a) and thermally annealed at 300°C (b), $Fe_{49.6}Ni_{27.9}Si_{7.5}B_{15}$ in as-cast (c) and thermally annealed at 300°C (d). At high temperature, the axial anisotropy is the strongest one. However, the domain structure of microwire undergoes a complex change when temperature is below 100K.

5.3 The effect of thermal treatment under the mechanical stress

Magnetization process of strongly magnetostrictive Fe-rich amorphous glass-coated microwires is determined mainly by magnetoelastic anisotropy. The magnetoelastic anisotropy depends on the geometric parameters (thickness of the glass), chemical composition (determining the coupling to mechanical stress) and the internal stress distribution (introduced in the wire during manufactory process). The observed experimental results on domain wall dynamics in samples subjected to the thermal treatment in previous section can be understood as a consequence of induced magnetic anisotropy arising from the counterbalance between internal stresses owing to the

difference in thermal expansion coefficients of the metal core an glass-coating. Enhancing of the domain wall dynamics by thermal treatment was controlled by properly selected temperature and by the time duration of the thermal annealing. However, the reduction of the internal stresses can be performed even more effectively. It was shown in the previous works that the thermal-mechanical annealing of amorphous glass-coated microwires leads to the drastic change in the shape of hysteresis loops (147) (148). Such change was attributed to the reduction of axial mechanical stresses as well as to the induction of the strong perpendicular anisotropy to the wire. Here we study the influence of thermal treatment under the mechanical stress on domain wall dynamics in FeSiB microwire. The effect of thermo-mechanical annealing on domain wall velocity is compared to the conventional thermal treatment performed in previous chapter.

The $Fe_{77.5}Si_{7.5}B_{15}$ microwire with 15 μm metallic nucleus in diameter was used for this experiment. The samples were subjected to the thermo-mechanical annealing at 300°C for 1 hour. The stress was applied to the wire by series of laboratory loads. It is worth mentioning that the sample was first loaded by the stress and then placed in the furnace.

The hysteresis loops of $Fe_{77.5}Si_{7.5}B_{15}$ microwire is shown in Fig. 70. As it is expected due to the magnetostrictive character, the corresponding hysteresis loop of as-cast FeSiB microwire exhibits spontaneous bistability (Fig. 70). The thermal annealing at 300°C changes a bit the magnetic coercivity; however, rectangular shape of hysteresis loops is maintained. This is in a good agreement with the previous measurements where thermal annealing decreased the critical propagation field (Fig. 64).

The conventional thermal treatment (at 300°C) of FeSiB as-cast microwire results in the domain wall mobility increase and in the critical propagation field decreases as it was shown in the previous section. In contrast, the thermal annealing at the same temperature, but under applied stress ($\sigma = 67 MPa$) leads to the drastic change in the shape of hysteresis loop (Fig. 70) as well as change in the domain wall dynamics. The spontaneous magnetic bistability disappears (Fig. 69) and the domain wall propagation is not possible to observe in that case.

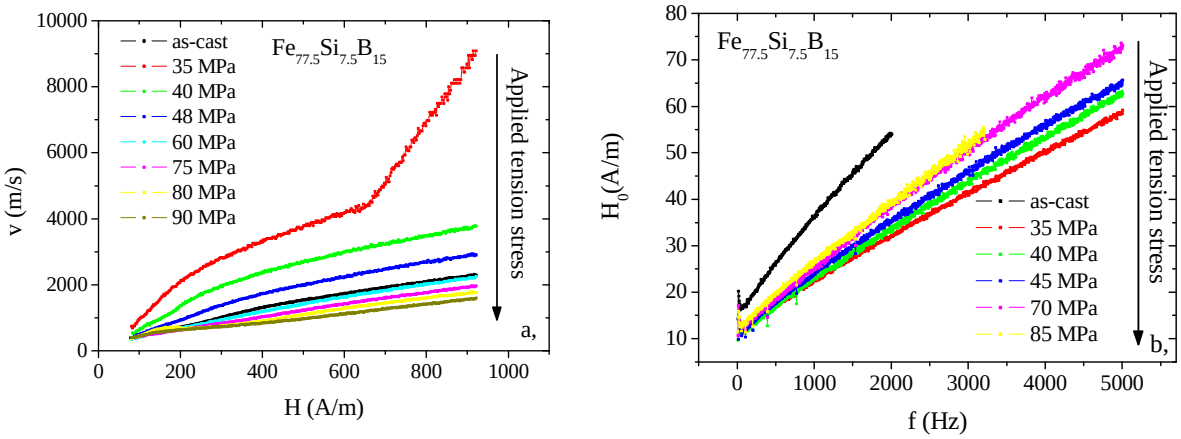

Fig. 69 (a,) The domain wall velocity of microwire subjected to thermal annealing at 300°C under the mechanical stress of 67 MPa during 1 hour and measured at room temperature under various values of applied stress. (b,) the frequency dependence of the critical field for as-cast and treated sample.

The different effect of conventional and thermo-mechanical annealing originates probably from the different relaxation processes during the thermal treatment. As it was noted above, the peculiarity of amorphous glass-coating microwires consists in the source of additional internal stresses resulting from the different thermal expansion coefficient of metallic core and glass-coating. Moreover, the axial stresses can be considered to be higher than radial one. In order to explain the measured data, it can be assumed that after thermo-mechanical annealing the axial stresses in annealed-out samples are reduced close to zero (loss of bistability). As a result, the easy magnetization of the sample is not in axial direction (as it was in as-cast state), but the direction is more influenced by radial or circular stresses. In order to explain the effect of thermo-mechanical annealing on internal stress-distribution, it must be suggested that the annealing under the stress results in re-distribution of internal stresses in order to minimize the magnetoelastic energy and to fit to the stressed state. For this reason, the removal of mechanical load after thermo-mechanical annealing leads to the strong decrease of axial stresses component and even in appearance of compressive stresses.

Fig. 70 shows that the application of tensile stress to the samples treated by thermo-mechanical annealing leads to the progressive recovery of magnetic bistability observed in as-cast state. The rectangular shape of hysteresis loops appears at tensile stress as low as 12 MPa (red curve). Further increase of the applied stress provides higher volume of hysteresis loop, which can be associated with the increase of axial domain when tension axial stress was applied. Such a tendency can be observed at the applied tension up to 52 MPa where the shape of the as-cast hysteresis loop is completely recovered.

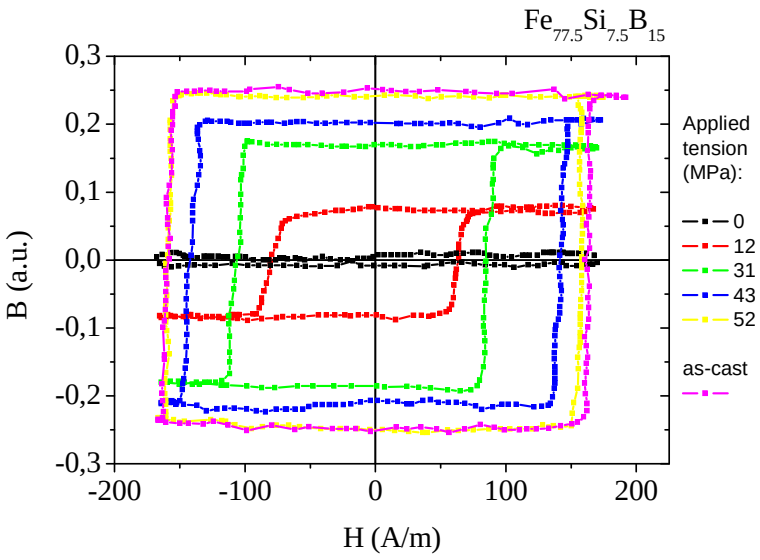

Fig. 70 The hysteresis loops (room temperature, various applied stress) of $Fe_{77.5}Si_{7.5}B_{15}$ microwire treated by thermal annealing under the mechanical stress (300°C, 67MPa, 1h). As it is seen, the complete recovery of magnetic bistability (as compared to as-cast) was observed at the applied tension value of 52 MPa.

This behavior can be attributed to the increase of axial stress component under the application of tensile stress that results to the alignment of easy magnetization to the axial direction. Observed changes of the hysteresis loop of the sample subjected to the thermal treatment when measured under tensile stress confirm such assumption. This effect should be attributed to the increase of the longitudinal stress component under the application of axial tensile stress and consequently to align of the magnetization along the highest stress component due to the positive magnetostriction coefficient of studied alloy.

A similar recovery of magnetic properties typical for as-cast state is observed in domain wall dynamics (Fig. 69). It was not possible to measure the domain wall velocity in treated sample without applied tension due to the spontaneous bistability loss. However, the application of 35 MPa tensile stresses recovers the bistable character enabling the domain wall dynamics measurements. As it is seen, the v (H) dependence, measured under the lowest value of applied tension (35 MPa), consists of (at least) 3 regimes: (1,) adiabatic (149) followed by previously discussed (2,) primary regime and (3,) fast secondary regime.

The domain wall dynamics of conventionally treated FeSiB microwire was examined in previous section (Fig. 64). As it is seen here, the thermo-mechanical annealing performed at the same temperature but under the mechanical stress, leads to a more drastic domain wall velocity increase as compared to conventional treatment. Such effect can be attributed to a more effective relaxation of internal stresses during thermo-mechanical annealing. Thanks to it, the secondary regime of domain wall propagation appears which results in 4 time's higher domain wall velocity as compared to the as-cast

state (at 800A/m). Further increase of externally applied tensile stress leads to the suppression of the secondary regime. Moreover, the domain wall velocity of as-cast state is recovered completely at the value of applied tension stress of 60 MPa.
As it was noted above, the heat treatment results in structural and stress relaxation in metallic core. In the case of amorphous microwires, the switching field is proportional to the energy required to form the domain wall involved in bistable process (150) (151):

$$H_{SW} \approx (A(3/2)\lambda_S\sigma)^{1/2} \quad (119)$$

where A is exchange energy constant, λ_S coefficient of saturation magnetization and σ mechanical stresses. Fig. 69 shows that the thermo-mechanical treatment decreases the switching field, which can be associated with the residual stresses decrease. The switching field increases as a result of higher axial stress component under the application of axial stresses. However, the switching field of thermo-mechanically treated microwire never reaches the high values measured in as-cast state.

The influence of thermal annealing on domain wall dynamics of highly magnetostrictive Fe-rich microwires was examined in this section. It was shown that the thermo-mechanical annealing provides a more efficient decrease of axial anisotropy as compared to the conventional thermal annealing. Moreover, it results in the loss of sample bistability. Further application of relatively small tension stress (35 MPa) restores the bistable character. At the same time, the maximum domain wall velocity is more than five times higher as compared to the as-cast state due to the presence of secondary regime of domain wall propagation in this case. Such high sensitivity of microwires to the external stress field should be employed in potential sensor applications based on the detection of domain wall velocity or critical field (152) (153).

5.4 The domain wall dynamics tailored by current annealing of microwires

Magnetic properties of magnetostrictive amorphous glass-coated microwires were found in previous sections to be strongly influenced by magnetoelastic anisotropy that arises from residual mechanical stresses introduced to wires during their manufactory process. Thanks to it, the domain wall velocity of microwires can be tailored very effectively by tuning the residual stresses. This was presented in section 5.1 where the domain wall velocity was tailored by the residual stresses increase via externally applied tension and the same in section 5.2 where the residual stresses were decreased by thermal annealing performed at proper selected temperature. The influence of thermal annealing on domain wall dynamics in microwires can be explained within three terms: (a,) decrease of residual stresses (b,) redistribution of internal stresses (especially between radial one and axial one by thermal annealing under the mechanic tress) and (c,) induced anisotropy via pair ordering.

Another kind of thermal treatment of microwires was proposed in previous theoretical (154) (155) as well as experimental (159) (158) works, namely the current annealing. Electric current produces an Oersted magnetic field which induces the magnetic anisotropy of circular orientation in the wire (155) (156). If DC electric current is used during the treatment, the temperature can be considered to be homogenous in the whole cross-section and the wire is annealed in constant circular field. On the other hand, an AC current is usually used to enhance soft magnetic properties of wire surface (159). Especially, this is was found to be very useful for enhancing GMI effect in those wires with negative magnetostriction (157).

In this part, the magnetoelastic anisotropy of microwires is tailored by current annealing and its influence on domain wall dynamics is studied with a special attention paid to high domain wall velocities.

Microwires with compositions of $Fe_{77.5}Si_{7.5}B_{15}$, $Fe_{49.6}Ni_{27.9}Si_{7.5}B_{15}$ and $Fe_{42.6}Ni_{34.9}Si_{7.5}B_{15}$ have been used for this measurement. Samples were treated by electric current up to 50 mA during standard processing time of 10 minutes. Such values of electric current were found to heat up microwires close to crystallization temperature, which can be recognized in Fig. 71 showing the temperature dependence of electric

resistance (thermoanalysis). The initial smooth resistance increase can be attributed to more effective electron scattering due to higher temperature achieved by heat released by current. Sudden breakdown of resistance at 57 mA points to the strong structural changes which can be associated with the crystallization of amorphous state (which is in the case of $Fe_{77.5}Si_{7,5}B_{15}$ around 400 °C). Further electric current decrease beyond this point is characterized by much lower value of resistance. Hence, the thermo-analysis is a very easy method for determination the "crystallization" current (which was found to be around 57 mA) and this value has never been exceeded in thermal treatments in order to preserve the amorphous state of the studied wires.

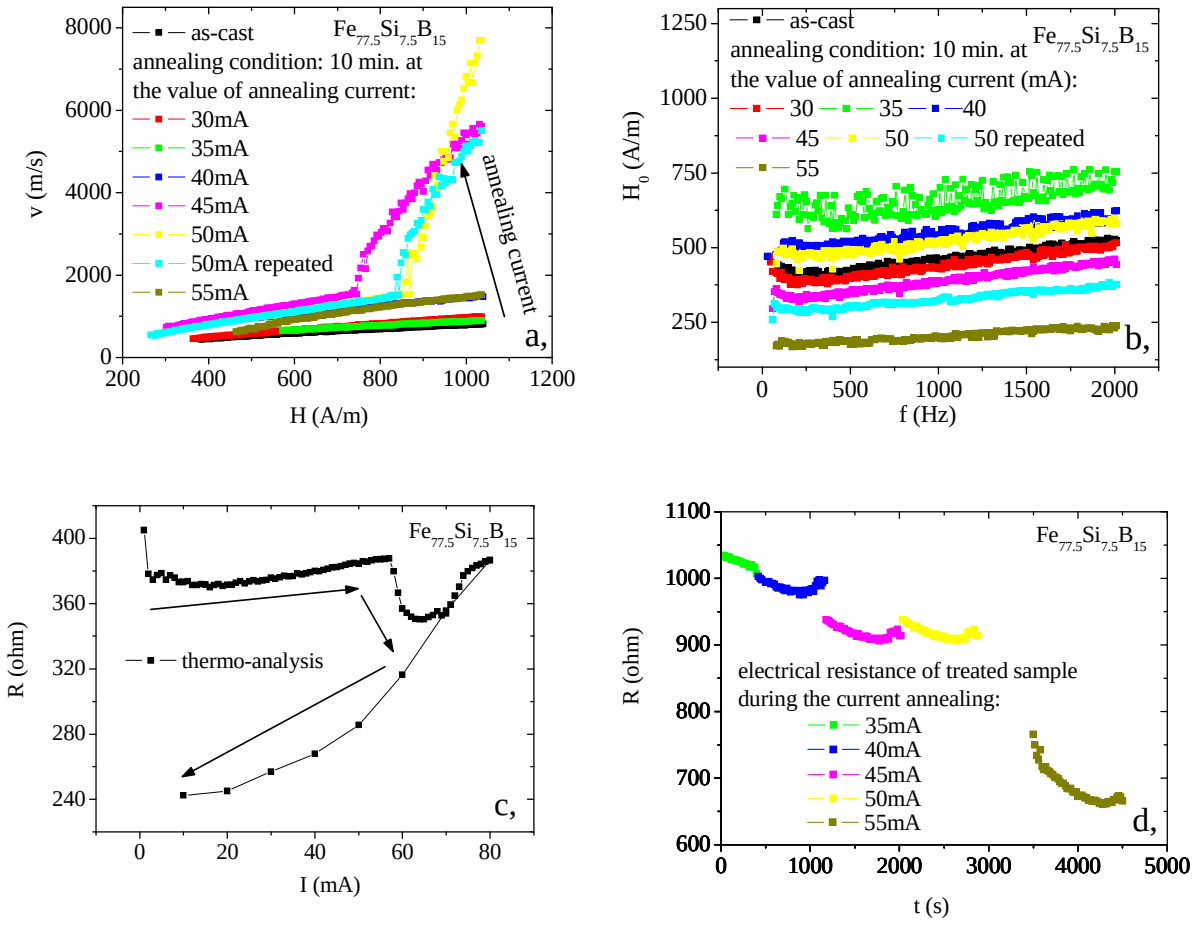

Fig. 71 The Influence of current annealing on domain wall dynamics : (a,) the field dependance of domain wall velocity and (b,) the frequency dependance of critical field of $Fe_{77.5}Si_{7,5}B_{15}$ amorphous glass-coated microwire. (c,) thermo-analysis showing the value of electric current when the crystallization of amorphous state starts to occur. (d,) the time evolution of microwire electrical resistance during the thermal treatment by current annealing.

Fig. 71 shows the magnetic field dependence of domain wall velocity in the same piece of $Fe_{77.5}Si_{7.5}B_{15}$ microwire subjected to the current annealing. Generally, the thermal

treatment increases the domain wall velocity and decreases the switching field. The domain wall velocity in as-cast state is described by linear dependence on applied field in the same way as it was shown in the previous measurements. Thermal treatment at 30mA smoothly decreases the switching field, however the domain wall mobility is not affected significantly. The temperature at the 30 mA current is perhaps not sufficient to perform irreversible changes in amorphous state of the wire. This was possible to observe at the time evolution of electric resistance during annealing (Fig. 71 d,) where the treatment at 30 mA didn't change the resistance remarkably. A similar behavior was observed in section 5.2, where the conventional annealing at 200°C was able to change neither velocity nor switching field.

A higher value of annealing current (35mA) leads to a smooth increase in switching field; however the domain wall mobility seems to be not influenced (Fig. 71). Since the total domain wall damping arises from three contributions (the structural one proportional to the free volumes concentration, the magnetoelastic one proportional to mechanical stress and the eddy-current one proportional to the alloy resistance), it can be expected that treatment at 35mA changed none of this individual contributions. On the other side, switching field increase could be explained within the term of magnetic domain stabilization.

As it is seen in Fig. 71, the remarkable change of domain wall dynamics can be observed if the annealing current exceeds the value of 40mA. The switching field from this point starts to monotonously decrease with current and (in contrary to previous cases) the domain wall mobility increases. Further increase of annealing current leads to appearance of secondary domain wall propagation regime.

As it was noted before, the change of domain wall mobility beyond 40mA can be discussed in terms of the three contributions to the domain wall damping. Thermal treatment leads to removal of the free volumes (that contributes to the decrease of structure relaxation) and to the relaxation of internal stresses (which is responsible for decrease of magnetic relaxation domain wall damping). Simultaneous measurements of electric resistance during current annealing confirm such structural changes (Fig. 71 d,). However, comparing the domain wall velocity in microwires treated by current and by furnace (in conventional way), one may see, that current annealing during 10 min is as effective as the conventional treatment during 1hour. The difference between the current annealing and the conventional treatment may consist in the circular magnetic field that induces additional perpendicular anisotropy via pair ordering during current annealing.

However this effect can be considered to be not so strong in composition containing one transition metal.

Fig. 72 shows the domain wall dynamics in current-treated microwires with composition of $Fe_{49.6}Ni_{27.9}Si_{7.5}B_{15}$ and Fig. 73 the domain wall dynamics of treated $Fe_{42.6}Ni_{34.9}Si_{7.5}B_{15}$ wire.

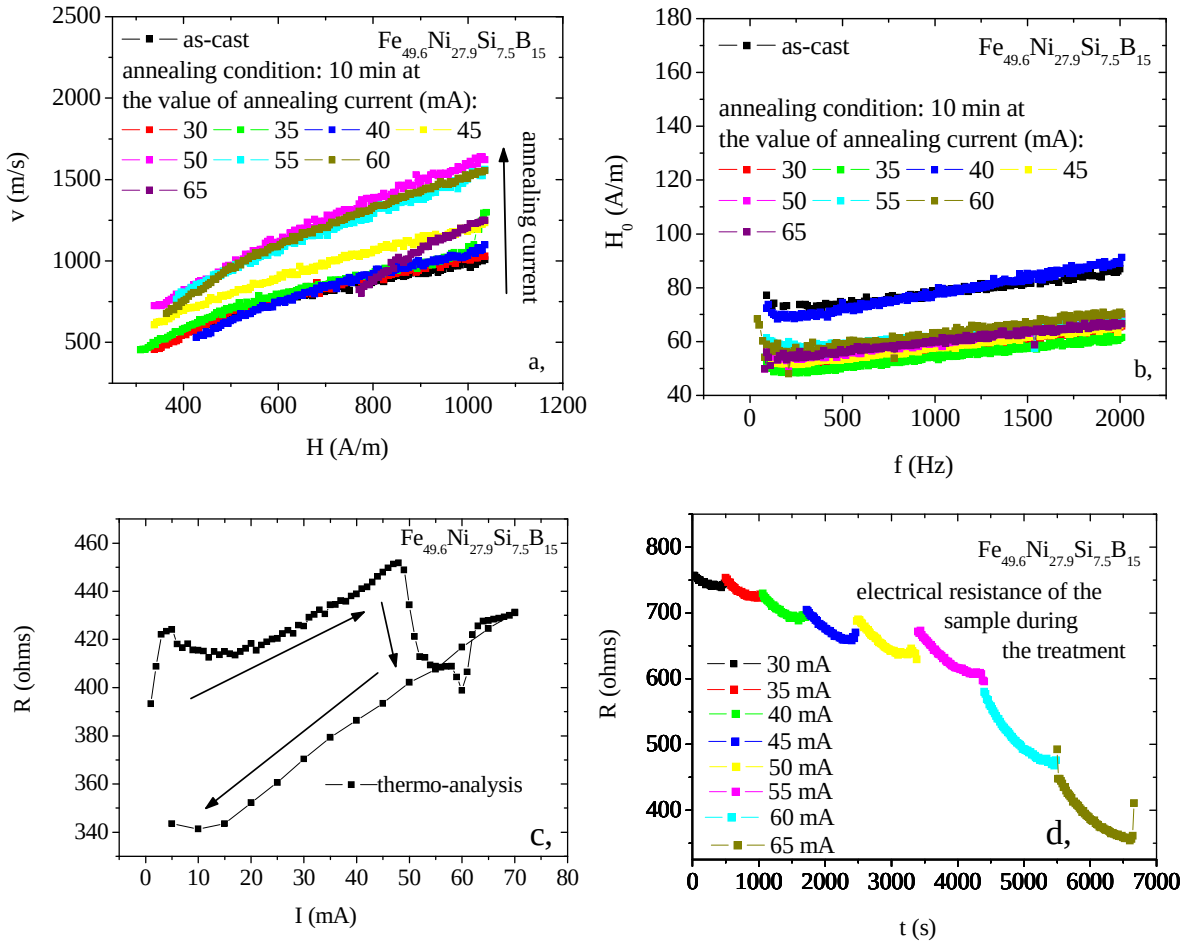

Fig. 72 The Influence of current annealing on domain wall dynamics : (a,) the field dependance of domain wall velocity and (b,) the frequency dependance of critical field of $Fe_{49.6}Ni_{27.9}Si_{7.5}B_{15}$ amorphous glass-coated microwire. (c,) thermo-analysis showing the value of electric current when the crystallization of amorphous state starts to occur. (d,) the time evolution of microwire electrical resistance during the thermal treatment by current annealing.

These samples are characterized by the presence of two transition metals (bi-metal compound), hence the induced perpendicular anisotropy via pair ordering should be higher in these wires.

As it is seen in Fig. 72 the current annealing of $Fe_{49.6}Ni_{27.9}Si_{7.5}B_{15}$ microwire leads to the small domain wall velocity increase from 900 m/s (in as-cast state) to more than 1500 m/s (in the wire annealed at the highest current). As in the previous case, such changes of domain wall mobility can be attributed to the stress relaxation as well as to the reduction of free volumes concentration.

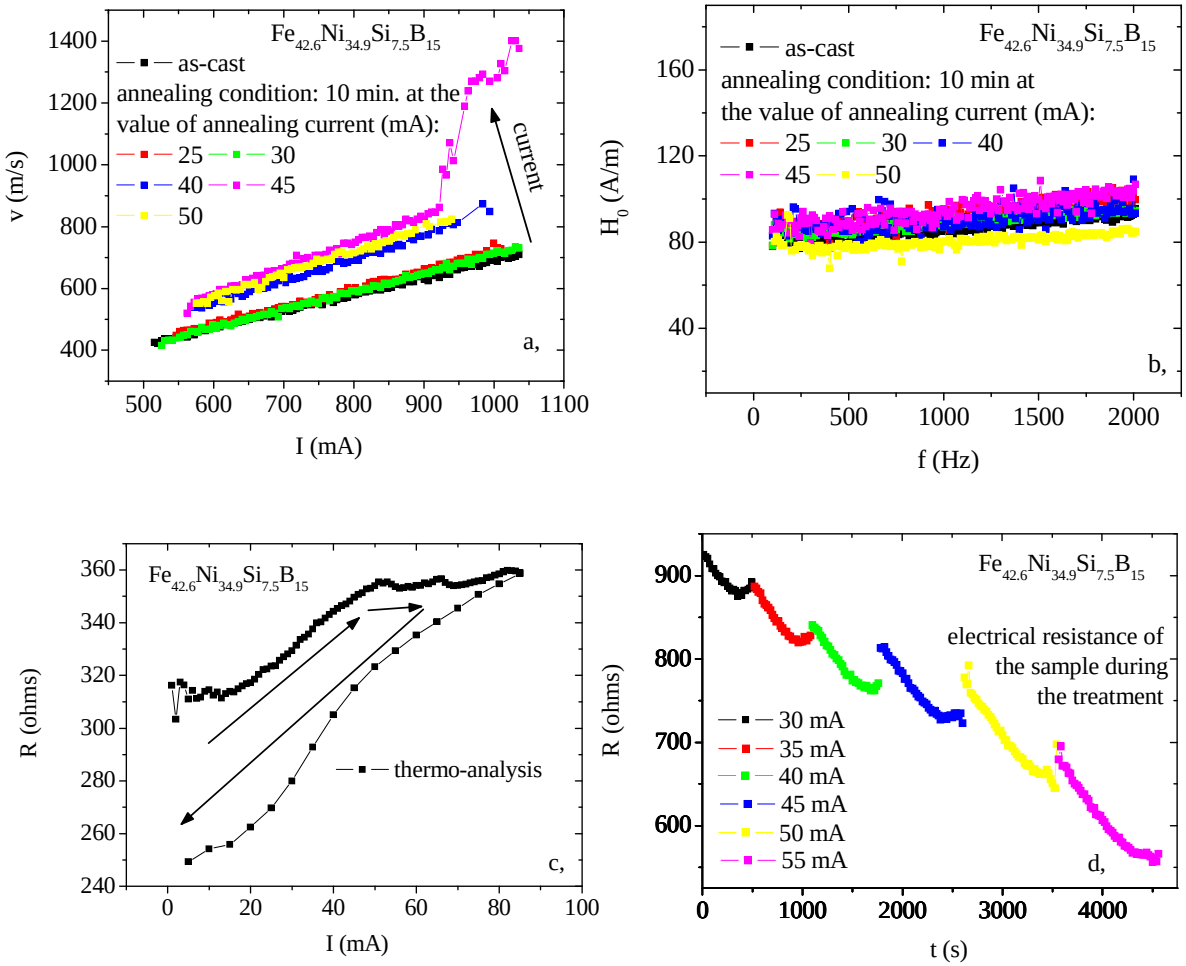

Fig. 73 The Influence of current annealing on domain wall dynamics : (a,) the field dependance of domain wall velocity and (b,) the frequency dependance of critical field of $Fe_{42.6}Ni_{34.9}Si_{7.5}B_{15}$ amorphous glass-coated microwire. (c,) thermo-analysis showing the value of electric current when the crystallization of amorphous state starts to occur. (d,) the time evolution of the microwire electrical resistance during the thermal treatment by current annealing.

The structural changes take place in microwire during the treatment, which is confirmed by the resistance decrease during annealing (Fig. 72 d,). However, one may conclude, that the influence of current annealing on fast domain wall dynamics in this composition is much lower as compared to the previously discussed sample characterized by higher magnetostriction coefficient.

The situation is similar in the last $Fe_{49.6}Ni_{27.9}Si_{7.5}B_{15}$ microwire characterized by the lowest magnetostriction coefficient. The domain wall velocity is modified remarkably but only in the treatment performed at the highest values of current. However, the relative change of velocity is not so high (30 %) in this case. The low sensibility of domain wall dynamics to the current annealing in this composition is confirmed by frequency dependence of switching field (Fig. 73 b,).

Taking into account the above mentioned the influence of current annealing on domain wall dynamics; one may conclude that the lower magnetostriction coefficient of alloy, the weaker effect of current annealing on domain wall dynamics in microwires is observed. It means, the most important effect of such treatment consists in the relaxation and in the redistribution of internal mechanical stresses. Relaxation of internal stresses overcomes the effect of induced circular anisotropy by annealing in Oersted field via pair ordering. This is in a good agreement with the initial estimations, since the effect of induced anisotropy by pair ordering is very weak in comparison to the strong magnetoelastic anisotropy which is typical for microwires.

Chapter 6

Study of the surface domain structure of microwires

The domain wall dynamics in amorphous glass-coated microwires is well-known by very high domain wall velocities, which reach up 10 km/s. Its understanding attracts great attention from the technological as well as from the theoretical point of view. In particular, recently developed spintronic logic devices are based on the transport properties of uniaxial magnetic wires. Speed, at which the domain wall is able to run through the wire, is a key factor that determines the operational rate of these devices. Hence, a big attention is paid to find the mechanisms that allow controlling the domain wall velocity of a given wire.

In previous chapter, the domain wall velocities in thin wire were controlled by tailoring of magnetoelastic anisotropy. Along with geometry of anisotropies, the domain wall dynamics is strongly influenced by surface domain structure, too. Most of recent papers on surface domain structure of microwires were devoted to the study of Co-rich samples with negative (162) or nearly-zero (160) coefficient of magnetostriction. In this kind of wires, the circular domains appear on the surface that makes them promising candidate for sensor applications based on GMI effect (161). In case of highly positive magnetostriction microwires, the situation becomes more complex. According to the magneto-elastic model (81), the domain structure of such wires consists of one large axial domain covered by thin surface of radial and circular domains (Fig. 74). However, it was shown in the previous works that the domain wall velocity can be measured by use of surface MOKE. It means that the domain wall propagating in axial domain interacts with the shell of radial domains and, consequently, the change of surface magnetization occurs as a result of domain wall propagation. Hence a strong influence of the surface domain structure on domain wall propagation can be expected.

Later studies by magneto-optical imaging film (MOIF) on FeSiB microwires (163) confirmed periodic surface domain structure, however its relation to the fast domain wall propagation in microwires is still not so clearly understood.

In this chapter, the study of spontaneous surface magnetization in FeSiB microwires is carried out by two comparative methods: 1, Bitter technique and 2, Magneto-optical observations by polarizing microscope.

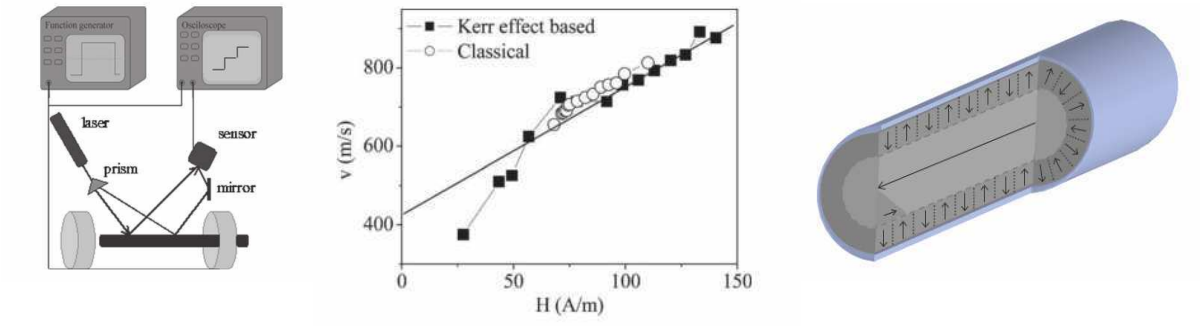

Fig. 74 The domain wall velocity measured by inductive method (two pick-up coils) and by the surface MOKE. Right, the illustration of domain structure of amorphous glass-coated microwire with positive magnetostriction coefficient is shown. Image adopted from (164).

6.1 Imaging the surface domain structure by Bitter colloid

The pieces of amorphous $Fe_{77.5}Si_{7.5}B_{15}$ samples with 2 cm in length were used for these measurements. The glass-coat of microwires has been removed mechanically from the sample. Such glass-removal is usually delicate process, because of additional mechanical stresses that can be introduced to the sample by improper removing technique. For this reason, the glass coat was removed mechanically in several ways (by rolling and by tearing off) and many times at different pieces of sample in order to be sure that surface pattern of Bitter colloid corresponds to the surface domain structure of as-cast sample. The remains of glass dust were cleaned off the metallic core surface by pressured nitrogen. Cleaned sample of microwire was placed on a glass sheet with 100 μm thickness. The optimum colloid concentration was applied to the sample and 1 mm covering glass sheet was placed at the top of examined wire. The metallurgical microscope supplied by D5000 Nikon photo camera was used for the observation. The objective providing magnification of 40x was found to be optimal for this kind of observations.

Fig. 75 compares the Bitter colloid pattern observed at the surface of microwires with various diameters. As it is seen, the surface pattern in each sample consists of bright and dark parts that can be associated with the accumulation of magnetic particles of Bitter colloid to the position of high gradient of stray magnetic field produced by surface domain structure. Due to this, the high values of stray fields can be attributed to the dark parts and vice versa. As it is seen, the sample of biggest diameter (100 μm) is characterized by periodic zigzag domain walls twisting all around the wire (Fig. 75 a,). A similar structure has been observed previously in wires of such diameter (166).

Microwire with reduced diameter of 50 μm doesn't show the zigzag structure; however, it is still possible to observe some kind of periodic inclined domains. At the smallest diameter (15 μm), corresponding to the wires used in domain wall dynamics measurements, the periodic tilting domain structure was observed (Fig. 75 c,). In order to determine the effect of surface domain structure on domain wall dynamics, two parameters were measured: (i) the size of domains (measured as a distance between two bright parts) and (ii) tilting angle of domains (measured with respect to the axis of wire).

It was shown in the previous chapters that the domain wall dynamics of as-cast FeSiB amorphous wires is characteristic by low domain wall mobility (units of $m^2/A.s$) and relatively low domain wall velocity reaching up to 1.5 km/s. Thermal annealing of the samples at 300° C leads to drastic increase of maximum domain wall velocity (up to 4 km/s), which was attributed to the faster domain wall with vortex structure. Despite the high change in domain wall dynamics, the thermal treatment of FeSiB was not sufficient to influence the surface magnetic structure, as it is seen in Tab. 3 (d,).

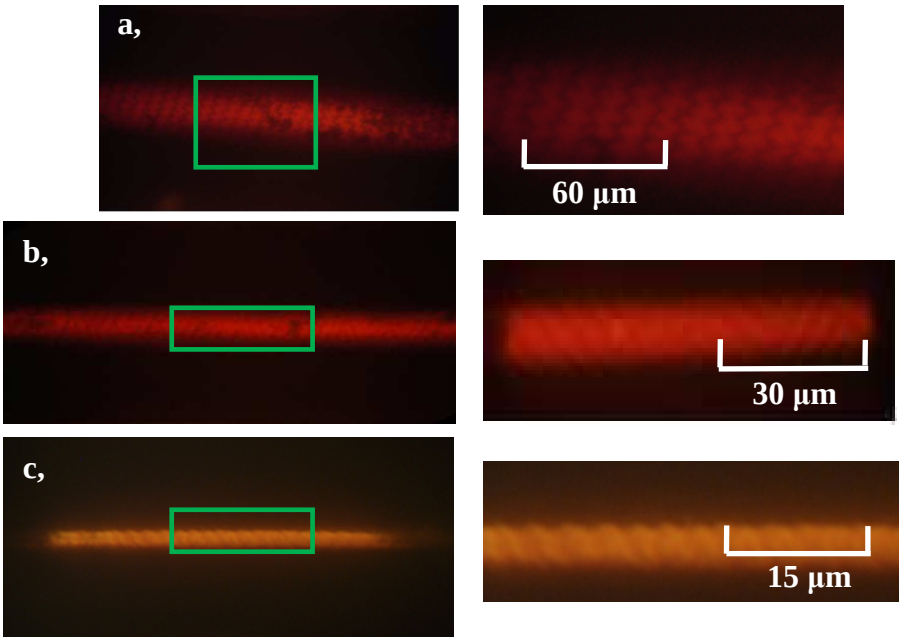

Fig. 75 The surface domain structure of microwires with total diameter of 120um (a), 54um (b) and 30um (c) obtained by Bitter colloid. The green rectangulars depict the position of zoom pictures figured at right side.

The apparent size of surface magnetic domains (4 μm) is the same in both as-cast and thermal treated samples (Tab. 3). Moreover, the tilting angle of surface Bitter pattern is not strongly affected by thermal treatment as well. It proves that the rapid increase in

the domain wall velocity of thermally annealed FeSiB was not result of the change in the surface domain structure. Such assumption was confirmed by the observation of FeNiSiB microwires, too. This kind of sample is characterized by the lower magnetostriction coefficient and by the higher domain wall velocity as compared to that of FeSiB samples. As it is seen in Tab. 3, the Bitter pattern of FeNiSiB microwire is characterized by higher apparent size of domains (from 8 to 11 μm) as compared to FeSiB. However, tilting angle of domains was not changed essentially (from 43° to 46°). The domain wall dynamics of FeNiSiB sample discussed in previous chapter was found to be characterized by the presence of secondary regime (vortex domain wall). Although the thermal treatment increases the size of the domains, the maximum domain wall mobility doesn't seem to be strongly affected by annealing (Tab. 3). This can be explained by additional stresses introduced to the sample during glass-removing. For this reason, the surface domain structure was examined by microscope in the next step.

Sample	treatment	tilting angle	size of domains	max.domain wall mobility
$Fe_{77.5}Si_{7,5}B_{15}$	as-cast	41°	4 μm	1.6 m^2/A.s
	annealed 300° C	43°	4 μm	12 m^2/A.s
$Fe_{49,6}Ni_{27,9}Si_{7,5}B_{15}$	as-cast	43°	8 μm	11 m^2/A.s
	annealed 300° C	46°	11 μm	12 m^2/A.s

Tab. 3 The comparison of domain's size and tilting angles obtained by Bitter colloid. The maximum values of domain wall mobility has been obtained from measurements discussed in previous chapter.

6.2 Surface magneto-optical observations by polarizing microscope

6.2.1 Surface magnetization process of amorphous glass-coated microwires

Classification of the main surface magnetization processes

As it was mentioned above, the amorphous glass-coated microwires are typical by very high residual stresses introduced to the wire during its manufactory process. In accordance to the magneto-elastic model (81), the highest values of stresses should be present in the surface shell of the metallic core due to the close proximity of glass-

coating. This assumption is confirmed by the comparison between the volume and surface hysteresis loops (Fig. 76). The magnetic field was applied in perpendicular direction with respect to the main axis of microwire in both cases. As it is seen, the surface magnetic anisotropy field value (measured by use of MOKE) is very close to value of saturation magnetization measured by MPMS ($H_K = 0.5\ T$). It seems that the magnetic anisotropy reaches the highest values at the top of the metallic core. This is in a good agreement with the calculated internal stress distribution in microwires (81).

Generally, the full surface magnetization process in the amorphous glass-coated microwires in Fig. 76 consists of two parts. At very high magnetic fields, a non-hysteresis rotation of magnetic moments prevails, which results in characteristic linear shape of the loop. However, a small jump can be distinguished at low magnetic fields. As it was noted above, such jump was previously attributed to the internal domain wall propagation. If the domain wall propagation is blocked by two small coils at the wire ends, (hence, no internal domain wall propagation occurs), the surface magnetization jump in surface MOKE disappears.

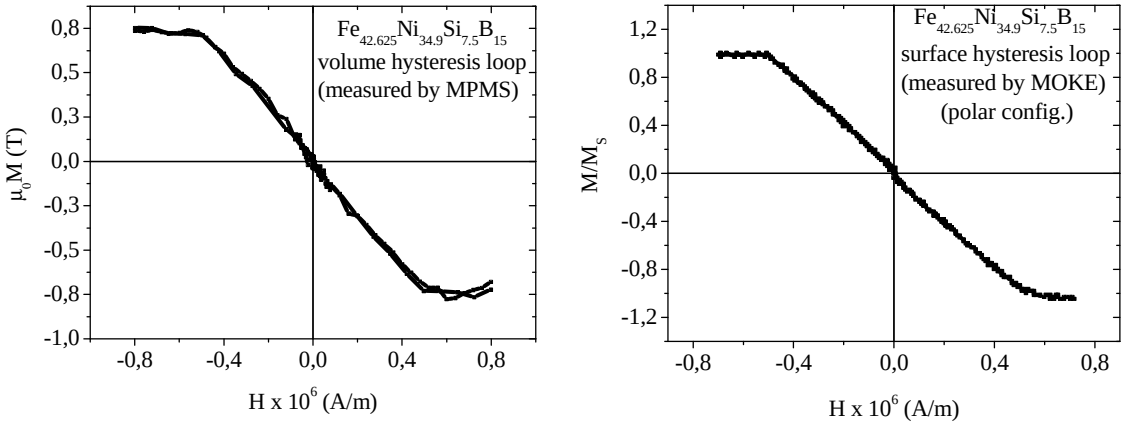

Fig. 76 Comparison of the volume (left) and surface (right) hysteresis loop of FeNiSiB amorphous glass-coated microwire. The magnetic field direction was perpendicularly oriented to the microwire axis in both measurements.

For this reason, two magnetization processes (a) magnetization rotation due to externally applied magnetic field and (b) the surface magnetization change due to the internal domain wall propagation must be distinguished in our study.

The specific optical properties of amorphous glass-coated microwires are given by two factors: 1, the presence of the glass coat at the core surface and 2, the cylindrical shape of observed sample. The influence of glass coat on microwire optical properties was briefly discussed in chapter 4. It was shown that the undesirable high glass-coating

reflectivity can be suppressed by proper selected conditions of observation (p-polarized light used in the experiment, the optimal angle of incidence equal to Brewster angle, at which the total glass transmission of the p-polarized light occurs, therefore the glass coat doesn't contribute to the amount of reflected light) or by use of immersion oil.
However, the second problem related to the cylindrical shape of the sample is not so easy to avoid. Fig. 78 compares the intensity profiles of the light reflected from microwire surface for two cases (a) without use of analyzer and (b) with crossed polarizer and analyzer. As it is seen, the highest intensity of reflected light is obtained at the top of wire (see the case without analyzer). For this reason, the two light strips that can be observed with crossed polarizer and analyzer (in right column of Fig. 78) cannot be explained in term of polarizers imperfections. On the other hand, the plane of polarization or ellipticity (or both) must be changed significantly by the reflection from metallic core in order to produce the light stripes without magnetic state change Fig. 78.
A detail explanation of this phenomenon is proposed in the next section. However, it is important to note that the magnetic contrast (contrast which appears as a result of surface magnetization change) could be detected by the light intensity change of these two stripes only.

6.2.2 Optical observation of the sample of cylindrical geometry

Assume a cylindrical metallic sample oriented along the x axis with the incident light along the main axis of the cylinder (Fig. 77).

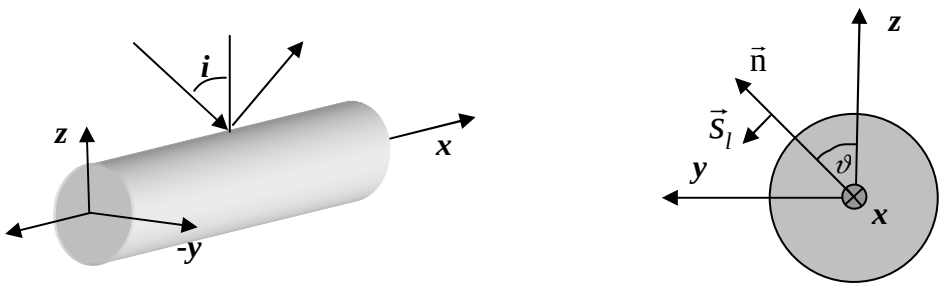

Fig. 77 Description of the geometric parameters used in the calculation.

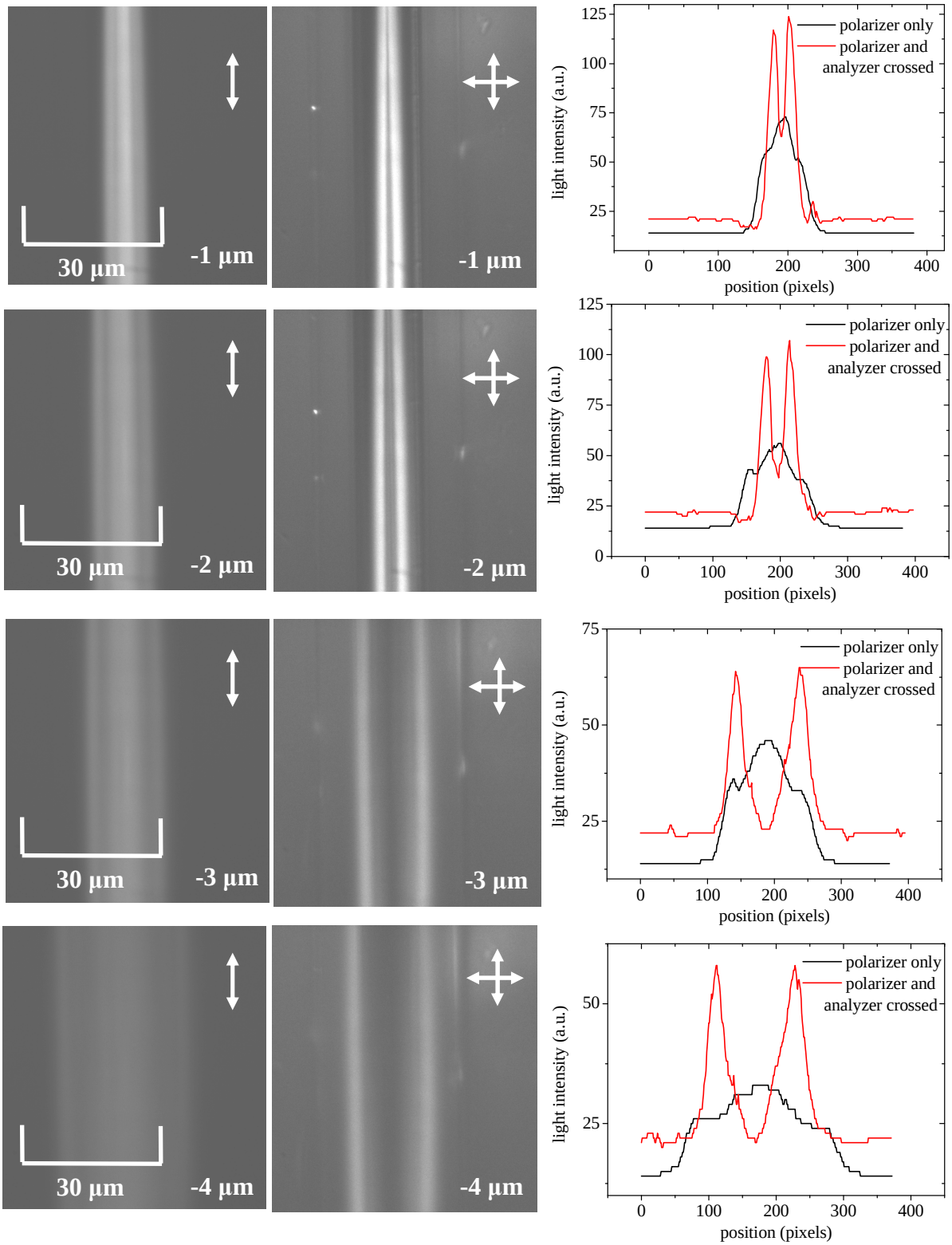

Fig. 78 The intensity profile of light reflected from cylindrical surface of $Fe_{77.5}Si_{7,5}B_{15}$ amorphous glass-coated microwire for different focusing depths. The left column shows the optical image of microwires observed by polarized light, whereas the right column compares the images obtained by use of crossed polarizer and analyzer. Right graphs right compare the number of maxima in both profiles. Note, the scale of light intensity values differs from those obtained without analyzer. Mutual inclination of two light stripes is given by non-horizontal position of the sample. Samples were observed by use of immersion oil. Focusing depth z = 0 was chosen at the top of glass-coating.

Suppose that the incident light beam consists of parallel rays only, which is the good assumption for laser beam. The geometry is then fully described by two parameters. First of them is incident angle *i*, which is constant for all rays. The second parameter, angle ϑ defines the position on the cylinder surface, being $\vartheta=0$ for cylinder top and $\vartheta>0$ for left side of cylinder (Fig. 77, right picture) and vice versa. The main goal is to evaluate the light intensity profile for the case of crossed polarizer and analyzer.

The incident ray is described by incident vector $\vec{i}$ *:*

$$\vec{i} = \begin{pmatrix} \sin i \\ 0 \\ -\cos i \end{pmatrix} \tag{120}$$

which has the same orientation for all rays in the beam. The normal to the cylindrical sample can be obtained (Fig. 77):

$$\vec{n} = \begin{pmatrix} 0 \\ \sin \vartheta \\ \cos \vartheta \end{pmatrix} \tag{121}$$

The plane of incidence is defined by two vectors: (i) normal $\vec{n}$ and (ii) incident vector $\vec{i}$. It means that the direction of the plane of incidence is not constant for each ray on the cylinder, because of the ϑ angle dependence on normal $\vec{n}$. This is important result because it shows that even if the cylinder is illuminated by linearly polarized light, the mutual orientation of the oscillating electric vector $\vec{E}$ (which defines the direction of linear polarization) and the plane of the incidence is not constant for each position on the cylinder surface. As the angle ϑ increases, the oscillating electric field intensity vector is more out-of perpendicular direction with respect to the plain of incidence for s-polarization. The reflected rays have the plane of polarization, which is neither perpendicular nor parallel to the plane of incidence (as the angle ϑ increases). For this reason, it is useful to distinguish two components of linear polarization; the component of linear polarization which is perpendicular to the local plane of incidence (local s-polarization) and the component of linear polarization which is parallel to the local plane of incidence (local p- polarization).

The (normalized) component of polarization which is oriented perpendicularly to the plane of incidence (local s-polarization) has a direction given by:

$$\vec{s}_l = \frac{1}{\sqrt{\sin^2\vartheta + \cos^2\vartheta \sin^2 i}} \begin{pmatrix} -\sin\vartheta\cos i \\ \cos\vartheta\sin i \\ -\sin\vartheta\sin i \end{pmatrix} \tag{122}$$

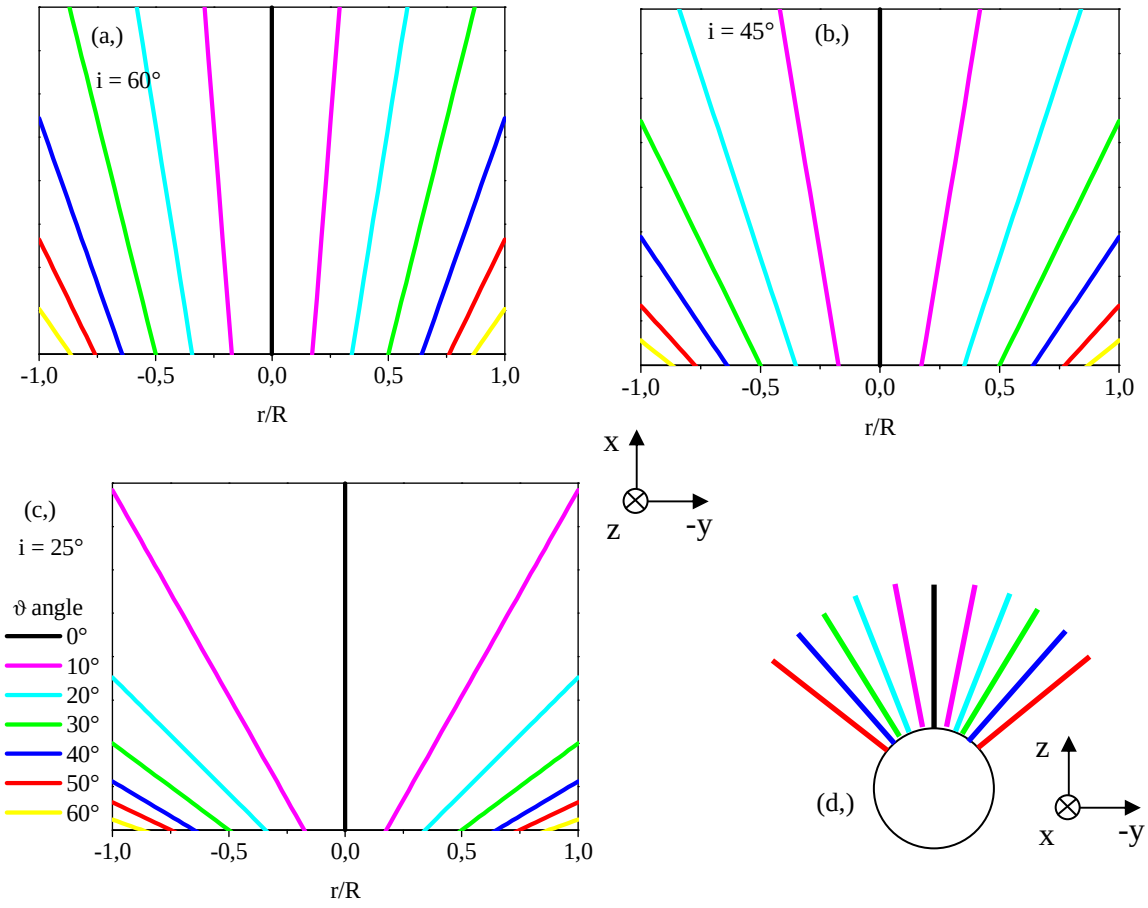

Fig. 79 The plane of incidence has not constant orientation for each ray reflected from a cylindrical surface. Figures (a,) (b,) and (c,) compares the plane of incidence orientation in xy plane. It is calculated from the *x* and *y* components of eq. (122) and (123). The effect of cylindrical surface seems to disappear progressively as the incidence angle *i* increases. However, the opposite is true, because the plane of incidence in not perpendicular to the yz plane but additional inclination in yz plane (d,) must be taken into account. As it will be shown later lines for the angle $\vartheta = 60°$ are not reflected back to the objective plane.

whereas the component of polarization which is parallel to the plane of incidence (local p-polarization) is defined by the direction that can be obtained from $\vec{p}_l = \vec{i} \times \vec{s}_l$, which yields:

$$\vec{p}_l = \frac{1}{\sqrt{\sin^2\vartheta + \cos^2\vartheta \sin^2 i}} \begin{pmatrix} \cos\vartheta \sin i \cos i \\ \sin\vartheta \\ \cos\vartheta \sin^2 i \end{pmatrix} \tag{123}$$

Hence, even the “s” or “p” linearly polarized light is used for measurements; the resulting magnetic contrast consists of the Kerr-effect of locally s-polarized and locally p-polarized contributions. For “s” polarized incident light beam one may obtain:

$$\vec{S} = \begin{pmatrix} 0 \\ 1 \\ 0 \end{pmatrix} = \frac{\cos\vartheta \sin i\, \vec{s}_l + \sin\vartheta\, \vec{\mathrm{p}}_1}{\sqrt{\sin^2\vartheta + \cos^2\vartheta \sin^2 i}} \tag{124}$$

And for “p”polarized incident light beam:

$$\vec{P} = \begin{pmatrix} \cos i \\ 0 \\ \sin i \end{pmatrix} = \frac{-\sin\vartheta\, \vec{s}_l + \cos\vartheta \sin \mathrm{i}\, \vec{\mathrm{p}}_1}{\sqrt{\sin^2\vartheta + \cos^2\vartheta \sin^2 i}} \tag{125}$$

The amplitude of the light transmitted by crossed polarizer and analyzer is defined as a product of multiplication (for “s” polarized incident light):

$$A_{SP} = \vec{P}.\vec{\vec{R}}.\vec{S} \tag{126}$$

And vice-versa for “p” polarized incident light beam:

$$A_{PS} = \vec{S}.\vec{\vec{R}}.\vec{P} \tag{127}$$

where $\vec{\vec{R}}$ denotes the reflection matrix which consists of Fresnel coefficients. For non-magnetic sample (the Voigt parameter is zero, hence, the off-diagonal components R_{SP} and R_{PS} of reflection matrix $\vec{\vec{R}}$ can be neglected) the light intensity profile for crossed polarizer and analyzer can be obtained in the form:

$$A_{PS} = A_{SP} = \frac{\sin\vartheta\cos\vartheta\sin i_1}{\sin^2\vartheta + \cos^2\vartheta\sin^2 i}(R_{PP} - R_{SS}) \tag{128}$$

The intensity of reflected light for the case without analyzer (and for "s" polarized incident light) is given by:

$$\vec{\vec{R}}\vec{S} = \frac{\cos\vartheta\sin i\, R_{SS}\vec{s}_l + R_{PP}\sin\vartheta\,\vec{p}_1}{\sqrt{\sin^2\vartheta + \cos^2\vartheta\sin^2 i}} \tag{129}$$

$$I_S = \left|\vec{\vec{R}}\vec{S}\right|^2 = \frac{\left|R_{PP}\right|^2\sin^2\vartheta + \left|R_{SS}\right|^2\cos^2\vartheta\sin^2 i}{\sin^2\vartheta + \cos^2\vartheta\sin^2 i} \tag{130}$$

The plot of intensity profile for non-magnetic sample for two cases (a) without polarizer and (b) crossed polarizer and analyzer (b) is shown in Fig. 80.

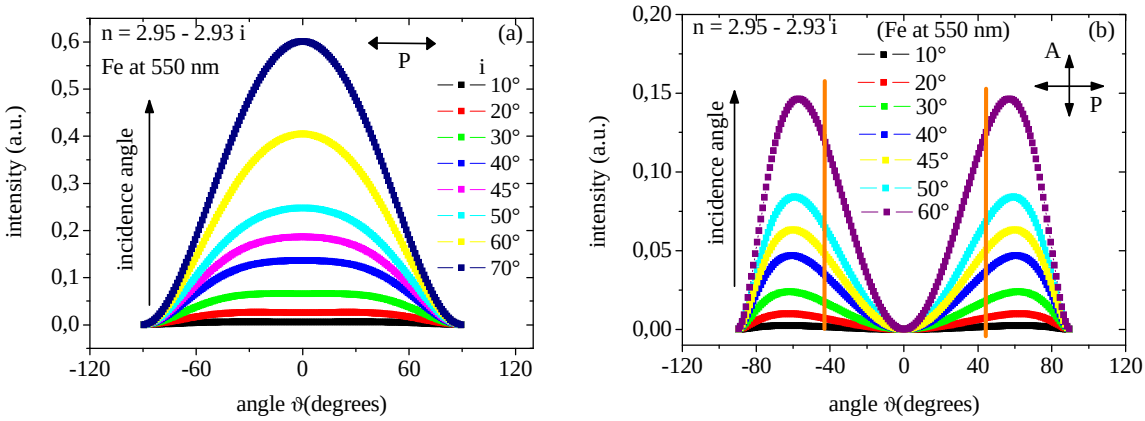

Fig. 80 The calculated intensity profiles for non-magnetic cylindrical surface without analyzer (a) and with crossed analyzer and polarizer (b). The profiles are calculated for incident angle $i = 45°$. Orange vertical lines denote the maximum angle of ϑ at which the surface of cylinder can be observed by microscope. However, this limitation is not valid for laser-based MOKE, where detector can positioned.

As it is seen in Fig. 80 (a) the maximum light intensity without analyzer is achieved at the top of cylinder (angle $\vartheta = 0°$) for each incident angle i. As ϑ angle increases, the intensity decreases because the more scattered rays by curved surface of cylinder and drops to zero at $90°$ ($0°$). In contrary, the reflected light intensity profile for crossed polarizer and analyzer is characterized by two maxima as it can be seen in Fig. 80. Such calculated profile can be explained as follows. Assume the (globally) s-polarized incident light. The oscillating electric field intensity vector is perpendicular to the plane of incidence at the top of the wire only ($\vartheta = 0°$). As the angle ϑ increases, the global polarization doesn't correspond to the local polarization and a strong ellipticity is

introduced to the ray, which produces a non-zero light transmitted by analyzer. On the other hand, the field intensity vector of (globally) s-polarized light is parallel to the plane of incidence at the wire boundary defined by angle $\vartheta = 90°$. Situation is qualitatively the same for a p-polarized light. The oscillating electric field intensity vector is parallel to the plane of incidence at the wire top. However, the (globally) p-polarization corresponds to the local s-polarization for the ray reflected from the wire boundary ($\vartheta = 90°$). For this reason, the reflected light intensity profile of cylinder consists of two sharp maxima due to the strong ellipticity introduced by local polarization, which is neither ”s” nor “p” out of (i) the top and (ii) boundary of the wire. As it is seen at Fig. 80, the relative change in the intensity due to the cylindrical shape increases with incident angle, but the position of both maxima is more or less constant ($\vartheta = \pm 60°$). Apparently, such calculated light intensity profile describes well the observed data on microwires shown in Fig. 78 where two maxima appeared with crossed polarizer and analyzer.

In order to calculate the intensity profile for the reflection from magnetic cylinder, the same equations (eq. 126) (eq. 127) are considered, however the non-zero Voigt constant must be taken into account in this case. Then, the off-diagonal components of the reflection matrix $\ddot{R}$ are not zero. The components of reflection matrix $\ddot{R}$ were taken in the form (167):

$$R_{SS} = \frac{\cos\vartheta_i - \hat{n}\cos\vartheta_r}{\hat{n}\cos\vartheta_r + \cos\vartheta_i} \tag{131}$$

$$R_{SP} = \frac{-iQ\sin\vartheta_i\cos\vartheta_i m_l}{(\hat{n}\cos\vartheta_r + \cos\vartheta_i)\cos\vartheta_r(\cos\vartheta_r + \hat{n}\cos\vartheta_i)} \tag{132}$$

$$R_{PP} = \frac{\cos\vartheta_r - \hat{n}\cos\vartheta_i}{\cos\vartheta_r + \hat{n}\cos\vartheta_i} + \frac{2iQn\cos\vartheta_i\sin\vartheta_r}{(\cos\vartheta_r + \hat{n}\cos\vartheta_i)^2} m_s \tag{133}$$

$$R_{PS} = R_{PS} \tag{134}$$

where ϑ_i is incident angle and ϑ_r the angle of refraction. Both angles are measured relative to the normal of cylinder. Index of refraction is denoted by $\hat{n}$. Fig. 81 A compares the light intensity profiles $I_{SP}(-M)$ and $I_{SP}(M)$ corresponding to the cylinder magnetized in both axial directions. As it is seen, the magnetic interaction results in very small change in the light intensity (the highest difference can be observed close to

the maxima). However, such difference is the function of magnetization at the cylinder surface. Fig. 81 shows the difference $I_{SP}(M)$- $I_{SP}(-M)$ which corresponds to the change in the intensity as a result of axial magnetization reversal.

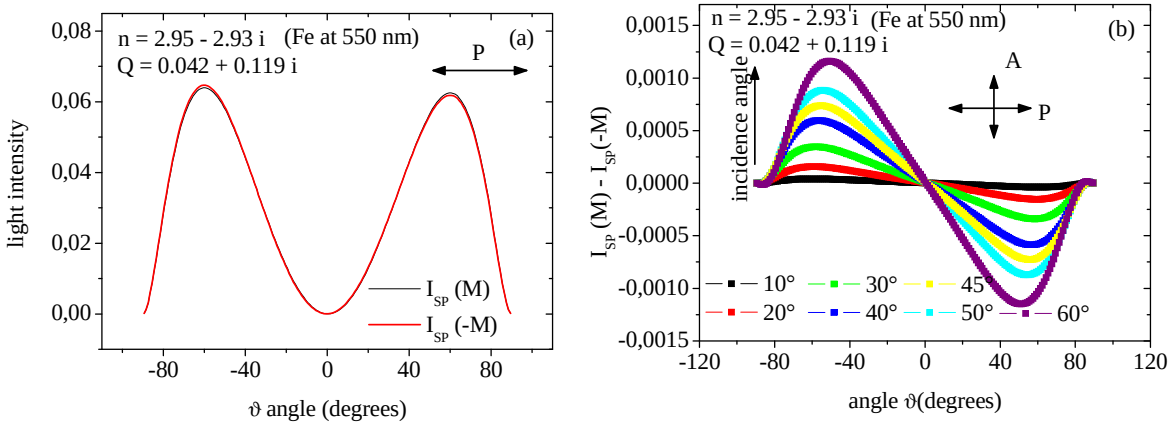

Fig. 81 A The intensity profile of light reflected from cylinder magnetized in axial direction (left). Change in the light intensity profile that occurs during the reversal (right). Curves are calculated for the incident angle value of i = 45°.

As it is seen, the intensity increases for the negative values of ϑ angle (left side of cylinder), whereas the intensity decreases for another side of cylinder (positive values of ϑ angle). Such curves describe well the black-and-white magnetic contrast that was observed in case of microwires. This observation will be treated more detailed in the next section.

6.2.3 Comparison with the experiment

In order to compare the light intensity profile calculated in previous section with the real magneto-optical observation on microwires made by microscope, the additional assumptions must be taken into account, which is discussed briefly in this section.

Microscope observations

As it was noted at the beginning of previous chapter, the calculation of light intensity profiles was done for the simple case when incident light beam consists of parallel rays and the influence of objective was not included. However, the real observation by microscope introduces more factors that must be taken into account. For example, not all rays scattered from cylindrical surface can be seen in microscope as a result of variable value of numerical aperture across the angle ϑ. The maximum angle ϑ for

which the beam can be reflected back to the objective is given by numerical aperture *NA*:

$$NA = \sqrt{\sin_i^2 + \sin^2 2\vartheta \cos_i^2} \qquad (135)$$

Fig. 81 B shows plot of the numerical aperture for incident angle of i = 45°. As it is seen, the light ray is reflected back to the objective plane for values of angle ϑ <45°.

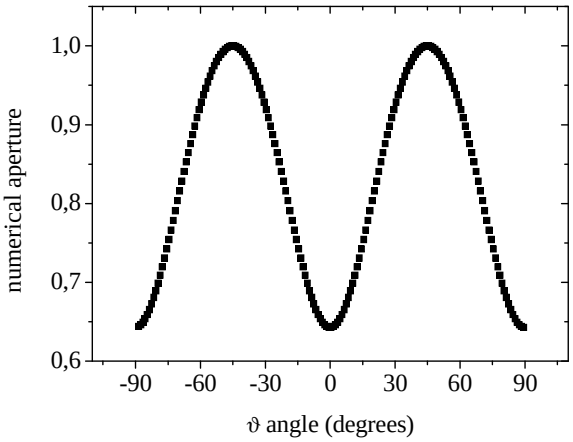

Fig. 81 B Plot of the numerical aperture as a function of ϑ angle on the cylindrical surface. The calculation is done for incident angle if *i = 45°*.

Another important feature of objective that must be considered is the focus depth. As it was shown in the Fig. 78, the distance of two light stripes observed with crossed polarizer and analyzer is function of the focus depth.

If the microscope is focused at the metallic core top (zero focus depth), only one light stripe can be observed. When microscope is focused deeper, two light stripes appear and the distance between them progressively increases with focus depth (Fig. 78). However, the calculation of the light intensity profiles gives the position of maxima almost constant (around ϑ = 60°). In order to find the value of focus depth at which the best agreement of the model with experiment occurs, the light intensity profiles of microwire were compared for three conditions: (i) for the p-polarized incident light (without analyzer) (Fig. 82 (a,)) (ii) for a crossed polarized and analyzer when the objective is focused below the metallic core (Fig. 82 (b,)) (iii) for crossed polarized and analyzer when objective focused above the glass-coat (Fig. 82 (c,)).

Amorphous glass-coated microwires consist of two cylinders from the optical point of view. The first cylindrical surface corresponds to the metallic core. The second cylindrical surface is formed by glass-coat, that cannot be completely neglected even the immersion oil is used during the measurements. This is confirmed indirectly by light

intensity profiles measured with crossed polarized and analyzer (Fig. 82 (b,) and (c,)) where intensity doesn't drop to zero at the top of wire *(ϑ = 0°)*.

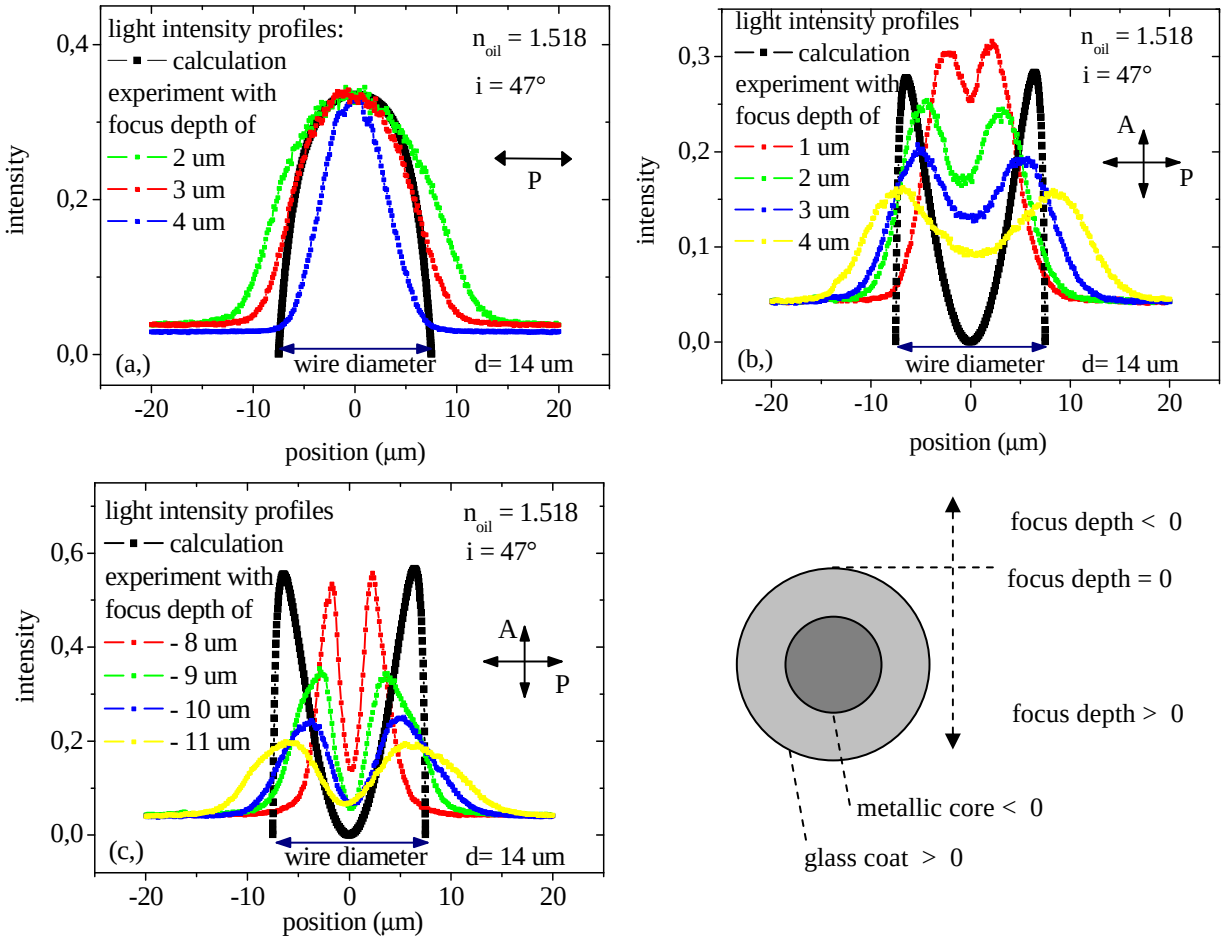

Fig. 82 The calculated light intensity profile comparison with experiment for various experimental conditions: (a,) for (globally) p-polarized light without analyzer (b,) for incident (of globally) p-polarized light with crossed polarizer and analyzer when microscope was focused below the metallic core surface (positive values of focus depth) and (c,) for the same conditions but negative focus depth (above the metallic core surface). The profiles are calculated for incident angle *i = 47°*. Calculated curves were multiplied by factor sin ϑ, as it gives the amount of incident light per unit wire surface.

If the microscope is focused below the metallic core surface (positive values of focus depth in Fig. 82 (b,)), the effect of glass-coat disappears partially. However, the measured light intensity profile is wider than the wire diameter in each case. The same result was obtained qualitatively in the case without analyzer (Fig. 82 (a,)).

6.2.4 Study of the surface magnetization change invoked by the internal domain wall propagation in microwires

As it was noted above, the domain wall propagation was found to be responsible for the surface magnetization change that occurs at small magnetic fields. In order to study this effect, the microwire was switched in first (axial) direction and the change of the corresponding surface domain structure was detected when microwire was reversed. This change in the surface domain structure (before and after reversal) was obtained by digital image processing technique. In order to avoid the strong Faraday effect of glass-coat and objective, the study of the surface magnetization change due to the internal domain wall propagation was done in a series of following steps:

1, microwire under investigation was switched by axial magnetic field in the first direction, then the field was reduced to zero and background image was taken (Fig. 83 (a,)).
2, the background image was subtracted from live image in the second step. The wire was reversed by an opposite magnetic field, and then the field was reduced to zero.
3, magnetic contrast was obtained by software averaging of the accumulated images.

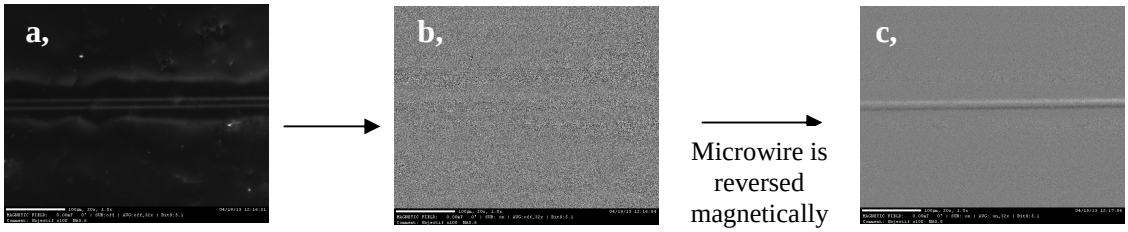

Fig. 83 The magnetic contrast corresponding to the surface magnetization change that occurs as a result of internal domain wall propagation in microwire was obtained by digital image processing that consists of three steps. All images are observed by crossed polarizer and analyzer.

It is worth mentioning that the image which results from this process corresponds to the change of surface domain structure that occurs by the domain wall propagation during reversal rather than to the surface domain structure in remanent state (Fig. 83).
Within the study, the surface magnetization change by domain wall propagation was found to be different (a,) in the central part of the wire (above the axial domain) and (b,)

close to the ends of microwire (due to the closure domain structure presence). For this reason, these two cases were investigated separately.

Study of the surface magnetization change above the axial domain

As it can be recognized in Fig. 84 and Fig. 86 the digital image processing revealed a magnetic contrast consisting of two parallel black and white stripes in all studied samples above the axial domain. Moreover, the position of black and white stripes was found to be dependant on the initial configuration of microwire: if the background image is taken when microwire is switched to first direction, the resulting magnetic contrast is opposite as compared to the case when background image is taken when microwire is switched to opposite direction. Fig. 84 also shows that the magnetic (black and white) contrast on microwires doesn't depend on the configuration of microscope. The same contrast is obtained if the oblique incident light (Fig. 84 (a,) (b,)) or normal incident light (Fig. 84 (c,)) at the different sample orientation (Fig. 84 (d,)) is used for observation. Moreover, the magnetic contrast was found to be independent on the direction of incident light beam at the longitudinal configuration of microscope (Fig. 84 (a,) and (b,)).

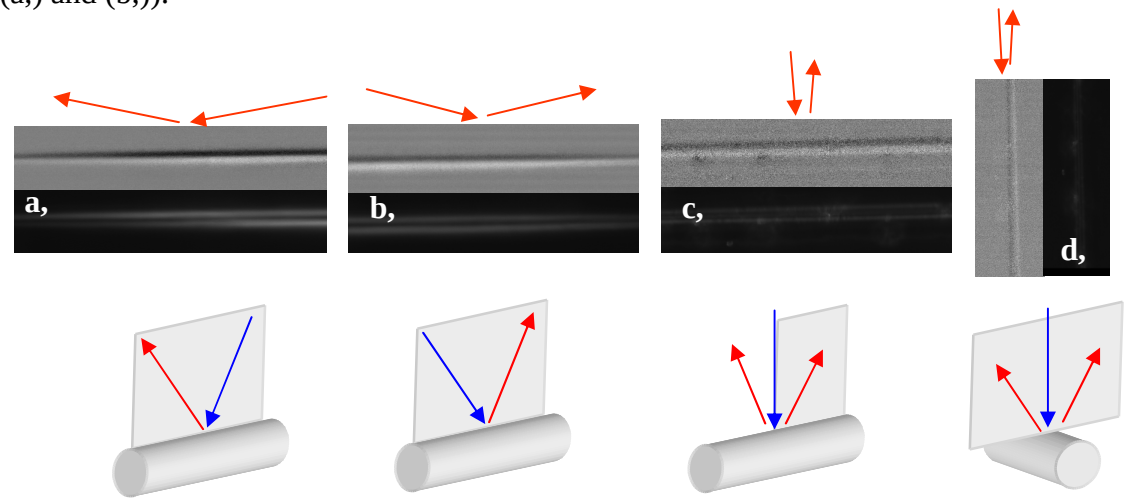

Fig. 84 The magnetic contrast at the surface of amorphous glass-coated $Fe_{49,6}Ni_{27,9}Si_{7,5}B_{15}$ microwire obtained by magneto-optic Kerr effect in longitudinal (a), (b), and polar (c), (d) configuration of microscope. The pictures at the bottom shows the orientation of the plane of incidence for the ray inciding at the wire top. The mutual orientation of incident beam (blue arrow) and reflected beam (red arrows) with respect to the plane of polarization and microwire is illustrated at the bottom.

However, it is well know from the theory, that the longitudinal Kerr effect is odd function of incident angle (it is proportional to *sin i*). This proves that the resulting

magnetic contrast is determined by the sample shape rather than by configuration of microscope (normal incident light for polar Kerr-effect and inclined for longitudinal Kerr-effect with respect to the wire axis). As it was noted above, the presence of black and white contrast at the sample of cylindrical geometry can be attributed to the change in the axial component of spontaneous magnetization at the wire surface. It seems, that the domain wall propagating in the axial domain changes the surface structure of the shell of domains in the way where the axial component of surface magnetization changes. The experimental observation that the magnetic (black and white) contrast doesn't change with the orientation of the incident light (Fig. 84 (a,) and (b,)) can be explained qualitatively as follows. The transverse Kerr-effect is proportional to the transverse component of magnetization change with respect to the plane of incidence. As it was noted above, the planes of incidence at the cylinder surface are characterized by oblique orientation with respect to the main axis. Fig. 85 compares the directions of the transverse components (red arrows) of the same axial magnetization change (blue arrow) for two directions of incident light: (i) antiparallel to the $\Delta\vec{M}$ (figure left) and (ii) parallel to the $\Delta\vec{M}$ (figure right). As it is seen, even if the direction of the axial magnetization change is the same; the transverse projection of axial magnetization change is maintained for both directions of incident light.

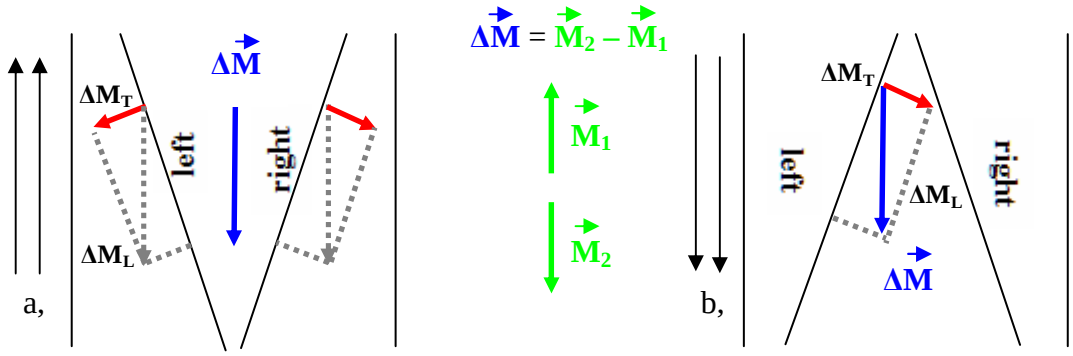

Fig. 85 The magnetic contrast at the surface of cylinder can be found to be independant on the direction of incident light. Figure (a,) shows the mutual orientation of the plane of incidence and the transverse components (red arrows) of the axial magnetization change (blue arrows). Figure (b,) right shows the same but for opposite direction of incident light. Direction of the incidence light is figured by double arrow.

The same magnetic contrast consisting of two black and white parts was observed in all samples under the investigation. Fig. 86 compares the surface magnetic contrast

invoked by internal domain wall propagation in three types of microwires characterized by different surface domain shell thickness.

Composition	Max. domain wall velocity	Estimated thickness of the surface shell of domains (122)
$Fe_{77.5}Si_{7.5}B_{15}$	1.5 km/s	< 100 nm
$Fe_{49.6}Ni_{27.9}Si_{7.5}B_{15}$	6 km/s	~ 150 nm
$Fe_{42.6}Ni_{34.9}Si_{7.5}B_{15}$	10 km/s	~ 500 nm

As it is seen, the as-cast $Fe_{77.5}Si_{7.5}B_{15}$ amorphous glass-coated microwire characterized by thin surface domain structure (<100 nm) (122) showed (Fig. 86 (a,)) a big change in the surface magnetization direction during the domain wall propagation.

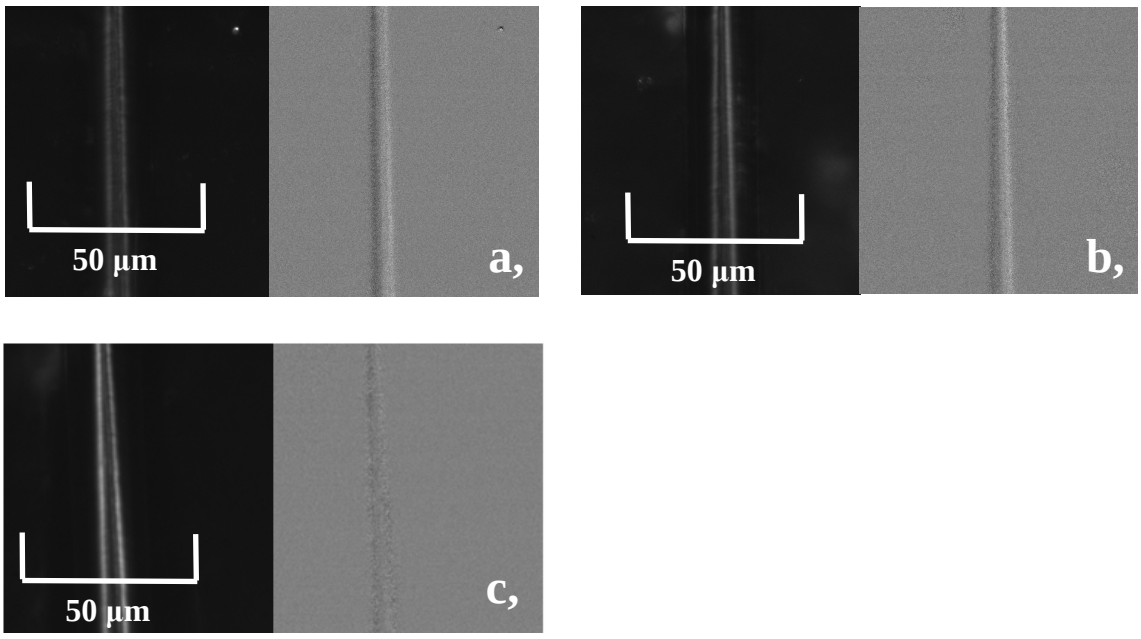

Fig. 86 The change of the surface domain structure invoked by internal domain wall propagation. The images were done above the axial domain of (a,) $Fe_{77.5}Si_{7.5}B_{15}$ (b,) $Fe_{49.6}Ni_{27.9}Si_{7.5}B_{15}$ and (c,) $Fe_{42.6}Ni_{34.9}Si_{7.5}B_{15}$.amorphous glass-coated microwires characterized by different thickness of surface shell of domains (see tab. in the text).

On the other hand, the interaction of the propagating domain wall with the shell of surface structure was not observed in the $Fe_{42.6}Ni_{34.9}Si_{7.5}B_{15}$ microwires characterized by thicker shell of surface domains. The above result can be explained by different interaction of propagating domain wall with the surface magnetization. Domain wall is able to reverse the surface shell magnetization direction in case of $Fe_{77.5}Si_{7.5}B_{15}$

microwire, because of the low thickness of surface shell of domain and vice versa for the sample of thicker surface shell of domains ($Fe_{42.6}Ni_{34.9}Si_{7.5}B_{15}$ Fig. 86 (c,)).

It is important to note that the sample with very fast domain wall propagation ($Fe_{42.6}Ni_{34.9}Si_{7.5}B_{15}$ Fig. 86 (c,)) displays no change in the surface magnetization direction and vice versa for the sample of slow domain wall ($Fe_{77.5}Si_{7.5}B_{15}$ Fig. 86 (a,)). This confirms that the presence of the surface shell of magnetic domains may play an important role on fast domain wall propagation in microwires.

Another contribution to the different magnetic contrast (Fig. 86 (a) – (c)) can be found in the much smaller magneto-optical effect of Ni as compared to Fe. Hence, the magnetic contrast decrease with nickel content can be attributed to the smaller magneto-optical effect of FeNiSiB alloy too. However, this cannot explain fully the almost vanished magnetic contrast of $Fe_{42.6}Ni_{34.9}Si_{7.5}B_{15}$ alloy, where the nickel content is almost the same as that of iron.

Study of the surface magnetization change above closure domain structure

The magnetic contrast obtained close to the ends of microwire differs remarkably from that discussed in previous section (in the central part of microwire). It consists of two black and white stripes as previously; however, one may recognize the progressive disappearance of the contrast as the end of wire is approached.

Fig. 87 shows the magnetic contrast of $Fe_{77.5}Si_{7.5}B_{15}$ microwire. As it is seen, the application of magnetic field parallel to the axial magnetization direction results in the suppression of the closure domain. As the magnetic field increases, the domain wall is pushed closer to the end of wire. Note, the closure domain structure is not removed fully even if the magnetic field of highest value (0.18 T) is applied (Fig. 87 (a,)). The magnetic field applied in opposite direction (Fig. 87 (d,)) results in the Large Barkhaussen jump (Fig. 87 (d,)).

The magnetic contrast is opposite here as compared to the previous case (white – black as compared to the black-white contrast, see Fig. 87 (a,) and (d,)). Such change can be attributed to the opposite change in the axial magnetization that occurs (i) above the axial domain and (ii) closure domain. The length of the closure domain in remanent state was found in this composition to be around 100 μm. A more complex magnetic contrast above the closure domain structure was found in $Fe_{49.6}Ni_{27.9}Si_{7.5}B_{15}$ microwire (Fig. 88). The apparent length of closure domain reached more than 1 cm in this case. Moreover, the magnetic contrast obtained as a difference between two remanent states

of microwire is characterized by small parts where no change in surface magnetization direction occurs.

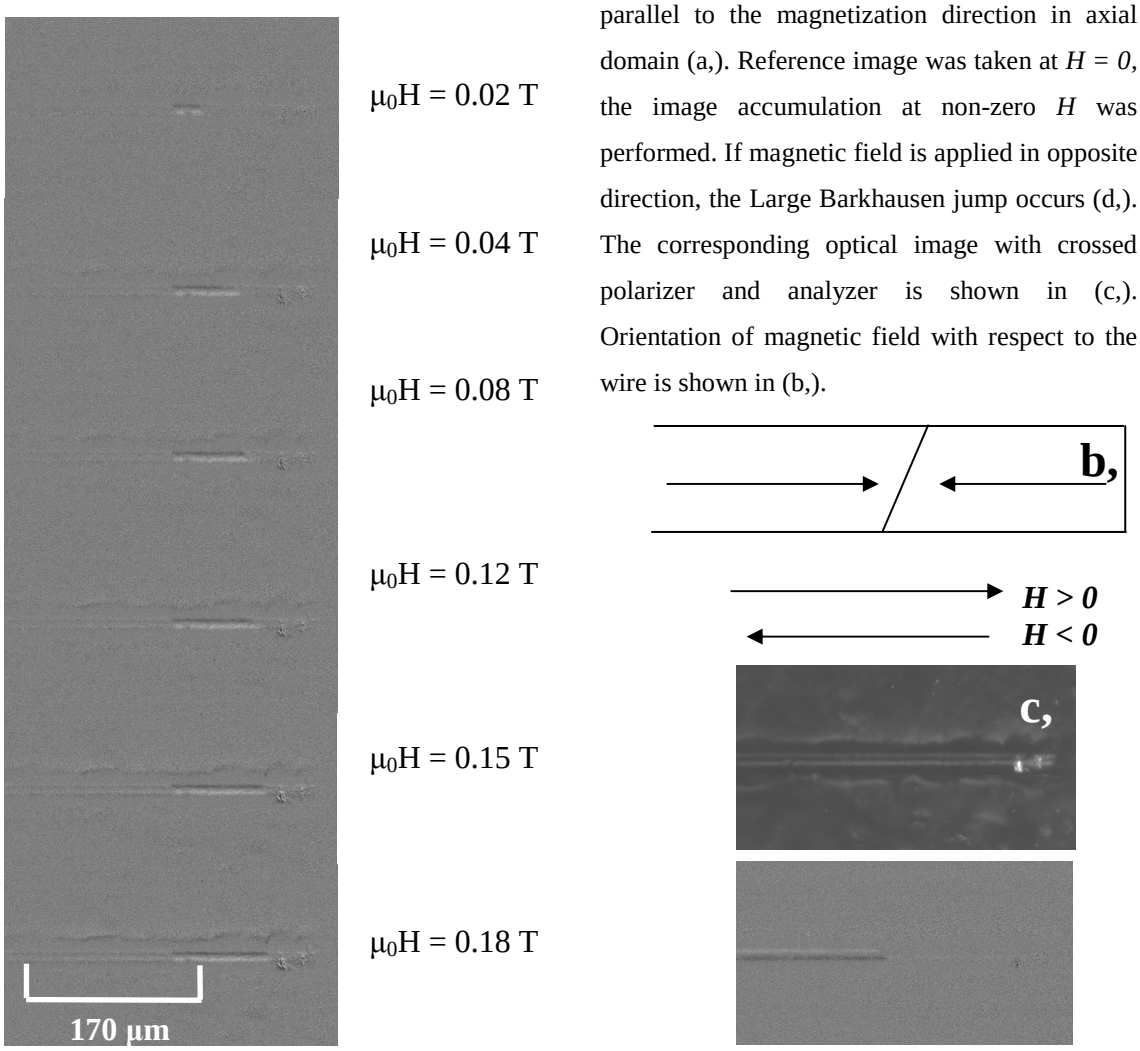

Fig. 87 Suppression of the closure domain structure by application of magnetic field oriented parallel to the magnetization direction in axial domain (a,). Reference image was taken at $H = 0$, the image accumulation at non-zero H was performed. If magnetic field is applied in opposite direction, the Large Barkhausen jump occurs (d,). The corresponding optical image with crossed polarizer and analyzer is shown in (c,). Orientation of magnetic field with respect to the wire is shown in (b,).

A more detailed study is necessary to confirm the shape of closure structure that would be able to produce such magnetic contrast. However, application of magnetic field oriented parallel to the axial magnetization resulted to the progressive disappearance of the closure structure (as it was observed in the previous case).

One possible explanation of such complex structure of closure domain can be found in the introduction of mechanical stresses during the microwire cutting by scissors. Note that the structure of closure domain in the last composition ($Fe_{42.6}Ni_{34.9}Si_{7.5}B_{15}$) could not be detected from the same reason as it was discussed in previous section (probably due to the big thickness of surface shell of domains).

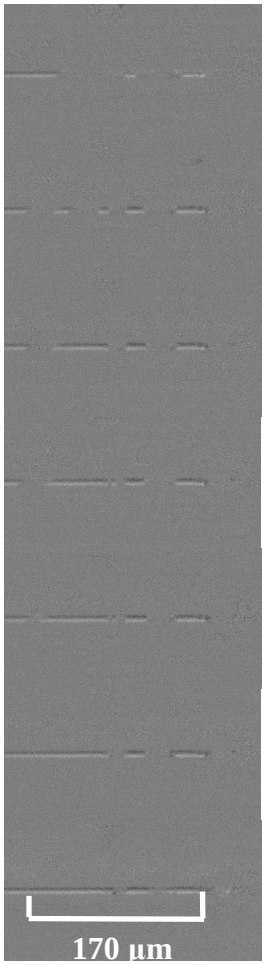

Fig. 88 Magnetic contrast which was obtained above the closure domain structure of $Fe_{49.6}Ni_{27.9}Si_{7.5}B_{15}$ amorphous glass-coated microwire. The magnetic contrast was obtained as the difference between two remanent states of microwire: (i) where the axial domain is switched to the one and (ii) to the opposite direction. Schematic drawing (b,) shows the orientation of magnetic field with respect to the wire.

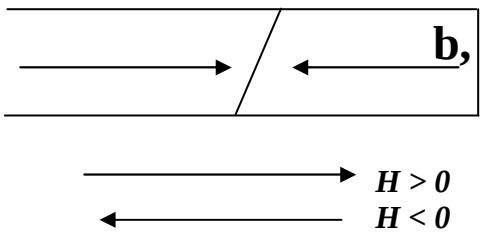

6.2.5 Non-hysteretic surface magnetization rotation

It was found in the previous section that the internal domain wall propagation (above the axial domain and above the closure structure too) leads to the surface magnetization process that can be registered as a black and white contrast by difference image processing. As it was noted above, such magnetic contrast can be interpreted as a change in the axial component of surface magnetization in the case of the sample of cylindrical geometry. However, the surface domain structure is still not so clear. In order to understand better the direction of surface magnetization, the hysteresis loops in high axial magnetic field were measured in the next step.

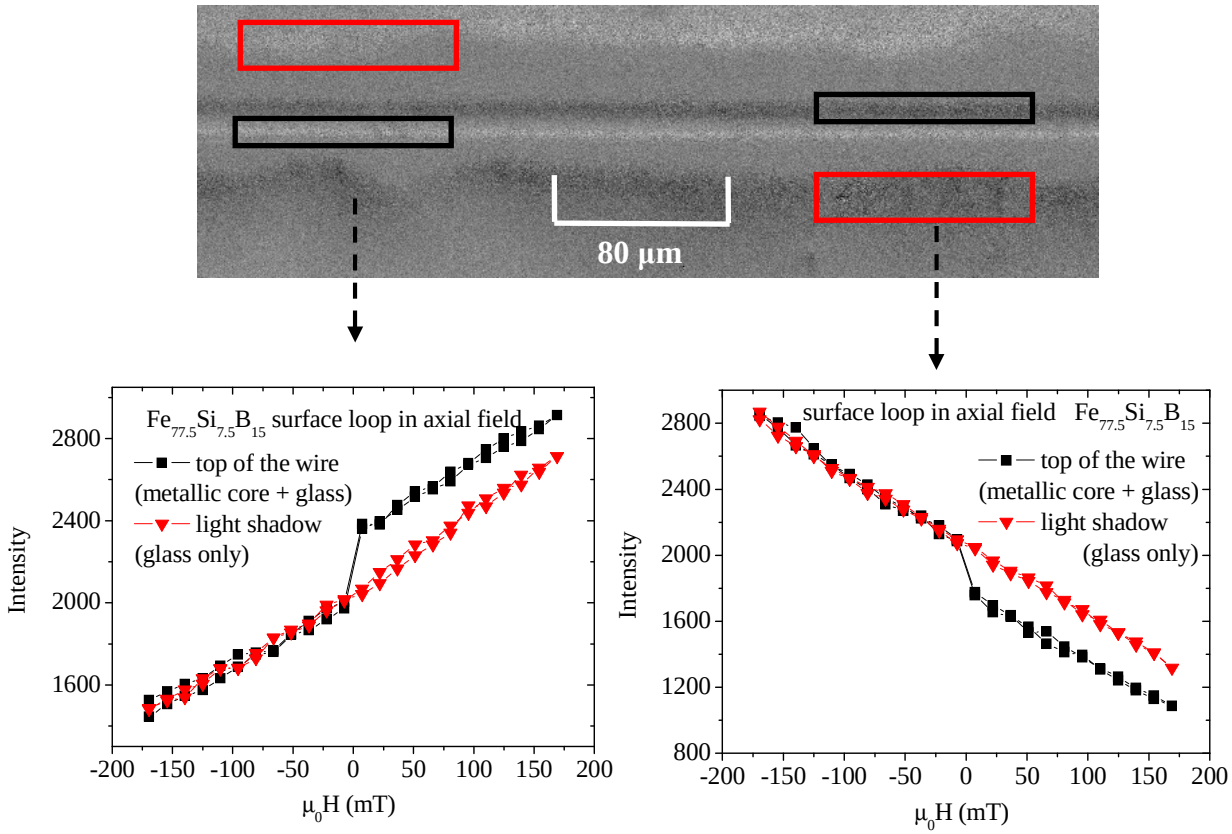

Fig. 89 The surface hysteresis loops of $Fe_{77.5}Si_{7.5}B_{15}$ microwire measured in high axial magnetic field (up to 0.2 T). The region of interest that corresponds to hysteresis loops is depicted by the same colour in the top picture. The magnetic contrast was obtained at the focus depth of 5 µm.

As it was noted in section 6.2.1, the surface of microwires is characterized by very high value of magnetic anisotropy. The application of high magnetic field to the sample introduces many undesired phenomena, namely Faraday effect of glass coat as well as the Faraday effect of objective used for observations. Such effect rotates the polarization plane of incident light that can obscure the true Kerr rotation produced by surface magnetization change.

Fig. 89 shows the surface hysteresis loops measured in high magnetic field (up to 0.2 T) oriented along the main axis of $Fe_{77.5}Si_{7.5}B_{15}$ microwire. The surface hysteresis loops were measured for the black and the white part of the resulting magnetic contrast separately (black curves in the Fig. 89). These hysteresis loops were measured at the top of the wire, where both Farady effect of glass-coat and Kerr-effect of metallic core must be considered. The hysteresis loops depicted by red curves are measured at the light shadows that can be recognized far away from the microwire border.

As it is seen, the surface magnetization process at the top of the wire (black curves) consists of the apparent magnetization rotation at high magnetic field and small jump that appears at low values of magnetic field (which was attributed to the internal domain wall propagation above). However, the hysteresis loops measured at the light shadows are characterized by the rotation of the same slope, but the low-field jump is missing here. One of possible explanation is that the light shadows observed far away from microwire are formed by primary light reflected from glass-coat. Hence, the corresponding hysteresis loops (depicted by red colours) are background proportional to the Faraday effect of glass coat only. If this assumption is accepted, it means that there is no change in the surface magnetization direction if the axial magnetic field is applied to the wire. Then it means that the surface domain structure of the surface shell of domains is given by the axial component of magnetization only. Or, even simpler, there is no surface shell of domains and the axial domain can be seen directly. This allows observing the surface domain wall structure in microwire directly, which is discussed in the next section.

The optical image of the same pieces of microwires (made by microscope with crossed polarizer and analyzer) is shown in Fig. 90.

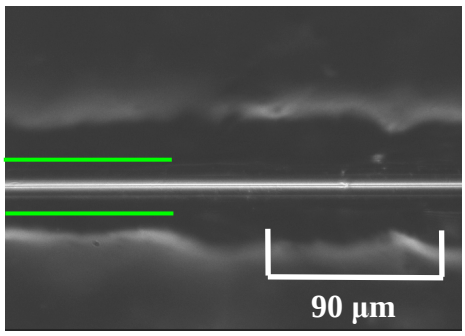

Fig. 90 Optical image of $Fe_{77.5}Si_{7.5}B_{15}$ microwire made by crossed polarizer and analyzer. The boundary of glass-coat is marked by green lines.

Microscope is focused at the boundary between the metallic core and glass-coat in this case in order to see that the position of light shadows is far away from the microwire. Another important fact is that the light shadows disappear when the microwire was observed by use of immersion oil (which reduces the light primary reflected from glass-coat).

Figure 91 shows the surface hysteresis loops measured in the same way, but for different composition ($Fe_{49.6}Ni_{27.9}Si_{7.5}B_{15}$) of microwires. The size of low-field magnetization jump (invoked by internal domain wall propagation) is much smaller as compared to the previous case. The slope of hysteresis loops measured at the light shadow is close to that at the wire top. However, the agreement is not as remarkable as it was in high iron content sample.

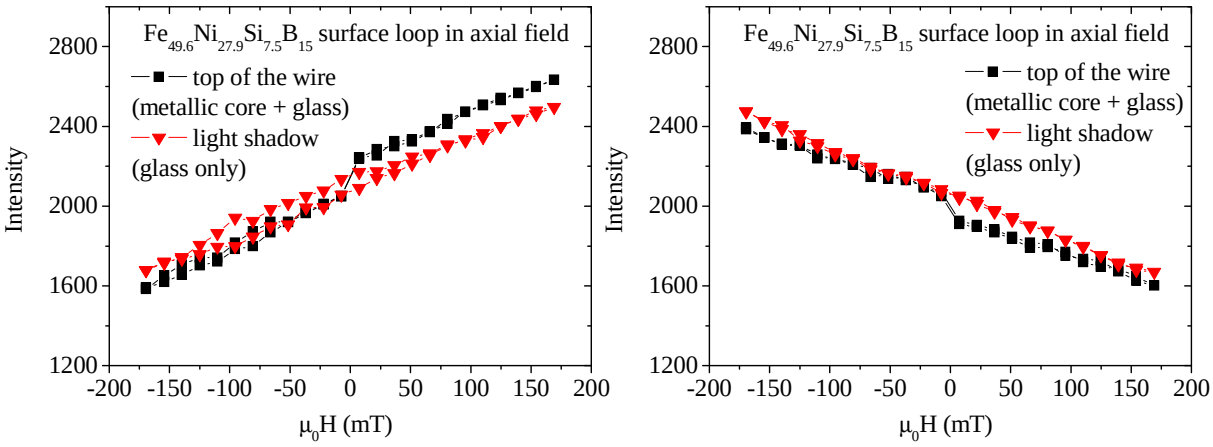

Fig. 91 The surface hysteresis loops of $Fe_{49.6}Ni_{27.9}Si_{7.5}B_{15}$ microwire measured in high axial magnetic field (up to 0.2 T). The region of interest that corresponds to hysteresis loops is depicted by the same colour in the top picture.

Such observed result may be explained by the presence of surface shell. However, more data are needed to conclude the surface structure.

The axial hysteresis loops of third composition (with the highest nickel content) are shown in Fig. 92. As it was noted above, this composition is characterized by very small intensity of (black and white) magnetic contrast (see the images in previous section). One can recognize the same behavior here. A small jump in the surface magnetization invoked by the internal domain wall propagation cannot be recognized in both hysteresis loops. Moreover, the slope of hysteresis loops measured at the light shadows is very noisy in order to subtract it from resulting hysteresis loops measured at the top of the wire.

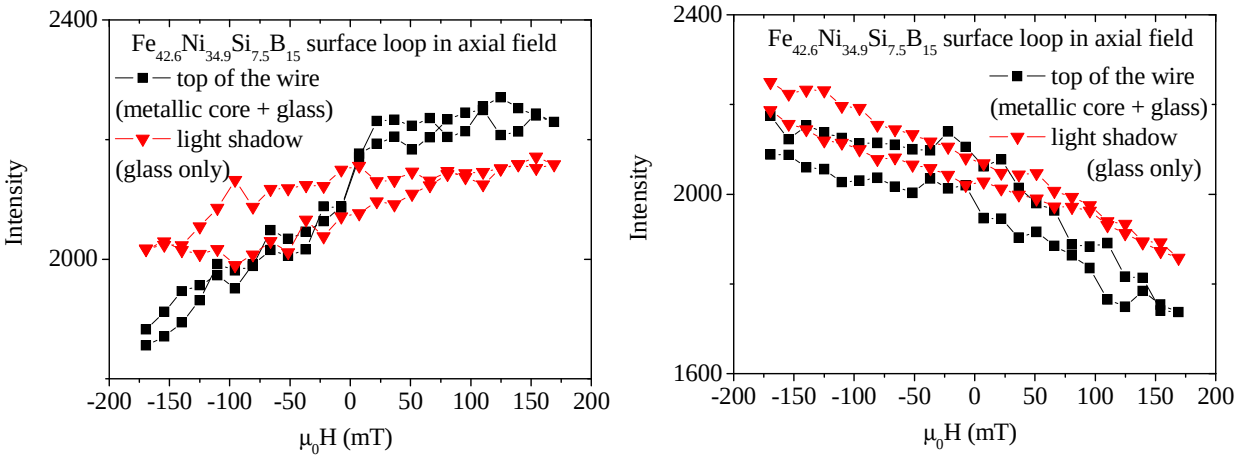

Fig. 92 The surface hysteresis loops of $Fe_{42.6}Ni_{34.9}Si_{7.5}B_{15}$ microwire measured in high axial magnetic field (up to 0.2 T).

6.2.6 The domain wall trapping in a potential well

As it was noted above, the main surface reversal process is related to the domain wall propagation in the axial domain at low magnetic field in microwires. It means that the boundary between two axial domains (domain wall) could be seen directly too. In order to study the surface structure of the domain wall, the domain wall was trapped in a potential well. In fact, this was done by two comparative experiments.

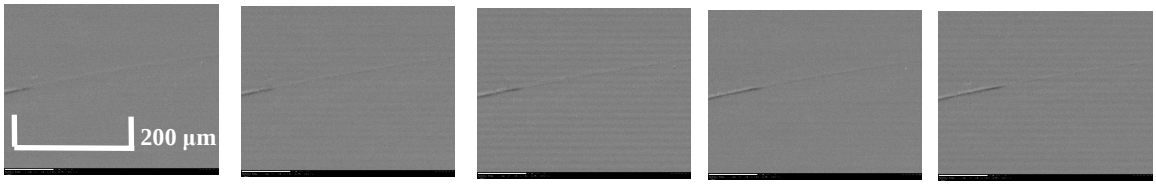

Fig. 93 Images showing the domain wall at different position in bent $Fe_{77.5}Si_{7.5}B_{15}$ amorphous glass-coated microwire. The images were captured in static mode using different orientations of the magnetic field.

The microwire under investigation was bent to the shape of “U” letter within the first approach. The position of the domain wall was controlled by rotating in-plane magnetic field (Fig. 93). The magnetic contrast was performed as a difference between two states: (i) remanent state at zero magnetic field and (ii) state with applied magnetic field, where domain was kicked-out from the wire end (Fig. 94). Such a way of domain wall trapping was used in previous experiments with nanowires (174). However, the

advantage of microwires consists in the presence of the closure structure, so that a domain wall does not have to be created artificially here.

Fig. 94 b, shows the zoomed detail of the boundary between two domains from Fig. 93. As it is seen, the change of contrast between two domains is not abrupt, but one may observe a continuous white part of magnetic contrast disappearance in a total length of 70 μm. Such tilted surface domain wall structure could be attributed to the tilted domain wall, which was previously predicted for glass-coated microwires (175-177). However, this is one of the first direct observations that confirms such hypothesis.

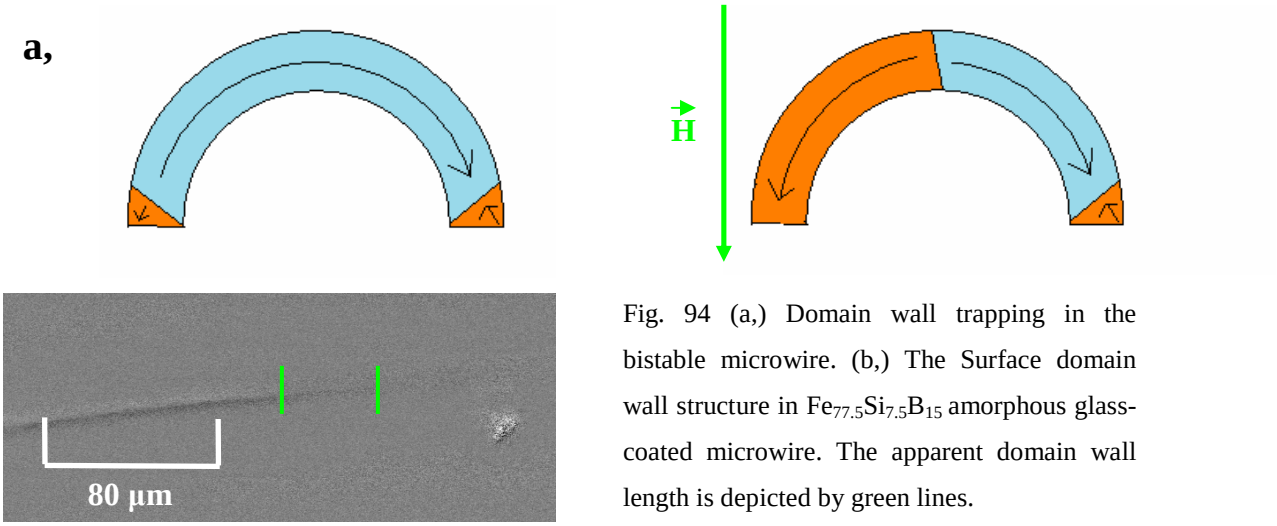

Fig. 94 (a,) Domain wall trapping in the bistable microwire. (b,) The Surface domain wall structure in $Fe_{77.5}Si_{7.5}B_{15}$ amorphous glass-coated microwire. The apparent domain wall length is depicted by green lines.

The surface domain wall length was measured in a following way: firstly, the light intensity profile of the black and white magnetic contrast was determined by use of graphic processor. Next, the intensity value of the gray part of the image (corresponding to the background) was measured far away from microwire. The surface domain wall length was measured as a distance at which the value of magnetic black and white contrast drops to the value of the background intensity.

As it is seen in Fig. 95, increase in the magnetic field intensity results in the domain wall compression. Such observed result may be explained by Zeeman interaction of domain wall (or magnetic domains) with external field. Note, despite the observed surface, the internal structure of the domain wall cannot be identified from such surface observation. For this reason, the corresponding images are treated as *"surface domain wall structure"* in the following text.

One disadvantage of such observation method is that the domain wall is not under zero magnetic fields during the observation. As it can be recognized (Fig. 95), the external magnetic field strongly influences the surface domain wall length.

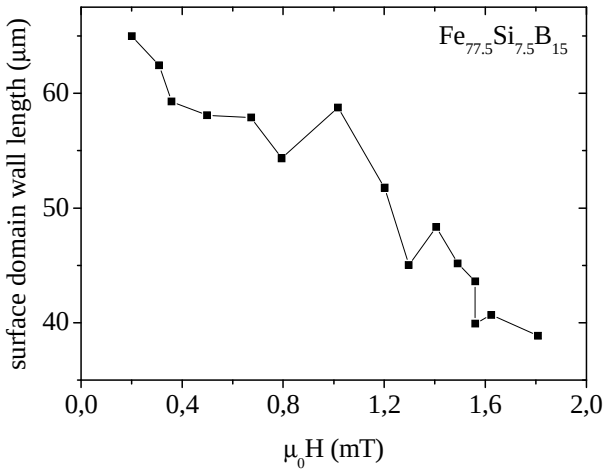

Fig. 95 Magnetic field dependence of the surface domain wall length in $Fe_{77.5}Si_{7.5}B_{15}$ amorphous glass-coated microwire.

For this reason, another important issue appeared: whether the surface domain wall length (observed in the experiment) is the effect of magnetic field only or it is the effect of additional stresses introduced by bending of the wire or it is the intrinsic property of the microwire domain wall structure.

For this reason, the surface domain wall structure was observed differently in the comparative experiment. The whole magneto-optic system (microscope together with the sample) was placed between two coils producing magnetic fields of opposite direction (Fig. 96). Both magnetic coils were powered independently by two power supplies used as current sources. Firstly, the magnetic field intensity of primary coil was set to the certain value by power supply. Adjusting the electric current at the second power supply allowed to shift the region of zero magnetic field between two coils (and domain wall too, consequently) along the microwire. Thus, the stable position of the domain wall was always at zero magnetic field. Such experimental approach allowed us: (i) to avoid the influence of the bent wire shape on the surface domain wall structure, because the additional mechanical stresses (from wire bending) vanishes in the straight sample and (ii) to observe the domain wall at zero magnetic field (which allowed to exclude the magnetostatic interaction, at least partially).

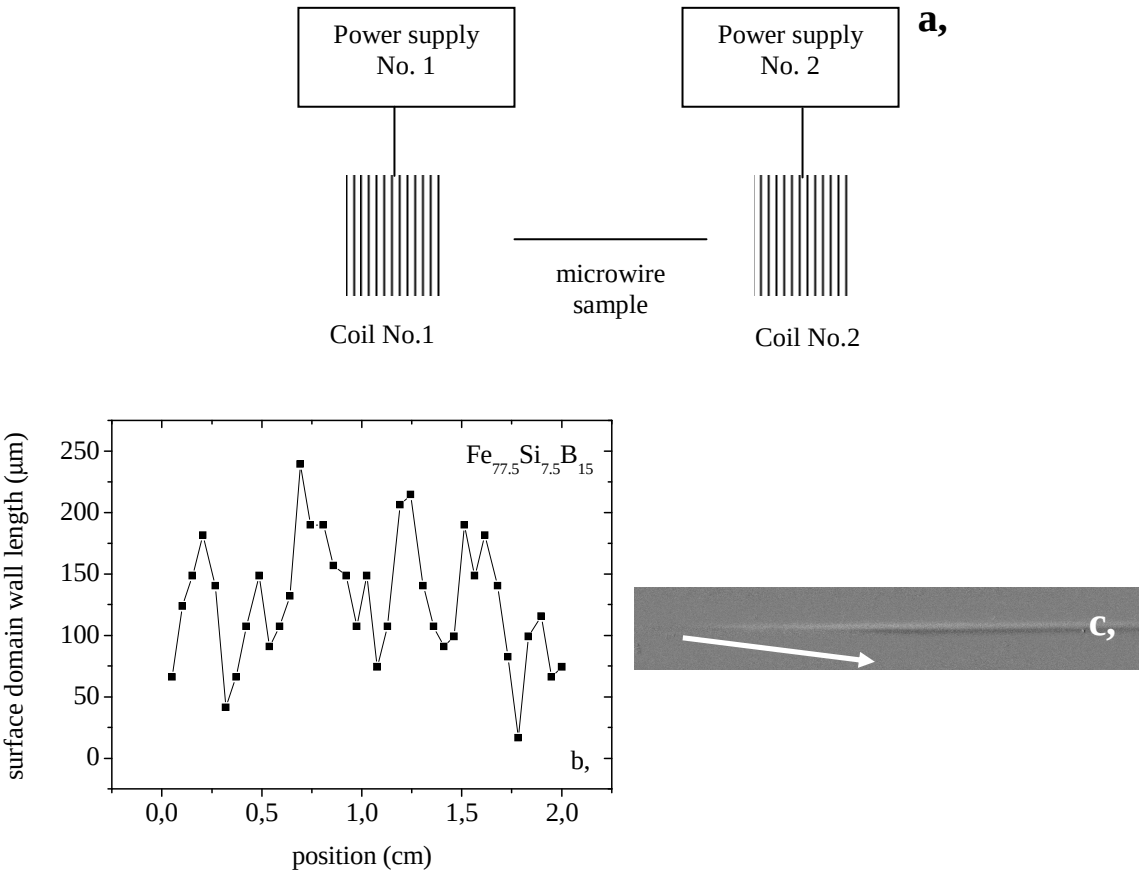

Fig. 96 (a,) Schematic depiction of the domain wall stabilization technique used for magnto-optical observation of the surface domain wall structure of $Fe_{77.5}Si_{7.5}B_{15}$ amorphous glass-coated microwire. (b,) surface domain wall length measured at various positions along the microwire sample with length of 2 cm. (c,) magnetic contrast shows the inclined surface domain wall structure in this experiment. Direction of the surface domain wall inclination is depicted by green arrow. Note, the apparent surface domain wall length doesn't depend on the focus depth.

As it is seen in Fig. 96, the apparent tilting of the surface domain wall structure was observed in this case too. Moreover, the measurements of the surface domain wall length were performed at different positions of microwire with 2 cm in length. As it is seen in Fig. 96 (b,) the inclination of domain wall (apparent surface domain wall length) is not constant along the microwire axis, but one may observe that the surface domain wall length varied from *40 μm* to *210 μm.*

Such high fluctuation of the surface domain wall length can be attributed to the local mechanical stresses that vary along the wire.

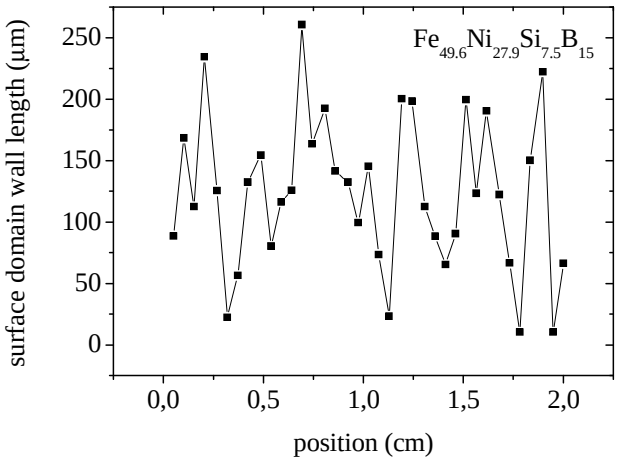

Fig. 97 surface domain wall length measured at various positions along the $Fe_{49.6}Ni_{27.9}Si_{7.5}B_{15}$ microwire sample with length of 2 cm. Note, the focus depth was constant.

The surface domain wall length was measured in the second group of microwires ($Fe_{49.6}Ni_{27.9}Si_{7.5}B_{15}$) where the surface magnetic contrast invoked by internal domain wall propagation was possible to detect (Fig. 86). As it is seen (Fig. 97), the surface domain wall length fluctuated around its *120 μm* average value. The direction of domain wall inclination was the same as before. We tried to change the domain wall inclination direction by application of magnetic field oriented perpendicularly to the microwire main axis. However, the inclination direction was found neither to be the function of the position along the sample nor externally applied perpendicular magnetic field. This shows that the origin of the surface domain wall inclination should be associated with the much stronger (as compared to Zeeman interaction) magnetoelastic magnetic anisotropy, which is discussed in the next section.

On the other hand, the surface domain wall length as well as the direction of surface domain wall inclination was found to be a function of the position around the microwire. The sample pieces with 2 cm length were cut from one long microwire. Each 2 cm piece of microwire was rotated around the main axis and stock on the sample holder. As it is seen in Fig. 98 the average value of the surface domain wall length (as well as the inclination of the surface domain wall structure) is not constant around the microwire.

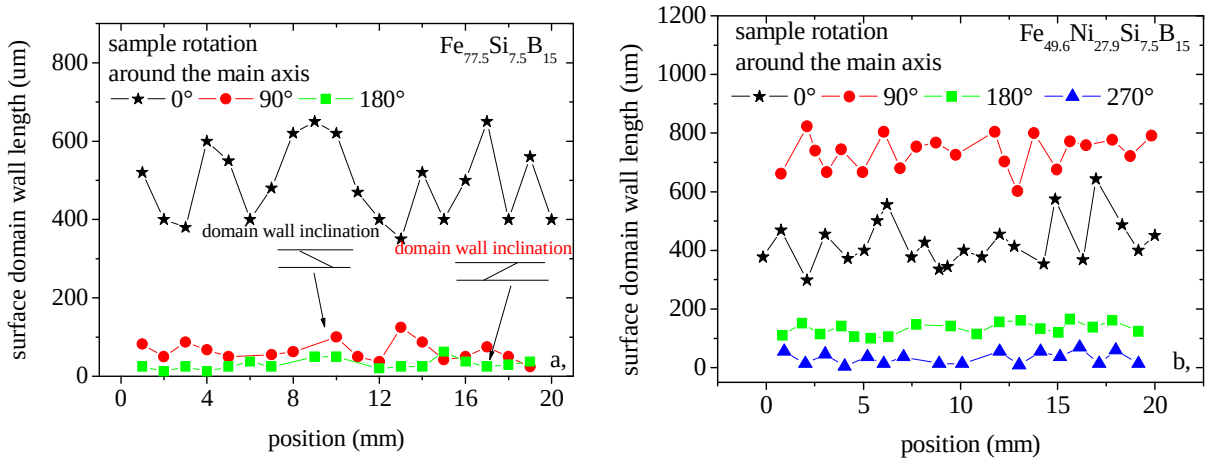

Fig. 98A, Comparison of the surface domain wall length measured in (a,) $Fe_{77.5}Si_{7.5}B_{15}$ and (b,) $Fe_{49.6}Ni_{27.9}Si_{7.5}B_{15}$ amorphous glass-coated microwires.

A different surface domain wall length around the microwire can be explained by domain wall orientation that is fixed relative to the main axis of microwire. As far as the tilted domain wall cannot rotate around the main axis during its propagation, the surface domain wall length depends on the point of view.

In order to compare the homogeneity of microwire surface when microwire is rotated around its main axis, a series of SEM images have been done. The glass-coat of microwires was removed in two ways: (i) mechanically by tearing off and by rolling and (ii) by etching in ultrasonic bath of HF. As it is seen in Fig. 98B (d,), mechanical removal of glass-coating doesn't leave any remarkable defects on the metallic core. On the other hand, etching of microwires introduces many small holes with app. diameter of 800 nm. Moreover, one apparent line can be recognized along the core surface, as it is seen in Fig. 98B. These lines were observed in many pieces of microwire samples (different position along the wire and different sample composition). However, these lines appear only at a certain position on the surface (fig. 98B (a,) (c,) but not if the sample is rotated (b,)), which means that the microwire surface under investigation were probably not homogeneous.

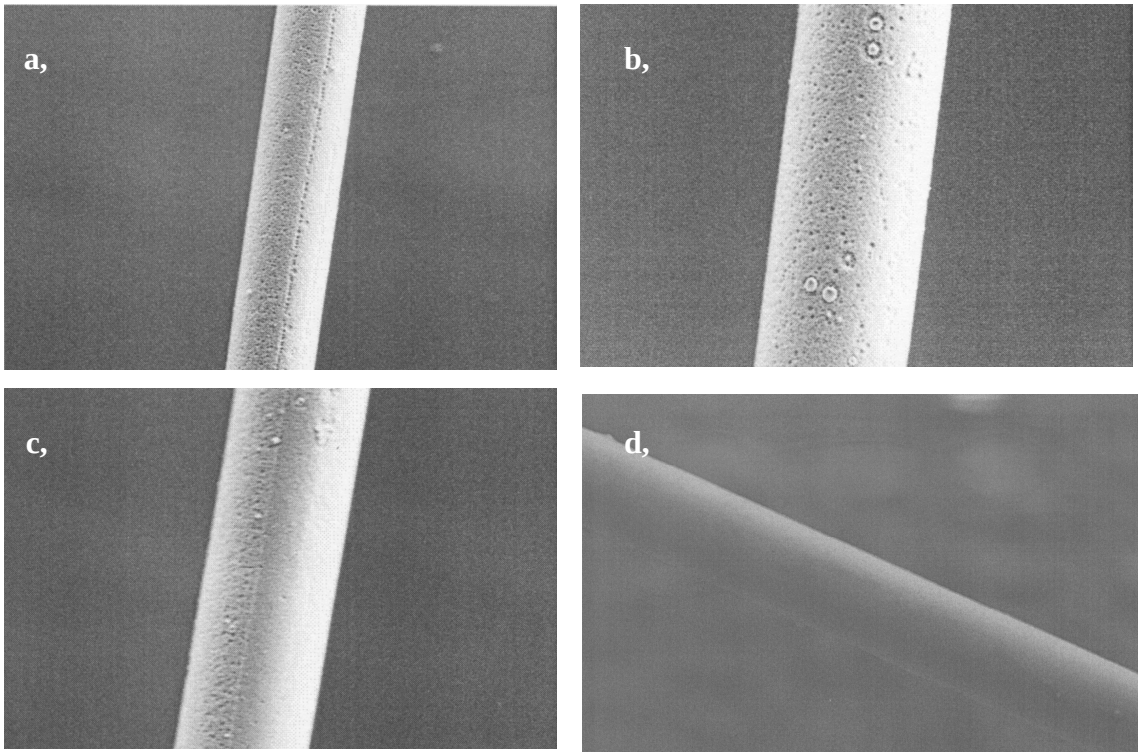

Fig. 98B, SEM images of the metallic core surface of $Fe_{77.5}Si_{7.5}B_{15}$ amorphous glass-coated microwires. The glass-coat was removed chemically (by etching in HF) (a,) (b,) (c,). The mechanical way of glass-removal (d,) doesn't introduce remarkable surface defects.

The surface domain wall structure was found to be tilted in all above described conditions. However, when the domain wall is deppining from the defect, the situation becomes more complex, as it can be seen in Fig. 99.

The domain wall deppining process doesn't start at the boundary between two domains, but one may observe the rotation of magnetic moments within the small region apart the boundary Fig. 99 (b,). Further domain wall movement results in the increase of that region (Fig. 99 (c,)) up to the complete disappearance of the magnetic contrast at one half of the wire (Fig. 99 d,). The domain wall deppining process is finished by progressive disappearance of the magnetic contrast at the opposite part of the wire (Fig. 99 e, f,). Finally, the domain wall of tilted surface structure is observed as it was presented in previous measurements. Right column of Fig. 99 shows the schematic depiction of the surface magnetization direction (made under the assumption that the black and white magnetic contrast on cylindrical wires corresponds to the change in the axial component of surface magnetization, which was discussed in previous section). It

may be very difficult to determine the internal structure of the domain wall from the surface observation. However, some images (Fig. 99 (d,), right column) apparently corresponds well to the surface structure of the twisted planar domain wall (see a micromagnetic simulation of the domain wall structure in the next section for the anisotropy energy value of 1xE5 J/m^3).

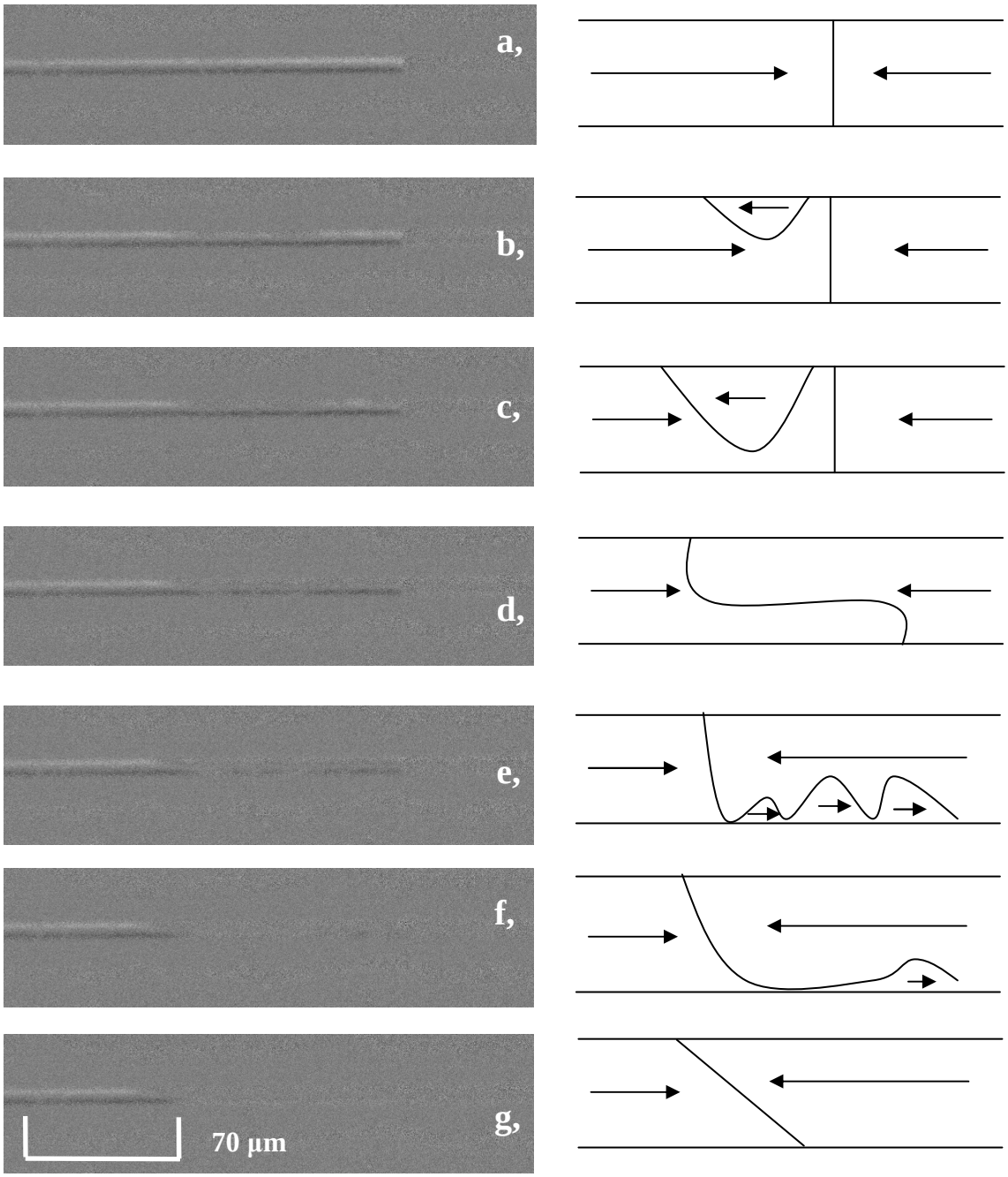

Fig. 99 The domain wall depinning from the defect in FeNiSiB amorphous glass-coated microwire. Left, the magnetic contrast of the doamin wall obtained from the observation of microwire. Right, the schematic depiction of the surface magnetization is shown.

6.2.7 Tilted surface domain wall structure

In order to propose the simple model which explains the tilted surface domain wall structure assume a head to head domain wall of small thickness (Fig. 100).

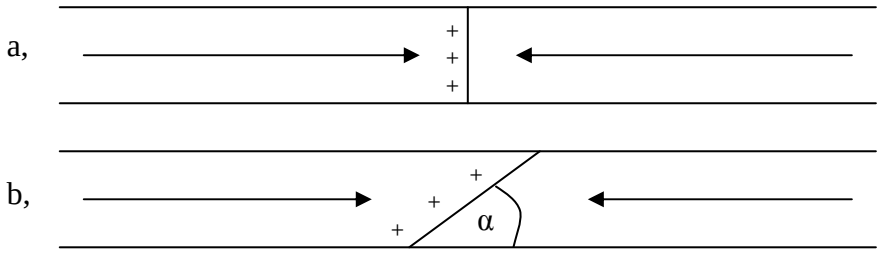

Fig. 100 Schematic description of the perpendicular (a,) and tilted head to head domain wall. Tilting the domain wall results in the magnetic charges density decrease.

The magnetic charge density of perpendicular (with respect to the main axis) head to head domain (Fig. 100 (a,)) wall is:

$$\sigma = 2M_S \tag{136}$$

However, the domain wall inclination reduces the total density of magnetic charges (due the domain wall surface increase) (Fig. 100 (b,)):

$$\sigma = 2M_S \sin\alpha \tag{137}$$

The corresponding demagnetizing energy of surface magnetic charges decreases with the domain wall inclination too:

$$E_d \approx \frac{2\mu_0 M_S^2 \sin^2\alpha}{\sin\alpha} \tag{138}$$

The factor $\sin\alpha$ in the denominator is because of the energy increase due to the increase of the wall length.

On the other hand, the more domain wall is tilted, the higher domain wall surface is. Assume the energy of perpendicular head to head domain (Fig. 100 (a,)) in the form:

$$E_0 = 2A/\Delta \tag{139}$$

where A is the exchange constant and Δ^2 the square of domain wall width. This energy increases with domain wall inclination because of the higher domain wall surface:

$$E_\alpha = \frac{E_0}{\sin\alpha} \tag{140}$$

The tilting angle of domain wall may is given by the competition between the demagnetizing energy of surface magnetic charges (decreases with the tilting angle) and the energy of the domain wall (increase with the tilting angle because of higher surface). The total energy of the domain wall is then given by:

$$E_{total} \approx \frac{E_0 + 2\mu_0 M_S^2 \sin^2\alpha}{\sin\alpha} \tag{141}$$

The minimum energy is achieved at the tilting angle given by condition:

$$\sin\alpha \approx \sqrt{\frac{E_0}{\mu_0 M_S^2}} \tag{142}$$

In the case of very high magnetic anisotropy, the domain wall thickness is very small and the demagnetizing energy of the surface magnetic charges may play an important role which can result in the tilted domain wall shape.

In order to confirm such behavior a series of micromagnetic simulations in OOMMF (195) has been done. The minimal value of mesh size δ must be chosen in accordance to the magnetic anisotropy strength K and to the value of exchange constant A:

$$\delta \approx \sqrt{A/K}$$

For the value of exchange constant $A = 13 \times 10^{-12}\, J/m^3$ (which corresponds to Permalloy) and for the value of energy density of magnetic anisotropy $K \cong 1 \times 10^5\, J/m^3$ (measured on microwires by use of AGFM) it gives

$$\delta \cong 10\, nm$$

In order to run the OOMMF simulation on microwires with 15 μm diameter and 1 mm length, one needs to simulate 10^{11} cells to maintain the 10 nm mesh size. Such number of cells costs a lot of simulation time that cannot be done by use of standard PC in a reasonable time.

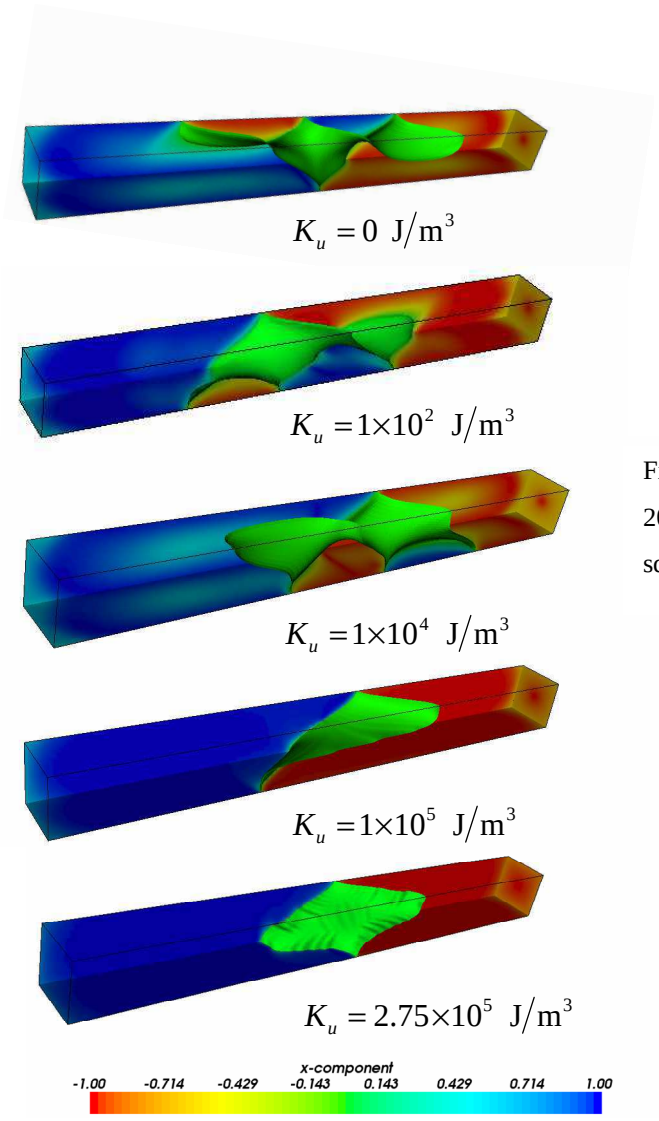

Fig. 101 simulated shape of the domain wall in 200 nm x 200 nm x 2000 nm nanowire of square cross-section.

For this reason, the simulation was performed on thin magnetic wires of reduced diameter (*200 nm*) and length (*2000 nm*) with the total number of 4×10^4 cells. The simulation time was found to be dependent on the magnetic anisotropy strength (in axial direction, given to the software as an initial parameter), but usually it didn't take more than 20 hours per one simulation.

The domain wall structure was simulated in two steps: Firstly an initial head to head magnetization configuration was chosen. It consisted of two axial domains with opposite axial magnetization and the region between two domains with a perpendicular magnetization direction (with respect to the main axis). This region served as the initial core for head to head domain wall.

The surface magnetic charges appearing in both ends of wire were compensated by magnetic field that was calculated separately for each cell. The simulations were run for various initial magnetization configurations: (i) different width of the region between two domains, (ii) different initial orientation of the magnetization in the region between two domains in order to be sure that the simulated structure of the domain wall corresponds to the global minimum. The stopping criterion $dm/dt = 0.0001\,\mathrm{deg/ns}$ was used to define stable (relaxed) structure.

In order to be sure that the 10 nm mesh size is reasonable for our simulation, the highest value of magnetic anisotropy (the last simulation in Fig. 101) was simulated with 5 nm mesh size too. Such simulation took more than 5 days; however the resulting domain wall structure was the same as in 10 nm mesh size simulation.

Fig. 101 compares the relaxed domain wall structure in *200 nm x 200 nm x 2000 nm* wire of square cross-section for different values of uniaxial magnetic anisotropy. As it is seen, the domain wall shape is very similar to the screw at the lowest value of magnetic anisotropy. Accidentally, this structure describes the surface domain wall structure obtained on microwires, where domain wall was pinned by defect (see Fig. 99, right column). As the magnetic anisotropy strength increases, the number of turns decreases (Fig. 101). One may observe the planar domain wall (or one turn in screw) for the value $K_u = 1\times10^5\,J/m^3$ of uniaxial magnetic anisotropy. Such tilted shape of the domain wall is maintained for higher value of magnetic anisotropy (see fig. 102), however, the tilting angle varies slightly.

Generally, the complex shape of the domain wall at low anisotropy becomes simpler as the magnetic anisotropy increased.

The tilted surface domain wall structure appeared at the highest value of uniaxial anisotropy ($K_u = 2.75\times10^5\ \mathrm{J/m^3}$) only. Accidentally, this value corresponds roughly to that measured in amorphous glass-coated microwires (magnetoelastic anisotropy $K \cong 1\times10^5\ \mathrm{J/m^3}$, see chapter on the sample description).

The domain wall width parameter Δ was calculated by the Thiele formula, which is the definition relevant to estimate the domain wall velocity in steady state:

$$\frac{2S}{\Delta} = \int\left(\frac{dm}{dx}\right)^2 dx\,dy\,dz \qquad (143)$$

As it is seen in Fig. 102 the calculated domain wall width is governed by magnetostatics at low values of magnetic anisotropy parameter. On the other hand, the domain wall width follows to square root formula for the magnetic anisotropy parameter higher than app. $K_u > 10^5\ \mathrm{J/m^3}$. Accidentally, this value of magnetic anisotropy is the same as it was obtained in microwires by AGFM measurements.

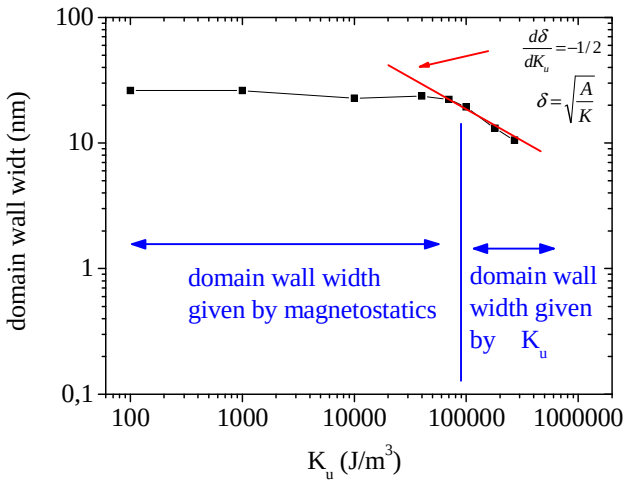

Fig. 102 simulated shape of the domain wall in 200 nm x 200 nm x 2000 nm nanowire of square cross-section.

Chapter 7

The domain wall dynamics in microwires of reduced diameter

The domain wall dynamics in amorphous microwires of diameters 10 μm – 70 μm has been extensively studied in previous works (187), (188), (189). The results have been attractive especially for potential application in spintronic devices based on domain wall propagation. Generally, the reported domain wall velocities were very high and were found to depend on many parameters, like applied tension stress (190), glass thickness (191), structure (192) or temperature (193) of studied samples. The most reasonable parameter determining the domain wall velocity of 10 μm microwires was found in the strong magnetoelastic anisotropy.

The main goal of this chapter is to investigate the domain wall dynamics in microwires of reduced diameter down to 1 μm and to compare the influence of the reduced size on fast domain wall propagation.

The series of $(Fe_{97}Co_3)_{75}Si_{7,5}B_{15}$ amorphous glass-coated microwires with four different diameters of metallic nucleus (2.8 μm 2 μm 1.6 μm and 1 μm) have been used for this measurement. Hysteresis loops of the samples used in this measurement are shown in Fig. 103. A remarkable switching field increase from 200 A/m (for the sample of 2.8 μm diameter) to 800 A/m (for the thinnest sample of 1 μm diameter) can be recognized when the ferromagnetic nucleus diameter decreased. On the other side, the rectangular hysteresis loop shape is maintained in each sample, even in the microwire with the smallest diameter (1 μm).

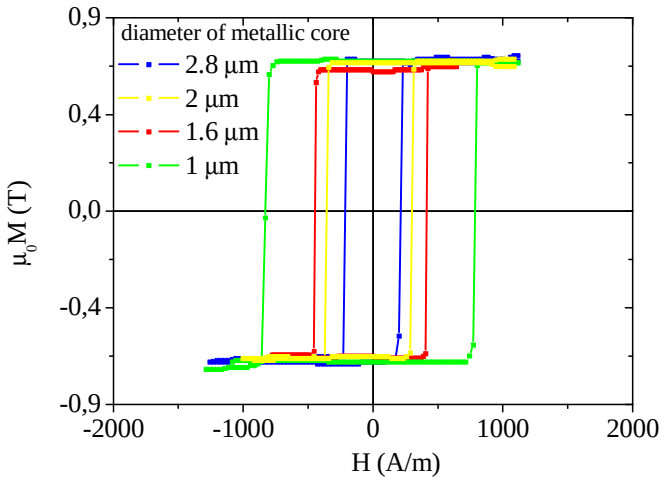

Fig. 103 Hysteresis loops of $(Fe_{97}Co_3)_{75}Si_{7.5}B_{15}$ amorphous glass-coated microwires measured by SQUID. All the pieces are of the same length (5 mm) and of the same chemical composition. Sample of d_m = 2.8 μm and D = 10 μm has ratio p = 0.28, sample of d_m = 2 μm and D = 11 μm p = 0.18, sample of d_m =1.6 μm D = 10 μm p = 0.16 and sample of d_m = 1 μm D = 9 μm p = 0.11.

I was shown in the previous works (178) (179) that the strength of residual stresses introduced to the microwires during preparation is mainly determined by the ratio between the glass and metal thickness which is expressed by parameter p :

$$p = d / D \tag{144}$$

where d is the core diameter and D the total diameter of microwire. The high increase of the switching field with decrease the core diameter should be attributed to the higher shape anisotropy and to the higher magnetoelastic anisotropy arising from the enhanced internal residual stresses when p is small. Such a relation between the core diameter and the switching field magnitude has been observed in previous works (180) (181) (182).

The rapid increase of switching field with core diameter decrease can be recognized in the field dependence of domain wall velocity (Fig. 104) too. The values of switching field are in this case a bit higher than in previous measurements. The considerable difference can be attributed to the higher shape anisotropy of longer samples used in domain wall velocity measurements (10 cm).

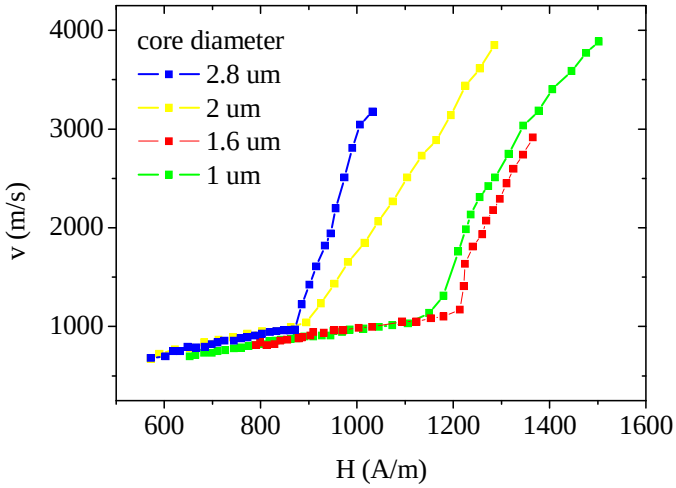

Fig. 104 The domain wall dynamics of $(Fe_{97}Co_3)_{75}Si_{7.5}B_{15}$ amorphous glass-coated microwires. All the pieces of microwires provide fast domain wall dynamics with two regimes of domain wall propagation, similarly to thicker samples.

As it can be seen, the domain wall velocity reaches very high values up to 4 km/s in all samples used in measurements. Two regimes of domain wall propagation can be clearly recognized; the first one characterized by low domain wall mobility (units of $m^2/A.s$) and the secondary one with high domain wall mobility (tens of $m^2/A.s$). Note that the domain wall mobility of primary and secondary regime doesn't change when the core

diameter decreased. This confirms that the size of metallic core doesn't influence the energy dissipation by domain wall propagation which is expressed by phenomenological parameter of domain wall damping. However, the transition field (the field at which the transformation from the primary to the secondary regime occurs) steeply increases when core diameter became smaller than 2 μm.

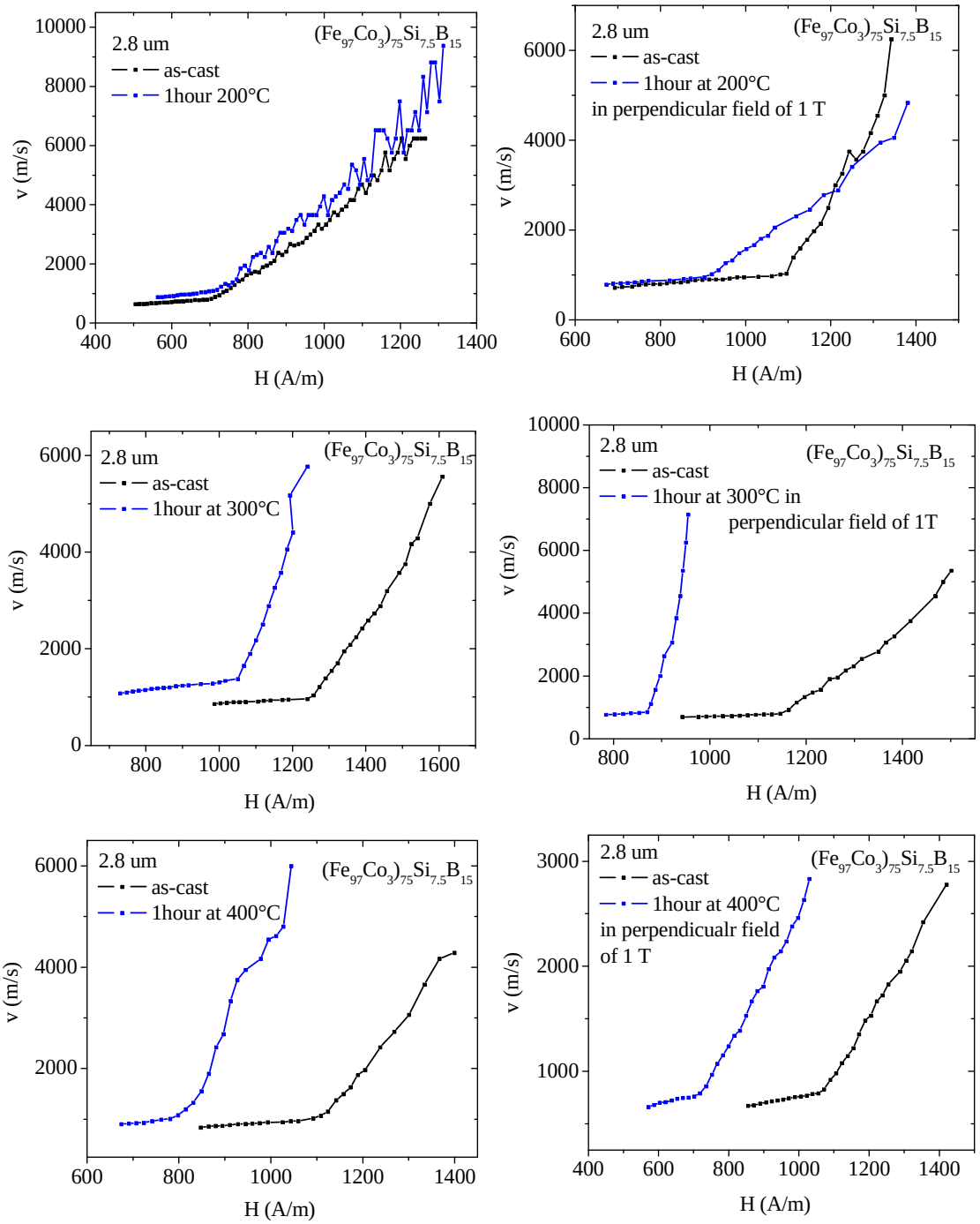

Fig. 105 The influence of thermal treatment on domain wall velocities in $(Fe_{97}Co_3)_{75}Si_{7.5}B_{15}$ amorphous glass-coated microwires of 2.8 um diameter. Left column represents thermal treatment without externally applied field; the annealing in perpendicular field is shown in right column.

Even if the origin of secondary regime of domain wall propagation is not so clear, the high influence of transversal field applied simultaneously with the driving axial field during the domain wall propagation was found (183) to be an important parameter determining the value of the transition field.

In this regard, the change in transition field when the core diameter decreased below 2 μm can be associated with different geometry of residual stresses. In this way, the strength of perpendicular stresses can be considered to be higher in microwires with small diameter.

Regardless of the values of transition field, the maximum domain wall velocity in thin wires reached very high values (up to 10 km/s) comparable with the velocities measured in previously discussed thicker microwires.

However, even if the velocities are high, they can be enhanced by proper thermal annealing. Fig. 105 shows the influence of thermal treatment on domain wall velocities in microwires of 2.8 μm diameter. In order to avoid the additional effect of triple annealing (at 200°C, 300°C and 400°C), the domain wall velocities were measured in three different samples, each subjected to thermal annealing performed at different temperature.

As it is seen, thermal annealing at 200°C is not sufficient to change domain wall mobility remarkably; however the switching field is slightly decreased. Further increase of annealing temperature results in two effects: decrease the switching field more than two times (from 1100 A/m in as-cast to less than 500 A/m in the sample treated at 300°C) and increase the domain wall mobility of both primary and secondary regime. Such an effect can be explained in terms of the three contributions to the total domain wall damping. Thermal annealing leads to decrease the magnetic relaxation domain wall damping (by reduction of internal stresses) and to decrease structural relaxation domain wall damping (by reduction of concentration of free volumes) as it was shown in previous chapters. Another important effect of thermal annealing can be recognized in the shift of the transition field, which was observed in the each treated sample. A similar shift of transition field was found to be the effect of perpendicular anisotropy (6). In this regard, the observed shift of transition field could be attributed to the redistribution of internal stresses between the radial and axial one during thermal annealing. However, one needs more information on the origin of secondary regime to explain the observed data.

The influence of thermal annealing in perpendicular field on domain wall dynamics in the wires of the same composition is shown in right column of fig. 105. The presence of perpendicular field during the treatment leads to the same above mentioned effects (the switching field decrease, the domain wall mobility and transition field increase).

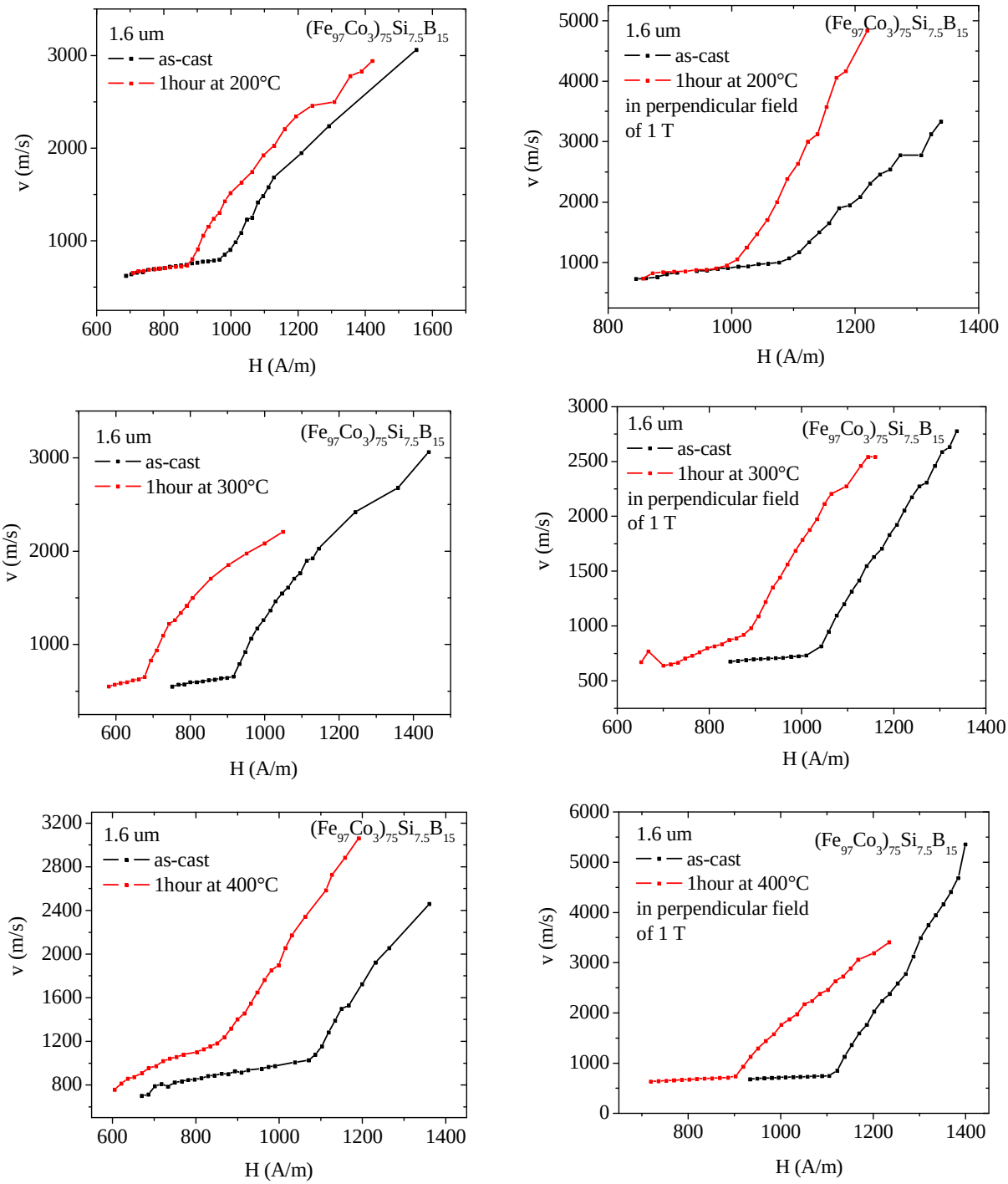

Fig. 106 The influence of thermal treatment on domain wall velocities in $(Fe_{97}Co_3)_{75}Si_{7.5}B_{15}$ amorphous glass-coated microwires of 1,6 um diameter. Left column represents thermal treatment without externally applied field; the annealing in perpendicular field is shown in right column.

The only difference between the standard and field annealing consists in the direction of presented field. Whereas the microwires are annealed in an internal field given by the direction of spontaneous magnetization in standard annealing (without field), annealing in perpendicular field leads to the structure relaxation in the total field given by the sum of the internal and the externally applied field, which results in the induction of perpendicular anisotropy.

As it was noted at the beginning of this chapter, the strength of residual stresses is indirectly proportional to the parameter p expressing the ratio between the glass and core thickness (eq. 144). The lower the parameter p (i.e. higher glass thickness and lower core thickness) the higher residual stresses are present in the sample (184). Fig. 106 compares the influence of thermal treatment on domain wall velocity in the wire of smaller diameter (d = 1.6 μm and p = 0.16) where residual stresses can be considered to be higher because of smaller parameter p.

Regarding experimentally obtained data in fig. 106, there are few typical features. First of all, there is a considerably higher influence of thermal annealing on domain wall velocity in each treated sample. Thermal annealing at 200°C changes neither the domain wall mobility nor switching field. However, the transition field is significantly decreased (from 1000 A/m to 880 A/m). Such a difference between the transition field of as-cast and of treated sample increases with annealing temperature (fig. 106). In contrary to the previous sample, the domain wall mobility of primary and secondary regime of domain wall dynamics surprisingly shows a low dependence on annealing conditions. On the other side, thermal treatment in perpendicular field increases the domain wall mobility of secondary regime, while the mobility of primary regime doesn't seem to be affected (fig. 84 annealing at 200°C and annealing at 400°C). Such a curious result might point to the different origin of magnetization process that occurs within the primary and secondary regime of domain wall propagation. Regardless to the low change in domain wall mobility, the maximum domain wall velocity of 1.6 μm microwire is ranging between 2 km/s – 3 km/s. This is almost twice lower as compared to previously discussed 2.8 μm microwire (with maximum velocity of about 8km/s – 10 km/s). The lower maximum velocity should be explained in terms of higher magnetoelastic anisotropy in 1.6 μm microwire since ratio $p = d / D$ determining the strength of residual stresses is for thinner wire (1.6 μm) p = 0.16 while for thicker wire p = 0.28. It means that the decrease the metallic core with maintaining the same glass

thickness results in the higher residual stresses, which can be recognized by lower domain wall velocities. Such a tendency can be clearly seen in *v(H)* dependence of the thinnest (1 μm, p = 0.11) microwire showed in Fig. 107, where domain wall velocity of as-cast samples reached maximum of about 2 km/s. This value of maximum velocity is much lower as compared to maximum velocity obtained in thicker wires (1.6 μm and 2.8 μm). On the other side, a significant influence of thermal treatment on domain wall dynamics in maintained.

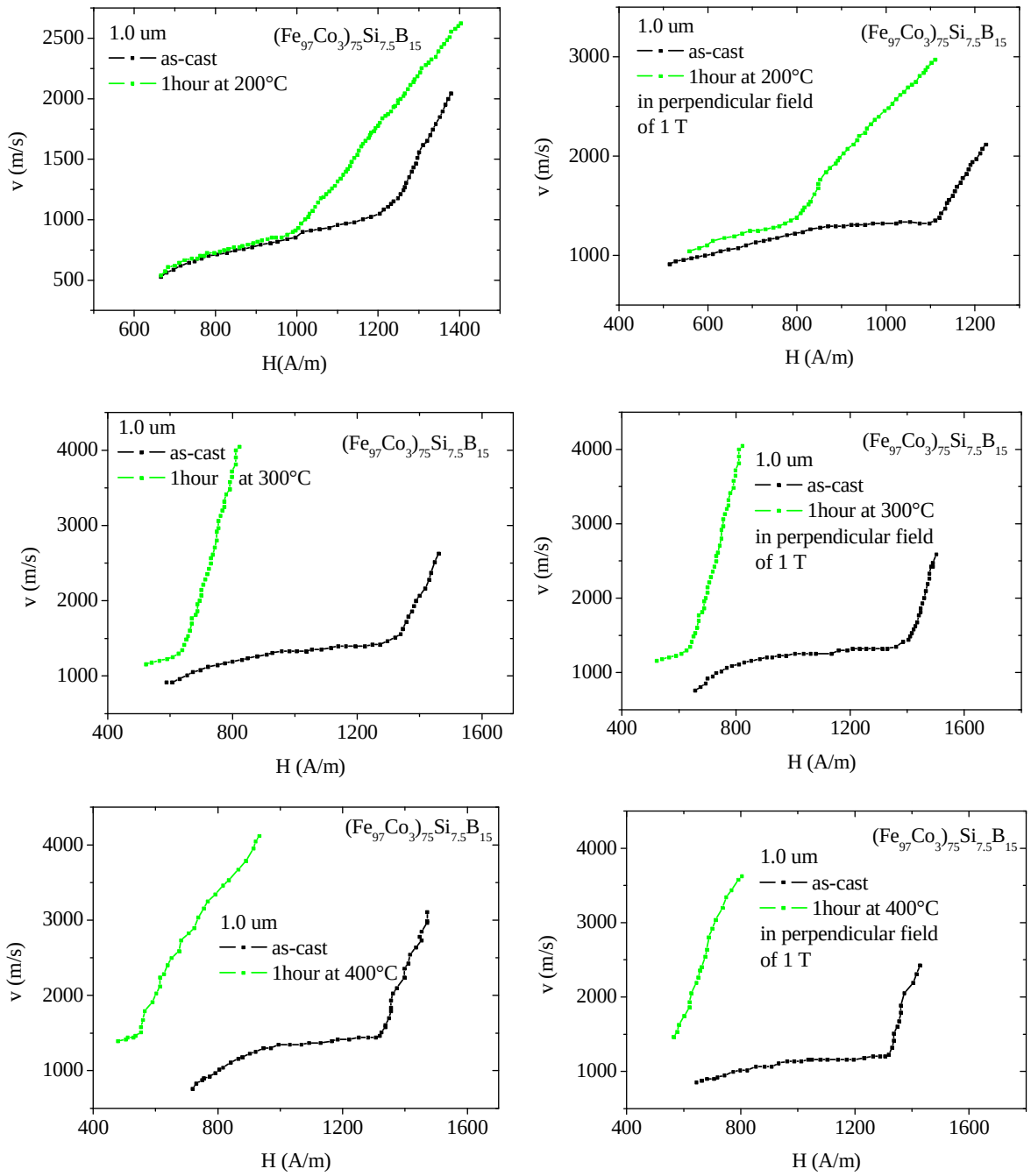

Fig. 107 The influence of thermal treatment on domain wall velocities in $(Fe_{97}Co_3)_{75}Si_{7.5}B_{15}$ amorphous glass-coated microwires of 1 um diameter. Left column represents thermal treatment without externally applied field; the annealing in perpendicular field is shown in right column.

Thermal annealing of 1 μm microwires without applied perpendicular field increased the domain wall velocity more than two times (the highest enhancement can be observed at annealing temperature 400°C where the velocity increased from 1 km/s to 3 km/s at 800 A/m). Such considerable effect was achieved by the transition field decrease and by the domain wall mobility increase in each observed sample. The highest change in domain wall mobility was found in the sample treated at 300°C without perpendicular field (Fig. 107), whereas the highest shift of transition field was observed in the sample treated at 400°C without perpendicular field. Note that microwires of the smallest diameter (1 μm) were found to be extremely sensitive to thermal treatment. In contrary to the previously discussed thicker wires (of 2.8 μm and 1.6 μm), the thermal annealing of 1 μm at 200°C (Fig. 107) was sufficient to change the domain wall mobility. Such result can be understood only in terms of higher residual stresses in the thinnest wire, because the chemical compositions of the all studied wires are the same.

Comparing the *v(H)* diagrams of the studied samples, one may conclude that the highest enhancement of the domain wall velocity was achieved by thermal annealing in perpendicular magnetic field (right columns). The domain wall velocities of treated samples were more than three times higher (4 km/s) as compared to the as-cast state (Fig. 107 annealing at 300°C).The obtained domain wall velocities in 1 μm as-cast samples are comparable to those (~ 1.5 km/s) measured in submicron amorphous glass coated microwires (185) (186) as well as to those reported in planar magnetic nanowires (~ 1 km/s). However, here it is shown that such fast magnetization reversal process can be enhanced by thermal treatment that results even in the higher domain wall velocity.

The amorphous glass-coated microwires with metallic core diameter below 3 μm have been studied in this chapter. It is shown, that the domain wall dynamics of thin wires (~ 1 μm) is similar to those observed in thicker samples (~ 10 μm) discussed in previous chapters. Two regimes of domain wall propagation characterized by different values of domain wall mobilities were observed at each sample diameter. Moreover, the high maximum domain wall velocities of about 2 km/s for primary and 9 km/s for secondary regime are maintained when the core diameter decreased. The correlation between the domain wall velocity and the core diameter was explained within the term of magnetoelastic anisotropy.

It is demonstrated that the fast domain wall dynamics of thin wires can be tailored by an appropriate selection of the core diameter and annealing conditions. An investigation of the influence of the annealing condition on domain wall velocity has shown the great potential use of these materials for miniaturized sensor applications.

Conclusions

This work deals with the fast domain wall dynamics in amorphous glass-coated microwires. Three main potential factors allowing the fast reversal process in microwires were investigated: (a) a relatively low value of magnetic anisotropy (b) the presence of the surface domain structure and (c) the complex geometry of magnetic anisotropies in microwires. The influence of various external parameters (temperature too, if a high mechanical stress induced by particular treatments) on domain wall dynamics in microwires was studied. It has been shown that:

- Application of tensile stress on FeNiSiB microwire characterized by multi-regime domain wall dynamics leads to the domain wall velocity decrease in the whole interval of applied tension stress.

- Fitting the stress dependence of the domain wall damping parameters revealed the possible origin of four domain wall propagation regimes in FeNiSiB microwire. The stress-dependant structure relaxation domain wall damping can describe the experimentally obtained stress dependence of the overall domain wall damping in the first regime. It means that the structural relaxation domain wall damping can play an important role at room temperature, too if the high tension stress is present. The second regime of the domain wall propagation could by explained within the term of domain wall width contraction due to the high domain wall velocity. The domain wall damping in the third regime of domain wall propagation can be fitted by neglecting the structural relaxation contribution to the overall domain wall damping. The fourth regime of domain wall dynamics characterized by the highest domain wall velocities is not possible to fit by mechanical model of domain wall propagation.

- Conventional thermal treatment at the properly selected annealing condition (300°C during 1 hour) leads to the remarkable increase in maximum domain wall velocity in FeSiB microwires from 1.5 km/s in as-cast state to 6 km/s in treated sample.

- The conventional thermal treatment of FeNiSiB microwire characterized by lower magnetostriction coefficient resulted in smaller increase in domain wall velocity as compared to more magnetostrictive FeSiB microwire. This result confirms that the magneto-elastic coupling between the residual stresses and spontaneous magnetization is probably the most important factor that influences the change of the domain wall dynamics during the conventional thermal treatment.

- Thermal annealing under the mechanical tension stress (70 MPa) results in the loss of spontaneous bistability in amorphous FeSiB microwire. Further application of tensile stress (35 MPa) leads to the recovery of the initial domain wall velocity observed in the as-cast sample. Thermal annealing under the mechanical tension stress was found to be more effective to decrease the residual stresses than the conventional annealing.

- The current annealing of Fe-rich amorphous microwires during 10 min. was found to be as much effective in domain wall velocity increase as the conventional thermal treatment during 1 hour.

- The imaging of microwires without glass by Bitter colloid revealed a periodic pattern in each studied FeNiSiB microwires.

- Despite the high change in domain wall velocity during the thermal treatment, this surface periodic structure does not seem to be affected.

- Methodics for the magneto-optical observations of cylinder was proposed.

- The magneto-optical observation of surface structure revealed that the boundary between two axial domains is not abrupt, but the tilted surface domain wall structure was observed. Tilted surface domain wall structure could points to the tilted domain wall structure that can explain the high domain wall velocity in microwires.

- Simple model for tilted domain wall structure was proposed. It was shown that the high magnetic anisotropy can be found to be responsible for tilted domain wall structure. Such structure should explain well the tilted surface domain wall structure observed in microwires. The tilted domain wall structure could explain apparent high domain wall velocities measured in microwires by use of Sixtus-Tonks method.

- Preliminary micromagnetic simulations on thin magnetic wires of reduced diameters (*200 nm*) have been done by use of OOMMF. It was shown that tilted surface domain wall structure appears in *200 nm* magnetic wires under the condition of high magnetic anisotropy $K > 1 \times 10^5 J/m^3$.

- Amorphous glass-coated microwires of reduced diameter (down to 1μm) are characterized by the same domain wall dynamics as in thicker wires. The conventional thermal treatment of microwires results in the high domain wall velocity increase.

- Thermal annealing of microwires in the perpendicular field increases the domain wall velocity even more than the conventional annealing without the presence of perpendicular field during the treatment. This point to the importance of the perpendicular anisotropy in fast domain wall propagation in microwires.

Conclusions related to further development of science and potential practical applications

The work presented in this dissertation served as the introduction to the problematic of the fast domain wall propagation in microwires.

Despite the new direct confirmation of the tilted surface domain wall structure in microwires, there is a great degree of future work to understand better the structure of the domain wall during the propagation. Especially, understanding the dynamical processes occurring in such big domain wall (as it is in microwire) during its motion would be a great value. The field dependence of the domain wall velocity in some kind of microwires is very similar to that observed in magnetic nanowires: linear curve followed by breakdown of the velocity. It would be very surprising result if a Walker model had been valid in such “big” magnetic wires. Due to the absence of micromagnetic simulations made on this material, the model of domain wall propagation would be very interesting.

From the application point of view, the high sensitivity of the domain wall dynamics (i.e. the domain wall velocity and the critical field) to the applied mechanical stress found in this work may be employed in the potential sensor devices to detect external forces. Due to the very fast domain wall propagation of microwire, the relatively low change in the input parameter (magnetic field, mechanical stress, etc..) results in a big change in the value of domain wall velocity. Hence, the parameters that allows to achieve the higher domain wall velocities studied in this work (various thermal treatments, etc) would be useful to produce new sensors of enhanced sensitivity.

Thermal annealing of microwires under the mechanical stress was shown as a very effective method for the internal tension stress removal. On the other hand, application of relatively low tension stress recovers the bistable-character to the initial (in as-cast sample) state. Therefore, the microwire treated in such way would be employed as a high sensitive detector of mechanical stress.

Abstract in English

The domain wall propagation in thin magnetic wires becomes in the centre of interest due to the development of spintronics. Spintronics or spin-oriented electronics is an emerging technology that uses magnetic moment of electron to transport and store information. One of recently developed spintronics conceptions is that based on the magnetic properties of thin bistable magnetic wires. The level of logical value is coded by the magnetization direction within the domains, whereas the change of logical value is performed by domain wall propagation. In the previous works, many prototypes of spintronic devices using the domain wall propagation were proposed: domain wall logical gates performing operations “xor”, “and” or “not”, spintronic diode or spintronic race-track memory that uses multiple domain wall propagation for reading/writing data. Within these devices, the velocity of domain wall movement is one of the most important factors that influence the operational speed of these devices. Hence, it is paid a big attention to understand better the mechanism of fast domain wall propagation in thin magnetic wires. The maximum domain wall velocities used in recently proposed domain wall logical gates doesn’t exceed 2 km/s. The maximum domain wall velocity measured in amorphous glass-coated microwires reach up to 20 km/s.

Another motivation for the domain wall dynamics in amorphous glass-coated microwires study is related to their potential sensor applications. Amorphous glass-coated microwires are recently employed in many sensory devices for sensing of (i) external magnetic field intensity (ii) mechanical stress or (iii) mechanical strain. Most of these sensors use the domain wall dynamics (domain wall velocity and critical field), to detect the external forces. Hence, the knowledge of domain wall propagation in microwires is needed from application point of view, too.

The main goal of this work is to examine mechanisms that can be used to tailor the domain wall dynamics in microwires. The second goal is to understand better the origin of fast domain wall propagation that can be observed in amorphous glass-coated microwires.

Amorphous glass-coated microwires are composite material that consists of metallic core which is covered by glass-coat at the surface. It is worth mentioning that most of magnetic properties of amorphous glass-coated microwires are given by their

fabrication process by Taylor-Ulitovski method. Within this preparation process, amorphous glass-coated microwires are produced by rapid quenching and drawing. As a result of different thermal expansion coefficient of metallic core and glass coat a very strong mechanical stresses of axial and radial directions are introduced to the wire by rapid quenching. Moreover, microwires are pulled out from the molten master alloy during the preparation, which introduces additional mechanical stresses in axial directions. The geometry of resulting mechanical stresses in amorphous glass-coated microwires is very complex. According to the magneto-elastic model, the mechanical stress in amorphous glass coated microwires can be roughly described by the domination of axial stress in central part of the wire, whereas radial and circular mechanical stresses prevails just below the metallic core surface. Moreover, the magnitude of residual stresses is very high according to the model. The highest mechanical stresses achieved at the boundary between the metallic core surface and glass-coat is very close to the ultimate strength of material which the metallic core is made of. Maybe, this is the reason why the magnetoelastic coupling is very important in case of amorphous glass-coated microwires. This assumption is confirmed by the experiment, where the domain structure of amorphous glass-coated microwires is solely given by the sign of magnetoelastic coefficient of material which the metallic core is made of. This proves that the shape anisotropy for domain structure of microwires is not as important as it is in case of Py magnetic nanowires.

If amorphous glass-coated microwire is made of the alloy of positive sign magnetostriction coefficient, the minimum magnetoelastic energy is achieved by parallel orientation of magnetization to the direction of internal residual mechanical stresses. For this reason, the domain structure of amorphous glass coated microwires of positive magnetostriction coefficient consists of large axial domain which is surrounded by thin shell of surface domains (according to the recent theoretical models describing the residual mechanical stresses). Moreover, closure domains appear at the ends of wire in order to decrease the stray fields. The main magnetization process of positive – magnetostriction amorphous glass-coated microwires is related to the Large Barkhaussen jump characterized by single domain wall propagation across the microwire.

The domain wall dynamics in amorphous glass-coated microwires was examined within the mechanical model of domain wall propagation used by Kittel in early fifties of 20th

century. The dynamic properties of domain wall movement are compared to the motion of mass point in a viscous media. Under this assumption, the domain wall movement is described by equation similar to that of linear harmonic oscillator. Then, the equation of domain wall motion can be evaluated, where the domain wall velocity is directly proportional to the applied magnetic field. The domain wall velocity is given by two parameters that appear in equation of motion. The parameter of domain wall mobility (which is proportional to the slope of curve in field dependence of domain wall velocity) expresses the braking forces that oppose the domain wall motion (domain wall damping). The second parameter of domain wall velocity is called the critical field, which is related to the pinning mechanisms of domain wall.

Recently, at least three contributions to the domain wall damping were recognized. The first contribution arises from the eddy-currents induced in the neighbours of domain wall during the propagation. In the case of domain wall propagating between two axial domains covered by thin shell of surface domains, the corresponding term of domain wall damping arising from eddy current that was found to be inversely proportional to the axial domain diameter. The second contribution to the overall domain wall damping arises from the fact that the domain wall cannot move faster than magnetic moments which the domain wall consists of. The domain wall damping from magnetic relaxation of magnetic moments was found previously to be indirectly proportional to the domain wall width. Physically this dependence comes about because for a given domain wall velocity the spins in a thin wall must rotate more rapidly than in a thick one. The third contribution to the domain wall damping arises from the structural relaxation of mobile defects in amorphous materials. It was found previously, that this contribution becomes important at low temperatures, especially where the relaxation time of mobile defects remarkably increases as compared to the higher temperatures. The influence of domain wall damping from structural relaxation on domain wall dynamics is given by the relation between three times constants: (i) the relaxation time of mobile defects in amorphous material, (ii) the time of interaction between the domain wall in movement and the mobile defect (which is given by the domain wall thickness and the domain wall velocity) and (iii) the time between two reversals. Thanks to it, the domain wall damping by structural relaxation can be observed at lest in four distinct different regimes. Moreover, the domain wall damping from structural relaxation was found previously to be directly proportional to the concentration of mobile defects and inversely proportional to the temperature.

Since the magnetoelastic anisotropy was found to be very important in the case of amorphous glass-coated microwires, the domain wall dynamics was tailored by externally applied mechanical tensile stress in the first experiment. The FeNiSiB microwire with domain wall dynamics characterized by presence of four regimes of domain wall propagation was used for this measurement. The first regime was characterized by negative critical field and the lowest domain wall mobility. The negative value of critical field was maintained in the second regime, however, the field dependence of domain wall velocity was not linear in this case, but slight saturation of domain wall velocity was observed. The third regime of domain wall propagation was characterized by remarkable increase in domain wall mobility and by positive value of critical field. The fourth regime of domain wall propagation with positive value of critical field and higher domain wall mobility as compared to the third regime was observed at the highest domain wall velocities. Four regimes of domain wall propagation were observed at each value of applied tension stress, which allowed their study separately.

The tensile stress dependence of domain wall mobility was examined on amorphous cold-drawn wires in previous works. The low-tensile stress concave dependence of domain wall mobility was explained within two contributions to the domain wall damping (domain wall damping from magnetic relaxation of magnetic moments and domain wall damping from eddy-currents) in that case. However, the tensile stress dependence of domain wall damping at high values of tensile stress was characterized by convex shape of curve. The tensile stress dependence of domain wall damping in FeNiSiB amorphous glass-coated microwire was found to have a convex shape too. Such shape of the curve cannot be explained within the two contributions to the domain wall damping (from magnetic relaxation of magnetic moments and from eddy-current) as before, because of their concave stress-dependence. However, the domain wall is damped by structural relaxation during its motion, too. In accordance to the two-level model of Kronmuller theory, the overall interaction energy of mobile defect with amorphous matrix can be considered as the sum of dipole-dipole, exchange and magnetoelastic interaction energy. If the stress dependence of magnetoelastic contribution to the interaction energy of mobile defects with amorphous matrix is taken into account, the formula of domain wall damping from structure relaxation becomes square dependant on applied tensile stress and such convex dependence can explain qualitatively the measured data. Fit of the measured data confirmed that the domain

wall motion is damped by structure relaxation in the first regime of domain wall propagation. Such regime was observed previously as a diffusion damped regime of domain wall propagation. The magnetic moments of mobile defects try to follow the change in the magnetization direction, which occurs during the domain wall propagation. Since the relaxation time of mobile defects was comparable to the interaction time of the domain wall with mobile defects, a strong domain wall damping by structural relaxation occurred.

The domain wall damping value in second regime is very close to that observed in the first regime. However, one may observe a slight saturation of the domain wall velocity which can be recognized in v-H dependence. It was shown in the previous theoretical works that the domain wall compress its width above some critical domain wall velocity. The field dependence of domain wall velocity in second regime was fitted by the equation of domain wall motion containing the domain wall thickness for each value of applied tensile stress.

Within the first two regimes, the domain wall movement was damped by structure relaxation because of a relaxation time of mobile defects comparable to the interaction time of the domain wall with mobile defects in these regimes. However, as the domain wall velocity increases, the relaxation time of mobile defects becomes much higher than the interaction time of domain wall with mobile defects and domain wall is detached from the structure relaxation. This was probably observed in third regime of domain wall propagation, where domain wall mobility increased sharply and critical field became positive. The above mentioned assumption was confirmed by the fitting the tensile stress dependence of the domain wall mobility, where domain wall damping from structure relaxation had to be neglected in order to reach the agreement of model with measured data.

The fourth regime of domain wall propagation was characterized by the highest domain wall velocities. Unfortunately, the stress dependence of domain wall damping was not possible to fit by mechanical model of domain wall propagation because of very low values of fitted parameters.

Generally, the domain wall velocity decreased with applied tensile stress. In order to understand the influence of magnetic anisotropy strength on domain wall velocity in microwires, the magnetic anisotropy of microwires was reduced in a several comparative ways.

Firstly, amorphous glass coated microwires were treated thermally in conventional furnace. FeSiB amorphous glass-coated microwires were used for this experiment. Such composition is characterized by relatively low domain wall velocity, which doesn't exceed 1 km/s. It was shown in the previous works that the highest contribution to the domain wall damping arises from magnetic relaxation of magnetic moments at room temperature. On the other hand, magnetic relaxation of magnetic moment could be decreased by reduction of magnetic anisotropy. Since the strongest magnetic anisotropy in amorphous glass-coated microwires is the magnetoelastic one, magnetic anisotropy could be decreased by reduction of residual stresses via thermal annealing. However, the value of annealing temperature must be selected properly in order to meet the sufficient stress relaxation.

Thermal annealing at 200°C was not sufficient to change the domain wall dynamics remarkably. On the other hand, the thermal annealing at 300°C resulted in two remarkable effects: (i) domain wall mobility increase (ii) the appearing of the fast regime of domain wall propagation, which was not observed in the as-cast state. The domain wall mobility increase can be understand in term of reduced magnetic relaxation of magnetic moments contribution to the domain wall propagation (via relaxation of internal stresses) and by reduction of structural relaxation contribution to the domain wall damping (via volume concentration decrease of mobile defects).

An alternative way to the reduction of internal stresses was found in the thermal annealing under the mechanical tensile stress. The internal stress relaxation occurs more remarkably in the metallic core of microwire, as compared to glass-coat because of a higher melting temperature of glass. Removal of the tensile stress after thermal treatment results in the introduction of compressive mechanical stresses that fully compensates the tensile stress that was in the as-cast state. For this reason, amorphous glass-coated microwire thermally treated under the mechanical stress lost their magnetic bistability. In order to recover the magnetic bistability of the treated sample, a tensile stress of about 35 MPa had to be applied to the wire. The domain wall dynamics was characterized by very high domain wall velocity (7 km/s), which is three times higher than the domain wall velocity of as-cast sample. Further increase in applied tensile stress resulted in the full recover of the domain wall dynamics (domain wall mobility and critical field).

Taking into account the above discussed results, one may conclude that the low value of magnetic anisotropy seems to be necessary for the high domain wall velocities in microwires.

However, the highest domain wall velocities were observed in materials characterized by very high values of magnetic anisotropy: iron whiskers with maximum domain wall velocities of about 25 km/s has been examined by Deblois in late fifties of 20^{th} century, or orthoferrites with maximum velocities of about 60 km/s studied by Demokritov et al. in the late eighties of 20^{th} century. However, the magnetic anisotropy of these materials was not uniaxial. The same situation seems to be typical for amorphous glass-coated microwires, where the axial stresses are partially balanced by radial and circular mechanical stresses.

In order to understand better the influence of the geometry of magnetic anisotropies on domain wall dynamics, the microwires under investigation were thermally annealed in perpendicular field. Thermal annealing in perpendicular field induced a perpendicular anisotropy to the material, which resulted in the domain wall velocity increase and in the shift of the transition point between two regimes of domain wall propagation. A similar effect was observed in previous attempts, where domain wall velocity was measured in perpendicular field (with respect to the microwire axis).

Even more effective method of domain wall velocities tailoring was found in the current annealing. Current annealing of the sample during 10 minutes was found as much effective (from the domain wall velocity point of view) as thermal annealing during 1 hour at the same temperature by conventional way (annealing furnace). The domain wall velocity of FeSiB samples increased more than four times (from 1 km/s to more than 4 km/s) as compared to the as-cast state.

Finally, the domain wall velocity was studied in the microwire samples of reduced diameter down to 1 μm. The domain wall dynamics of these samples is characterized by the same dynamics as compared to thicker wires. This confirms that the high domain wall velocities of microwires are not result of the big size only, but perhaps the geometry of internal stresses (given by the glass-coat presence) play an important role. Moreover, the thermal annealing of microwires with reduced diameters resulted in the domain wall velocity increase. Such an effect was more remarkable in the samples treated in perpendicular field. The thermal annealing of 1 μm microwire increased the both domain wall mobility and the maximum domain wall velocity more than five times

as compared to the as-cast state. Such results are attractive for potential application especially where thin magnetic wires of well-defined domain wall dynamics are needed.

Along with the geometry of magnetic anisotropy and the strength of magnetic anisotropy, the presence of the surface shell of domain may play an important role for fast domain wall propagation in microwires, too. It was shown in previous works that the presence of the surface shell of domain can avoid the surface domain wall pinning by defects and therefore a higher domain wall velocities can be observed. In order to understand better the role of surface domain structure on fast domain wall propagation in microwires, the surface domain structure of the sample characterized by different domain wall velocities were compared.

The surface domain structure of amorphous glass-coated microwires of negative magnetostriction coefficient were studied previously, where typical bamboo surface domain structure consisting of circular surface domains was found in this material. All the previous magneto-optical observations of these samples were done under the common assumption that the cylindrical wires can be approximated by planar sample. However, this assumption failed to explain fully the observed surface domain structure of microwires with positive magnetostriction coefficient of metallic core studied in this work. For this reason, the method of magneto-optical observation of cylindrical samples was firstly examined. The main optical properties of amorphous glass-coated microwires are given by the presence of two factors: (i) glass-coat that decreases the light intensity reflected from the metallic core (therefore, glass-coat decreases the effective signal of Kerr-effect that arises from the light reflected from the metallic surface) and (ii) the cylindrical shape of the sample surface.

In order to determine the optimal experimental conditions for magneto-optical observation of composite materials, the reflectivity calculation of the bilayer structure consisting of the metal covered by thin layer of glass was performed. The reflectivity of s-polarized light was found to be higher as compared to p-polarization in the whole interval of incident angles. For this reason, the s-polarized light seems to be optimal for magneto-optical observation of composite material if high intensity of reflected light is needed. On the other hand, the total intensity of the light reflected from the metallic surface is higher if the p-polarized light is used for observations. Moreover, the highest portion of the total light reflected from microwire corresponds to that reflected from the metallic surface if the p-polarized light with incident angle equal to Brewster angle is

used in the magneto-optical observation. The total transmission of the incident light at the air to glass interface occurs, which means that the whole light is reflected by metal in this case.

Another important feature of magneto-optical observation of microwires consists in their cylindrical shape. This was confirmed by the optical observation on microscope with crossed polarizer and analyzer, where the light reflected from the cylindrical surface of microwire formed two light stripes. As it is well known from the optics, the linearly “s” or “p” polarized light is reflected from the non - magnetic planar sample as a linearly polarized light. Therefore, there is not reason for the remarkable light intensity transmitted by crossed polarizer and analyzer. In order to be sure that the magneto-optical observations of microwires are interpreted well, a detail calculation of the intensity profile of light reflected from the cylindrical surface was performed firstly. The calculation was done under two conditions: that the incident light beam consists of parallel rays only and the incident light beam is oriented parallel the main axis of the cylinder. The reflected light intensity profile was found to depend on two parameters only in that case: (i) the incident angle and (ii) the angle theta which defines the position on the cylinder surface. Detailed calculation of the reflected light intensity revealed that the plane of incidence orientation is the function of both parameters for each ray of the light beam. It means that the plane of incident has not constant orientation along the cylinder surface, but one may observe the complex inclination of planes of incident. It means, even if the linearly (“s” or “p” polarized) light is used for observations, the mutual orientation of the plane of incidence and the oscillating electric field intensity vector differs for each ray. If the s-polarized (p-polarized) light is used for magneto-optical observation, the oscillating electric field intensity vector is perpendicular (parallel) to the plane of incidence on the top of the wire only. Apart from the top of wire, the linear polarization is neither parallel nor perpendicular to the plane of incidence. For this reason, two component of linear polarization with respect to the local plane of incident is useful to distinguish: (i) the component of linear polarization oriented perpendicularly to the local plane of incidence (local s-polarization) and (ii) the component of linear polarization oriented parallel to the local plane of incidence (local p-polarization). The resulting magneto-optical observation of microwire is composed of two effects: (i) the magneto-optical Kerr effect of locally s-polarized light and (ii) the magneto-optical Kerr effect of locally p-polarized light that must be taken into account.

The intensity profile of the light reflected from cylindrical surface was calculated for two cases: (i) observation made by crossed polarizer and analyzer and (ii) for the case of polarized incident light only (without analyzer). While linearly polarized incident light beam produce the light intensity profile characterized by one remarkable maximum (above the top of wire), the light intensity profile consisting of two sharp maxima was obtained in the case of crossed polarizer and analyzer. Such calculated profiles apparently describe well the light intensity profiles of microwires observed at the microscope.

In order to calculate the profile of the light reflected from the cylinder magnetized in axial direction, a non-zero Voigt parameter was introduced to the reflection matrix. Magnetic interaction of the light with the surface magnetization of cylinder results in very small change as compared to the shape of the light intensity profile of non-magnetic cylinder. It was shown that the magnetic contrast consisting of two black and white stripes is characteristic for the change in the axial component of the surface magnetization in the case of cylindrical samples.

The characteristic black and white magnetic contrast resulting from the cylinder reversal in axial direction may be explained within the transverse Kerr-effect domination. The vector of axial magnetization change has non-zero component with respect to the normal to the plane of incidence. Due to symmetric inclination of planes of incidence with respect to the main axis, the normal component of the axial magnetization change is the same in magnitude (but opposite) for both sides of cylinder.

Comparison of the volume hysteresis loop measured by MPMS and the surface hysteresis loop measured by MOKE for the same orientation of magnetic field (perpendicular to the main axis) revealed that the saturation field of the volume hysteresis loop is very close to that measured in the surface hysteresis loop. This confirms that the highest magnetic anisotropy is present at the microwire surface. Moreover, the value of saturation field was found to be much higher than $M_S/2$, which points to the presence of additional (magnetoelastic) magnetic anisotropy in each sample of microwire under the investigation. The surface magnetization process was found to consist of two processes: (i) non-hysteretic magnetization rotation that occurs at high magnetic field and (ii) jump in the surface magnetization direction that appears at low magnetic field. It was shown previously, that the low-field change in the surface magnetization direction is due to the internal domain wall propagation. The domain wall

propagating inside the wire strongly interacts with the shell of surface domains and it changes the orientation of surface magnetization direction, consequently. For this reason, two surface magnetization processes (non-hysteretic rotation at high field and surface magnetization change invoked by the internal domain wall propagation) had to be examined separately.

The change in the surface magnetization direction invoked by the internal domain wall propagation was detected by the digital image processing. The whole process consisted of three steps: (1,) microwire was switched to one axial direction and the magnetic field was reduced to zero when background image was captured (2,) microwire under investigation was reversed by axial field oriented in opposite direction and the field was reduced to zero when the image was captured (3,) background image was subtracted from the image obtained in step (2,) and the result was averaged. It is worth mentioning that the magnetic contrast obtained in such way corresponds to the surface magnetization change that occurs during the Large Barkhaussen jump in microwires.

The magnetic contrast invoked by the internal domain wall propagation was studied in the series of FeNiSiB samples of microwires characterized by different thickness of the surface domain structure measured previously.

A different magnetic contrast was observed in the (i) central part of the microwire and (ii) close to the microwire ends. The magnetic contrast consisting of black and white stripes was found in the each sample under the investigation. It confirms that the domain wall propagation leads to the change in the axial component of the surface magnetization during the domain wall propagation. Moreover, the strength of magnetic contrast was found different in the samples of thin and thicker shell of the surface domains.

The as-cast FeSiB amorphous glass-coated microwires characterized by thin surface domain structure (<100 nm) showed a big change in the surface magnetization direction during the domain wall propagation, whereas they display relatively low domain wall velocity (< 1.5 km/s). On the other hand, the interaction of the propagating domain wall with the shell of surface structure was not observed in the FeNiSiB microwires characterized by thicker shell of surface domains. At the same time, the domain wall velocity reached much higher values (up to 10 km/s) in this microwire. The above results confirm that the presence of surface domain structure can play an important role for achieving the high domain wall velocity in microwires.

A different magnetic contrast was observed close to the end of the wire, where closure domain structure would appear according to the recent models. The black and white magnetic contrast continuously disappears as the end of the wire was approached. Application of the magnetic field parallel to the axial magnetization resulted in the compression of the closure domain structure. Note, that the closure domain structure was not completely removed even at the highest values of applied field of 0.2 T. Application of the magnetic field oriented parallel to the magnetization in the closure domain structure resulted in Large Barkhaussen jump. The length of the closure domain structure doesn't exceeded the value of 100 μm in each studied piece of FeSiB microwire, while the closure domain structure length of more than 5 mm was observed in the sample of higher nickel content (FeNiSiB microwire). The apparent size of the closure domain structure may be attributed to the shape anisotropy of the wire as well as to the mechanical stresses introduced to the wire ends during the sample cutting.

Magneto-optical observation of the surface magnetization processes invoked by the internal domain wall propagation revealed that the axial component of magnetization changes during the domain wall motion in microwires. However, the surface domain structure was not clarified.

In order to understand better the surface magnetization direction and its possible interplay on the fast domain wall propagation, the surface hysteresis loops of microwires in high magnetic field by use of microscope were measured in the next step. Application of high magnetic field leads to the many undesirable magneto-optical effects (in parallel to the Kerr-effect) which must be taken into account: (i) rotation of the plane of polarization by glass-coat (Faraday Effect of glass-coat) (ii) rotation of the plane of polarization by objective used in the experiment (Faraday Effect of the objective). The axial surface hysteresis loops revealed that the surface magnetization process at the wire top consists of two processes: (i) apparent magnetization rotation and (ii) the jump in magnetization direction that occurs due to the domain wall propagation. However, hysteresis loop measured at the light shadow (probably formed by the light primary reflected from the glass-coat only) are characterized by the apparent magnetization rotation of the same slope as compared in the surface wire loops, but the jump due to the internal domain wall propagation was missing. One of possible explanations is that the apparent magnetization rotation measured at the surface hysteresis loop at the wire top corresponds to the Faraday Effect of glass-coat which

must be taken into account at such high magnetic fields (0.2T). It means that the surface magnetization direction is not changed by application of axial magnetic field in this case. It means that the shell of surface domains is characterized by axial magnetization at the surface. Another possible explanation of such observation may be interpreted in the absence of the shell of surface domains, which means the axial domain can be observed directly and the domain wall (as a boundary between two domains) can be observed directly too.

Magneto-optical observation of the domain wall was performed by two comparative methods, in which the domain wall was trapped in a potential well. The microwire under the investigation was bended to the shape of letter “U” within the first approach. Application of magnetic field along the magnetization in closure domain resulted in the single domain wall propagation to the microwire centre. The boundary between two domains (domain wall) was not abrupt, but one could observe a tilted domain wall. In order to avoid the mechanical stresses induced to the wire by its bending, the surface domain wall structure was examined in the next experiment where straight microwire was observed. The microwire was placed between two coils powered independently by two power supplies. The whole process of domain wall trapping was done in two steps. Firstly, the magnetic field intensity of primary coil was set to the certain value by power supply. Adjusting the electric current at the second power supply allowed to shift the region of zero magnetic field between two coils (and consequently domain wall, too) along the microwire. The domain wall was trapped by the gradient of magnetic field (in this case given by the ratio of magnetic field produced by both coils), however, the stable position of the domain wall was always at zero magnetic field.
Such experimental approach allowed: (i) to avoid the influence of the bended wire shape on the surface domain wall structure, because the additional mechanical stresses (from wire bending) vanishes in the straight sample and (ii) to observe the domain wall at zero magnetic field (which allowed to exclude the magnetostatic interaction).
The apparent tilting of the surface domain wall structure was observed in this case too. Moreover, the measurements of the surface domain wall length were performed at different positions of microwire with 2 cm in length. The domain wall tilting angle was not constant along the microwire axis, but one could observe that the surface domain wall length varied from *40 μm* to *210 μm* in case of $Fe_{77.5}Si_{7.5}B_{15}$ microwires.

The surface domain wall length was measured in the second group of microwires ($Fe_{49.6}Ni_{27.9}Si_{7.5}B_{15}$) where surface magnetic contrast invoked by internal domain wall propagation was possible to detect. The surface domain wall length fluctuated around its *120 μm* average value in this composition. The direction of domain wall inclination was the same as before. We tried to change the domain wall inclination direction by application of magnetic field oriented perpendicularly to the microwire main axis. However, the inclination direction was found neither to be the function of the position along the sample nor externally applied perpendicular magnetic field. This shows that the origin of the surface domain wall inclination should be associated with the much stronger (as compared to Zeeman interaction) magnetoelastic magnetic anisotropy.

The tilted surface domain wall structure should be explained by the reduction of demagnetizing energy associated with magnetic surface charge density which decreases by domain wall inclination. At the same time, the tilted surface domain wall structure can be found responsible for the apparent high domain wall velocities measured previously in Sixtus-Tonks experiment.

Abstrakt v slovenčine

Pohyb doménovej steny v tenkých magnetických drôtoch sa ocitá v centre pozornosti kvôli rozvoju spintroniky. Spintronika, alebo spinovo orientovaná elektronika je rozvíjajúca sa technológia, v ktorej sa na prenos informácie používa magnetický moment elektrónu. Jednou z koncepcií budovania spintroniky je spintronika vybudovaná na báze tenkých feromagnetických drôtov. Hodnota logickej úrovne je kódovaná smerom magnetizácie, kým zmena logickej úrovne je prevádzaná pohybom doménovej steny. V predchádzajúcich prácach bolo zostrojených viacero prototypov spintronických zariadení na báze tenkých feromagnetických drôtov: logické hradlá na báze pohybu doménových stien typu „xor“, „and“ alebo „not“, spintronická dióda alebo spintronická pamäť typu „race-track“, ktorá používa synchrónny pohyb veľkého množstva doménových stien na čítanie a zápis informácie. Vo všetkých spomenutých zariadeniach je rýchlosť pohybu doménovej steny jedným z rozhodujúcich parametrov, ktoré ovplyvňujú konečnú operačnú rýchlosť týchto zariadení. Z tohto dôvodu je rýchlosť pohybu doménovej steny v tenkých drôtoch jedným z predmetov štúdia v súčasnej spintronike na báze tenkých magnetických drôtov. Maximálna rýchlosť v súčasne konštruovaných prototypoch nepresahuje 2 km/s. Na druhej strane, maximálna rýchlosť pohybu doménových stien v mikrodrôtoch dosahuje rýchlosti až 20 km/s.

Štúdium pohybu doménových stien v mikrodrôtoch je atraktívne aj z hľadiska ich možných aplikácii v senzoroch. Amorfné, sklom potiahnuté mikrodrôty sú v súčasnosti používané v integrovaných zariadeniach, kde slúžia ako senzory (i) vonkajších magnetických polí, (ii) mechanického napätia alebo (iii) mechanického predĺženia. Tieto externé sily sa snímajú pomocou odozvy dynamiky doménovej steny. Detailná znalosť dynamiky doménovej steny je tak dôležitá aj z aplikačného hľadiska.

Hlavným cieľom tejto práce je preskúmanie mechanizmov, ktoré umožňujú ladenie dynamiky rýchlej doménovej steny v mikrodrôtoch. Druhým cieľom je lepšie pochopenie pôvodu tak veľkých rýchlostí doménovej steny v amorfných, sklom potiahnutých mikrodrôtoch.

Amorfné, sklom potiahnuté mikrodrôty sú kompozitný materiál, ktorý pozostáva z kovového jadra a skleneného obalu. Je dôležité zdôrazniť, že magnetické vlastnosti

mikrodrôtov sú dané najmä postupom ich výroby Taylorovou-Ulitovského metódou. Počas tohto procesu výroby sa mikrodrôty vyrábajú ťahaním a prudkým chladením. V dôsledku rozdielneho teplotného koeficientu rozťažnosti kovového jadra a skleneného obalu dochádza k indukovaniu silných pozdĺžnych a radiálnych mechanických pnutí do mikrodrôtov. Dodatočné ťahanie mikrodrôtov počas výroby do nich indukuje mechanické napätia pozdĺžneho smeru. Výsledná geometria mechanických pnutí je v mikrodrôtoch veľmi zložitá. Podľa magneto-elastického modelu môže byť napäťové pole mikrodrôtov zhruba popísané dominantným pozdĺžnym mechanickým pnutím v centrálnej časti mikrodrôtu, pričom radiálne a cirkulárne mechanické pnutia dominujú v okrajovej časti kovového jadra mikrodrôtu. Navyše, hodnoty mechanických pnutí v mikrodrôtoch dosahujú veľmi veľké hodnoty, ktoré sú blízko medze pevnosti daného materiálu. To je možno dôvod, prečo je megneto-elastické usporiadanie dominantné v prípade mikrodrôtov. To je potvrdené aj experimentom, kde sa ukazuje, že doménová štruktúra mikrodrôtov je daná iba znamienkom magnetostrikcie kovového jadra. To dokazuje, že dominantnou magnetickou anizotropiou nie je tvarová anizotorpia (ako v prípade Py magnetických nanodrôtov), ale magnetoelastická anizotorpia.

Ak je amorfný, sklom potiahnutý mikrodrôt vyrobený z kovovej zliatiny s kladnou magnetostrikciou, najmenšia energia magneto-elastického usporiadania je dodržané pre paralelný smer orientácie magnetizácie vzhľadom na vnútorné mechanické pnutia. Z tohto dôvodu sa doménová štruktúra takýchto drôtov skladá z jednej veľkej axiálnej domény, ktorá je obklopená tenkou vrstvou radiálnych domén (podľa súčasného teoretického modelu popisujúcom reziduálne mechanické pnutia v mikrodrôtoch). Navyše, hlavným magnetizačným procesom amorfných, sklom potiahnutých mikrodrôtov s kladnou magnetostrikciou je veľký Barkhaussenov skok pozostávajúcom pohybom doménovej steny pozdĺž celej dĺžky mikrodrôtu.

Dynamika doménovej steny v amorfných, sklom potiahnutých mikrodrôtoch bola skúmaná v rámci mechanického modelu pohybu doménovej steny prvýkrát zavedený Kittelom na začiatku 50-tych rokov 20. storočia. Pohyb doménovej steny bol porovnávané s pohybom hmotného bodu vo viskóznom prostredí. Pohyb doménovej steny je v tom prípade popísaný rovnicou podobnou rovnici mechanického harmonického oscilátora. Dá sa ukázať, že pohybová rovnica doménovej steny má v tom prípade lineárny tvar, kedy rýchlosť doménovej steny je priamo úmerná

aplikovanému magnetickému poľu. Rýchlosť doménovej steny závisí iba od dvoch parametrov a to: (i) pohyblivosťou doménovej steny (ktorá vyjadruje brzdné mechanizmy pôsobiace na doménovú stenu počas je pohybu) a (ii) kritickým poľom (ktoré vyjadruje záchytné mechanizmy pôsobiace na doménovú stenu počas jej odtrhávania od konca drôtu).

V súčasnosti sú známe tri príspevky k tlmeniu pohybu doménovej steny. Prvým z nich je príspevok od vírivých prúdov indukovaných v okolí pohybujúcej sa doménovej steny. V prípade doménovej steny pohybujúcej sa medzi dvoma axiálnymi doménami pokrytými tenkou vrstvou radiálnych domén je príslušný príspevok nepriamo úmerný priemeru axiálnej domény. Druhý príspevok ku koeficientu tlmenia pohybu doménovej steny súvisí s faktom, že doménová stena sa nemôže pohybovať rýchlejšie ako magnetické momenty, z ktorých sa doménová stena skladá. Bolo ukázané, že príspevok od magnetickej relaxácie magnetických momentov ku tlmeniu pohybu doménovej steny je nepriamo úmerný hrúbke doménovej steny. Fyzikálne táto závislosť vyjadruje to, že čím je doménová stena užšia, tým rýchlejšie sa magnetické momenty musia preklápať a tým je väčšie brzdenie pohybu doménovej steny pochádzajúce od magnetických momentov. Tretím príspevkom k tlmeniu pohybu doménovej steny je príspevok od štruktúrnej relaxácie pohyblivých defektov v amorfnej matrici. V predchádzajúcich prácach bolo ukázané, že tento príspevok k tlmeniu pohybu doménovej steny je výrazný najmä pri nižších teplotách, kde relaxačný čas pohyblivých defektov je omnoho vyšší ako pri vyšších teplotách. Prejavy tlmenia pohybu doménovej steny od štruktúrnej relaxácie závisia najmä od pomerov medzi troma časmi použitými v experimente: (i) relaxačný čas pohyblivých defektov, (ii) čas, ktorý doménová stena potrebuje na prejdenie pohyblivého defektu (ktorý je daný rýchlosťou doménovej steny a hrúbkou doménovej steny) a (iii) časom medzi dvoma pohybmi doménovej steny. Vďaka tomu, tlmenie pohybu doménovej steny od štruktúrnej relaxácie môže byť pozorované v štyroch rozličných režimoch. Navyše bolo ukázané, že príspevok k tlmeniu pohybu doménovej steny od štruktúrnej relaxácie je priamo úmerný objemovej koncentrácii voľných objemov a nepriamo úmerný teplote.

Keďže dominantnou magnetickou anizotropiou v mikrodrôtoch je magnetoelastická anizotropia, dynamika doménovej steny bola najprv ladená mechanickým pnutím aplikovaným na mikrodrôt. Amorfný, železo-niklový sklom potiahnutý mikrodrôt charakteristický štyrmi režimami pohybu doménovej steny bol použitý pre uvedené merania. Prvý režim sa vyznačoval zápornou hodnotou kritického poľa a najnižšou

hodnotou pohyblivosti doménovej steny. Záporná hodnota kritického poľa bola zachovaná aj v druhom režime pohybu doménovej steny, avšak rýchlosť doménovej steny nebola lineárnou funkciou rýchlosti v tomto režime. Tretí režim pohybu doménovej steny sa vyznačoval výrazným nárastom pohyblivosti doménovej steny a kladnou hodnotou kritického poľa. Štvrtý režim pohybu doménovej steny sa vyznačoval kladnou hodnotou kritického poľa a omnoho vyššou hodnotou pohyblivosti doménovej steny ako to bolo v treťom režime. Všetky štyri režimy pohybu doménovej steny sa objavovali pri každej hodnote aplikovaného napätia, čo umožňovalo poukázať na ich možný pôvod.

Napäťová závislosť koeficientu tlmenia pohybu doménovej steny bola študovaná už v predchádzajúcich prácach. Bolo ukázané, že konkávnu závislosť koeficientu tlmenia pohybu doménovej steny pri nízkych poliach je možné vysvetliť pomocou dvoch príspevkov k tlmeniu pohybu doménovej steny (príspevok od magnetickej relaxácie magnetických momentov a príspevok od vírivých prúdov). Na druhej strane, napäťová závislosť koeficientu tlmenia pohybu doménovej steny pri vysokých napätiach mala konvexný tvar. Napäťová závislosť koeficientu tlmenia pohybu doménovej steny má v železo-niklových vzorkách tiež konvexný tvar. Takáto napäťová závislosť nemôže byť vysvetlená príspevkami od vírivých prúdov a magnetickej relaxácie magnetických momentov, pretože obidva uvedené príspevky majú konkávny priebeh. Ako však bolo spomenuté vyššie, doménová stena je pri svojom pohybe brzdená aj príspevkom od štruktúrnej relaxácie. Podľa dvojhladinovej teórie Kronmullera, celková interakčná energia pohyblivého defektu s amorfnou matricou je daná súčtom dipól-dipólovej, výmennej a megnetoelastickej interakcie. Ak sa uvažuje, že magnetoelastická interakcia pohyblivého defektu so svojim okolím závisí od mechanického pnutia, koeficient tlmenia pohybu doménovej steny od štruktúrnej relaxácie sa dá vyjadriť ako člen priamo úmerný druhej mocnine pôsobiacich mechanických pnutí a takáto konvexná závislosť dokáže kvalitatívne dobre popísať nameranú napäťovú závislosť koeficientu tlmenia pohybu doménovej steny. Fitovanie nameraných dát potvrdzuje, že doménová stena je počas svojho pohybu v prvom režime brzdená najmä štruktúrnou relaxáciou. Keďže relaxačný čas pohyblivých defektov je porovnateľný s časom, ktorý potrebuje doménová stena na prejdenie defektu, dochádza k brzdeniu pohybu doménovej steny štruktúrnou relaxáciou.

Dynamika doménovej steny v druhom režime sa veľmi podobá na dynamiku doménovej steny v prvom režime. Záporná hodnota kritického poľa je zachovaná, avšak závislosť

rýchlosti doménovej steny od magnetického poľa nie je lineárna tak ako v predchádzajúcom režime. Namiesto toho je možné pozorovať jemnú saturáciu rýchlostí doménovej steny v druhom režime. V predchádzajúcich prácach bolo ukázané, že doménová stena zmenšuje svoju hrúbku pri prekročení istej kritickej rýchlosti. Poľová závislosť rýchlosti doménovej steny v druhom režime bola fitovaná modelom pohybu doménovej steny obsahujúcom predpoklad o premenlivej hrúbke doménovej steny.

V prvých dvoch režimoch pohybu doménovej steny bol relaxačný čas pohyblivých defektov porovnateľný s časom, ktorý doménová stena potrebuje na prekonanie polohy pohyblivého defektu. Ak však rýchlosť doménovej steny narastie, relaxačný čas pohyblivých defektov je omnoho väčší ako čas, ktorý doménová stena potrebuje na prekonanie pohyblivého defektu. Doménová stena je v takom prípade odtrhnutá od štruktúrnej relaxácie a príspevok k tlmeniu pohybu doménovej steny prudko klesá. To je pravdepodobne pozorované v treťom režime dynamiky doménovej steny, kde pohyblivosť doménovej steny prudko narastie a kritické pole je kladné. Tento predpoklad je potvrdený fitovaním napäťovej závislosti koeficientu tlmenia pohybu doménovej steny v treťom režime, kde príspevok od štruktúrnej relaxácie musí byť zanedbaný za účelom dosiahnutia dobrého súladu modelu s experimentom.

Štvrtý režim dynamiky doménovej steny je charakteristický najväčšími pozorovanými rýchlosťami. Napäťovú závislosť koeficientu tlmenia pohybu doménovej steny nie je možné vyfitovať pomocou mechanického modelu pohybu doménovej steny, nakoľko uvedený model dáva veľmi nízke hodnoty parametrov pohybu.

Rýchlosť doménovej steny s narastajúcim mechanickým pnutím vo všeobecnosti klesá. To by malo znamenať, že s klesajúcou magnetickou anizotropiou rýchlosť doménovej steny stúpa. Za účelom pochopenia vplyvu sily magnetickej anizotropie na rýchlosť doménovej steny, bola magnetická anizotropia v mikrodrôtoch ladená niekoľkými spôsobmi.

Dynamika doménovej steny bola skúmaná na mikrodrôtoch žíhaných v konvenčnej piecke. Na prvé merania bol použitý amorfný sklom potiahnutý mikrodrôt s vysokým obsahom železa ($Fe_{77.5}Si_{7.5}B_{15}$). Takéto zloženie je charakteristické nízkou rýchlosťou doménovej steny, ktorá nepresahuje 1 km/s. V predchádzajúcich prácach bolo ukázané, že najdôležitejším príspevkom k tlmeniu pohybu doménovej steny je príspevok od magnetickej relaxácie magnetických momentov pri izbovej teplote. Príspevok k tlmeniu pohybu doménovej steny od magnetickej relaxácie magnetických momentov môže byť

zmenšený redukciou magnetickej anizotropie. Keďže najdôležitejšou magnetickou anizotropiou v mikrodrôtoch je magnetoelastická anizotropia, magnetická anizotropia mikrodrôtov môže byť zredukovaná zmenšením reziduálnych pnutí tepelným žíhaním. Teplota tepelného žíhania však musí byť správne zvolená za účelom dosiahnutia účinnej relaxácie mechanických pnutí.

Tepelné žíhanie pri 200°C nebolo účinné na zmenu dynamiku doménovej steny. Na druhej strane, tepelné žíhanie pri 300°C vyústilo v dve významné zmeny: (i) nárast pohyblivosti doménovej steny (ii) objavenie rýchleho režimu pohybu doménovej steny (ktorý nie je možné popísať mechanickým modelom pohybu). Nárast pohyblivosti doménovej steny môže byť vysvetlený znížením príspevku k tlmeniu pohybu doménovej steny od magnetickej relaxácie magnetických momentov (znížením reziduálnych mechanických pnutí) a redukciou príspevku od štruktúrnej relaxácie ku koeficientu tlmenia pohybu doménovej steny (znížením koncentrácie voľných objemov).

Iný spôsob zníženia reziduálnych mechanických pnutí bol nájdený v tepelnom žíhaní pod mechanickým pnutím. Kvôli nižšej teplote topenia kovu prebieha relaxácia mechanických pnutí v kovovom jadre efektívnejšie ako v skle. Odstránenie mechanického pnutia po skončení žíhania vedie k indukcii kompresných pnutí axiálneho smeru, ktoré plne vykompenzujú reziduálne mechanické pnutia ťahového charakteru, ktoré boli naindukované do mikrodrôtu počas jeho výroby. To spôsobuje stratu bistabilného charakteru mikrodrôtov. Bistabilné správanie takto upravenej vzorky je možné následne docieliť aplikovaním vonkajšieho mechanického pnutia 35 MPa. Dynamika doménovej steny v takom prípade je charakteristická veľmi vysokou hodnotou rýchlosti doménovej steny (7 km/s), čo je takmer trikrát väčšia rýchlosť ako v as-cast vzorke. Ďalšie zvyšovanie mechanických pnutí (nad 35 MPa) vedie k úplnému obnoveniu dynamiky doménovej steny (rýchlosti doménovej steny a kritickému poľu) v žíhanej vzorke.

Z uvedeného vyplýva, že s narastajúcim mechanickým pnutím sa rýchlosť doménovej steny v mikrodrôtoch zmenšuje. To by mohlo naznačovať, že pre dosiahnutie veľkých rýchlostí doménovej steny v mikrodrôtoch sú nevyhnutné nízke hodnoty magnetickej anizotropie. Na druhej strane, najrýchlejšie doménové steny boli pozorované v materiáloch s vysokou hodnotou magnetickej anizotropie (štúdie De Bloisa na železných whiskeroch – 25km/s, štúdie Demokritova na ortoferitoch – doménové steny

s rýchlosťou až 60 km/s). Navyše, magnetická anizotropia v týchto materiáloch nie je jednoosá. V amorfných, sklom potiahnutých mikrodrôtoch je situácia podobná – dominantnej axiálna magnetická anizotropia je čiastočne kompenzovaná radiálnou a cirkulárnou magnetickou anizotropiou.

Za účelom lepšieho pochopenia vplyvu geometrie pôsobiacich anizotropií na dynamiku doménovej steny v mikrodrôtoch boli mikrodrôty žíhane v kolmom magnetickom poli. Tepelné žíhanie mikrodrôtov v kolmom magnetickom viedlo k miernemu nárastu pohyblivosti doménovej steny a posunu poľa prechodu medzi primárnym a sekundárnym režimom dynamiky doménovej steny. Podobný efekt bol pozorovaný v predchádzajúcich prácach, kde bola študovaná dynamika doménovej steny v kolmom magnetickom poli (s ohľadom na os drôtu).

Ešte účinnejší spôsob ladenia dynamiky doménovej steny bol nájdený v prúdovom žíhaní mikrodrôtov. Bolo zistené, že prúdové žíhanie vzoriek počas 10 minút je rovnako efektívne z hľadiska nárastu rýchlostí doménovej steny v mikrodrôtoch ako žíhanie konvenčným spôsobom (v žíhacej piecke) počas jednej hodiny. Rýchlosť doménovej steny pri prúdovom žíhaní narástla na 4 – násobnú hodnotu (z 1km/s na 4 km/s) v porovnaní s rýchlosťou doménovej steny v „as-castovom“ stave.

Dynamika rýchlej doménovej steny bola skúmaná na sade mikrodrôtoch s redukovaným priemerom (od 5 μm do 1 μm). Dynamika doménových stien takto tenkých drôtov je rovnaká ako v prípade drôtov s väčším polomerom (typicky 15 μm). To znamená, že veľké rýchlosti doménovej steny dosahované v mikrodrôtoch nie sú dôsledkom iba veľkosti materiálu, ale pravdepodobne súvisia s geometriou vnútorných pnutí (súvisiacimi s prítomnosťou skleneného obalu), ktoré sú dané postupom ich výroby. Navyše, tepelné žíhanie vedie k nárastu rýchlosti doménovej steny v mikrodrôtoch s redukovaným priemerom. Tento efekt bol špeciálne nápadný pri žíhaní v kolmom magnetickom poli, kedy tepelné žíhanie mikrodrôtov (s priemerom 1 μm) viac ako päťnásobne zvyšovalo maximálnu rýchlosť doménovej steny. Tieto výsledky sú atraktívne najmä pre potenciálne senzorické aplikácie, kde je potrebné pripraviť tenké magnetické drôty s dobre definovanou dynamikou doménovej steny.

Rýchlosť doménovej steny môže byť popri geometrii pôsobiacich magnetických anizotropií ovplyvnená aj prítomnosťou povrchovej vrstvy domén. V predchádzajúcich prácach bolo ukázané, že prítomnosť povrchovej vrstvy domén môže zabraňovať zachytávaniu doménovej steny na povrchových defektoch a tým umožňovať ešte väčšie

rýchlosti doménovej steny. Za účelom pochopenia tohto javu bola skúmaná povrchová doménová štruktúra mikrodrôtov na vzorkách s odlišnou rýchlosťou doménovej steny. V predchádzajúcich prácach bola študovaná povrchová doménová štruktúra mikrodrôtov so zápornou magnetostrikciou, kde cirkulárna doménová štruktúra bola nájdená ako typická pre tento typ materiálu. Všetky predchádzajúce magneto-optické pozorovania mikrodrôtov so zápornou magnetostrikciou boli vykonané na základe predpokladu, že pozorovaný valcový povrch mikrodrôtov je možné aproximovať rovinnou plochou. Tento predpoklad však nebol schopný vysvetliť všetky pozorované optické vlastnosti mikrodrôtov s kladnou magnetostrikciou. Z tohto dôvodu boli najprv študované optické vlastnosti valcových vzoriek. Hlavné optické (a z nich vyplývajúce magneto-optické) vlastnosti mikrodrôtov vyplývajú z dvoch faktorov: (i) prítomnosť skleneného obalu na povrchu mikrodrôtu, ktorý znižuje celkové množstvo svetla odrazeného od kovového povrchu a (ii) valcový tvar kovového jadra mikrodrôtu. Za účelom lepšieho pochopenia optických vlastností mikrodrôtov boli skúmané obidva tieto faktory teoreticky, pred začatím samotných meraní. Za účelom nájdenia optimálnych pozorovacích podmienok na vykonávanie magneto-optických pozorovaní mikrodrôtov, bol vykonaný výpočet reflektivity pre dvojvrstvu pozostávajúcu z kovu pokrytého tenkou vrstvou skla. Reflektivita s-polarizovaného svetla bola nájdená ako väčšia v porovnaní s reflektivitou p-polarizovaného svetla celom intervale uhlov dopadu. Z tohto dôvodu je výhodnejšie využívať na magneto-optické pozorovania mikrodrôtov s-polarizované svetlo; a to najmä tam, kde je kladený dôraz na vysokú intenzitu odrazeného svetla. Ak sa však prepočíta aké množstvo svetla odrazeného z mikrodrôtu je tvorené svetlom odrazeným z kovového povrchu, p-polarizované svetlo dáva viac efektívny signál. Navyše, najväčšia časť odrazeného svetla pripadá na odraz od kovového povrchu jadra mikrodrôtu ak uhol dopadu je rovný Brewsterovmu uhlu. Úplný prechod svetla rozhraním sklo-vzduch pri danom uhle spôsobuje, že všetko svetlo odrazené od mikrodrôtu je tvorené svetlom odrazeným od kovového jadra mikrodrôtu.

Druhou dôležitou optickou vlastnosťou mikrodrôtov je ich valcový tvar. To bolo potvrdené pozorovaniami na mikroskope so skríženým polarizérom a analyzérom, kde mikrodrôt bolo možné pozorovať ako dva svetelné pásy. Ako je z optiky známe, lineárne „s“ alebo lineárne „p“ polarizované svetlo sa odráža od rovinnej vzorky ako lineárne polarizované. Preto ak by sme predpokladali že povrch mikrodrôtov je tvorený rovinnou plochou, dva svetelné pásy pri skríženom polarizéri a analyzéri by nemali byť

pozorované. Za účelom potvrdenia toho, že výsledky magneto-optických pozorovaní sú spravené korektne, najprv bol vypočítaný profil intenzity odrazeného svetla od kovového valca. Výpočet profilu intenzity odrazeného svetla bol urobený pod dvoma podmienkami: (i) svetelný zväzok lúčov je tvorený len rovnobežnými lúčmi a (ii) zväzok lúčov dopadá na povrch valca v smere hlavnej osi valca. Profil intenzity odrazeného svetla je v tom prípade funkciou len dvoch parametrov: (i) uhla dopadu a (ii) uhla theta, ktorý udáva polohu na povrchu valca. Detailný výpočet profilu intenzity odrazeného svetla odhalil, že orientácia roviny dopadu je funkciou oboch týchto parametrov. To znamená, že rovina dopadu nie je konštantná pre každý lúč (každú polohu na povrchu valca), ale je možné pozorovať stočenie roviny dopadu vzhľadom na os valca. Aj keď je dopadajúce svetlo lineárne „s“ alebo „p“ polarizované, vzájomná orientácia polarizácie a roviny dopadu nie je na povrchu valca konštantná. Ak na magneto-optické pozorovania je použité „s“ polarizované svetlo, oscilujúci vektor intenzity elektrického poľa je kolmý vzhľadom na rovinu dopadu iba na vrchu valca. Mimo vrchu valca nie je svetlo ani „s“ polarizované (kolmo) ani „p“ polarizované (paralelne). Z toho dôvodu je výhodné rozlišovať dve zložky oscilujúcej intenzity elektrického poľa vzhľadom na rovinu dopadu: (i) zložka lineárnej polarizácie kolmá na lokálnu rovinu dopadu (lokálna s-polarizácia) a (ii) zložka lineárnej polarizácie paralelná vzhľadom na lokálnu rovinu dopadu (lokálna p- polarizácia). Výsledný magneto-optický Kerrov jav je daný súčtom (i) príspevku Kerrovho javu od lokálnej s-polarizácie a (ii) príspevkom Kerrovho javu od lokálnej p- polarizácie.

Profil intenzity odrazeného svetla od valcového povrchu bol počítaný pre dva prípady: (i) pre prípad lineárne polarizovaného svetla (bez analyzéra) a pre (ii) pozorovanie vykonané so skríženým polarizérom a analyzérom. Výpočet ukázal, že kým profil intenzity odrazeného svetla pre prvý prípad pozostával z jedného výrazného maxima, v druhom prípade profil intenzity odrazeného svetla pozostával z dvoch výrazných maximím. Tento výsledok popisuje kvalitatívne profil intenzity odrazeného svetla pozorovaného na mikroskope.

Za účelom vypočítania profilu intenzity odrazeného svetla pre zmagnetovaný valec, bola vzatá do úvahy nenulová hodnota Voightovho parametra. Interakcia svetla so zmagnetovaným povrchov valca vyústila do veľmi malej zmeny v profile intenzity odrazeného svetla v porovnaní s nemagnetickým valcom. Bolo ukázané, že charakteristický magnetický kontrast pozostávajúci z dvoch čiernobielych pásikov je

typický pre zmenu povrchovej magnetizácie v axiálnom smere. Takýto čiernobiely magnetický kontrast je možné vysvetliť príspevkom od transverzálneho Kerrovho javu. Vektor zmeny axiálnej zložky povrchovej magnetizácie má nenulovú zložku vzhľadom na normálu hlavnej osy. Kvôli symetrickému nakloneniu rovín dopadu voči hlavnej osi valca je kolmá zložka axiálnej zmeny magnetizácie vzhľadom na os drôtu rovnaká vo veľkosti (ale opačná) pre obe strany valca.

Porovnanie objemovej hysteréznej slučky meranej na MPMS a povrchovej hysteréznej slučky meranej pomocou MOKE pre rovnakú orientáciu magnetického poľa vzhľadom na os drôtu odhalila, že pole saturácie pre povrchovú hysteréznu slučku je veľmi blízke hodnote saturačného poľa objemovej hysteréznej slučky. To naznačuje, že na povrchu mikrodrôtu je magnetická anizotropia najsilnejšia. Navyše, hodnota poľa saturácie bola značne vyššia ako $M_S/2$, čo znamená, že okrem tvarovej anizotropie je vo vzorke mikrodrôtu aj iná (magnetoelastická) magnetická anizotropia. Magnetizačný proces na povrchu mikrodrôtu pozostáva z dvoch procesov: (i) nehysterézna magnetická rotácia ktorá nastáva v oblasti vysokých polí a (ii) skok v smere povrchovej magnetizácii, ku ktorému dochádza v oblasti nízkych polí. V predchádzajúcich prácach bolo ukázané, že nízkopoľový skok povrchovej magnetizácie je spôsobený pohybom doménovej steny vo vnútri mikordrôtu. Pohybujúca sa doménová stena silne interaguje s vrstvou povrchových domén, čím mení orientáciu povrchovej doménovej štruktúry. Za týmto účelom boli skúmané obidva povrchové magnetizačné procesy oddelene.

Zmena povrchovej doménovej štruktúry vyvolaná pohybom doménovej steny vo vnútri mikrodrôtu bola detekovaná digitálnym spracovaním obrázkov. Táto metóda pozostáva z troch krokov: (i) mikrodrôt je prepnutý do prvého smeru, magnetické pole sa zredukuje na nulu a sníma sa obrázok pozadia (ii) skúmaný mikrodrôt je premagnetovaný do opačného smeru a hodnota magnetického poľa je zredukovaná na nulu pri snímaní obrázku (iii) z obrázku získaného v druhom kroku sa odčíta obrázok pozadia a výsledok sa spriemeruje. Je dôležité zdôrazniť, že takto snímaný magnetický kontrast odpovedá zmene povrchovej doménovej štruktúry, ktorá je vyvolaná pohybom doménovej steny vo vnútri mikrodrôtu.

Magnetický kontrast vyvolaný pohybom doménovej steny bol študovaný na sérii vzoriek charakterizovaných rozdielnou hodnotou hrúbky povrchovej vrstvy domén.

Rozdielny magnetický kontrast bol pozorovaný v rôznych častiach mikrodrôtu a to: (i) na povrchu mikrodrôtu (nad axiálnou doménou v strede mikrodrôtu) a (ii) blízko

koncov mikordrôtu. Magnetický kontrast pozostávajúci z dvoch čiernobielych pásikov bol nájdený na všetkých študovaných vzorkách. To potvrdzuje, že pohyb doménovej steny vo vnútri mikrodrôtu vedie k takej zmene povrchovej doménovej štruktúry, pri ktorej sa mení axiálna zložka magnetizácie. Navyše, rôzna intenzita magnetického kontrastu bola nájdená na vzorkách s rôznou hrúbkou povrchovej vrstvy domén.

As-castová vzorka amorfného, sklom potiahnutého mikrodrôtu so zložením FeSiB charakterizovaná relatívne nízkou hrúbkou povrchovej vrstvy domén (menej ako 100 nm) vykazovala veľkú zmenu v povrchovej doménovej štruktúre pri pohybe doménovej steny. Toto zloženie je navyše charakterizované relatívne nízkou rýchlosťou doménovej steny (menej ako 1.5 km/s). Na druhej strane, interakcia doménovej steny s povrchovou magnetizáciou bola omnoho silnejšia pri vzorke s vyšším podielom niklu (zloženie FeNiSiB), ktorá je charakterizovaná väčšou hrúbkou povrchovej vrstvy domén. Navyše, je táto vzorka charakterizovaná omnoho vyššou hodnotou maximálnej rýchlosti doménovej steny (až do 10 km/s). Tieto výsledky prezrádzajú, že prítomnosť povrchovej vrstvy domén môže napomáhať väčším rýchlostiam doménovej steny v mikrodrôtoch.

Rozdielny magnetický kontrast bol pozorovaný v blízkosti koncov mikrodrôtu, kde by sa mala podľa súčasných modelov nachádzať uzatváracia doménová štruktúra. Čiernobiely magnetický kontrast postupne zaniká postupne ako sa blíži koniec drôtu. Aplikácia magnetického poľa v axiálnom smere vyústila v stlačenie uzatváracej doménovej štruktúry. Uzatváracia doménová štruktúra nebola plne potlačená ani pri najvyšších hodnotách axiálneho magnetického poľa (okolo 0.2 T). Aplikácia magnetického poľa v smere axiálnej magnetizácie v axiálnej doméne vedie k pohybu doménovej steny z jedného konca mikrodrôtu na druhý. Dĺžka uzatváracej doménovej štruktúry nepresahovala 100 μm pri každej študovanej vzorke FeSiB mikrodrôtu, kdežto bola pozorovaná uzatváracia doménová štruktúra s dĺžkou okolo 5 mm v prípade vzorky s vyšším obsahom niklu (FeNiSiB). Dĺžka uzatváracej doménovej štruktúry môže byť daná jednak tvarovou anizotropiou drôtu a jednak mechanickými pnutiami, ktoré sa naindukujú do materiálu počas strihania vzorky.

Magneto-optické pozorovania zmeny povrchovej doménovej štruktúry vyvolanej pohybom doménovej steny vo vnútri mikrodrôtu odhalili, že axiálna zložka povrchovej magnetizácie sa pri tomto procese mení. Doménová štruktúra mikrodrôtov bola ozrejmená v ďalších meraniach.

Za účelom lepšieho pochopenia smeru povrchovej magnetizácie v mikrodrôte a jeho vplyvu na rýchlosti doménovej steny v mikrodrôte, boli merané axiálne hysterézne slučky v silnom magnetickom poli. Aplikácia silných magnetických polí (viac ako 0.1 T) viedla k dvom neželaným javom (paralelne k žiadanému Kerrovmu javu): (i) rotácia polarizačnej roviny skleneným obalom (Faradayov efekt skleneného obalu) a (ii) rotácia roviny polarizácie v objektíve (Faradayov efekt objektívu). Meranie hysteréznych slučiek v axiálnom smere odhalilo, že pri aplikovaní silných magnetických polí (do 0.2 T) dochádza k dvom javom: (i) zjavnej rotácii povrchovej magnetizácie pri vysokých poliach a (ii) ku skoku vyvolanom pohybom doménovej steny vo vnútri mikrodrôtu. Hysterézne slučky merané na svetelných škvrnách (vytvorené pravdepodobne svetlom primárne odrazeným od skleneného povrchu) pozostávajú z rotácie magnetizácie pod rovnakým uhlom, avšak skok pri nízkych poliach (spôsobený pohybom doménovej steny vo vnútri mikrodrôtu) chýba. Jedným z možných vysvetlení je že zjavná rotácia magnetizácie v oblasti vysokých polí meraná na povrchu drôtu odpovedá Faradayovmu efektu skleneného obalu, ktorý pri tak veľkých magnetických poliach (0.2 T) musí byť vzatý do úvahy. To znamená, že smer povrchovej magnetizácie nie je zmenený aplikovaním relatívne silných magnetických polí axiálneho smeru. To znamená, že povrchová vrstva domén je charakteristická povrchovou doménovou štruktúrou s axiálnym smerom. Iným, jednoduchším vysvetlením je že povrchová vrstva domén na študovaných mikrodrôtoch neexistuje. To ale znamená, že axiálnu magnetickú doménu je možne pozorovať priamo a teda je možné priamo pozorovať aj povrchovú štruktúru doménovej steny.

Magneto-optické pozorovania povrchovej štruktúry doménovej steny boli vykonané dvoma metódami, kde doménová stena bola zachytená v potenciálovej jame. V rámci prvej metódy bol mikrodrôt ohnutý do tvaru písmena „U“. Aplikácia magnetického poľa pozdĺž magnetizácie v uzatváracej doméne vyústil v stabilizáciu doménovej steny v strede drôtu. Hranica medzi dvoma doménami (doménová stena) nebola pozorovaná ako skokovitá, ale mala naklonený tvar. Za účelom redukcie mechanických pnutí spôsobených ohnutím vzorky (ktoré by mohli spôsobovať naklonený tvar doménovej steny) sa povrchová štruktúra doménovej steny pozorovala v nasledujúcom experimente. Mikrodrôt bol vložený medzi dve magnetické cievky, ktoré boli napájané nezávisle dvoma zdrojmi prúdu. Celý proces zachytávania doménovej steny bol vykonaný v dvoch krokoch. Najprv bola hodnota prúdu v prvej magnetizačnej cievke

nastavená na istú hodnotu. Nastavenie intenzity elektrického poľa v druhej magnetizačnej cievke umožnilo posúvať oblasť nulového magnetického poľa pozdĺž mikrodrôtu (a tým aj posúvať doménovú stenu). Doménová stena bola v rámci tohto druhého prístupu zachytená gradientom magnetického poľa (ktorý bol daný v tomto prípade pomerom prúdu v oboch cievkach), kde sa doménová stena nachádzala v mieste jeho nulovej hodnoty.

Tento experimentálny prístup umožňoval (i) čo najviac zamedziť vplyvu mechanických pnutí na tvar steny (daných ohnutím vzorky ako v prvom experimentálnom prístupe) (ii) pozorovať povrchovú štruktúru doménovej steny v nulovom magnetickom poli.

Naklonená povrchová štruktúra doménovej steny bola pozorovaná aj v tomto experimente. Navyše, merania dĺžky povrchovej štruktúry (v axiálnom smere) boli merané pozdĺž vzorky mikrodrôtu s celkovou dĺžkou 2 cm. Merania odhalili, že naklonenie povrchovej štruktúry nie je konštantné pozdĺž drôtu, ale dĺžka bola premenlivá od *40 μm* do *210 μm* v prípade vzorky so zložením $Fe_{77.5}Si_{7.5}B_{15}$.

Dĺžka povrchovej štruktúry doménovej steny bola meraná aj na druhej skupine mikrodrôtov kde bolo možné pozorovať zmenu povrchovej doménovej štruktúry pohybom doménovej steny ($Fe_{49.6}Ni_{27.9}Si_{7.5}B_{15}$). Dĺžka povrchovej štruktúry doménovej steny v tomto prípade fluktuovala okolo strednej hodnoty *120 μm*. Smer naklonenia povrchovej štruktúry doménovej steny bol rovnaký ako v predchádzajúcom prípade. Bolo skúšané zmeniť sklon povrchovej štruktúry aplikáciou magnetického poľa v smere kolmom na os drôtu, avšak bez výsledne. To poukazuje na fakt, že naklonenie povrchovej štruktúry doménovej steny môže súvisieť s omnoho silnejšou interakciou (v porovnaní so Zeemanovskou), ktorou by mohla byť napr. magnetoelastická anizotropia.

Naklonená povrchová štruktúra doménovej steny by mohla byť vysvetlená redukciou demagnetizačnej energie rozptylových polí povrchových magnetických nábojov, ktorá klesá s narastajúcim sklonom doménovej steny. Naklonená štruktúra doménovej steny môže byť zodpovedná za veľké hodnoty rýchlosti doménovej steny meranej pomocou Sixtusovej-Tonksovej metódy na mikrodrôtoch.

Résumé en français

La propagation de parois dans des fils magnétiques de petites dimensions est redevenue un domaine d'intérêt du fait de la spintronique. La spintronique – ou électronique de spin – est une technologie émergente qui tire parti du moment magnétique de l'électron pour transporter et stocker de l'information. Un des concepts d'application récemment développés en spintronique est basé sur les propriétés magnétiques de petits fils magnétiques bistables. Le niveau logique est codé par la direction de l'aimantation des domaines, et le changement de valeur logique est obtenu par propagation d'une paroi. Différents types de dispositifs spintroniques utilisant la propagation de parois magnétiques ont été proposés : des portes logiques magnétiques à parois qui réalisent les fonctions « ou exclusif », « et » et « non », des diodes spintroniques, ou encore des registres à décalage spintroniques qui utilisent la propagation de plusieurs parois pour lire et écrire des données. Pour tous ces dispositifs, la vitesse de déplacement des parois est un des facteurs les plus importants pour déterminer la vitesse de travail. En conséquence, il est d'un grand intérêt de mieux comprendre les mécanismes permettant d'obtenir un déplacement rapide des parois dans des fils magnétiques de petites dimensions. Les vitesses maximales des parois dans les dispositifs récemment proposés de porte logique n'excèdent pas 2 km/s. En regard de cela, la vitesse maximum des parois dans les microfils magnétiques amorphes gainés de verre (MAGV) peut atteindre 20 km/s.

Une autre motivation pour l'étude de la dynamique de parois dans les MAGV provient de leur application comme capteurs. Les MAGV ont été récemment utilisés dans un grand nombre de dispositifs de capteurs de (i) champ magnétique (ii) contrainte mécanique et (iii) déformation mécanique. La plupart de ces capteurs utilisent la dynamique de parois (vitesse de paroi et champ critique) pour détecter des forces externes. En conséquence, la connaissance de la dynamique de parois dans les microfils est aussi requise pour les applications comme capteurs.

Le but principal de ce travail a été d'étudier les mécanismes qui peuvent être mis à profit pour contrôler la dynamique de parois dans les microfils. Le but secondaire a été de mieux comprendre l'origine de la propagation si rapide des parois qui est observée dans les MAGV.

Les MAGV sont des matériaux composites consistant en une âme métallique gainée de verre. Il faut mentionner que la plupart des propriétés magnétiques des MAGV proviennent de leur processus de fabrication par la méthode de Taylor-Ulitkovski. Dans ce procédé, les MAGV sont produits par trempe rapide et étirement rapide. Du fait de la différence des coefficients de dilatation thermique du verre et du métal, des fortes contraintes mécaniques dans les directions radiales et axiales sont induites dans le fil durant la trempe. De plus, les microfils sont préparés par étirement depuis l'alliage de base, ce qui introduit des contraintes axiales supplémentaires. La géométrie des contraintes totales dans les MAGV est très complexe. Selon le modèle magnéto-élastique, les contraintes mécaniques dans les MAGV sont en première approximation une contrainte axiale au centre du fil, alors que des contraintes radiales et circulaires dominent juste en dessous de la surface de l'âme métallique. Dans ce modèle, des contraintes très élevées sont calculées. Les contraintes les plus fortes, obtenues près de la surface du métal, sont proches de la limite de rupture du matériau constituant l'âme. Ceci permet de comprendre l'importance du couplage magnéto-élastique pour les MAGV. L'expérience confirme cette intuition, en montrant que la structure en domaines magnétiques dans les MAGV est déterminée par le signe du coefficient magnéto-élastique du matériau métallique de l'âme. Donc, l'effet magnétostatique (anisotropie de forme) n'est pas aussi important que pour les fils magnétiques doux en permalloy.

Pour des MAGV réalisés avec des alliages à magnétostriction positive, l'énergie magnéto-élastique minimum est atteinte pour une aimantation parallèle à la direction des contraintes mécaniques. De ce fait, la structure en domaines dans les MAGV à magnétostriction positive consiste en un grand domaine axial entouré par une fine couche de domaines de surface (selon les modèles récents décrivant les contraintes résiduelles). De plus, deux domaines apparaissent aux extrémités du fil afin de réduire l'énergie magnétostatique. Le processus d'aimantation principal dans les MAGV à magnétostriction positive consiste en un grand saut de Barkhausen généré par la propagation d'une paroi d'un bout à l'autre du fil.

La propagation de parois magnétiques dans les MAGV a été étudiée par le modèle mécanique introduit par Kittel dans les années 50 du siècle précédent. La dynamique de la paroi en mouvement est comparée à celle d'un point matériel dans un milieu visqueux. Le mouvement de la paroi est alors décrit par une équation semblable à celle

d'un oscillateur harmonique linéaire. On en déduit des équations de mouvement de la paroi dont il résulte que la vitesse est proportionnelle au champ appliqué. Deux paramètres déterminent cette relation. La mobilité de paroi (pente de la vitesse en fonction du champ) exprime les forces de freinage qui s'opposent au mouvement de la paroi (amortissement du mouvement de la paroi). Le second paramètre est appelé champ critique, et est relié aux mécanismes de piégeage de la paroi.

Au moins trois contributions à l'amortissement du mouvement de la paroi ont été récemment mises en évidence. La première provient des courants de Foucault induits au voisinage de la paroi en mouvement. Dans le cas d'une paroi entre deux domaines axiaux entourés d'une fine couche de domaines en surface, la contribution à l'amortissement a été trouvée inversement proportionnelle au diamètre du domaine axial. La seconde contribution à l'amortissement du mouvement de paroi provient du fait que la paroi ne peut pas aller plus vite que les moments qui la composent ne peuvent tourner. L'amortissement du mouvement de paroi du fait du taux de relaxation des moments magnétiques a été trouvé inversement proportionnel à la largeur de la paroi. Physiquement, cette dépendance provient du fait que pour une vitesse donnée de paroi les spins dans une paroi fine doivent tourner plus vite que dans une paroi large. La troisième contribution à l'amortissement du mouvement de paroi apparaît du fait de la relaxation de défauts mobiles dans les matériaux amorphes. Il a été vu que cette contribution devenait particulièrement importante à basse température car le temps de relaxation des défauts y augmente fortement. L'influence sur l'amortissement du mouvement de paroi de la relaxation structurale est donnée par l'ordre relatif de trois constantes de temps : (i) le temps de relaxation des défauts mobiles, (ii) le temps d'interaction de la paroi en mouvement avec un défaut, fixé par la largeur et la vitesse de la paroi, et (iii) le temps entre deux relaxations. De ce fait, l'amortissement du mouvement de paroi donné par la relaxation structurale a été observé dans au moins cinq régimes. De plus, cet amortissement a été trouvé auparavant directement proportionnel à la concentration en défauts mobiles et inversement proportionnel à la température.

Comme l'anisotropie magnéto-élastique a été reconnue comme très importante pour les MAGV, la dynamique de parois a été contrôlée par une tension mécanique lors de nos premières expériences. Les microfils de composition FeNiSiB dans lesquels la dynamique de paroi est caractérisée par cinq régimes ont été utilisés pour ces mesures. Le premier régime est caractérisé par un champ critique négatif et la plus faible mobilité

de parois. La valeur négative du champ critique persiste dans le second régime, mais la dépendance de la vitesse en fonction du champ n'était pas linéaire, avec une tendance observée à la saturation de la vitesse. Le troisième régime se définit par une forte augmentation de la mobilité et un champ critique positif. Le quatrième régime avec champ critique positif et mobilité encore plus forte a été observé aux vitesses les plus élevées. Ces quatre régimes de propagation ont été observés à chaque valeur de la tension, ce qui a permis leur étude séparée.

La dépendance avec la contrainte en tension de la mobilité de parois a été précédemment étudiée dans des fils amorphes étirés à froid. La dépendance concave à faible tension a été expliquée par deux contributions à l'amortissement du mouvement de la paroi (relaxation des moments magnétiques et courants de Foucault). Mais à forte tension une variation convexe a été observée. Dans les MAGV de FeNiSiB nous avons aussi trouvé une forme convexe. Une telle forme ne peut être expliquée avec ces deux premières contributions à l'amortissement. Mais la relaxation structurale intervient aussi comme mécanisme d'amortissement. Selon le modèle à deux niveaux de Kronmüller, l'énergie d'interaction d'un défaut mobile avec la matrice amorphe est prise comme la somme des énergies d'interaction dipôle-dipôle, échange et magnéto-élastique. Si on prend en compte la dépendance en contrainte de la contribution magnéto-élastique à l'énergie d'interaction des défauts mobiles avec la matrice amorphe, la formule donnant l'amortissement de paroi selon la relaxation structurale est quadratique en fonction de la tension, ce qui correspond qualitativement aux mesures. L'ajustement des données a confirmé que le mouvement de paroi est amorti par la relaxation structurale dans le premier régime de propagation. Un tel régime a été observé précédemment et appelé régime amorti par diffusion. Les moments magnétiques des défauts mobiles tentent de suivre le changement de l'aimantation qui se produit lorsque la paroi se propage. Comme le temps de relaxation des défauts mobiles était comparable au temps d'interaction de la paroi avec ceux-ci, un fort amortissement de la dynamique de paroi en résulte.

L'amortissement de la dynamique de paroi dans le second régime est très proche de celui observé dans le premier régime. Toutefois on observe une tendance à la saturation de la vitesse dans la courbe v-H. Les études théoriques antérieures ont montré que la paroi se comprime au-delà d'une certaine vitesse. La dépendance en champ de la vitesse dans le second régime a été ajustée par les équations de mouvement de la paroi avec variation de la largeur de paroi en fonction de la contrainte de tension.

Dans ces deux premiers régimes, le déplacement de la paroi était amorti par la relaxation structurale car le temps de relaxation des défauts mobiles était comparable à celui d'interaction avec la paroi. Toutefois, lorsque la vitesse de paroi augmente, le temps de relaxation des défauts devient très supérieur au temps d'interaction avec la paroi en mouvement et donc la paroi se libère de la relaxation structurale. C'est probablement ce qui a été observé dans le troisième régime, dans lequel la mobilité de paroi augmente fortement et le champ critique devient positif. Cette hypothèse a été confirmée par l'ajustement de la dépendance en tension de la mobilité de paroi, dans lequel l'amortissement par relaxation structurale a dû être négligé afin d'obtenir un bon accord.

Le quatrième régime de propagation de paroi est caractérisé par les plus fortes vitesses de paroi. Malheureusement, il n'a pas été possible d'ajuster la variation en tension de l'amortissement de paroi par le modèle mécanique de dynamique de paroi, du fait des très faibles valeurs des paramètres.

De manière générale, la vitesse décroît avec la contrainte de tension. Afin de comprendre l'influence de la force de l'anisotropie magnétique sur la vitesse de paroi dans les microfils, l'anisotropie magnétique des microfils a été réduite par plusieurs moyens qui ont été comparés.

Premièrement, les MAGV ont été traités thermiquement dans un four. Des MAGV de FeSiB ont été utilisés pour ces expériences. Cette composition se caractérise par une vitesse modeste des parois qui ne dépasse pas 1 km/s. Les études précédentes ont montré que la plus importante contribution à l'amortissement du mouvement de parois provient de la relaxation des moments magnétiques à l'ambiante. D'autre part, la relaxation magnétique des moments magnétiques pourrait être réduite en réduisant l'anisotropie magnétique. Comme la plus forte anisotropie dans les MAGV est celle d'origine magnéto-élastique, l'anisotropie magnétique pourrait être réduite en réduisant les contraintes résiduelles par un recuit. Il faut pour cela bien choisir la température de recuit afin d'obtenir suffisamment de relaxation de contraintes.

Un recuit à 200°C n'a pas suffi à changer nettement la dynamique de parois. Mais un recuit à 300°C a eu deux effets remarquables : (i) augmentation de la mobilité de parois et (ii) apparition d'un régime de propagation rapide de paroi, non observé dans l'état brut de préparation. L'augmentation de la mobilité de paroi peut s'interpréter par une baisse de la relaxation des moments magnétiques (du fait de la baisse de l'anisotropie),

et par réduction de la contribution due à la relaxation structurale (via une baisse de la concentration volumique de défauts mobiles).

Une autre voie pour réduire les contraintes internes a été trouvée : le recuit sous contrainte de tension. La relaxation de contraintes internes se produit davantage dans la partie métallique au centre, plutôt que dans la gaine de verre du fait de la plus haute température de fusion du verre. Lorsqu'on enlève la contrainte de tension après le recuit, une contrainte compressive apparaît qui compense la contrainte résiduelle en tension de l'état brut de dépôt. De ce fait, les MAGV recuits sous contrainte de tension perdent leur bistabilité magnétique. Pour la restaurer, une tension de 35 MPa environ a été appliquée. La vitesse de paroi mesurée a montré une très forte valeur (7 km/s), trois fois plus forte que la valeur mesurée sur l'échantillon brut. Pour des tensions supérieures, toute la dynamique de paroi a été restaurée (mobilité et champ critique).
Au vu de ces résultats, on pourrait conclure qu'une faible valeur de l'anisotropie semble nécessaire pour obtenir de fortes vitesses de parois dans les microfils.
Toutefois, les plus fortes vitesses de paroi ont été observées dans des matériaux à forte anisotropie : des monocristaux allongés (poils de chat) de fer avec des vitesses maximales de paroi de 25 km/s ont été observées par DeBlois à la fin des années 1950, ou bien des orthoferrites avec des vitesses maximum de 60 km/s ont été étudiées par S. Demokritov à la fin des années 1980. Il faut noter cependant que l'anisotropie de ces matériaux n'était pas uniaxiale. La même situation semble se rencontrer dans les MAGV, où les contraintes axiales sont partiellement compensées par les contraintes radiales et circulaires.
Afin de mieux comprendre l'influence de la géométrie des anisotropies sur la dynamique de parois, des microfils ont été recuits sous champ perpendiculaire. Ce recuit a induit une anisotropie perpendiculaire qui a donné une augmentation de vitesse de paroi et a décalé le point de transition entre les deux régimes de propagation de paroi. Un effet similaire a été observé précédemment, lors de la mesure de la vitesse de paroi sous champ perpendiculaire à l'axe du fil.
Une méthode encore plus efficace pour varier la vitesse de paroi a été trouvée en recuisant par un courant circulant dans le fil. Un tel recuit durant 10 minutes a été trouvé aussi efficace (du point de vue de la vitesse de paroi) qu'un recuit dans un four durant 1 heure. La vitesse de paroi dans les échantillons de FeSiB a augmenté de plus d'un facteur 4 (de 1 à plus de 4 km/s) comparé à l'état brut.

Finalement, la vitesse de paroi a été mesurée dans des microfils de petit diamètre, jusqu'à 1 micromètre. La dynamique des parois dans ces échantillons montre les mêmes régimes que les fils plus gros. Ceci confirme que les fortes vitesses observées dans les microfils ne sont pas le résultat de leur seul grand diamètre, mais probablement aussi que la géométrie des contraintes internes (du fait de la présence de la gaine de verre) joue un rôle important. Le recuit de ces microfils de petit diamètre a conduit à une augmentation de vitesses. L'effet a été le plus fort pour un traitement sous champ perpendiculaire. Le recuit de fils de 1 micron a augmenté la mobilité de paroi et la vitesse maximum de plus de cinq fois en comparaison à l'état brut. De tels résultats sont attractifs en vue d'applications, spécialement si une dynamique bien définie des parois est requise.

En plus de la géométrie et de la force de l'anisotropie magnétique, la présence de la couche de domaines en surface peut jouer un rôle important dans la propagation rapide des parois dans les MAGV. Des travaux précédents ont montré que cette couche peut éviter le piégeage des parois par des défauts et ainsi favoriser des grandes vitesses de paroi. Afin de mieux comprendre le rôle de cette structure en domaines en surface sur la propagation rapide des parois, les structures de domaines en surface pour des échantillons à différentes vitesses de parois ont été comparées.

Les structures en domaines en surface dans des MAGV à magnétostriction négative ont été étudiées précédemment, et des structures typiques en bambou avec des domaines à aimantation circulaire en surface ont été trouvées. Toutes les observations précédentes par magnéto-optique sur ces échantillons ont pris comme point de départ que les fils cylindriques sont assimilés à leur plan tangent. Mais cette hypothèse ne réussit pas à expliquer complètement les structures observées sur les MAGV à magnétostriction positive que nous avons effectuées dans ce travail. Pour cette raison, la méthode d'observation magnéto-optique d'échantillons cylindriques a été étudiée tout d'abord. Les principales propriétés optiques des MAGV sont déterminées par deux facteurs : (i) la couche de verre réduit la quantité de lumière réfléchie par le métal (ce qui réduit le signal par effet Kerr car ce dernier provient de la réflexion à la surface du métal) et (ii) la forme cylindrique de la surface de l'échantillon.

Afin de déterminer les conditions optimales pour l'observation par magnéto-optique de ces matériaux composites, le calcul de la réflectivité optique de la structure bicouche

consistant en un métal couvert par une fine couche de verre a été effectué. La réflexion de la lumière polarisée « s » a été trouvée supérieure à celle de la lumière polarisée « p » dans toute la gamme des angles d'incidence. Donc, afin de maximiser l'intensité réfléchie totale, il faudrait adopter cette polarisation. Toutefois, c'est avec la polarisation « p » que la lumière réfléchie par le métal est la plus importante. Enfin, la part réfléchie par le métal est maximale à l'angle de Brewster. Ceci résulte de la transmission totale de la lumière à l'interface air-verre à cet angle.

Un autre facteur important dans cette observation par magnéto-optique des microfls provient de la forme cylindrique des échantillons. Ceci a été confirmé par microscopie entre polariseurs croisés, où la lumière réfléchie forme deux lignes brillantes. Il est bien connu en optique qu'une lumière incidente polarisée « s » ou « p » est réfléchie par une surface plane en restant polarisée linéairement. Donc, avec l'approximation du plan tangent supérieur, cette observation ne s'explique pas. Afin de s'assurer que les images magnéto-optiques étaient bien interprétées, un calcul détaillé du profil de la lumière réfléchie par la surface cylindrique a été mené. Ce calcul a été fait selon deux hypothèses : un faisceau incident constitué par des rayons parallèles, avec une orientation le long de l'axe principal du microfil. Dans ces conditions, le profil de lumière réfléchie a été trouvé en fonction de deux paramètres seulement : (i) l'angle d'incidence et (ii) l'angle theta qui donne la position sur la surface du cylindre. Le calcul détaillé a révélé que le plan d'incidence est une fonction de ces deux paramètres, pour chaque rayon du faisceau qui arrive à la surface. Le plan d'incidence n'a donc pas une orientation constante sur toute la surface du cylindre, et sa variation n'est pas intuitive. Ceci veut dire que, même si une lumière polarisée linéairement (« s » ou « p ») est utilisée pour les observations, l'orientation mutuelle du champ électrique et du plan d'incidence varie pour chaque rayon. Si la lumière incidente polarisée « s » (resp. « p ») est utilisée pour l'observation, le vecteur champ électrique ne sera normal (resp. parallèle) au plan d'incidence que en haut du fil. En dehors du haut du fil, la polarisation linéaire ne sera ni parallèle ni perpendiculaire au plan d'incidence. Pour cette raison, il faut distinguer les deux composantes de cette polarisation par rapport au plan d'incidence local : (i) la composante linéaire orientée perpendiculairement au plan d'incidence local (polarisation « s locale ») et (ii) la composante linéaire orientée parallèlement au plan d'incidence local (polarisation « p locale »). Le signal magnéto-optique pour le microfil sera composé de deux effets (i) celui pour la polarisation s locale et (ii) celui pour la polarisation p locale. Le profil de l'intensité réfléchie par le

microfil a été calculé dans deux cas (i) observation entre polariseur et analyseur croisés et (ii) observation en lumière polarisée seule (sans analyseur). Alors que dans le second cas on trouve un seul maximum (au niveau du sommet du fil), un profil à deux maxima est obtenu dans le premier cas, de manière remarquable. Ces profils calculés semblent bien décrire les profils mesurés dans le microscope.
Pour calculer le profil d'intensité pour un cylindre aimanté axialement, un paramètre de Voigt différent de zéro a été introduit dans la matrice de réflexion. L'effet magnéto-optique en réflexion lié à l'aimantation en surface du cylindre donne lieu à un très petit changement du profil d'intensité par rapport à un cylindre non magnétique. On a montré que le contraste magnétique consistant en deux bandes, noire et blanche, était caractéristique d'une composante axiale de l'aimantation à la surface de l'échantillon cylindrique.
Ce contraste caractéristique noir et blanc résultant du renversement de l'aimantation axiale peut être simplement expliqué par l'effet Kerr transverse. Le vecteur aimantation axiale a en effet une composante normale au plan d'incidence local qui est non-nulle. Du fait de l'inclinaison symétrique de ce plan d'incidence de part et d'autre du plan médian du fil, la composante normale locale change de signe entre ces deux côtés.

La comparaison de cycles d'hystérésis mesurés pour la même orientation du champ (perpendiculaire à l'axe du fil), soit pour le volume (mesure par MPMS) ou pour la surface (effet Kerr), a révélé que le champ de saturation en surface était très proche de celui mesuré en volume. Ceci confirme que l'anisotropie reste aussi forte en surface. De plus, la valeur du champ de saturation a été trouvée supérieure à Ms/2, ce qui indique la présence d'une autre anisotropie (magnéto-élastique) dans tous les échantillons étudiés.
Le processus d'aimantation en surface a montré deux phénomènes (i) rotation anhystérétique de l'aimantation à forts champs et (ii) saut de la direction de l'aimantation de surface à faible champ. Or il a été montré précédemment que ce saut était dû à la propagation de la paroi à l'intérieur du fil. On en déduit que la propagation de la paroi à l'intérieur du fil interagit fortement avec la structure de domaines en surface et change l'orientation de l'aimantation en surface. Pour cette raison, les deux phénomènes d'aimantation en surface ont été étudiés séparément.
Le changement de l'aimantation en surface causé par la propagation de la paroi interne a été détecté par différence d'images. Cette opération se déroule en trois étapes : (1) le microfil est basculé dans une direction axiale, le champ magnétique est ramené à zéro,

et l'image de référence est acquise ; (2) le microfil est renversé par un champ axial orienté dans la direction opposée, le champ est réduit à zéro et une seconde image est acquise ; (3) l'image de référence est soustraite à l'image acquise en (2) et le résultat est moyenné en répétant acquisition et soustraction. Il est utile de mentionner que le contraste mesuré de cette manière correspond au changement d'aimantation qui se produit lors d'un grand saut de Barkhausen.

Le contraste magnétique relié à la propagation de la paroi interne a été étudié dans une série d'échantillons FiNiSiB caractérisés par différentes épaisseurs de structure de domaines en surface, selon les mesures précédentes.
Un contraste différent a été observé (i) au centre du fil et (ii) proche de ses extrémités. Le contraste magnétique avec bandes noire et blanche a été trouvé pour tous les fils observés. Il confirme que le déplacement de la paroi conduit à un changement de la composante axiale pour l'aimantation en surface. De plus, la force de ce contraste a été trouvée différente entre des échantillons à couche de domaines de surface fine ou plus épaisse.
Les échantillons de MAGV en FeSiB bruts de fabrication caractérisés par une fine couche de domaines de surface (< 100 nm) ont montré un fort changement de signal lié à la composante axiale lors du déplacement de la paroi, alors qu'ils montrent des vitesses de paroi relativement basses (< 1.5 km/s). D'un autre côté, l'interaction du déplacement de paroi avec le couche de domaines en surface n'a pas été observée pour les microfils de FeNiSiB possédant une couche de domaines de surface plus épaisse. Dans le même temps, la vitesse des parois atteint des valeurs bien plus élevées (jusqu'à 10 km/s) dans ces microfils. Ces résultats confirment que la présence de domaines de surface peut jouer un rôle important dans la propagation à grande vitesse des parois dans les microfils.
Des images différentes ont été obtenues près des extrémités du fil, là où des domaines de fermeture sont attendus d'après les modèles récents. Le contraste noir et blanc disparaît continûment à mesure que l'on s'approche de l'extrémité. L'application d'un champ parallèle à l'aimantation axiale a conduit à la compression de la structure en domaines de fermeture. Il est à noter que, même pour des champs aussi forts que 0.2 T, la structure en domaines de fermeture n'a pas disparu complètement. En appliquant un champ orienté parallèlement à l'aimantation dans les domaines de fermeture, le grand saut de Barkhausen est observé. La longueur de la structure en domaines de fermeture

n’a pas dépassé 100 microns pour tous les échantillons de FeSiB, alors que des longueurs de plus de 5 mm ont été observées pour des échantillons avec plus de nickel (microfils de FeNiSiB). Cette taille apparente de la structure en domaines de fermeture peut être atttribuée à l’anisotropie de forme des fils mais aussi aux contraintes mécaniques induites aux extrémités du fil lors de la coupe de l’échantillon.

L’observation magnéto-optique du processus d’aimantation en surface induit par le déplacement de la paroi interne a révélé que la composante axiale de l’aimantation change. Toutefois, la structure en domaines en surface n’a pas été ainsi clarifiée.
Afin de comprendre mieux la direction de l’aimantation en surface et sa possible intervention dans la propagation rapide des parois, le cycle d’hystérésis en surface des microfils a été mesuré à forts champ appliqués dans le microscope. L’application de tels champs entraîne de nombreux effets magnéto-optiques indésirables (en parallèle à l’effet Kerr) et qu’il faut prendre en compte : (i) rotation du plan de polarisation en traversant la gaine de verre (effet Faraday dans la gaine de verre) ; (ii) rotation de la polarisation dans la lentille de l’objectif utilisé (effet Faraday dans la lentille). Le cycle d’hystérésis axial en surface a révélé que l’aimantation subit 2 processus : (i) une rotation d’aimantation apparente et (ii) un saut d’aimantation lors du passage de la paroi. Toutefois, le cycle d’hystérésis mesuré dans une ombre portée à côté du fil (probablement formée par la lumière réfléchie par la gaine de verre) montre une rotation d’aimantation apparente avec la même pente que celle vue sur le fil, avec absence du saut lors de la propagation de la paroi. Une explication de ceci serait que la rotation apparente d’aimantation mesurée dans le cycle d’hystérésis de surface correspond à l’effet Faraday dans la gaine de verre, qu’il faut prendre en compte pour des champs aussi forts (0.2 T). Ceci voudrait dire que la direction d’aimantation en surface ne change pas par l’application d’un champ axial, donc que la structure en surface possède une aimantation axiale. Une autre interprétation de ces observations serait que la couche de domaines de surface est absente, et donc que l’aimantation interne axiale est directement observée.

L’observation magnéto-optique de la paroi a été réalisée de deux manières qui ont été comparées, dans lesquelles la paroi est maintenue dans un puits de potentiel. Dans la première méthode, le fil étudié a été plié en forme de U. L’application d’un champ magnétique dans la direction de l’aimantation dans les domaines de fermeture a entraîné

la propagation de la paroi jusqu'au centre du fil. La frontière entre les domaines est alors observée comme étant non abrupte, avec présence d'une paroi inclinée. Dans le but d'éviter les contraintes induites par la courbure du microfil, la surface du fil a été observée sur un fil rectiligne. Le microfil a été placé entre deux bobines alimentées indépendamment par deux alimentations. La capture de la paroi dans la zone d'observation a été réalisée en deux temps. Tout d'abord, le courant a été mis à une certaine valeur dans la bobine première bobine. En ajustant ensuite le courant dans la seconde, la zone de champ nul a été balayée entre les deux bobines le long du microfil (ainsi que la paroi). La paroi est alors maintenue par le gradient du champ magnétique (dont la force est donnée par le courant dans les bobines), alors que la paroi se situe toujours à l'endroit du champ nul.

Cette expérience a permis (i) de supprimer l'influence de la courbure du fil sur la structure de domaines en surface, du fait des contraintes additionnelles (provenant de cette courbure) et (ii) d'observer la paroi à champ nul (afin d'exclure un effet du champ appliqué, du moins partiellement).

L'inclinaison apparente de la structure de paroi a été observée dans ce cas aussi. De plus, la mesure de la longueur de la paroi a été effectuée à différentes positions de la paroi pour un fil long de 2 cm. L'angle d'inclinaison de la paroi n'a pas été constant le long du fil, et on a pu observer que la longueur de la paroi variait entre 40 et 210 microns dans le cas des fils de $Fe_{77.5}Si_{7.5}B_{15}$. La longueur de paroi a été mesurée dans le second groupe de microfils de composition $Fe_{49.6}Ni_{27.9}Si_{7.5}B_{15}$, où il est possible de détecter du contraste lors de la propagation de la paroi interne. Pour cette composition, la longueur de paroi fluctuait autour d'une valeur de 120 microns. La direction d'inclinaison de la paroi était identique à celle vue sur les autres fils. Nous avons tenté de changer cette direction d'inclinaison en appliquant un champ perpendiculairement à l'axe du fil. Mais cette direction d'inclinaison n'a pas été trouvée varier avec la position le long du fil ni avec le champ perpendiculaire. Ceci montre que l'origine de l'inclinaison de la paroi doit être associée à l'anisotropie magnéto-élastique, bien plus forte que l'interaction Zeeman.

La forme inclinée de la paroi pourrait être expliquée par la réduction de l'énergie démagnétisante associée à la densité de charges magnétiques, qui diminue lors de cette inclinaison. Dans le même temps, cette structure inclinée de la paroi peut être rendue

responsable des fortes vitesses apparentes de paroi mesurées plus haut par méthode Sixtus-Tonks.

Bibliography

(1) P. Weiss, „The hypothesis of the molecular field and the property of ferrromagnetism", J. de Phys. Rad. 6, 661 (1907) (in French).

(2) H. Barkhaussen, „Two phenomena, discovered with the help of the new amplifiers", Phys. Z. 20, 401 (1919) (in German).

(3) L. Tonks and K. J. Sixtus, „Propagation of Large Barkhausen Discontinuities", Phys. Rev. 37, 930 (1931).

(4) L. Tonks and K. J. Sixtus, „Propagation of Large Barkhausen Discontinuities. II", Phys. Rev. 42, 419 (1932).

(5) L. Tonks and K. J. Sixtus, „Propagation of Large Barkhausen Discontinuities. III. Effect of a circular field with torsion", Phys. Rev. 43, 70 (1933).

(6) L. Tonks and K. J. Sixtus, „Further Experiments on the Propagation of Large Barkhausen Discontinuities", Phys. Rev. 39, 357 (1932).

(7) L. J. Dijkstra and J. L. Snoek, „A nucleation problem in ferromagnetism", Philips Research Repts. 4, 334 (1949).

(8) F. Bloch, „On the theory of exchange problem and the remanence phemonenon of ferromagnets", Z. Phys 74, 295 (1932) (in German).

(9) F. Bitter, „On inhomogenities in the magnetization of ferromagnetic materials", Phys. Rev. 38, 1903 (1932).

(10) H. J. Williams, W. Shockley, „A Simple Domain Structure in an Iron Crystal Showing a Direct Correlation with the Magnetization", Phys. Rev. 75 178, (1949).

(11) H. J. Williams, W. Shockley and C. Kittel, „Studies of the Propagation Velocity of a Ferromagnetic Domain Boundary", Phys Rev. 80, 1090 (1950).

(12) D. S. Rodbell, C. P. Bean, „Influence of Pulsed Magnetic Fields on the Reversal of Magnetization in Square‐Loop Metallic Tapes", J. Appl. Phys. 26 1318 (1955).

(13) C. Kittel and J. K. Galt in Solid State Physics, edited by F. Seitz and D. Turnbull (Academic Press Inc., New York, 1956), Vol. 3, p. 439.

(14) R. W. Deblois, „Domain wall motion in metals", J. Appl. Phys. 29, 459 (1958).

(15) J. J. Becker, „Magnetization changes and looses in conducting ferromagnetic materials", J. Appl. Phys. 34, 1327 (1963).

(16) C. C. Tsuei, P. Duwez, „Metastable amorphous ferromagnetic phases in palladium-base alloys", J. Appl. Phys. 37, 435 (1966).

(17) R. C. O´Handley, „Domain wall kinetics in soft ferromagnetic matellic glasses", J. Appl. Phys. 46, 4996 (1975).

(18) F. J. A. den Broeder and J. van der Borst, „Magnetization reversal in $Fe_{80}B_{15}Si_5$ metallic glass with large uniaxial magnetostrictive anisotropy" ,J. Appl. Phys. 50, 7116 (1979).

(19) H. S. Chen, S. D. Ferris, E. M. Gyorgy, H. J. Leamy, and R. C. Sherwood, „Field heat treatment of ferromagnetic metallic glasses", Appl. Phys. Lett. 26, 405 (1975).

(20) T. Egami, P. J. Flanders, and C. D. Graham, „Low−field magnetic properties of ferromagnetic amorphous alloys", Appl. Phys. Lett. 26, 128 (1975).

(21) V. V. Randoshkin, L. P. Ivanov, and R. V. Telesnin, „Dynamics of domains in iron garnet films in a homogeneous magnetic field", Sov. Phys. JETP 48, 486 (1978).

(22) M. V. Chetkin, S. N. Gadetski, A. P. Kuzmenko, and A. I. Akhutkina, „Investigation of supersonic dynamics of domain walls in orthoferrites", Sov. Phys. JETP 59, 825 (1984).

(23) M. V. Chetkin and A. I. Akhutkina, „Dynamics of domain walls in weakly ferromagnetic orthoferrites", Sov. Phys. JETP 51, 383 (1980).

(24) M. V. Chetkin, A. N. Shalygin, and A. de la Campa, „Velocity of domain walls in weak ferromagnets", Sov. Phys. JETP 48, 1184 (1978).

(25) D. A. Allwood, et al., „Magnetic Domain-Wall Logic", Science 309, 1688 (2005).

(26) D. Atkinson, „ Domain-Wall Dynamics in Magnetic Logic Devices", Appl. Phys. Lett. 101, 207 (2006).

(27) D. A. Allwood, et al, „Domain wall diodes in ferromagnetic planar nanowires", Appl. Phys. Lett. 85, 14 (2004).

(28) S. S. P. Parkin, M. Hayashi, L. Thomas, „Magnetic Domain-Wall Racetrack Memory", Science 11, 190 (2008).

(29) R. Varga, A. Zhukov, V. Zhukova, J. M. Blanco, and J. Gonzalez, „Supersonic domain wall in magnetic microwires", Phys. Rev. B 76, 132406 (2007).

(30) S.O. Demokritov, et al, „Interaction of the moving domain wall with phonons",J. Magn. Magnt. Mat. 102, 339 (1991).

(31) W. Doring, „On the inertia of walls between Weiss domains", Z. Naturforschung 3a, 373 (1948) (in German).

(32) A. Zhukov, „Domain wall propagation in a Fe-rich glass-coated amorphous microwire", Appl. Phys. Lett. 78, 3106 (2001).

(33) V. Zhukova, J. M. Blanco, M. Ipatov, R. Varga, J. Gonzalez, A. Zhukov, „Domain wall propagation in Fe-rich microwires", Phys. B: Cond. Mater. 403, 382 (2008).

(34) R. Varga, A. Zhukov, N. Usov, J. M. Blanco, J. Gonzalez, V. Zhukova, P. Vojtanik, „Domain-wall dynamics in glass-coated magnetic microwires", J. Magn. Magn. Mater. 316, 337 (2007).

(35) R. P. del Real, C. Prados, D. X. Chen, A. Hernando, and M. Vazquez, „Eddy current damping of planar domain wall in bistable amorphous wires", Appl. Phys. Lett. 63, 3518 (1993).

(36) H.-L. Hunag, „Theory of Domain-Wall Mobility in Ferromagnetic Insulators", J. Appl. Phys. 40, 855 (1969).

(37) M. Guyot, and V. Cagan, „Temperature dependance of the domain wall mobility in YIG, deduced from the frequency spectra of the initial susceptibility of polycrystals", J. Magn. Magn. Mater. 27, 202 (1982).

(38) L. D. Landau, E. Lifshitz, „On the theory of the dispersion of magnetic permeability in ferromagnetic bodies", Phys. Z. Sowjetunion 8, 153 (1939).

(39) T.H. O'Dell , Ferromagnetodynamics, Imperial College of Science and Technology, University in London, Printed in Hong Kong, ISBN 0 333 26413 4, p. 40.

(40) Soshin Chikazumi, „Physics of Ferromagnetism", Clarendon Press, Oxford, ISBN 0198517769 (1997).

(41) M. Mizutani, K. Mohri, F. B. Humphrey, I. Ogasawara, „Dynamics and relaxation of large Barkhaussen discontinuity in amorphous wires", IEEE Trans. Magn. 27, 5331 (1991).

(42) H. Kronmüller, „Theory of the coercitive fields in amorphous ferromagnetic alloys", J. Magn. Magn. Mater. 24, 159 (1981).

(43) H. Kronmüller, „The rôle of tho-level systems in amorphous metallic alloys", Phys. Status Solidi B 118, 661 (1983).

(44) D. X Chen, N. M. Dempsey, M. Vazquez and A. Hernando, „Propagating domain wall shape and dynamics in iron-rich amorphous wires", IEEE Trans. Magn. 31, 781 (1995).

(45) R.Varga, et al, „Single-Domain Wall Propagation and Damping Mechanism During Magnetic Switching of Bistable Amorphous Microwires", Phys. Rev. Lett. 94, 017201 1 (2005).

(46) J. Oliviera, R. Varga, V. M. Prida, M. L. Sanchez, B. Hernando and A. Zhukov, „Domain wall dynamics during the devitrification of $Fe_{73.5}CuNb_3Si_{11.5}B_{11}$ magnetic microwires", Phys. Rev. B 82, 094414 (2010).

(47) L. M. Garcia, J. Bartolome and F. J. Lazaro, „Magnetic disaccommodation phenomena in rare-earth intermetallic compounds", Phys. Rev. B 54, 15238 (1996).

(48) R. Varga, G. Infante, G. A. Badini-Canfolentieri and M. Vazquez, „Locally induced domain wall damping in a thin magnetic wire", Appl. Phys. Lett. 95, 012503 (2009).

(49) R. Varga, G. Infante, G. A. Badini-Confalonieri and M. Vazquez, „Diffusion-damped domain wall dynamics", J. Phys. Conf. Ser. 200, 042026 (2010).

(50) R. Varga, K. L. Garciaa, M. Vazquez, A. Zhukov, and P. Vojtanik, „Switching-field distribution in amorphous magnetic bistable microwires", Phys. Rev. B 70, 024402 (2004).

(51) J. Gamcova, P. Klein, J. Kovac, A. Zhukov, „Tailoring the Switching Field Dependence on External Parameters in Magnetic Microwires", IEEE Trans. on Magn. 49, 30 (2013).

(52) R. Varga, K. L. Garcia, and M. Vázquez, „Single-Domain Wall Propagation and Damping Mechanism during Magnetic Switching of Bistable Amorphous Microwires", Phys. Rev. Lett. 94, 017201 (2005).

(53) R. Sabol, R. Varga, J. Hudak, J. Blazek, D. Praslicka, P. Vojtanik, G. Badini, and M. Vazquez, „Temperature and frequency dependencies of the switching field in glass-coated FeNbSiB microwires", J. Appl. Phys. 111, 053919 (2012).

(54) E. Komova, M. Varga, R. Varga, P. Vojtanik, J. Torrejon, M. Provencio and M. Vazquez, „Frequency dependence of the single domain wall switching field in glass-coated microwires", J. Phys. Condens. Mater. 19, 236229 (2007).

(55) P. Allia and F. Vinai, „New approach to the study of the magnetic permeability aftereffect of amorphous ferromagnetic alloys", Phys. Rev. B 26, 6141 (1982).

(56) N. L. Schryer, L. R. Walker, „The motion of 180°domain walls in uniform dc magnetic fields", J. Appl. Phys. 45, 5406 (1974).

(57) D. A. Allwood, C. C Faulkner, X. Gang, M. D. Cooke, R. P. Cowburn, „Magnetic domain wall dynamics in a permalloy nanowire", J. Magn. Magn. Mater. 39, 2663 (2003).

(58) H. Tanigawa, T. Koyama, M. Bartkowiak, S. Kasai, K. Kobayashi, T. Ono, Y. Nakatani, „Dynamical pinning of domain wall in magnetic nanowire induced by Walker breakdown", Phys. Rev. Lett. 101, 207203 (2008).

(59) M. Kläui, P.-O. Jubert, R. Allenspach, A. Bischof, J. A. C. Bland, G. Faini, U. Rüdiger, C. A. F. Vaz, L. Vila, and C. Vouille, „Direct Observation of Domain-Wall Configurations Transformed by Spin Currents", Phys. Rev. Letters 95, 026601 (2005).

(60) G.S.D. Beach, M. Tsoi, J.L. Erskine, „Current-induced domain wall motion", J. Magn. Magn. Mater. 320, 1272 (2008).

(61) R.D. McMichael, M. J. Donahue, „Head to head domain wall structures in thin magnetic strips", IEEE Trans. Magn. 33, 4167 (1997).

(62) Y. Nakatani, A. Thiaville, J. Miltat, „Head-to-head domain walls in soft nano-strips: a refined phase diagram", J. Magn. Magn. Mater. 290, 750 (2005).

(63) D. G. Porter, M. J. Donahue, „Velocity of transverse domain wall motion along thin, narrow strips", J. Appl. Phys. 95, 6729 (2004).

(64) M. T. Bryan et al., „Magnetic domain wall propagation in nanowires under transverse magnetic field", J. Appl. Phys. 103, 073906 (2008).

(65) A. Kunz, S. C. Reiff, "Enhancing domain wall speed in nanowires with transverse magnetic fields", J. Appl. Phys. 103, 07D903 (2008).

(66) V. L. Sobolev, H. L. Huang, and S. C. Chen, „Generalized equations for domain wall dynamics ", J. Appl. Phys. 75, 5797 (1994).

(67) Y. P. Kabanov, Y. L. Iunin, V. I. Nikitenko, A. J. Shapiro, R. D. Shull, L. Y. Zhu, C. L. Chien, „In-Plane Field Effects on the Dynamics of Domain Walls in Ultrathin Co Films With Perpendicular Anisotropy", IEEE Trans. Magn. 46, 2220 (2010).

(68) S. Allende1, D. Altbir, E. Salcedo, M. Bahiana, and J. P. Sinnecker, „Propagation of transverse domain walls in homogeneous magnetic nanowires", J. Appl. Phys. 104, 013907 (2008).

(69) Y. Nakatani, A. Thiaville and J Miltat, „Faster magnetic walls in rough wires", Nature Mater. 2, 521 (2003).

(70) E. R. Lewis et al, „Fast domain wall motion in magnetic comb structures", Nature Mater. 9, 980 (2010).

(71) A. Kunz and S. C. Reiff, „Fast domain wall motion in nanostrips with out-of-plane fields", Appl. Phys. Lett. 93, 082503 (2008).

(72) A. Hubert, R. Schafer, „Magnetic domains", Springler-Verlag Berlin Heidelberg New York, 1998.

(73) G. F. Taylor, „A Method of Drawing Metallic Filaments and a Discussion of their Properties and Uses", Phys. Rev. 23, 655 (1924).

(74) A.V. Ulitovski, Method of continuous fabrication of microwires coated by glass, Author certification (USSR patent), No. 128427 (3.9.1950).

(75) A.V. Ulitovsky, in: Micro-Technology in Design of Electric Devices, Vol.7, Leningrad, 1951, p.6.

(76) T. Goto, M. Nagano and N. Wehara, „Mechanical Properties of Amorphous Fe80P16C3B1 Filament Produced by Glass-Coated Melt Spinning", T. Jpn. I. Met. 18, 11 (1977).

(77) J. Nixdorf, Draht-Welt 53, 693 (1967).

(78) E. Y. Badinter, N. R. Birman, L. F. Drabenko, V.I. Zaborovski, Z.I. Zelikovski and V.G. Cheban, in: Cast microwire and its properties, p.320 (Shinitsa, Kishinev, 1973).

(79) V.S. Larin, A.V. Torcunov, A.Zhukov, J.Gonzalez, M.Vazquez, L.Panina, „Preparation and properties of glass-coated microwires", J. Magn. Magn. Mat. 249, 39 (2002).

(80) S.A. Baranov, V.N. Berzhanski, S.K. Zotov, V.L. Kokoz, V.S. Larin, A.V. Tornucov, Phys. Met. Metall. 67, 73 (1989).

(81) H. Chiriac, T.A. Ovari, and Gh. Pop, „Internal stress distribution in glass-coated amorphous magnetic wires", Phys. Rev. B 52, 10104 (1995).

(82) J. Velazquez, M. Vazquez, and A. Zhukov, „Magnetoelastic anisotropy distribution in glass-coated microwires", J. Mater. Res. 11, 2499 (1996).

(83) M. Vazquez, A. Zhukov, „Magnetic properties of glass-coated amorphous and nanocrystalline microwires", J. Magn. Magn. Mater. 160, 223 (1996).

(84) H. Chiriac, et al., „Amorphous glass-covered magnetic wires: Preparation, properties, applications", Prog. Mater. Sci. 40, 333 (1996).

(85) A. Chizhik, J. Gonzalez, A. Zhukov, and J. M. Blanco, „Circular magnetic bistability induced by tensile stress in glass-covered amorphous microwires", Appl. Phys. Lett. 82, 610 (2003).

(86) H. Chiriac, T.-A. Ovari, and M. Ţibu, „Domain Wall Propagation in Nearly Zero Magnetostrictive Amorphous Microwires", IEEE Trans. Magn. 44, 3931 (2008).

(87) T.A. Ovari, S. Corodeanu, and H. Chiriac, „Domain wall velocity in submicron amorphous wires", J. Appl. Phys. 109, 07D502 (2011).

(88) A. Zhukov, J. Gonzales, M. Vazquez, V. Larin, and A. Torcunov, „Nanocrystalline and Amorphous Magnetic Microwires“, Encyclopedia of Nanoscience and Nanotechnology, american Scientific Publishers, Valnecia, USA, 365 (2001).

(89) R. Weiser, U. Nowak, and K. D. Usadel, „Domain wall mobility in nanowires: Transverse versus vortex domain walls“, Phys. Rev. B 69, 064401 (2004).

(90) M. Yan, A. Kákay, S. Gliga, R. Hertel., „Beating the Walker limit with massless domain walls in cylindrical nanowires”, Phys. Rev. Lett. 104, 057201 (2010).

(91) R. Hertel, J. Kirschner, „Magnetization reversal dynamics in nickel nanowires”, Physica B 343, 206 (2004).

(92) H. Forster, T. Schrefl, D. Suess, W. Scholz, V. Tsiantos, R. Dittrich, and J. Fidler, „Domain wall motion in nanowires using moving grids“, J. Appl. Phys. 91, 6914 (2002).

(93) R.Varga, et al, „Single-Domain Wal Propagation and Damping Mechanism During Magnetic Switching of Bistable Amorphous Microwires“, Phys. Rev. Lett. 94, 017201 1 (2005).

(94) M. V. Chetkin, A. I. Akhutkina and A. N. Shalygin, „Supercritical velocities of domain walls in orthoferrites”, J. Exp. Theor. Phys. 28, 650 (1978).

(95) R. W. Deblois, “Domain wall motion in metals”, J. Appl. Phys. 29, 459 (1958).

(96) R. Varga, K. Richter, A. Zhukov, „Domain wall propagation in thin magnetic wires“, IEEE Trans. Magn. 44, 3965 (2008).

(97) R.D. McMichael, M. J. Donahue, „Head to head domain wall structures in thin magnetic strips”, IEEE Trans. Magn. 33, 4167 (1997).

(98) H. Forster, T. Schrefl, W. Scholz, D. Suess, V. Tsiantos, and J. Fidler, „Micromagnetic simulation of domain wall motion in magnetic nano-wires,” J. Magn. Magn. Mater. 249, 181 (2002).

(99) A. Zhukov, „The remagnetization process of bistable amorphous alloys“, Mater. Des. 5, 299 (1993).

(100) R. Varga, A. Zhukov, V. Zhukova, J. M. Blanco, J. Gonzalez, „Supersonic domain wall in magnetic microwires”, Phys. Rev. B 76, 132406 (2007).

(101) A Zhukov, V. Zhukova, „Magnetic Properties and Applications of Ferromagnetic Microwires with Amorphous and Nanocrystalline Structure”. New York: Nova Science Publishers, Inc.; 2009.

(102) K. Richter, R. Varga, A. Zhukov, „Influence of thermal treatment on domain wall dynamics in glass-coated microwires”, Acta Phys. Pol. A 118 (2010), 738

(103) J. Yang, C. Nistor, G. S. D. Beach, and J. L. Erskine, „Magnetic domain-wall velocity oscillations in permalloy nanowires", Phys. Rev. B 77, 014413 (2008).

(104) M. Hayashi, S. Kasai, and S. Mitani, „Time resolved inductive detection of domain wall dynamics in magnetic nanowires", Appl. Phys. Express 3, 113004 (2010).

(105) D. Treves, „Limitations of the magneto-optic Kerr technique in the study of microscopic magnetic domain structures", J. Appl. Phys. 32, 358 (1961).

(106) M. Knobel, P. Allia, C. GomezPolo, et al., „Joule heating in amorphous metallic wires", J. Phys. D: Appl. Phys. 28, 2398 (1995).

(107) Handbook chemistry and physics, 47th edition, The chemical rubber Co., Superial Avenue, Cleveland, Ohio 1966.

(108) R. Carey and E. D. Isaac, „Magnetic domains and techniques for their observation", English Universities Press Limited, 1966 London, p.67.

(109) M. Born and E. Wolf, „Principles of optics", Cambridge university press, New York 1999, 7th edition.

(110) E. Hecht, „Optics", Addison Wesley Longman, Inc. printed in USA 1998, 3rd edition.

(111) A. Yamaguchi, Y. Kasatani and H. Miyajima, „Domain wall propagation in single crystalline iron wires", J. Phys.: Conf. Ser. 266, 012024 (2011).

(112) T. Ono, H. Miyajima, K. Shigeto, K. Mibu, N. Hosoito, T. Shinjo, „Propagation of a Magnetic Domain Wall in a Submicrometer Magnetic Wire", Science 284, 468 (1999).

(113) D. Atkinson, D. A. Allwood, G. Xiong, M. D. Cooke, C. C. Faulkner and R. P. Cowburn, „Magnetic domain-wall dynamics in a submicrometre ferromagnetic structure", Nature Mater. 2, 85 (2003).

(114) S. Puerta, D. Cortina, H. G. Miquel, D.-X. Chen and M. Vazquez, „Propagation of domain walls in bistable amorphous wires and microwires", J. Crystall. Sol. 287, 370 (2001).

(115) Z.Q. Qiu and S. D. Bader, „Surface magneto-optic Kerr effect (SMOKE)", J. Magn. Magn. Mater. 200, 664 (1999).

(116) J. Zak, E. R. Moog, C. Liu, and S. D. Bader, „Magneto-optics of multilayers with arbitrary magnetization directions", Phys. Rev. B 43, 6423 (1991).

(117) J. Zak, E. R. Moog, C. Liu, and S. D. Bader, „Universal approcah to magneto-optics", J. Magn. Magn. Mater. 89, 107 (1990).

(118) W. Voigt, Magneto-und Elektrooptic, B.G. Teubner, Leipzig, 1908.

(119) M. Ghezzo and K. M. Busen, „The generalized Fresnel reflection coefficients as linear fractional transformations and their representation in the Smith chart", J. Phys. D: Appl. Phys. 2, 655 (1969).

(120) A. Hubert, R. Schäfer, Magnetic domains, Springer-Verlag Berlin Heidelberg New York, printed in Germany, 1998.

(121) H. F. Ding, S. Putter, H. P. Oepen, and J. Kirschner, „Spin-reorientation transition in thin films studied by the component-resolved Kerr effect", Phys. Rev. B 63, 134425 (2001).

(122) J. Olivera, M. L. Sanchez, V. M. Prida, R. Varga, V. Zhukova, A. P. Zhukov, B. Hernando, „Temperature Dependence of the Magnetization Reversal Process and Domain Structure in FeNiSiB Magnetic Microwires", IEEE Trans. Magn. 44, 3946 (2008).

(123) A. Himeno, T. Ono, S. Nasu, T. Okuno, K. Mibu, T. Shinjo, „Propagation velocitymeasurement of a magnetic domain wall in a submicron magnetic wire", J. Magn. Magn. Mater. 272, 1577 (2004).

(124) R. Hudak, R. Varga, J. Zivcak, J. Hudak, J. Blazek, D. Praslicka, „Application of Magnetic Microwires in Titanium Implants – Conception of Intelligent Sensoric Implant", Aspects of Computational Intelligence: Theory and Applications, Topics in Intelligent Engineering and Informatics 2, 413 (2013).

(125) R. Sabol,R. Varga, J. Hudák, J. Blažek, D. Praslička, P. Vojtaník, „1D and 2D Sensor of Magnetic Field Based on the Measurement of Switching Field in Bistable Microwire", Magnetic Measurements 2012 : International Conference : Programme and Book of Abstracts : Tatranske Matliare, Slovakia, 2-4, September 2012. - Bratislava : STU, 2012. - ISBN 978-80-227-3770-8. - S. 18.

(126) E. Ia. Badinter, E.M Lys'ko, Microwire and resistivity devices, Shtinitsa, Kishinev, 1962, pp. 52 – 62.

(127) V. Zhukova, V.S. Larin, A.P. Zhukov, „Stress induced magnetic anisotropy and giant magnetoimpedance in Fe-rich glass-coated magnetic microwires", J. Appl. Phys. 94, 1115 (2003).

(128) Weast, Robert C., Handbook of Chemistry and Physics,65th ed., Chemical Rubber Comp. Press, Cleveland, Ohio, (1984).

(129) J.M. Blanco,V. Zhukova,M. Ipatov and A.Zhukov, „Effect of applied stresses on domain-wall propagation in glass-coated amorphous microwires", Phys. Stat. Solidi (a) 208, 545 (2011).

(130) V. Zhukova, J.M. Blanco, M. Ipatov and A. Zhukov, „Magnetoelastic Contribution in Domain-Wall Dynamics of Magnetically Bistable Microwires", IEEE Trans. Magn. 47, 3783 (2011).

(131) L. V. Panina, H. Katoh, M. Mizutani and K. Mohri, „Analysis for Domain Dynamics in Amorphous Magnetostrictive Wires of the Composition ($Fe_{77.5}Si_{7.5}B_{15}$)", IEEE Transl. J. Magn. Jpn 8, 306 (1993).

(132) H. Chiriac, M. Lupu, „Effect of thermal treatments on the magnetic inhomogeneities distribution in magnetic amorphous wires and microwires", IEEE Trans. Magn. 39, 3043 (2003).

(133) A. Zhukov, „Glass-coated magnetic microwires for technical applications", J. Magn. Magn. Mater. 242, 216 (2002).

(134) D. Djuhana, H.-G. Piao, J.-H. Shim, S.-H. Lee, S.-H. Jun, S.-C. Yu, S.K. Oh, D.-H. Kim, „Spontaneous Domain Wall Motion at Zero External Magnetic Field in Ferromagnetic Nanowire", IEEE Trans. Magn. 46, 217 (2010).

(135) R.L. Novak, J.P. Sinnecker, H. Chiriac, „Annealing effects on the magnetization reversal and domain wall dynamics in bistable amorphous glass-covered microwires", J. Phys. D, Appl. Phys. 41, 095005 (2008).

(136) R. Varga, K. Richter, Zhukov, „Domain wall propagation in thin magnetic wires.", IEEE Trans. Magn. 44, 3965 (2008).

(137) K. Richter, Y. Kostyk, R. Varga, a. A. Zhukov, V. Larin, „Domain wall dynamics in amorphous microwires", Acta Phys. Pol. A 113, 7 (2008).

(138) P. Klein, R. Varga and M. Vazquez, „Stable and fast domain wall dynamics in nanocrystalline magnetic microwire", J. Alloy. Comp. 550, 31 (2013).

(139) R. Varga, K. Richter and A. Zhukov, „Negative Mobility of Single Domain Wall in Magnetic Microwires", Acta Phys. Pol. A 118, 747 (2010).

(140) A. Zhukov, J. Gonzales, A. Torcunov, E. Pina, M.J. Prieto, A.F. Cobeno, J.M. Blanco, V. Larin, S. Baranov, „Ferromagnetic resonance, magnetic behaviour and structure of Fe-based glass-coated microwires", J. Magn. Magn. Mater. 203, 238 (1999).

(141) S. A. Baranov, D. Laroze, P. Vargas, M. Vazquez, „Domain structure of Fe-based microwires", Physica B 372, 324 (2006).

(142) M. Vazquez, A.P. Zhukov, „Magnetic properties of glass-coated amorphous and nanocrystalline microwires", J. Magn. Magn. Mater. 160, 223 (1996).

(143) Y. Takemura, H. Tokuda, K. Komatsu, S. Masuda, T. Yamada, K. Kakuno, K. Saito, „Dependence of magnetization dynamics and magneto-impedance effect in FeSiB amorphous wire on annealing conditions“, IEEE Trans. Magn. 32, 4947 (1996).

(144) R. D. McMichael and M. J. Donahue, „Head to head domain wall structures in thin magnetic strips", IEEE Trans. Magn. 33, 4167 (1997).

(145) W. M. Haynes, CRC Handbook of Chemistry and *Physics, 94th ed.*, National Institute of Standards and Technology, Boulder, Colorado, USA (2013).

(146) Kanno, T., K. Mohri, T. Yagi, T. Uchiyama, and L. P. Shen, „Amorphous wire MI microsensor using C-MOS IC multivibrator", IEEE Trans. Magn. 22, 3358 (1997).

(147) A. Zhukov, V. Zhukova, J. Gonzalez, L. Panina and J.M. Blanco, „Development of stress and temperature sensitive microwires for the sensor application and tunable composite materials", Sci. Tech. Adv. Mater. 54, 180 (2008).

(148) V. S. Larin., V. Zhukova, A. Zhukov, A. V. Torcunov and M. Vazquez, „Tailoring of magnetic anisotropy by thermo-mechanical annealing", Sensors and actuators A 106, 96 (2003).

(149) F. Becka, R.C. Gomesa, K.D. Sossmeiera, F. Bohnb and M. Carara, „Stress dependence of the domain wall dynamics in the adiabatic regime", Journal of Mag. and Mag. Materials 323, Issue: 3-4, 268 -271 (2011).

(150) P. Aragoneses, J. M. Blanco, L. Dominguez, J. González, A. Zhukov and M. Vázquez, „The stress dependance of switching field in amorphous glass-coated microwires", Journal of Physics D: Applied physics 31, 3040 (1998).

(151) J. González, N. Murillo, V. Larin, J.M. Barandiaran, M. Vázquez, A. Hernando, „Magnetic bistability of glass-covered Fe-rich amorphous microwire: influence of heating treatments and applied tensile stress", Sensors and actuators A 59, 100 (1997).

(152) H. H. Ouslimani, R. Abdeddaim, and A. C. Priou, „Free-space electromagnetic characterization of materials for microwave and radar applications“, PIERS Online 1, 132 (2005).

(153) A. Zhukov, M. Ipatov, C. Garcia, J. Gonzalez, L. Panina, J. M. Blanco, and V. Zhukova, „Development of Thin Soft Magnetic Amorphous Microwires for High Frequency Magnetic Sensors Applications", PIERS Proceedings, Hangzhou, China 650 (2008).

(154) I. Astefanoaei, D. Radu, and H. Chiriac, „On dc Joule-heating effects in amorphous glass-covered $Fe_{77.5}Si_{7.5}B_{15}$ microwires", J. Phys. D: Appl. Phys. 38, 235 (2005).

(155) I. Astefanoaei, D. Radu1, and H. Chiriac, „Internal stress distribution in DC joule-heated amorphous glass-covered microwires", J. Phys. D: Appl. Phys. 18, 2689 (2006).

(156) A. Zhukov, V. Zhukova, J. M. Blanco, and J. Gonzalez, „Recent research on magnetic properties of glass-coated microwires", J. Magn. Magn. Mater. 294, 182 (2005).

(157) V. Zhukova, A. F. Cobeno, A. Zhukov, J. M. Blanco, S. Puerta, J. Gonzalez, M. Vazquez, „Tailoring of magnetic properties of glass-coated microwires by current annealing", Journal of Non-Crystalline Solids 287, 31 (2001).

(158) J. Gonzalez, J. M. Blanco, M. Vazquez, J. M. Barandiaran, G. Rivero et al., „Influence of the applied tensile stress on the magnetic properties of current annealed amorphous wires", J. Appl. Phys. 70, 6522 (1991).

(159) K. D. Sossmeier, F. Bohn, H. Chiriac, and M. Carara, „Comparison between ac and dc current annealing in CoFeSiB glass-covered amorphous microwires", J. Phys. D: Appl. Phys. 40, 3233 (2007).

(160) H. Chiriac, T.-A. Óvári, and M. Ţibu, „Effect of surface domain structure on wall mobility in amorphous microwires", J. Appl. Phys. 105, 07A310 (2009).

(161) M. Ipatov, A. Chizhik, V. Zhukova, J. Gonzalez, and A. Zhukov, „Correlation of surface domain structure and magneto-impedance in amorphous microwires", J. Appl. Phys. 109, 113924 (2011).

(162) E.E. Shalyguina, L.M. Bekoeva, Kyung-Ho Shin, „Investigation of Co-rich amorphous microwires by help of magneto-optical method with micron resolution", J. Magn. Magn. Mater. 215, 472 (2000).

(163) N. N. Orlova,A. S. Aronin,S. I. Bozhko,Yu. P. Kabanov, and V. S. Gornakov, „Magnetic structure and magnetization process of the glass-coated Fe-based amorphous microwire", J. Appl. Phys. 111, 073906 (2012).

(164) A. Chizhik, R. Varga, A. Zhukov, J. Gonzalez, and J. M. Blanco, „Kerr-effect based Sixtus-Tonks experiment for measuring the single domain wall dynamics", J. Appl. Phys. 103, 07E707 (2008).

(165) H. Chiriac, M. Lostun, and T.-A. Ovari , „Surface Magnetization Processes in Amorphous Microwires", IEEE Trans. Magn. 46, 383 (2010).

(166) M. Letcher, G. A. Jones, D. G. Lord, M. WunFogle, and H. T. Savage, „Domain structure of as cast and annealed FeSiB amorphous wires", J. Appl. Phys. 69, 5331 (1991).

(167) G. Traeger, L. Wenzel, and A. Hubert, „Computer Experiments on the information depth and the figure of merit in magnetooptics", Phys. Stat. Sol. (a) 131, 201 (1992).

(168) A. Chizhik, A. Zhukov, A. Stupakiewicz, A. Maziewski, J.M. Blanco, and J. Gonzalez, „Kerr Microscopy Study of Magnetic Domain Structure Changes in Amorphous Microwires", IEEE Trans. Magn. 45, 4279 (2009).

(169) J. Oliviera, M.L. Sanchez, V.M. Prida, R. Varga, V. Zhukova, A.P Zhukov, and B. Hernando, „Temperature dependence of the magnetization reversal process and domain structure in $Fe_{77.5-x}$ $Ni_xSi_{7.5}B_{15}$ magnetic microwires", IEEE Trans. Magn. 44, 3946 (2008).

(170) V. Zhukova, P. Umnov, V. Molokanov, A.N. Shalygin, and A. Zhukov, „Magnetic Properties and Giant Magneto-Impedance Effect of Ductile Amorphous Microwires Without Glass Coating", Sens. Lett. 10, 731 (2012).

(171) H. Okuno, H. Murai, and Y. Sakaki, „Image processing system for magnetic domain observation", J. Appl. Phys. 64, 6014 (1988).

(172) M. Takezawa, T. Shimada, S. Kondo, S. Mimura, Y. Morimoto, T. Hidaka, and J. Yamasaki, „Domain observation technique for Nd–Fe–B magnet in high magnetic field by image processing using liquid crystal modulator", J. Appl. Phys. 101, 09K106 (2007).

(173) H.F. Ding, S. PuK tter, H.P. Oepen, J. Kirschner, „Experimental method for separating longitudinal and polar Kerr signals", J. Magn. Magn. Mater. 212, L5 (2000).

(174) J. Rhensius, L. Heyne, D. Backes, S. Krzyk, L. J. Heyderman, L. Joly, F. Nolting, and M. Klaui, „Imaging of Domain Wall Inertia in Permalloy Half-Ring Nanowires by Time-Resolved Photoemission Electron Microscopy", Phys. Rev. Let. 104, 067201 (2010).

(175) P. A. Ekstrom and A. Zhukov, „Spatial structure of the head-to-head propagating domain wall in glass-covered FeSiB microwire", J. Phys. D: Appl. Phys. 43, 205001 (2010).

(176) A. Zhukov, M. Vazquez, J. Velazquez , H. Chiriac and V. Larin, „The remagnetization process in thin and ultra-thin Fe-rich amorphous wires", J. Magn. Magn. Mater. 151, 132 (1995).

(177) L. V. Panina, M. Ipatov, V. Zhukova and A. Zhukov, „Domain wall propagation in Fe-rich amorphous microwires", Phys. B: Cond. Mater. 407, 1442 (2001).

(178) H. Chiriac, T. A. Ovari, G. Pop, „Internal stress distribution in glass-covered amorphous magnetic wires", Phys. Rev. B 52, 10104 (1995).

(179) A. Zhukov, M. Vázquez, J. Velázquez, H. Chiriac, V. Larin, „The remagnetization process of thin and ultrathin Fe-rich amorphous wires", J. Magn. Magn. Mater. 151, 132 (1995).

(180) A. Zhukov, M. Vázquez, J. Velázquez, H. Chiriac, V. Larin, „The remagnetization process of thin and ultrathin Fe-rich amorphous wires", J. Magn. Magn. Mater. 151, 132 (1995).

(181) H. Chiriac, T. A. Ovari, G. H. Pop, „Internal stress distribution in glass-covered amorphous magnetic wires", Phys. Rev. B 52, 10104 (1995).

(182) A. Zhukov, J. M. Blanco, M. Ipatov, A. Chizhik and V. Zhukova, „Manipulation of domain wall dynamics in amorphous microwires through the magnetoelastic anisotropy ", Nanoscale Res. Lett. 7, 223 (2012).

(183) K. Richter, R. Varga, G. A. Badini-Confalonieri and M. Vázquez, „The effect of transverse field on fast domain wall dynamics in magnetic microwires", Appl. Phys. Lett. 96, 182507 (2010).

(184) A. Zhukov, J. Gonzalez, „Processing of advanced magnetic materials", Advanced Magnetic Materials, Vol. 3, Cap. 5, 115{181, (Eds. David J. Sellmyer, Yi Liu and Daisuke Shindo), Kluwer Academic Publishers, Norwell, (2004).

(185) S. Corodeanu, H. Chiriac, and T.-A. Ovari, „Accurate measurement of domain wall velocity in amorphous microwires, submicron wires, and nanowires", Rev. Sci. Instr. 82, 094701 (2011).

(186) T. A. Ovari, S. Corodeanu, and H. Chiriac, „Domain wall velocity in submicron amorphous wires", J. Appl. Phys. 109, 07D502 (2011).

(187) V. Zhukova, J. M. Blanco, M. Ipatov, and A. Zhukov, „Effect of transverse magnetic field on domain wall propagation in magnetically bistable glass-coated amorphous microwires", J. Appl. Phys. 106, 113914 (2009).

(188) H. Garcia-Miquel, DX. Chen, M. Vazquez, „Domain wall propagation in bistable amorphous wires", J. Magn. Mag. Mater. 212, 101 (2000).

(189) K. D. Sossmeier, F. Beck, H. Chiriac, et al., „Spin relaxation and domain wall dynamics in glass-coated microwires", Phys. Status Solidi A 206, 635 (2009).

(190) J. D. Santos, A. Ruiz, R. F. Cobos, I. Ribot, V. Vega, P. Alvarez, M. L. Sanchez, J. L. Sanchez, V. M. de la Prida, B. Hernando, „Domain wall dynamics in Fe-rich glass covered amorphous microwires", Phys. Status Solidi A 206, 618 (2009).

(191) A. S. Antonov, N. A. Buznikov, A. L. D'yachkov, A. A. Rakhmanov, V. V. Samsonova, T. A. Furmanova, „The influence of the glass-cover thickness on the magnetoimpedance of amorphous microwires", Journal of Communications Technology and Electronics 54, 1315 (2009).

(192) M. Vazquez and C. Gomez–Polo, "Amorphous and Nanocrystalline Wires and Microwires with Giant Barkhausen Jumps for Magnetic Sensor Applications", J. Korean Phys. Soc. 31, 471 (1997).

(193) V. Rodionova, A. Nikoshin, J. Torrejon, G. A. Badini-Confalonieri, N. Perov, M. Vazquez, „Temperature-Dependent Magnetic Properties of Magnetically Biphase Microwires", IEEE Trans. Magn. 47, 3787 (2011).

(194) E. C. Stoner and E. P. Wohlfarth, „A mechanism of magnetic hysteresis in heterogeneous alloys", IEEE Trans. Magn. 27, 3475 (1991).

(195) M.J. Donahue and D.G. Porter, OOMMF User's Guide, Version 1.0, Interagency Report NISTIR 6376, National Institute of Standards and Technology, Gaithersburg, MD (1999).

Communication related to this work

In preparation process:

K. Richter, A. Thiaville, R. Varga, „Magneto-optical observation of metallic cylinders"
K. Richter, A. Thiaville, R. Varga, „Direct observation of the surface domain wall structure in amorphous glass-coated microwires"
K. Richter, R. Varga, A. Thiaville, „Imaging the surface domain structure of amorphous glass-coated microwires by Bitter colloid"

List of published articles:

1. R. Varga, K. Richter, P. Klein, A. Zhukov, M. Vázquez, „Domain wall dynamics in thin magnetic wires", Journal of Superconductivity and Novel Magnetism 26, 1713 (2013).
2. P. Klein, K. Richter, R. Varga, M. Vázquez, „Frequency and temperature dependencies of the switching field in glass-coated FeSiBCr microwire", Journal of Alloys and Compounds, 569, 9 (2012).
3. K. Richter, R. Varga, A. Zhukov, „Influence of the magnetoelastic anisotropy on the domain wall dynamics in bistable amorphous wires", J. Phys.: Condens. Matter 24 296003 (2012).
4. K. Richter, R. Varga, J. Kovac, A. Zhukov, „Controlling the domain wall dynamics by induced anisotropies" IEEE TRANS. MAGN. 48, 1266 (2011).
5. R. Varga, P. Klein, K. Richter, A. Zhukov and M. Vazquez, „Fast domain wall dynamics in amorphous and nanocrystalline magnetic microwires", Journal of Magnetism and Magnetic Material (2011).
6. K. Richter, R. Varga, G. A. Badini-Confalonieri and M. Vázquez, "The effect of transverse field on fast domain wall dynamics in magnetic microwires", Appl. Phys. Lett.96 (2010), 182507.
7. R. Varga, G. Infante, K. Richter, and M. Vazquez, "Anomalous effects in the domain wall dynamics in magnetic microwires", *Physica Status Solidi* 208 (2010), 509.
8. K. Richter, R. Varga, A. Zhukov, "Influence of thermal treatment on domain wall dynamics in glass-coated microwires", ACTA PHYSICA POLONICA A 118 (2010), 738.

9. K. Richter, R. Varga, G. Infante, G. A. Badini-Confalonieri and M. Vazquez, „Domain wall dynamics in thin magnetic wires under the influence of transversal magnetic field“, IEEE TRANS. MAGN. 46 (2010), 210.

10. R. Varga, K. Richter and A. Zhukov, „Negative Mobility of Single Domain Wall in Magnetic Microwires“, *ACTA PHYSICA POLONICA A* 118 (2010), 747.

11. R. Varga, Y. Kostyk, K. Richter, A. Zhukov, and M. Vazquez, „Domain wall dynamics in bistable magnetic microwires.“, Physica Status Solidi (a) 206 (2009), 608.

12. R. Varga, K. Richter, Zhukov, „Domain wall propagation in thin magnetic wires.“, IEEE TRANS. MAGN. 44 (2008), 3965.

13. K. Richter, Y. Kostyk, R. Varga, a. Zhukov, V. Larin, „Domain wall dynamics in amorphous microwires“, ACTA PHYSICA POLONICA A 113 (2008), 7.

Citations:

K. Richter, R. Varga, G. Infante, G. A. Badini-Confalonieri and M. Vazquez, „The effect of transverse field on fast domain wall dynamics in magnetic microwires“, Applied Physics Letters 96 (2010), 182507.

1. Otalora, J. A.; Lopez-Lopez, J. A.; Nunez, A. S.; et al. „Domain wall manipulation in magnetic nanotubes induced by electric current pulses“, Journal of physics-condensed matter 24, 436007 (2012).

2. O. Boulle, L. D. Buda-Prejbeanu, M. Miron, and G. Gaudin, Current induced domain wall dynamics in the presence of a transverse magnetic field in out-of-plane magnetized materials, J. Appl. Phys. 112, 053901 (2012).

3. A. Chizhik, A.Zhukov, J.M.Blanco, J.Gonzalez, „Magneto-optical study of domain wall dynamics and giant Barkhausen jump in magnetic microwires“, Journal of Magnetism and Magnetic Materials 324, 3563 (2012).

4. V. Rodionova, N. Kudinov, A. Zhukov, and N. Perov, „Interaction of bistable glass-coated microwires in different positional relationship“, Physica-B Condensed Matters 407, 1438 (2011).

5. Tzong Rong Ger, Chen-Chi Huang, Hao-Ting Huang, and Zung-Hang Wei, „Investigation of the magnetization process in a three-dimensional curled up structure“, Journal of Applied Physics vol. 109, 07E534 (2011)

6. S. Mukhopadhyay, A. Singh, A. Ghosh, „Field-tunable stochasticity in the magnetization reversal of a cylindrical nanomagnet“, Phys Rev. B, 82, 172404 (2010).

7. A. Kunz, J. D. Priem, S. C. Reiff, „Injecting, controlling, and storing magnetic domain walls in ferromagnetic nanowires“, Proceedings of the SPIE, 7760, 776005 (2010).

8. A. Kunz, S.C. Reiff, J.D. Priem, E.W. Rentsch, „Controlling individual domain walls in ferromagnetic nanowires for memory and sensor applications“, Proceeding – 2010 12th International Conference on Electromagnetics in Advanced Applications, ICAA 10, art. no. 5653609, 248.

R. Varga, K. Richter, Zhukov, „Domain wall propagation in thin magnetic wire.“, IEEE TRANS. MAGN. 44 (2008), 3965.

10. J. Ziman, M. Kladivova, J. Onufer, et al., „Domain Wall Dynamics in Amorphous Ferromagnetic Wire with Small Helical Anisotropy“, Acta Physica Polonica, 118, 778 (2010).

9. J. Onufer, J. Ziman, M. Kladivová, „Dynamics of closure domain structure in bistable ferromagnetic microwire“, Journal of Magnetism and Magnetic Materials, http://dx.doi.org/10.1016/j.jmmm.2013.05.033.

10. H.G. Piao,J.H. Shim,D. Djuhana,D.H. Kim, „Intrinsic pinning behavior and propagation onset of three-dimensional Bloch-point domain wall in a cylindrical ferromagnetic nanowire“, Applied Physics Letters 102, 112405 (2013).

11. P. Ma, H. G. Piao, J. H. Shim, et al. „Position-dependent spontaneous motion of the magnetic domain wall in ferromagnetic nanowires“, Journal of the Korean Physics Society 62, 288 (2013).

12. V. V. Zverev, B. N. Filippov, „Simulation of three-dimensional micromagnetic structures in magnetically uniaxial films with in-plane anisotropy: Static structures“, Physics of metals and metallography 114, 108 (2013).

13. J. Ziman, M. Kladivova, J. Onufer, et al., „Domain Wall Dynamics in Amorphous Ferromagnetic Wire with Small Helical Anisotropy“, Acta Physica Polonica, 118, 778 (2010).

14. H.-G. Piao, J.-H. Shim, S.-H. Lee, D. Djuhana, S.-K. Oh, S.-C. Yu, and D.-H. Kim, "Domain wall propagation in wavy ferromagnetic nanowire", IEEE Trans. Magn. 45, 3926 (2009).

15. Ziman, J., Onufer, J., Kladivová, „DC magnetization processes in bistable glass-coated ferromagnetic microwires“ Journal of Magnetism and Magnetic Materials volume 323, issue 23, 3098 - 3103 (2011).

16. H.-G. Piao, J.-H. Shim, D. Djuhana, S.-H. Lee, S.-H. Jun, C.-M. Heo, S.-K. Oh, S.-C. Yu, and D.-H. Kim, "Micromagnetic simulation of damped oscillatory behaviour of domain wall propagation in sinusoidal ferromagnetic nanowire", IEEE Trans. Magn. 46, 224 (2010).

R. Varga, Y. Kostyk, K. Richter, A. Zhukov, and M. Vazquez, „Domain wall dynamics in bistable magnetic microwires", Physica Status Solidi (a) 206 (2009), 608.

17. J.S. Liu, F.Y. Cao, D.W. Xing, L.Y. Zhang, F.X. Qin, H.X. Peng, X. Xue, J.F. Sun, „Enhancing GMI properties of melt-extracted Co-based amorphous wires by twin-zone Joule annealing" J. Alloys Comp.541, 215 (2012).

18. JF. Sun, JS Liu, DW. Xing, et al., „Experimental study on the effect of alternating-current amplitude on GMI output stability of Co-based amorphous wires", Physica Status Solidi A – Applications and materials science, 208, 910 (2011).

19. Jing-Shun Liu, Da-Yue Zhang, Fu-Yang Cao, Da-Wei Xing, Dong-Ming Chen, Xiang Xue, Jian-Fei Sun, „Multiangle combined magnetic-field annealing of Co-based amorphous microwires for sensor applications", physica status solidi (a) 209, 984, (2012).

K. Richter, R. Varga, G. Infante, G. A. Badini-Confalonieri and M. Vazquez, „Domain wall dynamics in thin magnetic wires under the influence of transversal magnetic field", IEEE TRANS. MAGN. 46 (2010), 210.

20. H. Chiriac, M. Lostun, G. Ababei, and T.-A. Ovari, „Comparative study of the magnetic properties of positive and nearly zero magnetostrictive submicron amorphous wires," Journal of applied physics, 109, 07B501, (2011).

K. Richter, Y. Kostyk, R. Varga, a. Zhukov, V. Larin, „Domain wall dynamics in amorphous microwires", ACTA PHYSICA POLONICA A 113 (2008), 7.

21. N. N. Orlova, A. S. Aronin, S. I. Bozhko, Yu. P. Kabanov, and V. S. Gornakov, „Magnetic structure and magnetization process of the glass-coated Fe-based amorphous microwire", J. Appl. Phys. 111 (2012), 073906; doi: 10.1063/1.3702448

List of results presented at conferences and workshops:

2013 – 15th Czech and Slovak Conference on Magnetism, CSMAG 2013, Kosice, Slovakia, poster “Magneto-optical observation of surface domain structure in amorphous glass-coated microwires”

2012 – The Joint Europan Magnetic Symposia JEMS 2012, Parma, Italy, poster “Optical study of the domain structure in glass-coated microwires”

2012 – Spring school, The week of doctorands, TDPO 2012 Vysoke Tatry, Slovakia, talk “Fast domain wall dynamics in thin magnetic wires”

2011 – The 20th Soft Magnetic Materials Conference SMM 20, Kos, Grece, poster “Controlling the domain wall dynamics by induced anisotropies”

2010 – The 18th Conference of Slovakian Physicists, Banska Bystrica, Slovakia, invited talk “Dynamika rychlych domenovych stien”

2010 – The Joint Europan Magnetic Symposia JEMS 2010, Krakow, Poľand, poster “Domain wall dynamics in microwires with induced perpendicular anisotropy”

2010 – 13th Czech and Slovak Conference on Magnetism CSMAG 2010, Kosice, Slovakia, poster “The influence of thermal treatment on domain wall dynamics in microwires”

2008 – International workshop on magnetic wires IWMW, Zumaia, Spain, poster

2008 – Workshop on shoft magnetic wires, Madrid, Spain, poster

2008 – Intermag 2008, Madrid, Spain, poster

2007 – 12th Czech and Slovak Conference on Magnetism CSMAG 2007, Kosice, Slovakia, poster